frontiers | Research Topics

Recent advances in cervical cancer radiotherapy

Edited by
Gene A. Cardarelli and John Varlotto

Published in
Frontiers in Oncology

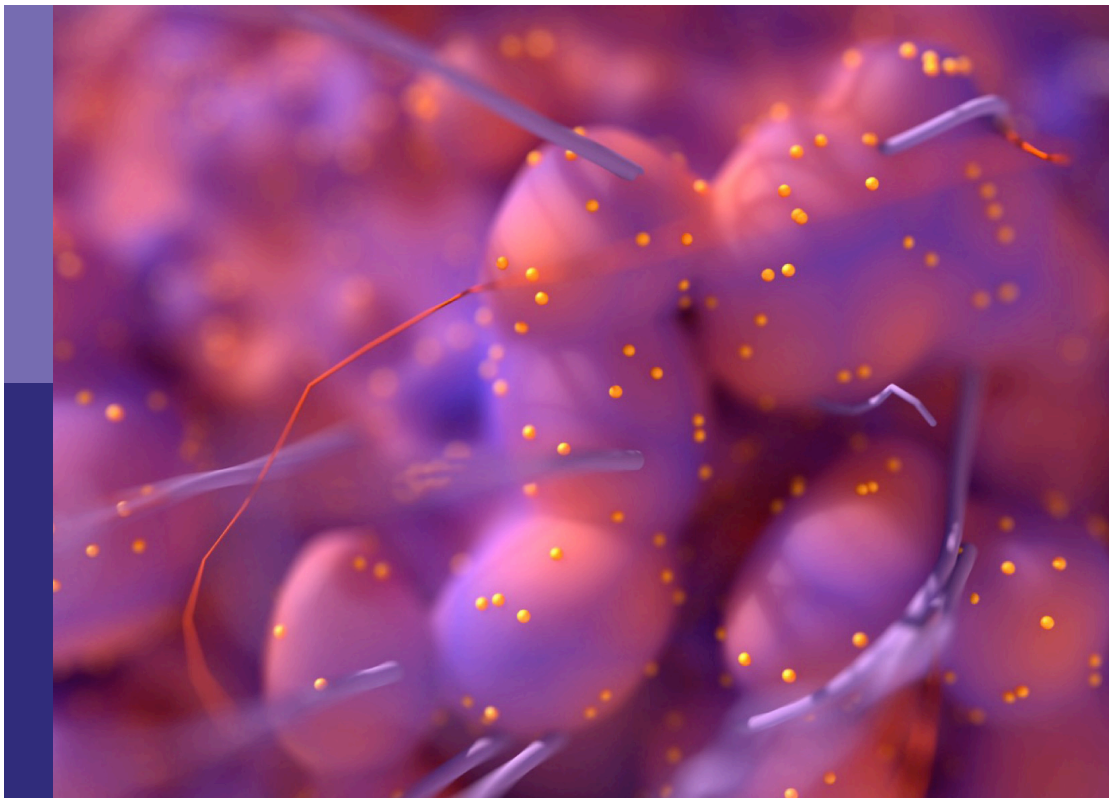

ISSN 1664-8714
ISBN 978-2-83251-798-7
DOI 10.3389/978-2-83251-798-7

About Frontiers

Frontiers is more than just an open access publisher of scholarly articles: it is a pioneering approach to the world of academia, radically improving the way scholarly research is managed. The grand vision of Frontiers is a world where all people have an equal opportunity to seek, share and generate knowledge. Frontiers provides immediate and permanent online open access to all its publications, but this alone is not enough to realize our grand goals.

Frontiers journal series

The Frontiers journal series is a multi-tier and interdisciplinary set of open-access, online journals, promising a paradigm shift from the current review, selection and dissemination processes in academic publishing. All Frontiers journals are driven by researchers for researchers; therefore, they constitute a service to the scholarly community. At the same time, the *Frontiers journal series* operates on a revolutionary invention, the tiered publishing system, initially addressing specific communities of scholars, and gradually climbing up to broader public understanding, thus serving the interests of the lay society, too.

Dedication to quality

Each Frontiers article is a landmark of the highest quality, thanks to genuinely collaborative interactions between authors and review editors, who include some of the world's best academicians. Research must be certified by peers before entering a stream of knowledge that may eventually reach the public - and shape society; therefore, Frontiers only applies the most rigorous and unbiased reviews. Frontiers revolutionizes research publishing by freely delivering the most outstanding research, evaluated with no bias from both the academic and social point of view. By applying the most advanced information technologies, Frontiers is catapulting scholarly publishing into a new generation.

What are Frontiers Research Topics?

Frontiers Research Topics are very popular trademarks of the *Frontiers journals series*: they are collections of at least ten articles, all centered on a particular subject. With their unique mix of varied contributions from Original Research to Review Articles, Frontiers Research Topics unify the most influential researchers, the latest key findings and historical advances in a hot research area.

Find out more on how to host your own Frontiers Research Topic or contribute to one as an author by contacting the Frontiers editorial office: frontiersin.org/about/contact

Recent advances in cervical cancer radiotherapy

Topic editors

Gene A. Cardarelli — Brown University, United States

John Varlotto — Marshall University Chief of Radiation Oncology, Edwards Comprehensive Cancer Center, United States

Citation

Cardarelli, G. A., Varlotto, J., eds. (2023). *Recent advances in cervical cancer radiotherapy*. Lausanne: Frontiers Media SA. doi: 10.3389/978-2-83251-798-7

Table of contents

frontiers | Frontiers in Oncology

TYPE Editorial
PUBLISHED 15 February 2023
DOI 10.3389/fonc.2023.1144797

OPEN ACCESS

EDITED AND REVIEWED BY
Giuseppe Giaccone,
Vice President Global Development,
United States

*CORRESPONDENCE
John Michael Varlotto
jmlotto@comcast.net
Gene A. Cardarelli
gcardarelli1@lifespan.org

SPECIALTY SECTION
This article was submitted to Radiation Oncology, a section of the journal Frontiers in Oncology

RECEIVED 15 January 2023
ACCEPTED 30 January 2023
PUBLISHED 15 February 2023

CITATION
Varlotto JM and Cardarelli GA (2023) Editorial: Recent advances in cervical cancer radiotherapy. *Front. Oncol.* 13:1144797. doi: 10.3389/fonc.2023.1144797

Editorial: Recent advances in cervical cancer radiotherapy

John Michael Varlotto[1]* and Gene A. Cardarelli[2]*

[1]Department of Oncology, Marshall University Chief of Radiation Oncology, Edwards Comprehensive Cancer Center, Huntington, WV, United States, [2]Department of Radiation Oncology, Warren Alpert Medical School, Rhode Island Hospital, Brown University, Providence, RI, United States

KEYWORDS

cervical cancer, anti-angiogenic therapy, vaginal microbiome, interstitial HDR brachytherapy, lexicographic optimization

Editorial on the Research Topic
Recent advances in cervical cancer radiotherapy

It is a great pleasure to serve as Editors for the Frontiers e-block, Recent Advances in Cervical Cancer.

Despite the availability of good screening and HPV vaccine strategies, cervical cancer remains the fourth most common cancer in women and still causes 570,000 new cases and 311,000 deaths globally as reported in 2018 (1). Nearly 90% of cervical cancer deaths occur in developing countries, with India and China accounting for 35% of the total cervical cancer burden (2). Meanwhile in the United States, the CDC has recommended to stop screening for most women age 65 years or older. However, The United States may be underscreening elderly women as shown by a recent retrospective review from the California Cancer Registry which demonstrated that 17.4% of cervical cancers were in women ≥ 65 yrs or older (3).

In 1999, 3 simultaneous prospective, randomized trials demonstrated the efficacy of concomitant cisplatin-based chemo/radiation (4–6) for locally advanced cervical cancer. Since this time, there has only been a refinement of our approach to the radiotherapeutic treatment for cervical cancer *via* the use of IMRT(proven in the adjuvant setting (7, 8), and the MRI-planning for cervical HDR brachytherapy as per EMBRACE (9), but there has been no recent trial that has shown a further improvement in survival in locally advanced cervical cancer.

Recently, the NRG Oncology Group reported the results of the phase I/Ib NRG-GY017 (10) and showed that the addition of atezolizumab to concurrent chemo/radiation in node-positive cervical cancer was feasible. Additionally, there was increase in peripheral blood T-cell receptor (TCR) clonal expansion and expansion of tumor-associated T-cell clones between the start of treatment and day 21 of concurrent chemo/radiation. Patients with higher pre-treatment TCR diversity had increased likelihood of biopsy-proven complete pathologic response. However, the role of immunotherapy remains to be determined.

This special issue of Frontiers will allow the reader to review cutting-edge research in radiation planning/treatment delivery and to assess valuable clinical studies on the use of re-irradiation of locally recurrent cervical cancer with interstitial HDR brachytherapy, the development of prognostic tools from conventional PETCT Scans, the optimal timing of radiotherapy as per the circadian cycle, the use of an anti-angiogenic agent concurrently with chemo/radiotherapy, and the changes of the vaginal microbiome during radiotherapy.

Five studies in this special issue have shown potential improvements in the efficacy and speed of treatment planning. The dosimetric study by Trivellato et al. compared plans for locally advanced cervical cancer using lexicographic optimization vs standard IMRT optimization. The lexicographic optimization mimics the conversations concerning treatment planning between the Radiation Oncologists and the treatment planning team by using inviolable dose constraints and a hierarchical list of objectives. By utilizing this technology, the median treatment planning/optimization period was reduced from 4 hours to just over 1 hour while increasing planning tumor volume coverage and plan complexity and offering similar organ-at-risk dose constraints. Researchers from Shanghai Sixth People's Hospital have proposed and verified a method of machine learning for optimization of cervical HDR-brachytherapy which allows for reduction of normal tissue doses and more efficient planning time (Li et al.). Investigators from The First Affiliated Hospital of Xi'an noted that an atlas-based auto-segmentation of volumes undergoing radiotherapy can be performed quickly and accurately for tumor and normal tissue volumes with the exception of rectum (Li et al.). Wu et al. from University of Science and Technology of China Anhui Provincial Hospital used a scatter-beam correction method in order to facilitate improved image quality of cone-beam ct scans to improve dosimetric accuracy of cervical brachytherapy. Zhou et al. from Affiliated Hospital of Southwest Medical University used a support vector machine model to predict the D2cm3 for the bladder, rectum, sigmoid colon, and small intestine in patients undergoing cervical cancer brachytherapy.

Two studies investigated potential prognostic factors that could, if proven in follow-up studies, help identify high-risk populations for treatment failure. Wang et al. from Peking Union Medical College Hospital (CAMS) assessed tumor/nodal metabolic parameters on PET/CT and their association with outcomes in 125 consecutive patients with locally advanced cervical cancer. This study noted that total lesion glycolysis and SUV max in the primary tumor volume and cervical lymph nodes, respectively are associated with overall survival, disease-free survival and distant metastasis-free survival. If confirmed, the results can hopefully identify patients who can benefit from treatment intensification. There have been intriguing studies of the microbiome and their effects of therapeutic outcomes of patients undergoing cancer therapy (11, 12). Jiang et al. demonstrated that the vaginal microbiome was different in 20 cervical cancer patients as compared to six healthy controls. Furthermore, the relative abundance of certain vaginal microbes increased over time. It will be interesting to see if follow-up studies can assess whether certain microbes are associated with treatment efficacy and if the microbial environment can be altered to improve outcomes in patients with cervical cancer undergoing radiotherapy.

Three clinical studies have demonstrated interesting strategies to improve outcomes for patients with cervical cancer undergoing radiotherapy. Based upon the concept that tumor and normal tissue both follow a circadian rhythm (13–15), Wang et al. report a very interesting prospective, randomized, multi-institutional clinical trial that randomized patients with locally advanced cervical cancer to morning (9:00–11:00 AM) or evening radiotherapy (7:00–9:00 PM) radiotherapy. Although the efficacy of therapy was similar in both groups, the evening group experienced less radiation enteritis and radiation diarrhea at the expense of a higher incidence of bone marrow suppression and hematologic toxicity. Ren et al. evaluated HDR interstitial brachytherapy for consecutive patients with locally recurrent cervical cancer in a previously irradiated area. Although the complete response rate was 56.5%, the 4-year post-relapse survival (PRS) rate was only 27.1% and 9 of the 23 patients(39.1%) experienced grade 3-4 late toxicity. Their approach to re-irradiation was quite daring because the average clinical tumor volume was quite large 82.9 cm3 (range: 26.9–208.3 cm3). Nevertheless, despite the high risk of serious toxicity, the authors noted that local tumor control was associated with overall survival. Authors from The First Affiliated Hospital of Anhui Medical University report an exciting prospective, randomized single-institution trial using the anti-angiogenic agent, Endostar, with concurrent chemo/radiation as compared to the same concurrent chemoradiotherapy regimen without Endostar. Endostar is a recombinant human vascular endostatin pharmaceutical agent that was made by adding 9 amino acids to the original endostatin molecule (16). Although the concurrent chemotherapy used was relatively non-standard(cisplatin, paclitaxel), the experimental arm yielded significantly higher complete response rates and a lower incidence of nausea at the expense of higher incidences of neutropenia, hypertension, and infection (Shu et al.). Although short and long-term survival are not available, the follow-up of this exciting trial is eagerly anticipated.

We hope that this issue and the involved studies promote further advances and refinement to the radiotherapeutic approach to cervical cancer. Furthermore, it is hoped that further evaluation of the sequencing of radiotherapy with anti-angiogenic agents and immunotherapy can start improving the survival of cervical cancer patients for the first time in over 23 years.

Author contributions

JMV provided the majority of the written manuscript. GC reviewed and provided edits as needed for submission. Both served as research editors for the Cervical Cancer research edition. All authors contributed to the article and approved the submitted version.

Acknowledgments

The Authors would like to acknowledge the opportunity to serve as editors for the Frontiers special research edition.

Conflict of interest

The authors declare that the research was conducted in the absence of any commercial or financial relationships that could be construed as a potential conflict of interest.

Publisher's note

References

1. Bray F, Ferlay J, Soerjomataram I, Siegel RL, Torre LA, Jemal A. Global cancer statistics 2018: GLOBOCAN estimates of incidence and mortality worldwide for 36 cancers in 185 countries. *CA Cancer J Clin* (2018) 68:394. doi: 10.3322/caac.21492

2. Arbyn M, Weiderpass E, Bruni L, de Sanjosé S, Saraiya M, Ferlay J, et al. Estimates of incidence and mortality of cervical cancer in 2018: A worldwide analysis. *Lancet Glob Health* (2020) 8(2):e191–203. doi: 10.1016/S2214-109X(19)30482-6

3. Cooley JP, Maguire FB, Morris CR, Parikh-Patel A, Abrahão R, Chen HA, et al. Cervical cancer stage at diagnosis and survival among women ≥ 65 years in California. *Cancer Epidemiol Biomarkers Prev* (2023) 32:91–7. doi: 10.1158/1055-9965.EPI-22-0793

4. Morris M, Eifel PJ, Lu J, Grigsby PW, Levenback C, Stevens RE, et al. Pelvic radiation with concurrent chemotherapy compared with pelvic and para-aortic radiation for high-risk cervical cancer. *N Engl J Med* (1999) 340:1137–43. doi: 10.1056/NEJM199904153401501

5. Whitney CW, Sause W, Bundy BN, Malfetano JH, Hannigan EV, Fowler WC Jr., et al. Randomized comparison of fluorouracil plus cisplatin versus hydroxyurea as an adjunct to radiation therapy in stage IIB-IVA carcinoma of the cervix with negative para-aortic lymph nodes: A gynecologic oncology group and southwest oncology group study. *J Clin Oncol* (1999) 17:1339–48. doi: 10.1200/JCO.1999.17.5.1339

6. Rose PG, Bundy BN, Watkins EB, Thigpen T, Deppe G, Maiman MA, et al. Concurrent cisplatin-based radiotherapy and chemotherapy for locally advanced 413 cervical cancer. *N Engl J Med* (1999) 340:1144–53. doi: 10.1056/NEJM199904153401502

7. Yeung AR, Deshmukh S, Klopp AH, Gil KM, Wenzel L, Westin SN, et al. Intensity-modulated radiation therapy reduces patient-reported chronic toxicity compared with conventional pelvic radiation therapy: Updated results of a phase III trial. *J Clin Oncol* (2022) 40(27):3115–9. doi: 10.1200/JCO.21.02831

8. Chopra S, Gupta S, Kannan S, Dora T, Engineer R, Mangaj A, et al. Late toxicity after adjuvant conventional radiation versus image-guided intensity-modulated radiotherapy for cervical cancer(PARCER): A randomized controlled trial. *J Clin Oncol* (2021) 39:3682–92. doi: 10.1200/JCO.20.02530

9. Berger T, Seppenwoolde Y, Potter R, Assenholt MS, Lindegaard JC, Nout RA, et al. Importance of technique, target selection, contouring, dose prescription, and dose-planning in external beam radiation therapy for cervical cancer: Evolution of practice from EMBRACE-I to II. *Int J Radiat Oncol Biol Phys* (2019) 104:885–94. doi: 10.1016/j.ijrobp.2019.03.020

10. Mayadev J, Zamarin D, Deng W, Lankes H, Pesci G, Park K, et al. (2022). Safety and immunogenicity of anti PD-L1 (Atezolizumab) given as an immune primer or concurrently with extended field chemoradiotherapy for node positive locally advanced cervical cancer: An NRG oncology trial, in: *2022 SGO Annual Meeting on Women's Cancer*, Phoenix, Arizona, March 18-21, 2022.

11. Zhu XX, Yang XJ, Chao YL, Zheng H-M, Sheng H-F, Liu H-Y, et al. The potential effect of oral microbiota in the prediction of mucositis during radiotherapy for nasopharyngeal carcinoma. *EBioMedicine* (2017) 18:23–31. doi: 10.1016/j.ebiom.2017.02.002

12. Bhatt AP, Redinbo MR, Bultman SJ. The role of the microbiome in cancer development and therapy. *CA Cancer J Clin* (2017) 67:326–44. doi: 10.3322/caac.21398

13. Radojevic MZ, Tomasevic A, Karapandzic VP, Milosavljevic N, Jankovic S, Folic M. Acute chemoradiotherapy toxicity in cervical cancer patients. *Open Med* (2020) 15:1:822–32. doi: 10.1515/med-2020-0222

14. Sato F, Bhawal UK, Yoshimura T, Muragaki Y. DEC1 and DEC2 crosstalk between circadian rhythm and tumor progression. *J Cancer* (2016) 7:2. doi: 10.7150/jca.13748

15. Nelson N, Lombardo J, Matlack L, Smith A, Hines K, Shi W, et al. Chronoradiobiology of breast cancer: The time is now to link circadian rhythm and radiation biology. *Int J Mol Sci* (2022) 23(3):1331. doi: 10.3390/ijms23031331

16. Guan L. Endostar rebuilding vascular homeostasis and enhancing chemotherapy efficacy in cervical cancer treatment. *Onco Targets Ther* (2020) 435:1312811–27. doi: 10.2147/ott.S277644

frontiers in Oncology

ORIGINAL RESEARCH
published: 23 February 2021
doi: 10.3389/fonc.2021.615439

Influence of Pelvic Intensity-Modulated Radiation Therapy With Concurrent Cisplatin-Based Chemotherapy of Cervical Cancer on the Vaginal Microbiome

Li Jiang[†], *Bo Li*[†], *Yong Zhang*, *Shanshan Ma*, *Chang Liu*, *Feifei Liang*, *Zhuxin Wei*, *Tingting Huang*[*] *and Rensheng Wang*[*]

Department of Radiation Oncology, The First Affiliated Hospital of Guangxi Medical University, Nanning, China

OPEN ACCESS

Edited by:
Xi Yang,
Fudan University, China

Reviewed by:
Qing Guo,
Jiangsu Taizhou People's Hospital, China
Mengying Shi,
University of Massachusetts, Lowell, United States

***Correspondence:**
Rensheng Wang
13807806008@163.com
Tingting Huang
httgxmu@163.com

[†]*These authors have contributed equally to this work and share first authorship*

Specialty section:
This article was submitted to Radiation Oncology, a section of the journal Frontiers in Oncology

Received: *09 October 2020*
Accepted: *06 January 2021*
Published: *23 February 2021*

Citation:
Jiang L, Li B, Zhang Y, Ma S, Liu C, Liang F, Wei Z, Huang T and Wang R (2021) Influence of Pelvic Intensity-Modulated Radiation Therapy With Concurrent Cisplatin-Based Chemotherapy of Cervical Cancer on the Vaginal Microbiome. Front. Oncol. 11:615439. doi: 10.3389/fonc.2021.615439

Pelvic intensity-modulated radiation therapy (IMRT) combined with concurrent chemotherapy is an effective treatment for cervical cancer; however, radiation resistance impairs its clinical benefit. The vaginal microbiome plays an important but poorly understood role in cancer radiochemotherapy. In this study, we investigated the effects of treatment on the overall composition and alteration of the vaginal microbiome in patients receiving pelvic IMRT with concurrent cisplatin-based chemotherapy. We collected samples from twenty patients with cervical cancer and six healthy controls and performed 16S rRNA sequencing. Vaginal microbial composition analysis revealed significant differences between the two groups, but no significant differences between radiation treatment time points. However, the relative abundances of *Gammaproteobacteria, Gemmatimonadetes, Gemmatimonadales, Pseudomonadales, Gemmatimonadaceae, Rikenellaceae, Acinetobacter, Desulfovibrio, Prevotella 9, Rikenellaceae RC9 gut group, Turicibacter*, and the *metagenome* increased with time. The results encourage further study into the effects of the vaginal microbiome on cervical cancer treatment strategies, especially radiochemotherapy. Better understanding of these effects could inform new therapeutic approaches to enhance the efficacy of radiochemotherapy.

Keywords: vaginal microbiome, cervical cancer, intensity-modulated radiation therapy, radiochemotherapy, 16S rRNA sequencing

INTRODUCTION

Cervical cancer, the most common gynecological malignancy, occurs in the epithelial lining of the cervix (1). For patients with locally advanced cervical cancer, radiotherapy combined with chemotherapy has become the mainstream treatment, usually involving intensity-modulated radiation therapy (IMRT) (2, 3). Although IMRT provides high dose conformity and spares organs at risk, resistance to treatment is an obstacle for patients with cervical cancer (4). Therefore,

strategies to enhance the effects of radiation and chemotherapy are required to obtain better clinical outcomes.

The human microbiome is the collection of microorganisms that inhabit the mucosal surfaces of the body, including the vagina (5). In recent years, sequencing technology has made great progress in cataloguing these populations, with 16S ribosomal RNA (rRNA) sequencing most commonly used. Changes in the vaginal microbiome (VM) are associated with cervical cancer development (6–8), and evidence is rapidly mounting that it can affect cancer treatment outcomes through diverse mechanisms (9, 10). The VM can therefore be considered a novel target to improve the treatment sensitivity of cervical cancer. However, the role of the VM in patients with cervical cancer who receive pelvic IMRT combined with chemotherapy is not well understood. To assess the effects of pelvic radiochemotherapy on the VM, we compared the VM profiles of patients with cervical cancer and healthy controls, and then tracked the changes to the VM in patients with cervical cancer during pelvic IMRT combined with concurrent cisplatin-based chemotherapy by bacterial 16S rRNA gene sequencing.

METHODS

Patients and Treatment

A prospective study was conducted by enrolling 20 patients with cervical cancer who received radical radiochemotherapy at the First Affiliated Hospital of Guangxi Medical University from April 2016 to May 2017. The inclusion criteria were: 1) patients were scheduled for pelvic IMRT at a dose delivered to a planning clinical target volume (PCTV) of 50 Gy in combination with concomitant cisplatin-based chemotherapy, 2) availability for vaginal sampling using a sterile swab stick, and 3) willingness to participate. The exclusion criteria were: 1) recent treatment with antibiotics, steroids, or immune-suppressants, 2) distant metastasis, and 3) previous pelvic radiotherapy for another tumor or with palliative intent. In addition, six healthy individuals were also enrolled from April 2016 to May 2017. Their inclusion criteria were 1) no history of malignancy, 2) a Karnofsky performance status ≥ 90, and 3) willingness to undergo vaginal sampling using a sterile swab stick. Written informed consent was obtained from all subjects, and the research protocol was approved by the Ethical Review Committee of the First Affiliated Hospital of Guangxi Medical University. Information that can be used to identify individual participants during or after the data collection is available and can be accessed. We confirm that all methods were performed in accordance with relevant guidelines and regulations.

All patients underwent a contrast-enhanced CT scan in the supine position with an immobilization device. The images datasets were imported to the treatment planning system (TPS). The gross tumor volume (GTV) and clinical target volume (CTV) was determined by CT and MRI. The CTV of the tumor bed (CTV-T) included the range of 10 mm from GTV as well as the entire uterus, cervix, parametria, and at least 3 cm proximal of the vagina. The nodal CTV (CTV-N) was delineated to include bilateral iliac, obturator, and presacral lymphatic drainage region with an expansion of the blood vessels by 7 mm. The planning clinical target volume (PCTV) was generated by a uniform expansion of 10 mm from CTV-T and 7 mm from CTV-N. The PCTV was prescribed such that > 95% was received at ≥ 50 Gy in 25 fractions, five times weekly for 5 weeks. The pelvic IMRT plan was generated using seven-field beam. In addition, all patients received weekly brachytherapy at a dose of 30 to 35 Gy following the pelvic IMRT. The constraints for organs at risk (OARs) were defined according to the institutional guidelines. Concurrent cisplatin-based chemotherapy was adopted in conjunction with IMRT as part of the treatment protocol. The concurrent chemotherapy regimen comprised the administration of cisplatin alone (80–100 mg/m^2) every 3 weeks for two cycles.

Sampling and DNA Extraction

A sterile swab stick was used to obtain a specimen from the cervical lesion using aseptic technique. When possible, four sequential samples were collected based on radiation treatment time points: before starting pelvic radiotherapy (the first time point sample, T1), after the fifth radiotherapy session (the second time point sample, T2), after the 15th radiotherapy session (the third time point sample, T3), and after the 25th radiotherapy session (the fourth time point sample, T4). T1 samples were obtained 1 week before starting radiotherapy. The swab tops were placed in 2-ml sterile DNAase/RNase-free cryovials containing phosphate-buffered saline (400 µl), and stored at −80°C until further processing. A cell lysis procedure including enzymatic lysis and bead beating was used prior to DNA extraction using a QIAamp DNA Mini Kit (Qiagen, Hilden, Germany) and amplification by polymerase chain reaction (PCR).

Library Preparation and Sequencing

In total, 71 vaginal swabs with sufficiently high-quality DNA were collected. The V3-V4 hypervariable regions of the 16S rRNA gene were amplified with the primers 338F (5′-ACTCCTACGG GAGGCAGCA-3′) and 806R (5′-GGACTACHVGGGT WTCTAAT-3′) on a 2720 Thermal Cycler (Applied Biosystems, USA) (11, 12). PCR was conducted using the following program: 2 min at 98°C, then 20 cycles of 30 s at 98°C, 30 s at 50°C, and 1 min at 72°C, followed by a final incubation at 72°C for 5 min. Reactions were performed in triplicate. The reaction mix (50 µl total) consisted of 2×TransStart FastPfu Fly PCR SuperMix (25 µl), each primer (1 µl of 10 µM), nuclease-free water (20 µl), and template DNA (10 ng). The resultant PCR products were purified using VAHTS DNA Clean Beads. Secondary PCR was performed under different conditions using special index primers. The PCR program was: 30 s at 98°C, then 10 cycles of 10 s at 98°C, 30 s at 65°C, and 30 s at 72°C, then a final 5 min incubation at 72°C. PCR reactions were performed in triplicate. The reaction mix (50 µl total) consisted of Phusion DNA Polymerase (25 µl), i5/i7 index primers (1 µl of 2.5 µM), UltraPure water (13 µl), and purified PCR product (10 µl). Reactions were analyzed on 1.8% agarose gels to ensure successful amplification. Unsuccessful reactions were repeated after a 10× dilution of the initial template

concentration, and removed from the experiment if unsuccessful again. PCR products were extracted from the agarose gels, further purified using an AxyPrep DNA Gel Extraction Kit (Axygen Biosciences, USA), and eluted with Tris-HCl. ImageJ (National Institutes of Health, Bethesda, MD, USA) was used to quantify the electrophoresis results. The library was pooled at equimolar concentrations and resolved on a 1.8% agarose gel, and the 600 bp band was extracted. The purified library was paired-end sequenced (2 × 250) on an Illumina HiSeq platform (Illumina, San Diego, CA, USA) according to the manufacturer's instructions.

Bioinformatic Analysis

FLASH (1.2.11) was used to merge paired end reads with a minimum overlap of 10 bp (13). Primer and barcode sequences were trimmed using cutadapt (v1.18) (14); and chimeric sequences were detected and removed with VSEARCH (v2.13.6) (15). The trimmed data were processed to form OTUs at 97% identity using VSEARCH, and a representative OTU was selected from each cluster (15, 16). Using the Silva_132 16S rRNA database as a reference, Ribosomal Database Project classifiers were used to assign taxonomic ranks to each OTU using Qiime (v1.9.1) (16, 17). The alpha-diversity and beta-diversity indices were calculated based on the rarefied OTU counts. Alpha-diversity was performed in Mothur (v1.38.1) (18, 19), and represents an analysis of the diversity in a single sample, reflected by parameters including the Sobs, Chao1, Ace, Shannon, and Simpson indices. The Wilcoxon rank-sum test was used to compare alpha-diversity indices. Beta-diversity is a measure of the microbiota structure between groups. Both weighted and unweighted UniFrac distance matrices were plotted in the PCA, and ANOSIMs were performed using the R package "ade4" (20). For taxa with a prevalence > 10%, differential abundance analysis was performed using the Wilcoxon rank-sum test at the phylum, class, order, family, and genus levels. For multiple comparisons of bacterial counts, the false discovery rate was calculated using the Benjamini-Hochberg method (21). Microorganism features used to distinguish gut microbiotas specific to cervical cancer were identified using the linear discriminant analysis effect size method, with an alpha cutoff of 0.05 and an effect size cutoff of 2.0 (22). Phylogenetic Investigation of Communities by Reconstruction of Unobserved States was used to predict the abundances of functional categories in Kyoto Encyclopedia of Genes and Genomes (KEGG) orthologs (23). Graphing of KEGG pathways at levels 2 (41 pathways) and 3 (328 pathways) was performed with STAMP, and p values were calculated using White's non-parametric t-test (24).

Statistics

R software (ver. 3.5.1, the R Project for Statistical Computing) was used for statistical analysis. In descriptive analyses, the mean ± standard deviation (s.d.) was used for normally distributed continuous variables and the median ± interquartile range (IQR) was used for continuous variables with skewed distributions. Comparisons of the relative abundance of detected genera between groups were conducted using the Wilcoxon rank-sum test. The Sobs, ACE, Simpson, Shannon, and Chao1 indices were compared using Student's t-test. $P<0.05$ was considered statistically significant.

RESULTS

Patient Characteristics

We analyzed 71 vaginal swab samples from 20 patients with cervical cancer and six healthy controls. **Table 1** shows the clinical characteristics of the patients with cervical cancer. Their median age was 54 years (range: 44–73). All patients received pelvic IMRT plus brachytherapy combined with cisplatin-based chemotherapy. Each radiation plan met the prescribed dose requirements, and the mean dose of the planning clinical target volume (PCTV) was calculated as 54 Gy. All 20 patients provided samples at T1, and 15/20 permitted the collection of samples at all four timepoints (T1–T4).

VM Diversity Estimations in Patients With Cervical Cancer and Healthy Controls

After quality control processes and the removal of chimeric sequences, we obtained 2,983 operational taxonomic units (OTUs) in total. **Table S1** summarizes the numbers of unique sequences and OTUs in each normalized sample. Of these, 612 OTUs (20.5%) were detected in healthy controls, 2,500 (83.8%) were detected in patients with cervical cancer, and 483 OTUs (16.2%) were detected in both groups (**Figure 1A**). Abundance comparisons of individual OTUs through principal component analysis (PCA) revealed differences in the VM composition of

TABLE 1 | Clinical characteristics of the patients with cervical cancer (n = 20).

Patient characteristic	Number (%)
Age (years)	
≤ 54	10 (50.0%)
>54	10 (50.0%)
FIGO[a] classification	
I B2	1 (5.0%)
II A2	3 (15.0%)
II B	8 (40.0%)
III B	4 (20.0%)
IV A	3 (15.0%)
V B	1 (5.0%)
Histology	
Squamous cell carcinoma	19 (95.0%)
Adenocarcinoma	1 (5.0%)
HPV[b] status	
Negative	2 (10.0%)
HPV 16	9 (45.0%)
HPV 18	6 (30.0%)
HPV 52	1 (5.0%)
HPV 58	1 (5.0%)
HPV 59	1 (5.0%)
Treatment	
Pelvic IMRT[c]+BT[d]+CT[e]	20 (100.0%)
Patients with four sequential samples (T1–T4)	15 (75.0%)

[a]*International Federation of Gynecology and Obstetrics;* [b]*human papillomavirus;* [c]*intensity-modulated radiation therapy* [d]*brachytherapy;* [e]*concurrent cisplatin-based chemotherapy.*

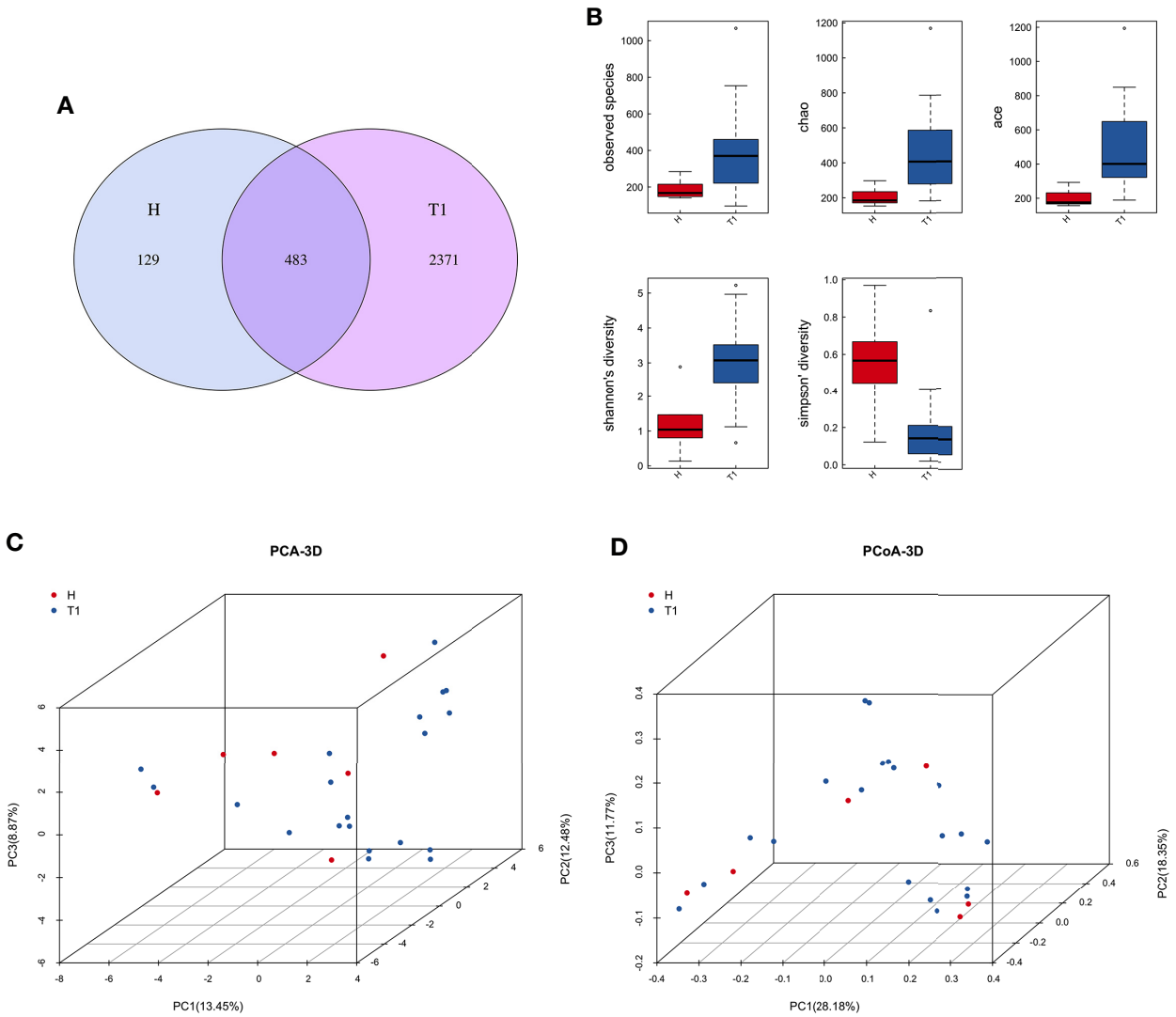

FIGURE 1 | **(A)** Venn diagram for the integration between healthy controls and cervix cancer patients OTUs. **(B)** Principal component analysis (PCA) of vaginal microbiome of 20 patients and 6 healthy controls. **(C)** The comparison between patients and healthy controls by alpha diversity analysis. **(D)** The comparison between patients and healthy controls by beta diversity analysis. H, Healthy controls; T1, the first time point sample of patients.

healthy controls and patients with cervical cancer (**Figure 1B**). Furthermore, species diversity and richness were also higher in cervical cancer samples than in control samples. The Chao, Ace, Shannon, and Simpson indices (p = 0.016, = 0.002, <0.001, <0.003, and <0.006, respectively) are shown in **Figure 1C** and **Table 2**. Beta diversity analysis revealed statistically significant differences between the two groups (p = 0.005; weighted UniFrac and analysis of similarity (ANOSIM); **Figure 1D**).

TABLE 2 | The comparison between patients with cervical cancer and healthy controls by alpha diversity analysis.

Alpha diversity	Mean (H)	s.d. (H)	Mean (T1)	s.d. (T1)	*P* value
Sobs	186.83	54.44	387.05	224.61	0.016
Chao	204.84	53.14	460.55	236.70	0.002
Ace	199.61	52.64	492.35	253.55	0.0001
Shannon	1.23	0.93	3.06	1.14	0.003
Simpson	0.56	0.28	0.19	0.19	0.006

T1, the first time point sample of patients; H, healthy controls; s.d., standard deviation.

VM Diversity Estimations in Patients With Cervical Cancer During Treatment

To explore the effects of radiation on the VM during the treatment process, we first analyzed VM richness and diversity at four time points (T1–T4). In total, 6,109 OTUs were obtained, and 1,382 were common among all timepoints. Then, the bacterial compositions at each timepoint were compared using overlap analysis (**Figure 2A**) and 3D-PCA (**Figure 2B**). Interestingly, in comparisons of T1 vs T2, T3 vs T2, T4 vs T3 and T4 vs T1, the timepoints were not spatially distinct, nor were they significantly different in VM richness and diversity according to alpha (**Figures 3A–D**) and beta diversity analyses (data not shown).

Impact of Radiation Therapy on the VM Composition of Patients With Cervical Cancer

Annotation analysis revealed the distribution of the microbiota at the phylum, class, order, family, genus, and species levels over time (**Figures 4A–F**). **Figure 5** shows changes in the relative abundances of major phylum-level taxa during radiation therapy. The relative abundances of Gammaproteobacteria, Gemmatimonadetes, Gemmatimonadales, Pseudomonadales, Gemmatimonadaceae, Rikenellaceae, Acinetobacter, *Desulfovibrio*, *Prevotella* 9, the Rikenellaceae RC9 gut group, *Turicibacter*, and the metagenome increased with radiation time.

DISCUSSION

Cervical cancer often results from persistent infection with human papillomavirus (HPV), which induces cervical epithelial cells to become cancerous (25). However, the process of cervical carcinogenesis can be affected by the VM (8), and increasing evidence indicates that VM changes play important roles in the process (26, 27). Conversely, cervical cancer disrupts the ratio between commensal and pathogenic microbiome species, resulting in microenvironmental changes (28). However, studies investigating the role of the VM in patients with cervical cancer who receive pelvic radiochemotherapy are scarce. The aim of our study was to examine associations between the use of pelvic radiochemotherapy and VM changes.

Currently, radiochemotherapy is a common treatment strategy for cervical cancer. The National Comprehensive Cancer Network guidelines (V1.2020) for cervical cancer recommend a dose of 45–50 Gy in standard fractionation with IMRT (29). In this study, all patients were prescribed a PCTV of 50 Gy. However, due to limitations in the radiation technique, the dose distribution in the target area is not absolutely uniform. To ensure quality radiation therapy, the patient received at least 50 Gy in 25 fractions, meaning that > 50 Gy was present in the PCTV. Dose data were recorded using a Varian Eclipse V8.0 treatment planning system. IMRT protects organs at risk better than two-dimensional radiation techniques; therefore, our results are based on pelvic IMRT combined with cisplatin-based concurrent chemotherapy.

In our study, there were more OTUs in patients with cervical cancer than in healthy controls, and the abundances of individual OTUs were significantly different between the two groups. When compared at different radiation treatment time points, there are no significant differences found in VM richness and diversity by alpha and beta diversity analysis. Nevertheless, changes in the relative abundances of several taxa were observed

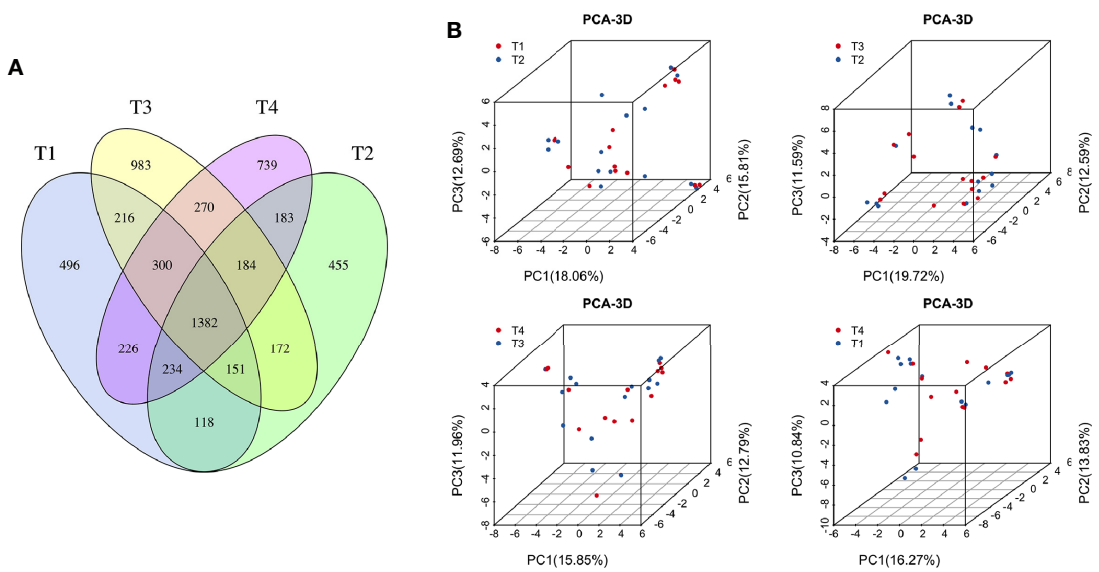

FIGURE 2 | **(A)** Venn diagram for the integration among the four time points of patient samples. **(B)** 3D scatter plot of PCA results for comparison among four time points of patient samples (T1 vs T2, T3 vs T2, T4 vs T3, and T4 vs T1). T1, the first time point sample; T2, the second time point sample; T3, the third time point sample; T4, the fourth time point sample.

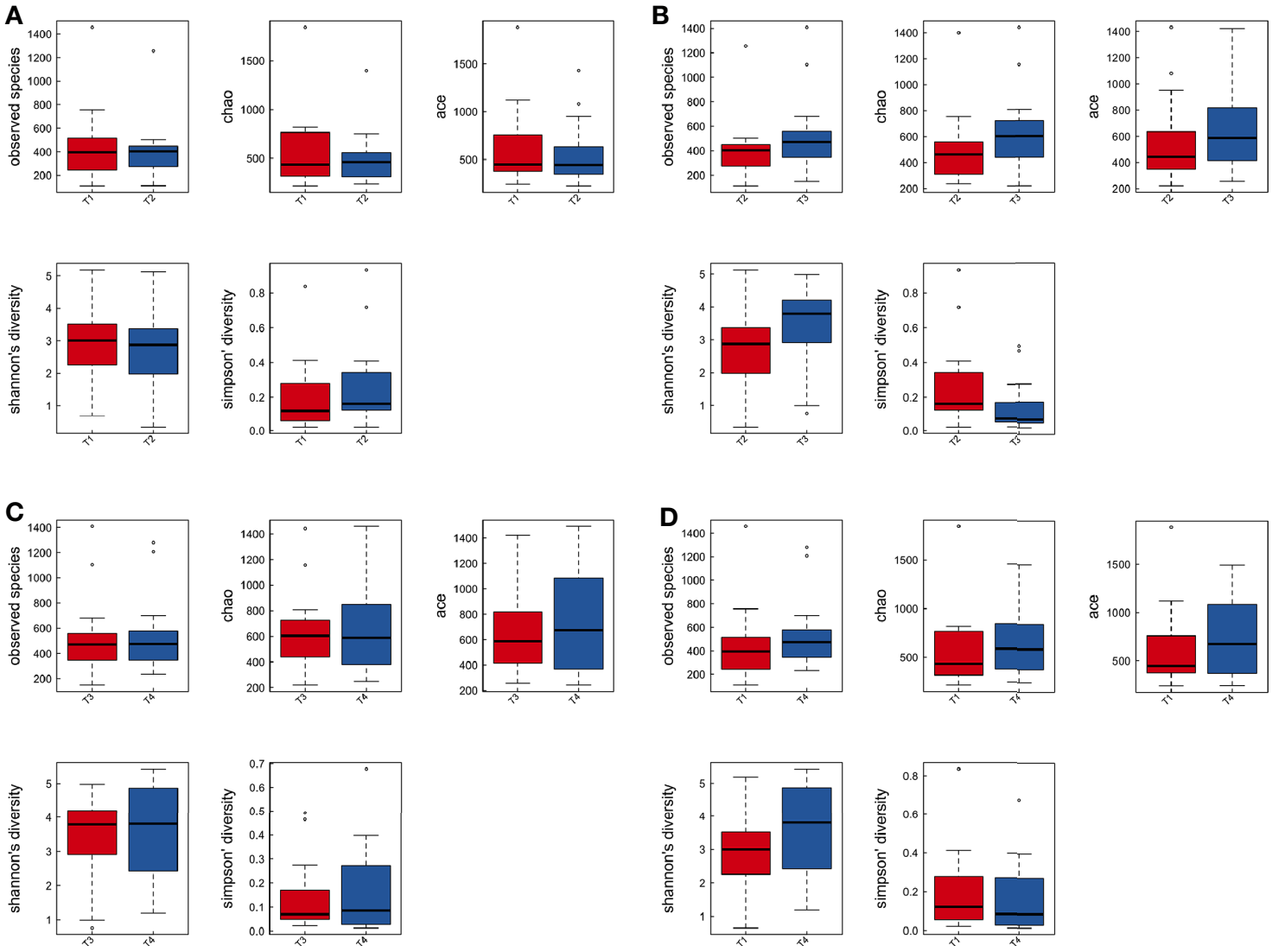

FIGURE 3 | The comparison among the four time points of patient samples by alpha diversity analysis. Boxplots of alpha diversity in T1 vs T2 **(A)**, T3 vs T2 **(B)**, T4 vs T3 **(C)**, and T4 vs T1 **(D)** using different metrics (observed OTUs, the Shannon index, and the Simpson index). T1, the first time point sample; T2, the second time point sample; T3, the third time point sample; T4, the fourth time point sample.

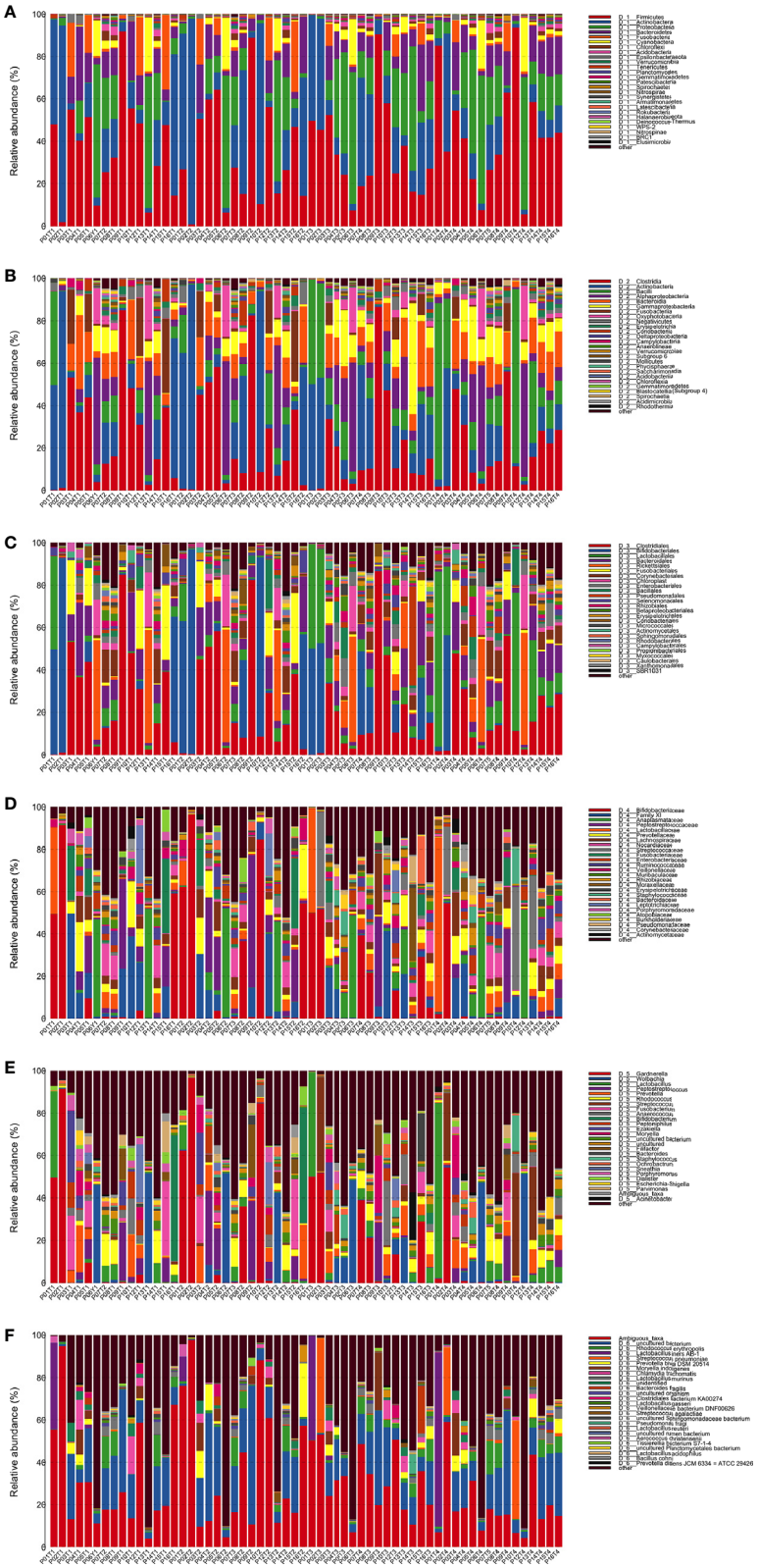

FIGURE 4 | Distribution of bacterial phyla **(A)**, classes **(B)**, orders **(C)**, families **(D)**, genera **(E)**, and species **(F)** obtained by next-generation sequencing of samples from 15 patients at four time points.

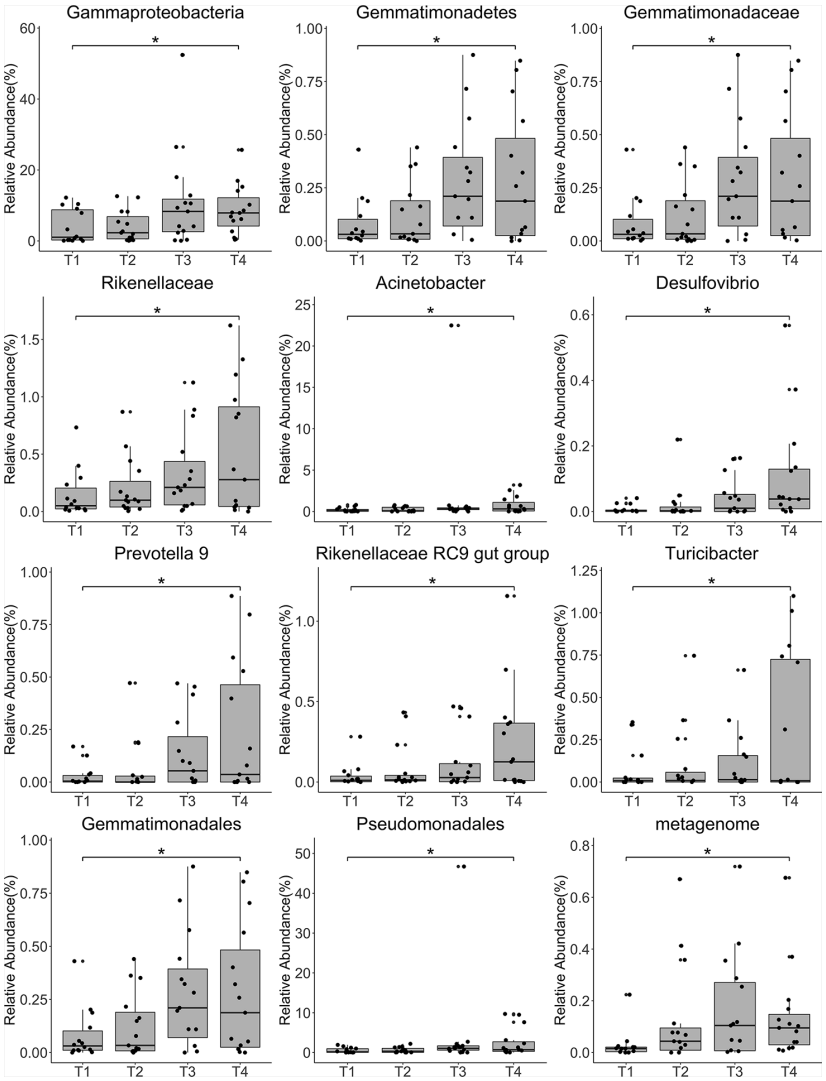

FIGURE 5 | Relative abundances of the top 12 most abundant genera at each time point. Each bar represents the mean abundance ± the standard error of the mean. *P<0.05.

during radiation therapy. The dose distribution of radiation is closely associated to the volume and the location of tumor, which might affect distribution of vaginal microbiome during the radiation treatment. The research endpoint may be insufficient to prove the vaginal microbiome as a key clinical index for cervical cancer patients, so a larger cohort is needed to determine the correlation between VM and cervical cancer patients in future study.

It is well established that VM imbalance is strongly correlated with cervical cancer. Vaginal dysbiosis (characterized by a non-*Lactobacillus*-dominant composition) and inflammation have been associated with HPV persistence and progression to cervical cancer (30). Compared to patients diagnosed with low – and high-grade squamous intraepithelial lesions, increased levels of *Lactobacillus crispatus*, *Lactobacillus iners*, and *Lactobacillus taiwanensis* were observed in the vaginal swabs of healthy women, while *Gardnerella vaginalis* and *Lactobacillus acidophilus* were absent. The bacterial dysbiosis observed in these patients, which featured a predominance of *G. vaginalis* and a concomitant paucity of *L. crispatus*, *L. iners*, and *L. taiwanensis*, may be associated with the development of HPV-dependent cervical cancer (31). However, whether pelvic IMRT affects the vaginal microbiome remains unknown.

A previous study compared differences in the proportions of bacteria isolated before and after radiotherapy using aerobic culture. The results showed no significant changes in the positive cultures of pathogens; however, the normal flora significantly increased after external beam irradiation (32). However, methods based on next-generation sequencing (NGS) were not used in this study. Using 16S rRNA sequencing, we observed no significant changes in overall diversity before, during, and after radiotherapy, consistent with the above study. However, the relative abundances of several taxa, including *Gammaproteobacteria,*

Pseudomonadales, Gemmatimonadaceae, and *Prevotell*a 9, increased significantly with irradiation time.

The tumor microenvironment can have great impact on radioresistance and tumor recurrence (33). The microbiome can also affect cancer by triggering DNA damage, modulating inflammation, and generating metabolites (10). Several previous studies have shown that patients receiving radiotherapy display obvious changes in the microbiomes of the irradiated areas as well as changes in the microenvironment, indicating that the microbiome may serve as an aberrant proinflammatory factor. A study by Wang *et al.* showed that *Gammaproteobacteria, Pseudomonadales*, and *Prevotella 9*, which showed increased abundance with radiation time in this study, were more abundant in the fecal microbiome after pelvic radiation, and were strongly associated with diagnoses of radiation enteritis. *In vitro* experiments indicated that radiation-induced microbiome dysbiosis results in epithelial cell damage, promoting inflammatory responses in the local mucosa by activating nuclear factor κB (NFκB) signaling and cytokine secretion (34). Radiation can reduce resistance to commonly used antibiotics, and vancomycin pretreatment can enhance the antitumor effects of radiation *in vivo* by increasing antigen presentation and cytotoxic T cell infiltration into the tumor, through modulation of the gut microbiota (32, 35). It has been suggested that microbiome superantigens might promote radiotherapy-induced inflammation by activating T cells and attenuating epithelial cell recovery (36). Increasing evidence indicates that inflammatory signaling pathways such as the toll-like receptor/myeloid differentiation primary response 88, proinflammatory cytokine, NFκB, and cyclooxygenase-2 pathways are bridging factors between the microbiome and cancer (37). The detection of *Gemmatimonadaceae* DNA in the blood has been associated with tumor progression in patients treated with nivolumab (38). While some studies have found no benefit to probiotic use (39), a meta-analysis demonstrated a beneficial effect of probiotics in reducing the incidence of diarrhea (40). Furthermore, one study reported that the anaerobic bacteria *Clostridium novyi*-NT, which is missing its major toxin gene, is able to selectively destroy the hypoxic regions of tumors and improve the efficacy of radiation in mouse tumor models (41).

In conclusion, we conducted a bioinformatic analysis of the VM in patients with cervical cancer receiving pelvic radiochemotherapy and healthy controls by 16S rRNA sequencing. We firstly examined microbiome differences between the cervical cancer patients and health controls, and then investigated the impact of pelvic radiochemotherapy on the VM in patients with cervical cancer. Our data indicated some changes in the relative abundances of the microbiome, which might have critical effects on the efficacy of radiochemotherapy. Future studies will be required to understand the relationship between the VM and radiochemotherapy in cervical cancer.

DATA AVAILABILITY STATEMENT

The data sets presented in this study can be found in online repositories. The names of the repository/repositories and accession number(s) can be found below: 16S rRNA squencing data to SRA (https://www.ncbi.nlm.nih.gov/sra/). The SRA ID is PRJNA687644.

ETHICS STATEMENT

The studies involving human participants were reviewed and approved by The Ethical Review Committee of the First Affiliated Hospital of Guangxi Medical University. The patients/participants provided their written informed consent to participate in this study.

AUTHOR CONTRIBUTIONS

RW and TH designed the study. YZ and SM collected samples and followed up the patients. BL, FL, and CL performed the experiments. LJ and ZW performed the data analyses. LJ wrote the main manuscript text and BL prepared all figures and tables. RW and TH critically inspected the manuscript and participated in its revision. LJ and BL contributed equally to this study and are the co-first authors of this paper. All authors contributed to the article and approved the submitted version.

FUNDING

This study was supported by the Youth Science Foundation of Guangxi Medical University (GXMUYSF201505), the Basic Ability Enhancement Project for Young Teachers in Guangxi Zhuang Autonomous Region (2018KY0134), the Guangxi Zhuang Autonomous Region Health and Wellness Committee Science and Technology Project (S2017017), the Key Research and Development Program of Guangxi (Guike AB18281003), the "139" Program for high-level medical talents in Guangxi, Innovation Team of the First Affiliated Hospital of Guangxi Medical University, and the Guangxi Science and Technology Program Project (GK AD17129013). The funders had no role in study design, data collection and analysis, decision to publish, or preparation of the manuscript.

ACKNOWLEDGMENTS

We thank Mr. Jindong Zhu and Mr. Lucheng Zhang (Anrenxin Biotechnology Co., Ltd at Nanning, China) for their helpful discussions and bioinformatics analysis.

SUPPLEMENTARY MATERIAL

The Supplementary Material for this article can be found online at: https://www.frontiersin.org/articles/10.3389/fonc.2021.615439/full#supplementary-material

Supplementary Table 1 | The OTUs of cervical cancer patients and healthy controls. CV, cervical cancer patients; HC, healthy controls.

REFERENCES

1. Bray F, Ferlay J, Soerjomataram I, Siegel RL, Torre LA, Jemal A. Global cancer statistics 2018: GLOBOCAN estimates of incidence and mortality worldwide for 36 cancers in 185 countries. *CA Cancer J Clin* (2018) 68:394–424. doi: 10.3322/caac.21492
2. Vordermark D. Radiotherapy of Cervical Cancer. *Oncol Res Treat* (2016) 39:516–20. doi: 10.1159/000448902
3. Berger T, Seppenwoolde Y, Potter R, Assenholt MS, Lindegaard JC, Nout RA, et al. Importance of Technique, Target Selection, Contouring, Dose Prescription, and Dose-Planning in External Beam Radiation Therapy for Cervical Cancer: Evolution of Practice From EMBRACE-I to II. *Int J Radiat Oncol Biol Phys* (2019) 104:885–94. doi: 10.1016/j.ijrobp.2019.03.020
4. Kitahara O, Katagiri T, Tsunoda T, Harima Y, Nakamura Y. Classification of sensitivity or resistance of cervical cancers to ionizing radiation according to expression profiles of 62 genes selected by cDNA microarray analysis. *Neoplasia* (2002) 4:295–303. doi: 10.1038/sj.neo.7900251
5. Babu G, Singaravelu BG, Srikumar R, Reddy SV, Kokan A. Comparative Study on the Vaginal Flora and Incidence of Asymptomatic Vaginosis among Healthy Women and in Women with Infertility Problems of Reproductive Age. *J Clin Diagn Res* (2017) 11:Dc18–dc22. doi: 10.7860/JCDR/2017/28296.10417
6. Njoku K, Crosbie EJ. Does the vaginal microbiome drive cervical carcinogenesis? *BJOG* (2020) 127(2):181.
7. Champer M, Wong AM, Champer J, Brito IL, Messer PW, Hou JY, et al. The role of the vaginal microbiome in gynaecological cancer. *BJOG* (2018) 125:309–15. doi: 10.1111/1471-0528.14631
8. Kyrgiou M, Mitra A, Moscicki AB. Does the vaginal microbiota play a role in the development of cervical cancer? *Transl Res* (2017) 179:168–82. doi: 10.1016/j.trsl.2016.07.004
9. Zhu XX, Yang XJ, Chao YL, Zheng HM, Sheng HF, Liu HY, et al. The Potential Effect of Oral Microbiota in the Prediction of Mucositis During Radiotherapy for Nasopharyngeal Carcinoma. *EBioMedicine* (2017) 18:23–31. doi: 10.1016/j.ebiom.2017.02.002
10. Bhatt AP, Redinbo MR, Bultman SJ. The role of the microbiome in cancer development and therapy. *CA Cancer J Clin* (2017) 67:326–44. doi: 10.3322/caac.21398
11. Zakrzewski M, Goesmann A, Jaenicke S, Junemann S, Eikmeyer F, Szczepanowski R, et al. Profiling of the metabolically active community from a production-scale biogas plant by means of high-throughput metatranscriptome sequencing. *J Biotechnol* (2012) 158:248–58. doi: 10.1016/j.jbiotec.2012.01.020
12. Klindworth A, Pruesse E, Schweer T, Peplies J, Quast C, Horn M, et al. Evaluation of general 16S ribosomal RNA gene PCR primers for classical and next-generation sequencing-based diversity studies. *Nucleic Acids Res* (2013) 41:e1. doi: 10.1093/nar/gks808
13. Magoc T, Salzberg SL. FLASH: fast length adjustment of short reads to improve genome assemblies. *Bioinformatics* (2011) 27:2957–63. doi: 10.1093/bioinformatics/btr507
14. Park CH, Yeo HJ, Park YE, Baek SA, Kim JK, Park SU. Transcriptome Analysis and Metabolic Profiling of Lycoris Radiata. *Biol (Basel)* (2019) 8 (3):63. doi: 10.3390/biology8030063
15. Rognes T, Flouri T, Nichols B, Quince C, Mahe F. VSEARCH: a versatile open source tool for metagenomics. *PeerJ* (2016) 4:e2584. doi: 10.7717/peerj.2584
16. Quast C, Pruesse E, Yilmaz P, Gerken J, Schweer T, Yarza P, et al. The SILVA ribosomal RNA gene database project: improved data processing and web-based tools. *Nucleic Acids Res* (2013) 41:D590–6. doi: 10.1093/nar/gks1219
17. Caporaso JG, Kuczynski J, Stombaugh J, Bittinger K, Bushman FD, Costello EK, et al. QIIME allows analysis of high-throughput community sequencing data. *Nat Methods* (2010) 7:335–6. doi: 10.1038/nmeth.f.303
18. Schloss PD, Gevers D, Westcott SL. Reducing the effects of PCR amplification and sequencing artifacts on 16S rRNA-based studies. *PLoS One* (2011) 6: e27310. doi: 10.1371/journal.pone.0027310
19. Paul D, Kumbhare SV, Mhatre SS, Chowdhury SP, Shetty SA, Marathe NP, et al. Exploration of Microbial Diversity and Community Structure of Lonar Lake: The Only Hypersaline Meteorite Crater Lake within Basalt Rock. *Front Microbiol* (2015) 6:1553. doi: 10.3389/fmicb.2015.01553
20. Sun CH, Liu HY, Liu B, Yuan BD, Lu CH. Analysis of the Gut Microbiome of Wild and Captive Pere David's Deer. *Front Microbiol* (2019) 10:2331. doi: 10.3389/fmicb.2019.02331
21. Keich U, Noble WS. Controlling the FDR in imperfect matches to an incomplete database. *J Am Stat Assoc* (2018) 113:973–82. doi: 10.1080/01621459.2017.1375931
22. Segata N, Izard J, Waldron L, Gevers D, Miropolsky L, Garrett WS, et al. Metagenomic biomarker discovery and explanation. *Genome Biol* (2011) 12: R60. doi: 10.1186/gb-2011-12-6-r60
23. Langille MG, Zaneveld J, Caporaso JG, McDonald D, Knights D, Reyes JA, et al. Predictive functional profiling of microbial communities using 16S rRNA marker gene sequences. *Nat Biotechnol* (2013) 31:814–21. doi: 10.1038/nbt.2676
24. Abel S, Abel zur Wiesch P, Chang HH, Davis BM, Lipsitch M, Waldor MK. Sequence tag-based analysis of microbial population dynamics. *Nat Methods* (2015) 12:223–6. 3 p following 226. doi: 10.1038/nmeth.3253
25. Cohen PA, Jhingran A, Oaknin A, Denny L. Cervical cancer. *Lancet* (2019) 393:169–82. doi: 10.1016/S0140-6736(18)32470-X
26. Mitra A, MacIntyre DA, Lee YS, Smith A, Marchesi JR, Lehne B, et al. Cervical intraepithelial neoplasia disease progression is associated with increased vaginal microbiome diversity. *Sci Rep* (2015) 5:16865. doi: 10.1038/srep16865
27. Zhang C, Liu Y, Gao W, Pan Y, Gao Y, Shen J, et al. The direct and indirect association of cervical microbiota with the risk of cervical intraepithelial neoplasia. *Cancer Med* (2018) 7:2172–9. doi: 10.1002/cam4.1471
28. Mitra A, MacIntyre DA, Marchesi JR, Lee YS, Bennett PR, Kyrgiou M. The vaginal microbiota, human papillomavirus infection and cervical intraepithelial neoplasia: what do we know and where are we going next? *Microbiome* (2016) 4:58. doi: 10.1186/s40168-016-0203-0
29. Howe HL, Wu X, Ries LA, Cokkinides V, Ahmed F, Jemal A, et al. Annual report to the nation on the status of cancer, 1975-2003, featuring cancer among U.S. *Hispanic/Latino Popul Cancer* (2006) 107:1711–42. doi: 10.1002/cncr.22193
30. Laniewski P, Cui H, Roe DJ, Barnes D, Goulder A, Monk BJ, et al. Features of the cervicovaginal microenvironment drive cancer biomarker signatures in patients across cervical carcinogenesis. *Sci Rep* (2019) 9:7333. doi: 10.1038/s41598-019-43849-5
31. Kwasniewski W, Wolun-Cholewa M, Kotarski J, Warchol W, Kuzma D, Kwasniewska A, et al. Microbiota dysbiosis is associated with HPV-induced cervical carcinogenesis. *Oncol Lett* (2018) 16:7035–47. doi: 10.3892/ol.2018.9509
32. Mubangizi L, Namusoke F, Mutyaba T. Aerobic cervical bacteriology and antibiotic sensitivity patterns in patients with advanced cervical cancer before and after radiotherapy at a national referral hospital in Uganda. *Int J Gynaecol Obstet* (2014) 126:37–40. doi: 10.1016/j.ijgo.2014.01.013
33. Barker HE, Paget JT, Khan AA, Harrington KJ. The tumour microenvironment after radiotherapy: mechanisms of resistance and recurrence. *Nat Rev Cancer* (2015) 15:409–25. doi: 10.1038/nrc3958
34. Wang Z, Wang Q, Wang X, Zhu L, Chen J, Zhang B, et al. Gut microbial dysbiosis is associated with development and progression of radiation enteritis during pelvic radiotherapy. *J Cell Mol Med* (2019) 23:3747–56. doi: 10.1111/jcmm.14289
35. Uribe-Herranz M, Rafail S, Beghi S, Gil-de-Gomez L, Verginadis I, Bittinger K, et al. Gut microbiota modulate dendritic cell antigen presentation and radiotherapy-induced antitumor immune response. *J Clin Invest* (2020) 130:466–79. doi: 10.1172/JCI124332
36. Hill A, Hanson M, Bogle MA, Duvic M. Severe radiation dermatitis is related to Staphylococcus aureus. *Am J Clin Oncol* (2004) 27:361–3. doi: 10.1097/01.COC.0000071418.12121.C2
37. Kipanyula MJ, Seke Etet PF, Vecchio L, Farahna M, Nukenine EN, Nwabo Kamdje AH. Signaling pathways bridging microbial-triggered inflammation and cancer. *Cell Signal* (2013) 25:403–16. doi: 10.1016/j.cellsig.2012.10.014
38. Ouaknine Krief J, Helly de Tauriers P, Dumenil C, Neveux N, Dumoulin J, Giraud V, et al. Role of antibiotic use, plasma citrulline and blood microbiome

in advanced non-small cell lung cancer patients treated with nivolumab. *J Immunother Cancer* (2019) 7:176. doi: 10.1186/s40425-019-0658-1
39. Blanarova C, Galovicova A, Petrasova D. Use of probiotics for prevention of radiation-induced diarrhea. *Bratisl Lek Listy* (2009) 110:98–104.
40. Liu MM, Li ST, Shu Y, Zhan HQ. Probiotics for prevention of radiation-induced diarrhea: A meta-analysis of randomized controlled trials. *PLoS One* (2017) 12:e0178870. doi: 10.1371/journal.pone.0178870
41. Bettegowda C, Dang LH, Abrams R, Huso DL, Dillehay L, Cheong I, et al. Overcoming the hypoxic barrier to radiation therapy with anaerobic bacteria. *Proc Natl Acad Sci U S A* (2003) 100:15083–8. doi: 10.1073/pnas.2036598100

Conflict of Interest: The authors declare that the research was conducted in the absence of any commercial or financial relationships that could be construed as a potential conflict of interest.

frontiers in Oncology

ORIGINAL RESEARCH
published: 15 July 2021
doi: 10.3389/fonc.2021.619384

Support Vector Machine Model Predicts Dose for Organs at Risk in High-Dose Rate Brachytherapy of Cervical Cancer

Ping Zhou[1†], Xiaojie Li[2†], Hao Zhou[3], Xiao Fu[3], Bo Liu[3], Yu Zhang[3], Sheng Lin[2] and Haowen Pang[2*]*

[1] Department of Radiology, The Affiliated Hospital of Southwest Medical University, Luzhou, China, [2] Department of Oncology, The Affiliated Hospital of Southwest Medical University, Luzhou, China, [3] Department of Nursing College, Southwest Medical University, Luzhou, China

OPEN ACCESS

Edited by:
Gene A. Cardarelli, Warren Alpert Medical School of Brown University, United States

Reviewed by:
Aaron Howard Wolfson, University of Miami, United States
Mark Rivard, Brown University, United States

****Correspondence:***
Sheng Lin
lslinsheng@163.com
Haowen Pang
haowenpang@foxmail.com

[†]These authors have contributed equally to this work

Specialty section:
This article was submitted to Radiation Oncology, a section of the journal Frontiers in Oncology

Received: *20 October 2020*
Accepted: *25 June 2021*
Published: *15 July 2021*

Citation:
Zhou P, Li X, Zhou H, Fu X, Liu B, Zhang Y, Lin S and Pang H (2021) Support Vector Machine Model Predicts Dose for Organs at Risk in High-Dose Rate Brachytherapy of Cervical Cancer. Front. Oncol. 11:619384. doi: 10.3389/fonc.2021.619384

Introduction: This study aimed to establish a support vector machine (SVM) model to predict the dose for organs at risk (OARs) in intracavitary brachytherapy planning for cervical cancer with tandem and ovoid treatments.

Methods: Fifty patients with loco-regionally advanced cervical cancer treated with 200 CT-based tandem and ovoid brachytherapy plans were included. The brachytherapy plans were randomly divided into the training (N = 160) and verification groups (N = 40). The bladder, rectum, sigmoid colon, and small intestine were divided into sub-OARs. The SVM model was established using MATLAB software based on the sub-OAR volume to predict the bladder, rectum, sigmoid colon, and small intestine D_{2cm^3}. Model performance was quantified by mean squared error (MSE) and δ ($\delta = |D_{2cm^3}/D_{prescription}(actual) - D_{2cm^3}/D_{prescription}(predicted)|$). The goodness of fit of the model was quantified by the coefficient of determination (R^2). The accuracy and validity of the SVM model were verified using the validation group.

Results: The D_{2cm^3} value of the bladder, rectum, sigmoid colon, and small intestine correlated with the volume of the corresponding sub-OARs in the training group. The mean squared error (MSE) in the SVM model training group was <0.05; the R^2 of each OAR was >0.9. There was no significant difference between the D_{2cm^3} -predicted and actual values in the validation group (all $P > 0.05$): bladder $\delta = 0.024 \pm 0.022$, rectum $\delta = 0.026 \pm 0.014$, sigmoid colon $\delta = 0.035 \pm 0.023$, and small intestine $\delta = 0.032 \pm 0.025$.

Conclusion: The SVM model established in this study can effectively predict the D_{2cm^3} for the bladder, rectum, sigmoid colon, and small intestine in cervical cancer brachytherapy.

Keywords: brachytherapy, cervical cancer, organs at risk, support vector machine, dose prediction

INTRODUCTION

Cervical cancer is the most common malignancy among women in developing countries (1). Depending on the stage of diagnosis, the treatment strategies for cervical cancer mainly include surgery, along with radiotherapy and chemotherapy (2). For patients with locally advanced cervical cancer, brachytherapy combined with external-beam radiotherapy is the prevalent standard treatment (3). Three-dimensional brachytherapy is widely applied in clinical practice, and computed tomography (CT)- or magnetic resonance imaging (MRI)-based treatment planning systems (TPS) provide accurate tumor and organs at risk (OARs) dose information. However, the experience of brachytherapy planners and knowledge of the Radiation Therapy Oncology Group guidelines, as well as clinical expertise and intuition, have a significant effect on the quality of a brachytherapy plan (4). If a planner can predict the OAR dose before designing a brachytherapy plan, the quality of the brachytherapy plan can be controlled, and the interfering factors can be minimized. Previous reports on cervical cancer brachytherapy have described the effects of the volume of the OARs on the dose to the bladder, rectum, sigmoid colon, and small intestine (5). Although there is a correlation between the dose to the OARs and their volumes, information to predict the dose to the OARs is limited. In recent years, methods for predicting the dose to the OARs have been widely introduced in external irradiation intensity-modulated radiotherapy (6–10). These approaches typically use libraries of existing patient plans to create models that predict the extent of OAR sparing that can be achieved in a new patient based on, for example, the planning target volume (PTV)-OAR distance and overlap (11). In this study, we examined factors relevant for the dose to the bladder, rectum, sigmoid colon, and small intestine in cervical cancer brachytherapy based on the Fletcher applicator. The bladder, rectum, sigmoid colon, and small intestine were divided into sub-OARs. We analyzed the correlation between the sub-organ volume and D_{2cm^3} of each OAR, and the SVM prediction model based on the correlation was established to predict the dose of each OAR before brachytherapy; the model can be used as an evaluation standard for brachytherapy plans to minimize the effects of confounding factors on the quality of the plans. To our knowledge, this study is the first to apply the SVM model to OAR dosimetric prediction based only on the contours of the organs and targets. This approach has been granted a Chinese invention patent (patent no.: 201610529290.8).

MATERIALS AND METHODS

Patients

We retrospectively selected 50 patients with loco-regionally advanced cervical cancer treated with 200 CT-based tandem and ovoid brachytherapy plans between 2016 and 2018 in the Affiliated Hospital of Southwest Medical University. The patients treated with brachytherapy were randomly divided into the training (N = 160) and verification groups (N = 40). The cervical cancer stages ranged from IIB to IVA, according to the International Federation of Gynecology and Obstetrics system.

Targets and Delineation of the OARs

The high-risk clinical target volume (HR-CTV) contours were generated for each treatment based on the Gynaecological European Society for Radiotherapy and Oncology Working Group I (Gyn GEC-ESTRO WG I) recommendations (12). The HR-CTV covered the entire cervix and macroscopic extent of the disease, based on clinical examinations and as depicted in CT images. The OARs included the bladder, rectum, sigmoid colon, and small intestine. The same radiation oncologist performed the target and delineation of the OARs.

Prescription Dose and Limiting Requirements for the OARs

After receiving 45 Gy intensity-modulated radiation therapy (IMRT), the per fraction prescription dose ($D_{prescription}$) for the HR-CTV was defined as 7 Gy with a total of four fractions for brachytherapy. A prescription dose delivered to 90% of the HR-CTV was considered. Combined with the IMRT dose, the total EQD2 (equivalent dose in 2 Gy, $\alpha/\beta = 10$) for HR-CTV and IR-CTV was 85 and 60 Gy, respectively. We applied dose constraints for the OARs according to the following principles: combined IMRT dose, D_{2cm^3} of EQD2 of ≤90 Gy ($\alpha/\beta = 3$) for bladder, ≤75 Gy ($\alpha/\beta = 3$) for rectum, ≤75 Gy ($\alpha/\beta = 3$) for sigmoid colon, and ≤75 Gy ($\alpha/\beta = 3$) for small intestine. These dose constraints were primarily based on the Gynaecological European Society for Radiotherapy and Oncology Working Group II (Gyn GEC-ESTRO WG II) recommendations (13). The ^{192}Ir-source was delivered using the Fletcher applicator. To avoid bladder and rectum volume variations, the bladder of all patients was emptied and subsequently filled with 50 ml of saline solution; they accepted an enema to empty the rectum before brachytherapy.

Brachytherapy Plans

The Oncentra 4.3 treatment planning system (Elekta Brachytherapy, Veenendaal, the Netherlands) was used for the brachytherapy plans. All brachytherapy plans in this study were developed using a manual and/or graphical optimization approach to repeatedly optimize the plan and thus ensure that the dose administered to 90% of the HR-CTV reached the prescribed dose ($D_{prescription}$), whereas the dose to the OARs was lower. For the optimization of the single brachytherapy plan, the prescription dose (7 and 4.2 Gy) was administered to 90% of HR-CTV and IR-CTV; D_{2cm^3} of the bladder < 5.2 Gy, D_{2cm^3} of the rectum, sigmoid colon, and small intestine < 4.7 Gy.

Deriving Sub-OARs From the OARs

The HR-CTV was externally expanded to a plurality of rings (ring1–ringn) with a width of 0.5 cm using the Oncentra 4.3 treatment planning system. Ring1–ringn and different OAR intersection regions (ring1–ringn∩OAR) were used as independent sub-OARs, with ring1∩OAR defined as the sub-OAR1, and so on; ringn∩OAR was defined as sub-OARn. The total sub-OARs are controlled within 10 and the statistics of the

volume of each sub-OARs. The intersecting regions for ring1–ring9 and the bladder in patient 15 are shown in **Figure 1**.

SVM Model Development

In machine learning, support vector machine (SVM) are supervised learning models with the associated learning algorithms used to analyze data for classification and regression analysis. In our study, we applied a radial basis function kernel for binary classification. We used MATLAB (R2017a, MathWorks, Inc., Natick, MA, USA) software to read, prepare, process, and output the predicted value. The SVM models were trained, validated, and tested for prediction accuracy using a self-written algorithm in MATLAB. A common radial basis function kernel was used:

$$K(x_i, x_j) = e^{\left(-\gamma||x_i - x_j||\right)^2}$$

where x_i and x_j are two data points, and γ is the shape parameter that represents the equivalent to the standard deviation in Gaussian distribution. To deal with the problem of regularization for noisy data, a user-specified cost parameter C is introduced, which acts to soften the margin. The cost parameter C controls the trade-off between allowing transgression of data points across the margin edges toward the other class and a more complex boundary, which might lead to overfitting. The evaluation and choice of C and γ were conducted using a grid search. The optimal parameters were estimated using the training and validation sets. We analyze the correlation between the sub-organ volume and D_{2cm^3} of each OAR and establish the SVM prediction model based on the correlation. The volumes of the sub-OARs were used as the independent variable in the SVM model, and the $D_{2cm^3}/D_{prescription}$ ratios were used as the dependent variable.

For the verification group, the performance of the SVM model was investigated to predict $D_{2cm^3}/D_{prescription}$ per fraction in the bladder, rectum, sigmoid, and small intestine using the volumes of the corresponding sub-OARs. The volumes of the sub-OARs were used as the input values for the SVM model, and the $D_{2cm^3}/D_{prescription}$ ratios were used as the output values. The performance of the model can be characterized by mean squared error (MSE) and δ ($\delta = |D_{2cm^3}/D_{prescription}(\text{actual}) - D_{2cm^3}/D_{prescription}(\text{predicted})|$). The goodness of fit of the model was quantified by the coefficient of determination (R^2 = 1 – the ratio of the sum of squares regressed to the total sum of squares). R^2 indicates the proportionate amount of variation in the response variable explained by the independent variables in the model. They measure the fitting performance of a model from different perspectives. The closer the δ is to 0, the closer the actual and prescription values are to each other. Furthermore, the closer the R^2 is to 1, the higher the fitting degree.

Statistical Analysis

Significant differences were determined using a two-sided paired *t*-test with SPSS 19.0 software (SPSS, Inc., Chicago, IL, USA). Correlations were tested by performing the Pearson correlation coefficient analysis. $P < 0.05$ indicates that there is a correlation between the two variables, and $P < 0.01$ indicates that there is a significant correlation between the two variables.

RESULTS

The volume of each sub-OAR ($V_{sub\text{-}OAR}$) was correlated with the $D_{2cm^3}/D_{prescription}$ of the respective OAR. The volume of the HR-CTV ($V_{HR\text{-}CTV}$) was correlated with the $D_{2cm^3}/D_{prescription}$ of the

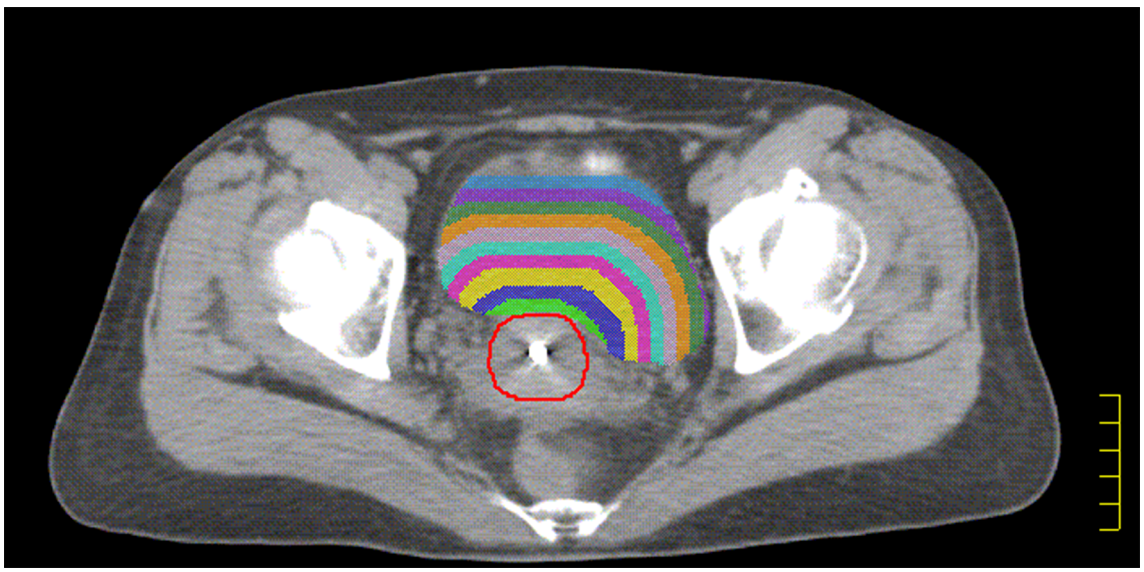

FIGURE 1 | The red line indicated HR-CTV, The green shadow indicated the intersection of $ring_1$ and bladder, the blue shadow indicated the intersection of $ring_2$ and bladder. The yellow shadow indicated the intersection of $ring_3$ and bladder. The purple shadow indicated the intersection of $ring_4$ and bladder. The sky blue shadow indicated the intersection of $ring_5$ and bladder. The lavender shadow indicated the intersection of $ring_6$ and bladder. The orange shadow indicated the intersection of $ring_7$ and bladder. The forest shadow indicated the intersection of $ring_8$ and bladder. The slate blue shadow indicated the intersection of $ring_9$ and bladder.

bladder, rectum, and sigmoid colon (all correlations, $P < 0.05$). The volume of the bladder ($V_{bladder}$) and the $D_{2cm^3}/D_{prescription}$ of the small intestine were correlated. The correlation coefficient (*r*, a statistical index used to describe the degree of linear correlation between two variables), and *P* values are shown in **Tables 1**–**4**. Therefore, these data can be used to predict the $D_{2cm^3}/D_{prescription}$ of each OAR using the SVM model. The MSE and the R^2 of each OAR in the SVM model prediction group are shown in **Table 5**.

The predicted and actual $D_{2cm^3}/D_{prescription}$ values for the bladder, rectum, sigmoid colon, and small intestine in the validation group are shown in **Figure 2**. There was no statistically significant difference between the predicted and actual $D_{2cm^3}/D_{prescription}$ values for the bladder ($P = 0.68$), rectum ($P = 0.16$), sigmoid colon ($P = 0.14$), and small intestine ($P = 0.77$) in the validation group. The δ value for the bladdera of the verification group was 0.024 ± 0.022, the corresponding rectum δ value was 0.026 ± 0.014, the sigmoid colon δ value was 0.035 ± 0.023, and the small intestine δ value was 0.032 ± 0.025.

DISCUSSION

The quality control of radiotherapy plan has always been a research hotspot in the field of radiotherapy (14–17). The most critical aspect is the prediction of the dose to the OAR before designing the radiotherapy plan. It has been reported that the OAR dose in the brachytherapy plan could be predicted by the overlapping volume of the OAR with the targeted area and knowledge-based tool (18, 19). Ours is a relatively simple mathematical model that uses prescription dose and $V_{sub\text{-}OAR}$ to predict the bladder, rectum, and sigmoid D_{2cm^3} for brachytherapy; this does not require buying new modules of TPS or extracting the distance of each sampling point of the OAR with the dose. We also divided the OARs into multiple sub-OARs to predict the OAR dose in the external IMRT plan (20, 21). In contrast to previous studies, the focus of our study is to determine the correlation between the $V_{sub\text{-}OAR}$ and $D_{2cm^3}/D_{prescription}$ of each OAR in brachytherapy, therefore, this method has been granted the Chinese invention patent. Owing to this correlation, we could fit the data of the training group using the SVM model approach. To rule out the effects of different prescription doses on the D_{2cm^3} of each OAR, we divided each D_{2cm^3} by 90% of the HR-CTV that reached the dose ($D_{prescription}$).

As shown in **Figure 2**, our SVM estimation system predicted that the $D_{2cm^3}/D_{prescription}$ of the OARs is very close to the actual value. There was no significant difference between the predicted and actual $D_{2cm^3}/D_{prescription}$ values for each OAR. The δ values

TABLE 1 | The correlation coefficient (r) and *P* value for bladder.

Relevant factors r, *P*	VHR-CTV	Vsub-bladder 1	Vsub-bladder 2	Vsub-bladder 3	Vsub-bladder 4	Vsub-bladder 5
r ($D_{2cm^3}/D_{prescription}$)	0.45**	0.58**	0.49**	0.45**	0.41**	0.37**
P ($D_{2cm^3}/D_{prescription}$)	0.001	<0.001	<0.001	0.001	0.003	0.008

***When the confidence (double test) is less than 0.01, the correlation is significant.*
Vsub-bladder, the volume of the sub-bladder.

TABLE 2 | The correlation coefficient (r) and *P* value for rectum.

Relevant factors r, *P*	VHR-CTV	Vsub-rectum 1	Vsub-rectum 2	Vsub-rectum 3	Vsub-rectum 4	Vsub-rectum 5
r ($D_{2cm^3}/D_{prescription}$)	0.40**	0.59**	0.37**	0.36**	-0.29*	-0.28*
P ($D_{2cm^3}/D_{prescription}$)	0.005	<0.001	0.009	0.009	0.028	0.033

***When the confidence (double test) is less than 0.01, the correlation is significant, *when the confidence (double test) is less than 0.05, the correlation is significant, the negative indicates that there is a negative correlation between the Vsub- rectum and* $D_{2cm^3}/D_{prescription}$ of rectum.
Vsub-rectum, the volume of the sub-rectum.

TABLE 3 | The correlation coefficient (r) and *P* value for sigmoid colon.

Relevant factors r, *P*	VHR-CTV	Vsub-sigmoid colon 1	Vsub-sigmoid colon 2	Vsub-sigmoid colon 3	Vsub-sigmoid colon 4	Vsub-sigmoid colon 5
r ($D_{2cm^3}/D_{prescription}$)	0.36**	0.85**	0.90**	0.85**	0.54**	0.57**
P ($D_{2cm^3}/D_{prescription}$)	0.010	<0.001	<0.001	<0.001	<0.001	<0.001

***When the confidence (double test) is less than 0.01, the correlation is significant.*
Vsub-sigmoid colon, the volume of the sub-sigmoid colon.

TABLE 4 | The correlation coefficient (r) and *P* value for small intestine.

Relevant factors r, *P*	VBladder	Vsub-small intestine 1	Vsub-small intestine 2	Vsub-small intestine 3	Vsub-small intestine 4	Vsub-small intestine 5
r ($D_{2cm^3}/D_{prescription}$)	0.75**	0.89**	0.89**	0.87**	0.84**	0.83**
P ($D_{2cm^3}/D_{prescription}$)	<0.001	<0.001	<0.001	<0.001	<0.001	<0.001

***When the confidence (double test) is less than 0.01, the correlation is significant.*
Vsub-small intestine, the volume of the sub-small intestine.

TABLE 5 | The MSE and the r-squared of each OAR for the SVM prediction model group.

	Bladder	Rectum	Sigmoid colon	Small intestine
MSE	0.00270	0.00024	0.00104	0.00102
R^2	0.938	0.991	0.957	0.964

MSE, mean squared error; SVM, support vector machine; R^2, the coefficient of determination.

of the bladder, rectum, sigmoid colon, and small intestine were 0.024 ± 0.022, 0.026 ± 0.014, 0.035 ± 0.023, and 0.032 ± 0.025, respectively. The abovementioned statistics, MSE, and R^2 of the SVM prediction model indicated that the prediction model was reliable. We used a relatively simple mathematical model, which does not require the acquisition of new modules of TPS software. The process model for the acquisition of the sub-OAR can be edited into scripts to improve efficiency and effectiveness.

Our model can be used as a component of a quality assurance tool to detect suboptimal treatment plans in OAR sparing. A properly

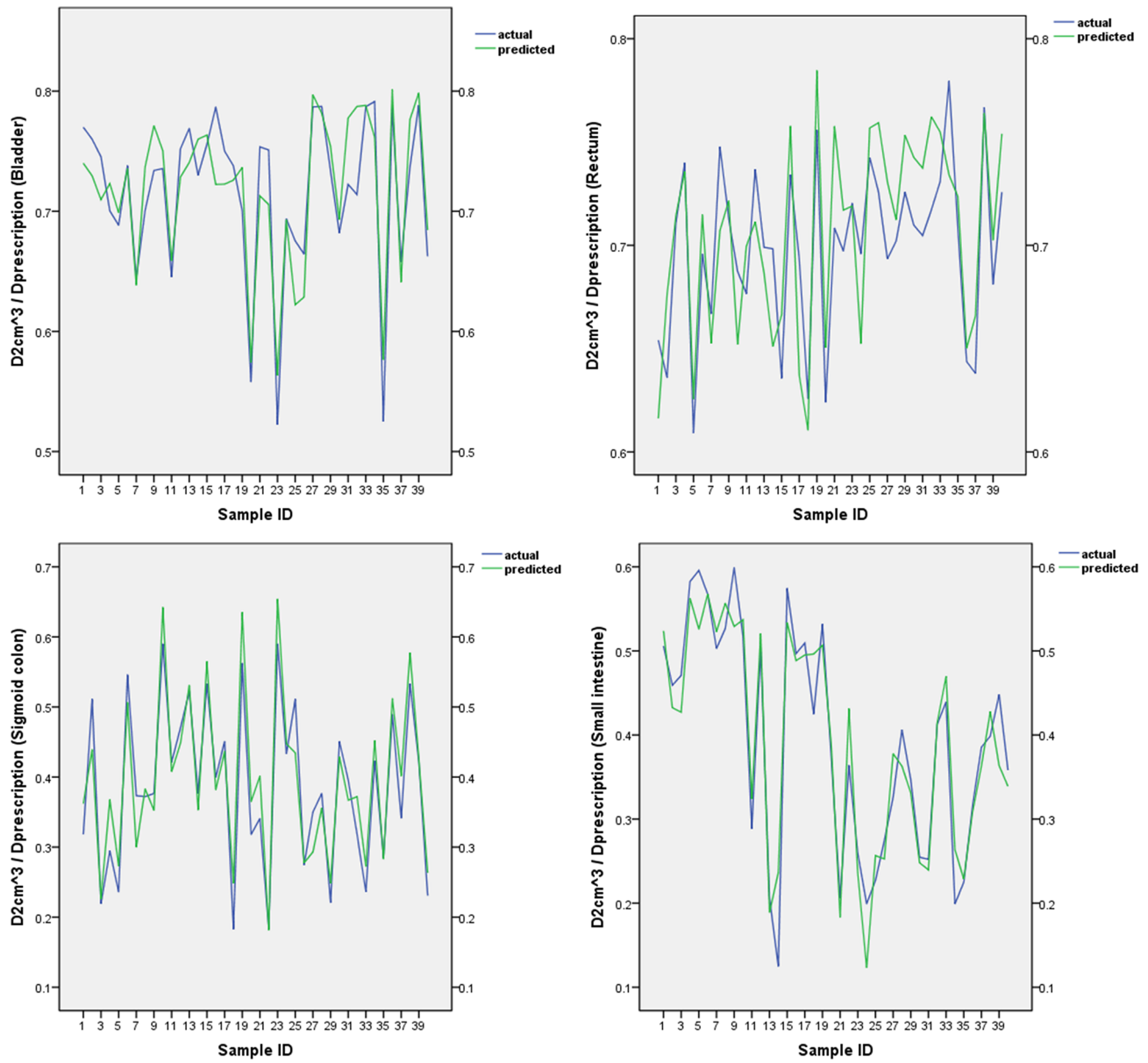

FIGURE 2 | The predicted and actual $D_{2cm^3}/D_{prescription}$ values for the bladder, rectum, sigmoid colon, and small intestine.

trained model will provide an estimate of the OAR doses required for appropriate planning and will detect outlines that require further review. Specifically, considering δ, a δ value closer to 0 indicated a closer relationship between the planned and predicted values of $D_{2cm^3}/D_{prescription}$. A standard δ threshold can be set for the D_{2cm^3} of each OAR, and the value above the threshold should be further optimized or the position of the applicator should be re-adjusted, until a satisfactory δ value is obtained. Predictions using the SVM model can be conducted for the quality control of the brachytherapy plan and for minimizing the effect of subjective factors (22).

Our study has some limitations. It was restricted to a single institution and considered only standard tandem and ovoid cases. Further research is needed comprising multiple centers and more cervical cancer brachytherapy plan data sets for analysis. If the data set is large enough, a neural network model can be developed, which will generate predictions with higher accuracy of the OAR dose for cervical cancer brachytherapy plans. The SVM models discussed herein may be applied beyond gynecologic brachytherapy. The application of our models to prostate brachytherapy as well can be considered after validation.

CONCLUSION

The SVM model can be applied to not only predict the dose to the OARs for the high-dose rate brachytherapy of cervical cancer but also develop quality assurance tools for designing brachytherapy plans.

DATA AVAILABILITY STATEMENT

The raw data supporting the conclusions of this article will be made available by the authors, without undue reservation.

ETHICS STATEMENT

The studies involving human participants were reviewed and approved by The Affiliated Hospital of Southwest Medical University Ethics Committee. The patients/participants provided their written informed consent to participate in this study.

AUTHOR CONTRIBUTIONS

Guarantors of integrity of entire study, HP. Study concepts/study design or data acquisition or data analysis/interpretation, all authors. Manuscript drafting or manuscript revision for important intellectual content, all authors. Resolution of any questions related to the work, all authors. Literature research, PZ, SL, and HP. Statistical analysis, PZ, XL, and HP. Manuscript editing, PZ, SL, and HP. All authors contributed to the article and approved the submitted version.

REFERENCES

1. Small W, Bacon MA, Bajaj A, Chuang LT, Fisher BJ, Harkenrider MM, et al. Cervical Cancer: A Global Health Crisis. *Cancer* (2017) 123(13):2404–12. doi: 10.1002/cncr.30667
2. Cibula D, Pötter R, Planchamp F, Avall-Lundqvist E, Fischerova D, Haie Meder C, et al. The European Society of Gynaecological Oncology/European Society for Radiotherapy and Oncology/European Society of Pathology Guidelines for the Management of Patients With Cervical Cancer. *Int J Gynecol Cancer* (2018) 28(4):641–55. doi: 10.1097/IGC.0000000000001216
3. Mayadev J, Viswanathan A, Liu Y, Li CS, Albuquerque K, Damato AL, et al. American Brachytherapy Task Group Report. American Brachytherapy Task Group Report: A Pooled Analysis of Clinical Outcomes for High-Dose-Rate Brachytherapy for Cervical Cancer. *Brachytherapy* (2017) 16(1):22–43. doi: 10.1016/j.brachy.2016.03.008
4. Wu B, Kusters M, Kunze-Busch M, Dijkema T, McNutt T, Sanguineti G, et al. Cross-Institutional Knowledge-Based Planning (KBP) Implementation and its Performance Comparison to Auto-Planning Engine (APE). *Radiother Oncol* (2017) 123(1):57–62. doi: 10.1016/j.radonc.2017.01.012
5. Siavashpour Z, Aghamiri MR, Jaberi R, Manshadi HR, Ghaderi R, Kirisits C. Optimum Organ Volume Ranges for Organs at Risk Dose in Cervical Cancer Intracavitary Brachytherapy. *J Contemp Brachytherapy* (2016) 8(2):135–42. doi: 10.5114/jcb.2016.59687
6. Moore KL, Brame RS, Low DA, Mutic S. Experience-Based Quality Control of Clinical Intensity-Modulated Radiotherapy Planning. *Int J Radiat Oncol Biol Phys* (2011) 81(2):545–51. doi: 10.1016/j.ijrobp.2010.11.030
7. Zawadzka A, Nesteruk M, Brzozowska B, Kukołowicz PF. Method of Predicting the Mean Lung Dose Based on a Patient's Anatomy and Dose-Volume Histograms. *Med Dosim* (2017) 42(1):57–62. doi: 10.1016/j.meddos.2016.12.001
8. Tol JP, Dahele M, Delaney AR, Slotman BJ, Verbakel WF. Can Knowledge-Based DVH Predictions be Used for Automated, Individualized Quality Assurance of Radiotherapy Treatment Plans? *Radiat Oncol* (2015) 10 (1):234. doi: 10.1186/s13014-015-0542-1
9. Ge Y, Wu QJ. Knowledge-Based Planning for Intensity-Modulated Radiation Therapy: A Review of Data-Driven Approaches. *Med Phys* (2019) 46(6):2760–75. doi: 10.1002/mp.13526
10. Jiao SX, Chen LX, Zhu JH, Wang ML, Liu XW. Prediction of Dose-Volume Histograms in Nasopharyngeal Cancer IMRT Using Geometric and Dosimetric Information. *Phys Med Biol* (2019) 64(23):23NT04. doi: 10.1088/1361-6560/ab50eb
11. Yang Y, Ford EC, Wu B, Pinkawa M, van Triest B, Campbell P, et al. An Overlap-Volume-Histogram Based Method for Rectal Dose Prediction and Automated Treatment Planning in the External Beam Prostate Radiotherapy Following Hydrogel Injection. *Med Phys* (2013) 40(1):011709. doi: 10.1118/1.4769424
12. Haie-Meder C, Pötter R, Van Limbergen E, Briot E, De Brabandere M, Dimopoulos J, et al. Recommendations From Gynaecological (GYN) GEC-ESTRO Working Group (I): Concepts and Terms in 3D Image Based 3D Treatment Planning in Cervix Cancer Brachytherapy With Emphasis on MRI Assessment of GTV and CTV. *Radiother Oncol* (2005) 74(3):235–45. doi: 10.1016/j.radonc.2004.12.015
13. Pötter R, Haie-Meder C, Van Limbergen E, Barillot I, De Brabandere M, Dimopoulos J, et al. Recommendations From Gynaecological (GYN) GEC ESTRO Working Group (II): Concepts and Terms in 3D Image-Based Treatment Planning in Cervix Cancer Brachytherapy-3D Dose Volume Parameters and Aspects of 3D Image-Based Anatomy, Radiation Physics, Radiobiology. *Radiother Oncol* (2006) 78(1):67–77. doi: 10.1016/j.radonc.2005.11.014
14. Yusufaly TI, Meyers SM, Mell LK, Moore KL. Knowledge-Based Planning for Intact Cervical Cancer. *Semin Radiat Oncol* (2020) 30(4):328–39. doi: 10.1016/j.semradonc.2020.05.009
15. Krayenbuehl J, Di Martino M, Guckenberger M, Andratschke N. Improved Plan Quality With Automated Radiotherapy Planning for Whole Brain With

Hippocampus Sparing: A Comparison to the RTOG 0933 Trial. *Radiat Oncol* (2017) 12(1):161. doi: 10.1186/s13014-017-0896-7
16. Court LE, Kisling K, Mccarroll R, Zhang L, Yang J, Simonds H, et al. Radiation Planning Assistant - A Streamlined, Fully Automated Radiotherapy Treatment Planning System. *J Vis Exp* (2018) 134(134):57411. doi: 10.3791/57411
17. Buschmann M, Sharfo AWM, Penninkhof J, Seppenwoolde Y, Goldner G, Georg D, et al. Automated Volumetric Modulated Arc Therapy Planning for Whole Pelvic Prostate Radiotherapy. *Strahlenther Onkol* (2018) 194(4):333–42. doi: 10.1007/s00066-017-1246-2
18. Damato AL, Viswanathan AN, Cormack RA. Validation of Mathematical Models for the Prediction of Organs-at-Risk Dosimetric Metrics in High-Dose-Rate Gynecologic Interstitial Brachytherapy. *Med Phys* (2013) 40 (10):101711. doi: 10.1118/1.4819946
19. Yusufaly TI, Kallis K, Simon A, Mayadev J, Yashar CM, Einck JP, et al. A Knowledge-Based Organ Dose Prediction Tool for Brachytherapy Treatment Planning of Patients With Cervical Cancer. *Brachytherapy* (2020) 19(5):624–34. doi: 10.1016/j.brachy.2020.04.008
20. Pang H, Sun X, Yang B, Wu J. A Quality Control Method for Intensity-Modulated Radiation Therapy Planning Based on Generalized Equivalent Uniform Dose. *J Appl Clin Med Phys* (2018) 19(3):276–82. doi: 10.1002/acm2.12331
21. Pang H, Sun X, Yang B, Wu J. Predicting the Dose Absorbed by Organs at Risk During Intensity Modulated Radiation Therapy for Nasopharyngeal Carcinoma. *Br J Radiol* (2018) 91(1092):20170289. doi: 10.1259/bjr.20170289
22. Klement RJ, Allgäuer M, Appold S, Dieckmann K, Ernst I, Ganswindt U, et al. Support Vector Machine-Based Prediction of Local Tumor Control After Stereotactic Body Radiation Therapy for Early-Stage Non-Small Cell Lung Cancer. *Int J Radiat Oncol Biol Phys* (2014) 88(3):732–8. doi: 10.1016/j.ijrobp.2013.11.216

Conflict of Interest: The authors declare that the research was conducted in the absence of any commercial or financial relationships that could be construed as a potential conflict of interest.

frontiers in Oncology

ORIGINAL RESEARCH
published: 13 August 2021
doi: 10.3389/fonc.2021.723193

The Efficacy and Safety of Continuous Intravenous Endostar Treatment Combined With Concurrent Chemoradiotherapy in Patients With Locally Advanced Cervical Squamous Cell Carcinoma: A Randomized Controlled Trial

Hang Shu[1], Yaqin Dong[1], Zhonghua Xu[1], Weiwei Luo[1], Lei Xu[1], Haochen Zhu[1], Linghui Cheng[2] and Yin Lv[1]**

[1] Department of Oncology Radiotherapy, The First Affiliated Hospital of Anhui Medical University, Hefei, China, [2] Department of Obstetrics and Gynecology, First Affiliated Hospital, Anhui Medical University, Hefei, China

OPEN ACCESS

Edited by:
John Varlotto,
Marshall University, United States

Reviewed by:
Bidhu K. Mohanti,
KIIT University, India
Yingming Sun,
Fujian Medical University, China

***Correspondence:**
Linghui Cheng
chenglinghui71@163.com
Yin Lv
Lvyin406@163.com

Specialty section:
This article was submitted to Radiation Oncology, a section of the journal Frontiers in Oncology

Received: 10 June 2021
Accepted: 30 July 2021
Published: 13 August 2021

Citation:
Shu H, Dong Y, Xu Z, Luo W, Xu L, Zhu H, Cheng L and Lv Y (2021) The Efficacy and Safety of Continuous Intravenous Endostar Treatment Combined With Concurrent Chemoradiotherapy in Patients With Locally Advanced Cervical Squamous Cell Carcinoma: A Randomized Controlled Trial. Front. Oncol. 11:723193. doi: 10.3389/fonc.2021.723193

Objective: To investigate the short-term efficacy and safety of Endostar combined with concurrent chemoradiotherapy in the treatment of locally advanced cervical squamous cell carcinoma (LACSC).

Methods: A total of 91 patients with LACSC admitted to the First Affiliated Hospital of Anhui Medical University from June 2019 to December 2020 were randomly assigned to either the experimental group (n = 48) or control group (n = 43). The control group received radiotherapy for cervical cancer and paclitaxel combined with platinum chemotherapy (CCRT), and the experimental group received Endostar continuous intravenous infusion of anti-angiogenic therapy plus CCRT. The short-term efficacy, common clinical indicators, tumor indicators, changes in serum vascular endothelial growth factor-A (VEGF-A), and the occurrence of adverse events (AEs) were explored after treatment.

Results: Compared with the control group, the complete response (CR) rate in the experimental group was significantly increased (83.33% *vs* 65.12%, $P < 0.05$). Both routine indicators and tumor indicators in the two groups were significantly decreased compared to before treatment. Compared with the control group, patients in the experimental group had higher incidences of neutropenia, hypertension, and infection, but lower incidence of nausea. After treatment, the serological expression of VEGF-A was significantly decreased in both groups.

Conclusion: Endostar combined with CCRT in the treatment of LACSC can further improve the efficacy of CR rate and significantly reduce serum tumor indicators and

VEGF-A levels, with mild and controllable AEs. Endostar combined with CCRT is expected to be a new treatment regimen for LACSC.

Keywords: locally advanced cervical cancer, endostar, concurrent chemoradiotherapy, short-term efficacy, safety

INTRODUCTION

Cervical cancer is a prevalent malignancy in women, ranking as the fourth most frequently diagnosed cancer and the leading cause of cancer death in women worldwide (1). Statistics show that there were approximately 570,000 new cases and 311,000 deaths globally in 2018 (1). Although the prevention and screening techniques of cervical cancer have improved, patients are being diagnosed with cervical cancer at a younger age (2). Cervical squamous cell carcinoma remains the major pathologic type, although the HPV vaccine has led to a decrease in its incidence (3, 4). In China, there are approximately 130,000 new cases and 53,000 deaths attributed cervical cancer each year (5). Therefore, cervical cancer remains a serious threat to women's health worldwide.

Locally advanced cervical squamous cell cancer (LACSC) refers to cervical squamous cell carcinoma with stages IB3-IVA according to the Federation International of Gynecology and Obstetrics (FIGO) classification system (2018). For patients with LACSC, concurrent chemoradiotherapy (CCRT) is the main treatment protocol, which consists of radiotherapy combined with platinum-containing chemotherapy. CCRT has become the "gold standard" treatment since the publication of five large sample, randomized controlled clinical trials conducted by the American Cancer Radiation Therapy Collegium (RTGG), the Gynecologic Oncology Group (GOG), and the Southwest Cancer Group (SWOG) (6–8). However, the 5-year overall survival (OS) rate for patients with LACSC remains only 66% (9), and within 2 years after the initial CCRT, about half of patients develop local recurrence or distant metastasis (10). Therefore, there is a need to identify new treatments for LACSC.

In 1971, Folkman proposed the hypothesis that tumor growth depends on angiogenesis (11). Many subsequent studies have confirmed that angiogenesis is the key mechanism underlying the occurrence and development of malignant tumors (12). Vascular endothelial growth factor (VEGF) and its receptor (VEGFR) have garnered much attention in the angiogenesis theory. As a monoclonal antibody to humanized VEGF, the GOG240 clinical trial showed that bevacizumab could significantly prolong the survival period of recurrent and metastatic cervical cancer, indicating that anti-angiogenic clinical treatment of cervical cancer could be beneficial. However, the incidence of adverse events (AEs) of bevacizumab, including bleeding, gastrointestinal perforation, and other adverse reactions, is very high (13, 14).

Chinese scholars developed a recombinant human vascular endostatin (Endostar; YP-16) by adding 9 amino acid sequences based on the original endostatin (15). Endostar has more stability and a longer half-life than bevacizumab and can inhibit tumor vascular growth through multiple targets. In addition, Endostar can help normalize the tumor vascular network, improve blood oxygen transport, and improve the treatment effect of radiotherapy (16). In 2005, Endostar was formally approved by the Chinese Food and Drug Administration as a first-line drug for recurrent and metastatic non-small cell lung cancer (NSCLC). In addition, Endostar is more affordable than other antiangiogenic drugs on the market, reducing the cost-burden on patients. Currently, studies involving NSCLC (17), nasopharyngeal carcinoma (NPC) (18), and bone and soft tissue sarcomas (19) have shown that clinical radiotherapy and chemotherapy have achieved a good effect when combined with Endostar. However, there are only a few reports on the efficacy and safety of Endostar combined with CCRT in the clinical treatment of LACSC.

The objective of the present study was to compare the efficacy and safety of CCRT combined with continuous intravenous pump Endostar with CCRT alone in patients with LACSC. This study provides new insights for optimal treatment of LACSC.

METHODS

The present study was a parallel, randomized, controlled clinical trial for LACSC clinical treatment. The protocol of the present study was approved by the Ethics Committee of the First Affiliated Hospital of Anhui Medical University (PJ2019-17-14). All participating patients signed informed consent before being enrolled in the study. The study protocol strictly followed the Declaration of Helsinki.

Patients

Consecutive patients with LACSC in the Department of Oncology Radiotherapy, Anhui Medical University, were screened from July 2019 to December 2020. The inclusion criteria were as follows: 1) LACSC patients with FIGO stage IB3-IVA tumors confirmed by pathological biopsy to be inoperable cervical squamous cell carcinoma; 2) age 18 to 75 years old; 3) KPS (Karnofsky Performance Status) score ≥ 60 points or ECOG (Eastern Cooperative Oncology Group) score

Abbreviations: AE, adverse event; ALB, Albumin; BMI, body mass index; CCRT, concurrent chemoradiotherapy; CEA, carcinoembryonic antigen; CR, complete response; CYFR21-1, cytokeratin 19 fragments; DCR, disease control rate; ELISA, enzyme-linked immunosorbent assay; FIGO, Federation International of Gynecology and Obstetrics; GOG, Gynecologic Oncology Group; Hb, Hemoglobin; IMRT, Intensity-modulated conformal radiotherapy; LACSC, Locally advanced cervical squamous cell carcinoma; NO, nitic oxide; NPC, nasopharyngeal carcinoma; ORR, objective response rate; OS, overall survival; PD, disease progression; PGI2, Prostaglandin; PLT, Platelet; PR, partial response; RTOG, Radiation therapy oncology group; SCC, squamous cell carcinoma antigen; SD, stable disease; SWOG, Southwest Cancer Group; VEGF, vascular endothelial growth factor; VEGF-A, vascular endothelial growth factor-A; VEGFR, vascular endothelial growth factor receptor; WBC, white blood cell.

0 – 2; 4) with evaluable tumor lesions; 5) no distant metastasis confirmed by imaging; 6) without serious liver, kidney, and other organ dysfunction; and 7) at least 6 months of expected survival time. The exclusion criteria were as follows: 1) patients who could not tolerate chemoradiotherapy or targeted therapy, including serious cardiovascular disease, serious liver or kidney failure, serious neurological or mental deficiency, and acute infectious diseases; 2) patients who received anti-tumor therapy previously; and 3) pregnancy and lactation patients.

Treatment

After providing informed consent, patients were randomly assigned in a 1:1 ratio to either the Endostar + CCRT arm (experimental arm) or the CCRT alone arm (control arm). The eligible patients were randomly assigned a sequence through a computer generation module to a study arm. The patient identification number was used to generate the sequence to ensure the anonymity of the assignment. Simple randomization was adopted without any restriction, such as stratification or blocking. The treatment process is shown in **Figure 1**.

CCRT for Both the Experimental Arm and the Control Arm

All included patients received CCRT, which consisted of radiotherapy combined with platinum-containing chemotherapy. Intensity-modulated conformal radiotherapy (IMRT) was used for external irradiation. A total dose of 50 – 51 Gy/25 – 30 F was administered to the pelvic cavity and planned target area of the lymphatic drainage area (PTV, planning target volume). Patients were located using a Varian Acuity simulation locator, and images were transmitted to the ELIPSE13.6 system. All involved radiotherapists received universal training to ensure the uniform standard of target area mapping. If imaging indicated positive metastatic lymph nodes in the para-aortic or pelvic cavity, the metastatic lymph nodes were administered PTVND (planning target volume of the metastatic lymph nodes) 60 Gy/30 F. For tumors larger than 4 cm, PTVG (planning target volume of gross tumor) was added to 60 Gy/30 F simultaneously. Intracavitary retro loading radiotherapy was performed at the dose of 30 Gy/5 F. The cumulative dose of point A was ≥ 80 – 84 Gy for intracavitary retro loading therapy and external irradiation. Synchronous chemotherapy started from the first week of concurrent chemoradiotherapy with the TP regimen of paclitaxel (40 mg/m^2, continuous intravenous infusion for more than 60 min) and Cisplatin (30 mg/m^2, continuous intravenous infusion for 30 – 60 min). Chemotherapy was administered once a week for 3 weeks. Routine prophylactic use of antiemetic drugs was provided during chemotherapy.

Endostar Therapy for the Experimental Arm

Anti-angiogenic therapy was performed with Endostar (Simcere Pharmaceutical, Nanjing, China) 15 mg/m^2, continuous intravenous pumping for 120 h (day 1 to 5 of the week of administration, coinciding with the time of weekly radiotherapy), with repeated administration every other week for a total of 3 cycles.

Endpoints and Assessment

The primary endpoint was short-term efficacy evaluated by the complete response (CR), partial response (PR), stable disease (SD), disease progression (PD), objective response rate (ORR), and disease control rate (DCR), and drug safety was evaluated by AEs. The CR, PR, SD, and PD were defined according to RECIST 1.1 (20). The equations for calculating ORR and DCR were ORR = (CR+PR)/total cases × 100% and DCR = (CR+PR+SD)/total cases × 100%, respectively. The short-term efficacy was evaluated by imaging all patients one month after assigned therapy. Therapy-related AEs, including drug-related and radiological AEs, during treatment were evaluated weekly in patients. The incidence of drug-related AEs was evaluated according to the International Cancer Organization Common Adverse Reactions Standard (NCI-CTCAE) 4.0, which were classified into Grades 1 - 5.

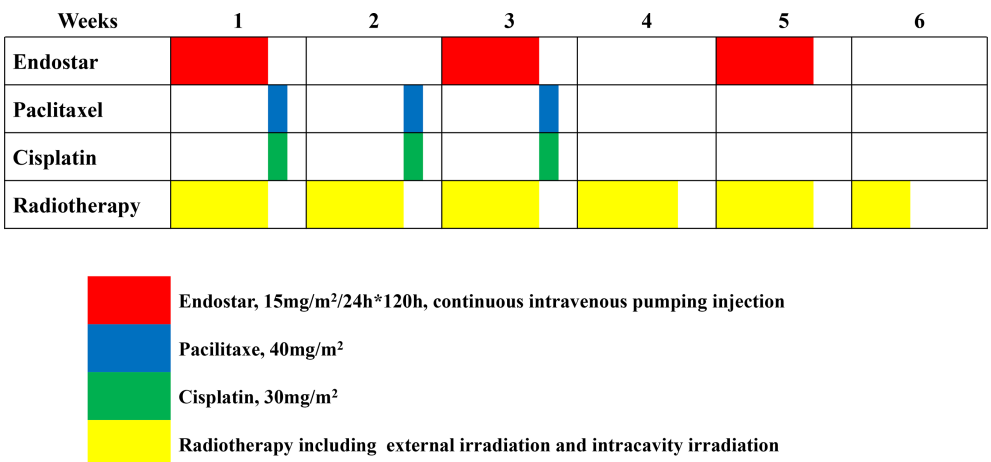

FIGURE 1 | Treatment flow.

The secondary endpoints included blood indicators and VEGF-A level. Before treatment and one month after treatment, blood indicators were examined respectively in the two groups. Blood indicators included tumor markers and routine markers tested in all participants both before and after the interventions. Tumor markers included squamous cell carcinoma antigen (SCC), carcinoembryonic antigen (CEA), and cytokeratin 19 fragments (CYFR21-1), which were detected using chemiluminescence. Routine indicators included white blood cell (WBC), hemoglobin (Hb), platelet (PLT), and albumin (ALB). Among the members of the VEGF family, VEGF-A plays the most important role in promoting blood vessel growth (21). In this study, serum VEGF-A levels were detected by timely extraction of venous blood from patients within 24 h before and after treatment. Fasting venous blood (3 ml) was collected from the patients after and before treatment for all included patients, which was centrifuged at 2,500 r/min for 10 min. VEGF-A levels were detected in the supernatant using enzyme-linked immunosorbent assay (ELISA, Jiangsu Enzyme Industrial Co. Ltd.).

Trial Oversight

To ensure the objectivity, authenticity, and reliability of the clinical trial, the sponsor assigned its inspectors to evaluate the study parameters regularly, supervise the case report form, check its qualification, and put forward suggestions for improvement.

Statistical Analysis

SPSS 24.0 statistical software was used for all data analysis. Continuous variables conforming to normal distribution are expressed as mean ± standard deviation (SD) and analyzed by t-test. Median and quaternary values (P_{25}, P_{75}) were used for expression data that did not conform to the normal distribution, and a rank-sum test (Z test) was used for comparison. Categorical variables are described with count and frequency. The rates of the two groups were compared using the Chi-square analysis or the Fisher's exact probability method. Logistic regression was used to explore the independent factors for efficacy and safety. $P < 0.05$ indicated statistical significance.

RESULTS

Patients

Of the 95 patients screened, 4 patients did not meet the eligibility criteria due to missing the follow-up. Thus, 91 patients underwent randomization; 48 patients were enrolled in the experimental group and 43 patients in the control group. Each enrolled patient completed the evaluation of short-term efficacy, therapy-related AEs, blood indicators, and VEGF-A levels. By the end of the study, no patients had recurrence or died during follow-up. Each patient was followed up from the beginning of treatment to one month after the end of treatment. Therefore, the long-term survival data were not available. There were no statistical differences between the groups in terms of the baseline characteristics including age, height, weight, body surface area, BMI, level of education, menopause, basic diseases, clinical stage, and tumor size. See **Table 1** for details.

Short-Term Efficacy

The experimental group achieved CR 83.33% (40/48), ORR 93.75% (45/48), and DCR 95.83% (46/48), while the control

TABLE 1 | Comparison of baseline characteristics between the two groups.

Clinical features	Control group (n=43)	Experimental group (n=48)	t/χ^2	P value
Age (years), mean ± SD	56.49 ± 11.65	56.52 ± 10.49	0.14	0.989
Height (cm), mean ± SD	157.98 ± 6.10	159.11 ± 4.95	0.982	0.329
Weight (kg), mean ± SD	56.59 ± 9.10	58.01 ± 10.86	0.648	0.519
Body surface area (m^2)	1.66 ± 0.14	1.68 ± 0.16	0.831	0.408
BMI	22.70 ± 3.94	22.87 ± 3.77	0.207	0.836
Level of education			0.729	0.393
Illiteracy	19	17		
Primary education or above	24	31		
Menopause			0.025	0.875
After	24	26		
Before	19	22		
Basis of disease (hypertension, diabetes, etc.)			0.288	0.591
No	32	38		
Yes	11	10		
FIGO stage			4.041	0.401
IIB	20	20		
IIIA	3	4		
IIIB	3	10		
IIIC	13	10		
IVA	4	4		
Tumor size (cm)			0.282	0.596
<4	20	25		
4 or higher	23	23		

SD, standard deviation; BMI, body mass index; FIGO, International Federation of Gynecology and Obstetrics.

group achieved CR 65.12% (28/43), ORR 39 90.70% (39/43), and DCR 95.35% (41/43). The CR rate was statistically different between the two groups (P < 0.05). No statistical difference was found for ORR and DCR (P > 0.05). The detailed comparison of the short-term efficacy is described in **Table 2**.

Therapy-Related AEs

Common drug-related AEs included leukopenia, neutropenia, thrombocytopenia, hematuria, proteinuria, hypertension, bleeding, infection, nausea, vomiting, and diarrhea. The incidence of neutropenia, hypertension, and infection in the experimental group was significantly higher than in the control group, but the incidence of nausea was significantly lower in the control group (all P < 0.05). Adverse reactions mostly occurred in grades 1 - 2 in the two groups. The detailed incidence with grades of each AE is described in **Table 3**.

We further explored the risk factors for the occurrence of neutropenia, hypertension, infection, and nausea using multivariate analysis. The results showed that CCRT combined with Endostar was an independent risk factor for the increased incidence of both neutropenia and infection; the risk of the experimental group was 2.885 and 4.455 times higher than the control group, respectively. The combination of Endostar in treatment was also an independent risk factor for reducing the risk of nausea (P = 0.011). Even when blood pressure was routinely controlled during treatment, patients with underlying diseases had a significantly further increased risk of hypertension following Endostar treatment (P = 0.004). The details of the multivariate regression are described in **Table 4**.

Radiation-related AEs included skin damage, lower gastrointestinal and pelvic reactions, genitourinary tract reactions, radiation cystitis, and radiation proctitis. Most of the radiation-related AES were grades 1 - 2 (see details in **Table 3**). No statistically significant difference was found for any radiation-related AEs between the two groups (P > 0,05). The statistical data are described in **Table 3**.

Blood Indicators and VEGF-A Levels

Among the common clinical indicators, white blood cells and platelets decreased in the Control group one month after treatment compared with before treatment (P < 0.001). However, the phenomenon did not appear in the treatment of CCRT combined with Endostar (P = 0.309). Compared with before treatment, hemoglobin in both groups decreased after treatment, and the difference was statistically significant (all P < 0.05). In terms of cervical cancer-specific tumor indexes, SCC, CEA, and CYRA21-1 in both groups significantly decreased after treatment compared with before treatment, (all P < 0.05) (**Table 5**). We also compared the range of changes in the indicators and found that there was no difference in the decrease ranges of four indicators of hemoglobin, SCC, CEA, and Cyra21-1 in the two groups (all P > 0.05) (**Supplementary Table 1**).

VEGF-A levels before treatment were 285.44 ± 53.25 and 285.44 ± 53.25 in the control and experimental groups, respectively (P > 0.05). After treatment, VEGF-A levels significantly decreased in both groups compared with before treatment (all P < 0.01). However, there was no statistically significant difference in VEGF-A levels between the two groups after treatment (P > 0.05). See details in **Table 5**.

TABLE 2 | Comparison of short-term efficacy between the two groups after treatment.

Short term efficacy	Control group (n=43)	Experimental group (n=48)	P value (chi-square test or Fisher's exact test)
CR, N (%)	28 (65.12)	40 (83.33)	0.046
PR, N (%)	11 (22.92)	5 (11.63)	0.058
SD, N (%)	2 (4.17)	1 (2.33)	0.601*
PD, N (%)	2 (4.17)	2 (4.65	1.00*
ORR, N (%)	39 (90.70)	45 (93.75)	0.703*
DCR, N (%)	41 (95.35)	46 (95.93)	1.00*

Fisher's exact test.
CR, complete response; PR, partial response; SD, stable disease; ORR, objective response rate; DCR, disease control rate.

DISCUSSION

As an anti-angiogenic drug, Endostar can block angiogenesis and directly kill tumor cells. Besides, Endostar can also improve systemic chemotherapy by increasing tumor perfusion (22) and optimizing the hypoxic environment to increase radiotherapy sensitivity (16). In the present study, we found Endostar combined with CCRT had a higher CR rate compared to CCRT alone (P = 0.046). Recently, Guan et al. reported a randomized controlled trial confirming Endostar's ability to restore vascular homeostasis and enhance chemotherapy in patients with cervical cancer (15), which is consistent with the results of the present study.

In terms of the safety, we found that Endostar plus CCRT was an independent risk factor for neutropenia and infection. Similarly, it was once reported that a higher incidence of neutropenia occurred in locally advanced NSCLC when combined with Endostar (23). The high frequency of infection could be due to neutropenia, as there is a potential connection between AEs. Furthermore, Senior et al. reported that infection seemed to block the growth of blood vessels in tumors (24). This unique observation seems to support the anti-angiogenic effect we observed in the experimental group. However, in terms of increased blood pressure, patients in the experimental group had significantly increased risks of hypertension. VEGF is critical for maintaining normal blood pressure and can induce the release of nitic oxide (NO) and prostaglandin (PGI2) from endothelial cells, promoting vasodilation (25). Endostar can down-regulate VEGF expression (26). Therefore, elevated blood pressure is more common following Endostar treatment. It is worth noting that the risk of nausea was lower in the experimental group in this study, providing a new insight for clinical treatment.

The levels of white blood cells and platelets in the control group decreased after treatment, but not in the experimental group. The data suggest that Endostar, as a targeted anti-angiogenic therapy, does not cause myelosuppression in patients after long-term combined treatment with CCRT. In the present study, patients in both groups experienced a slight decrease in hemoglobin during the one-month follow-up Most

TABLE 3 | The occurrence and comparison of acute toxic and side effects between the two groups.

	Arms	Classification of acute toxic reactions					Number of cases (%)	χ^2	*P*
		0	1	2	3	4			
leukopenia	Control	15	8	13	4	3	28 (65.12%).	1.062	0.303
	Experimental	12	14	16	6	0	36 (75.00%).		
Neutropenia	Control	24	5	7	3	4	19 (44.19%).	5.588	0.018
	Experimental	15	18	9	5	1	33 (68.75%).		
thrombocytopenia	Control	30	9	2	1	1	13 (30.23%).	0.276	0.599
	Experimental	31	12	5	0	0	17 (35.42%).		
Blood in the urine	Control	22	14	6	0	1	21 (48.84%).	0.008	0.930
	Experimental	25	16	6	1	0	23 (47.92%).		
proteinuria	Control	32	6	4	1	0	11 (25.58%).	0.653	0.419
	Experimental	32	12	4	0	0	16 (33.33%).		
hypertension	Control	42	1	0	0	0	1 (2.33%).		0.032*
	Experimental	40	8	0	0	0	8 (16.67%)		
bleeding	Control	34	7	2	0	0	9 (20.93%)	0.212	0.645
	Experimental	36	11	1	0	0	12 (25.00%).		
infection	Control	35	4	2	2	0	8 (18.60%)	9.806	0.02
	Experimental	24	16	8	0	0	24 (50.00%).		
nausea	Control	17	12	12	2	0	26 (60.47%).	3.957	0.046
	Experimental	29	9	10	0	0	20 (41.67%).		
vomiting	Control	28	8	5	2	0	15 (34.88%).	1.062	0.303
	Experimental	36	7	5	0	0	12 (25.00%).		
diarrhea	Control	32	6	2	3	0	11 (25.58%).	0.026	0.871
	Experimental	35	10	3	0	0	13 (27.08%).		
Skin damage*	Control	34	8	0	0	1	9 (20.93%)	0.052	0.819
	Experimental	37	10	1	0	0	11 (22.92%).		
Lower alimentary canal and pelvic cavity*	Control	35	5	2	1	0	8 (18.60%)	3.217	0.073
	Experimental	31	8	8	0	1	17 (35.42%).		
Genitourinary tract*	Control	40	0	2	0	1	3 (6.98%)		0.323*
	Experimental	41	5	1	1	0	7 (14.58%)		
Radiation cystitis*	Control	42	0	0	0	1	1 (2.33%).		1.00*
	Experimental	46	1	0	1	0	2 (4.17%).		
Radiation proctitis*	Control	38	3	1	1	0	5 (11.63%)	0.173	0.677
	Experimental	41	1	5	0	1	7 (14.58%)		

**denotes radiation-related injury.*

TABLE 4 | The adjusted odds ratios through multivariate regression for clarifying the correlation between toxicological reactions and Endostar.

Variables		Neutropenia	Hypertension	Infection	Nausea
Age	OR (95%CI)	0.993 (0.939-1.051)	1.069 (0.951-1.203)	0.967 (0.909-1.028)	0.962 (0.910-1.019)
	P value	0.817	0.263	0.280	0.183
Height	OR (95%CI)	1.038 (0.944-1.141)	1.196 (0.969-1.476)	0.950 (0.858-1.052)	1.000 (0.911-1.097)
	P value	0.438	0.095	0.325	1.000
Weight	OR (95%CI)	0.964 (0.916-1.014)	0.957 (0.874-1.048)	1.002 (0.950-1.057)	1.016 (0.969-1.065)
	P value	0.155	0.343	0.941	0.521
Level of education (Illiteracy *versus* literacy)	OR (95%CI)	2.35 (0.804-6.871)	1.198 (0.148-9.697)	1.870 (0.584-5.983)	2.317 (0.777-6.909)
	P value	0.118	0.866	0.292	0.132
Having basis of disease (yes *versus* no)	OR (95%CI)	2.489 (0.739-8.380)	19.801 (2.663-147.237)	0.483 (0.133-1.746)	0.704 (0.226-2.197)
	P value	0.141	0.004	0.267	0.545
Menopause (after *versus* before)	OR (95%CI)	1.112 (0.391-3.169)	0.846 (0.098-7.312)	0.701 (0.232-2.121)	0.364 (0.124-1.072)
	P value	0.842	0.879	0.530	0.067
FIGO stages (IIB-IIIB *versus* IIIC-IVA)	OR (95%CI)	0.823 (0.251-2.691)	1.759 (0.102-30.364)	0.669 (0.180-2.484)	0.401 (0.119-1.349)
	P value	0.747	0.697	0.548	0.140
Tumor size (< 4 cm *versus* ≥4 cm)	OR (95%CI)	0.684 (0.470-3.161)	3.544 (0.541-23.207)	1.697 (0.622-4.634)	1.237 (0.487-3.145)
	P value	0.684	0.187	0.302	0.655
Arms (Control *versus* Experimental)	OR (95%CI)	2.885 (1.063-7.833)	9.660 (1.062-87.835)	4.455 (1.472-13.485)	0.268 (0.097-0.744)
	P value	0.038	0.044	0.008	0.011

patients with LACSC have tumor bleeding, and concurrent radiotherapy can also decrease hemoglobin, as previously reported (27). SCC, CEA, and CYRA21-1 are tumor markers that are clearly related to tumor burden of cervical cancer (28, 29). These tumor indexes significantly decreased in both groups after treatment in this study. The results reconfirm the efficacy of Endostar in combination with CCRT in patients with LACSC. As for VEGF-A, we did not observe an improving effect of Endostar

TABLE 5 | Comparison of blood indicators and VEGF-A between the two groups before and after treatment.

	Indicators	Arms	Before the treatment	After treatment	Z/t	P value
Routine indexes (Unit)	WBC (x 10^9/L)	Control	*5.29 (3.89, 6.7)	*4.11 (3.09, 4.64)	3.592	<0.001
		Experimental	^4.230 ± 1.67	^4.70 ± 2.11	1.029	0.309
	HB (g/L)	Control	*111.00 (102.00, 122.00)	*106.00 (100.00, 116.00)	3.177	0.001
		Experimental	^113.02 ± 15.68	^107.00 ± 12.64	3.092	0.003
	PLT (x 10^9/L)	Control	^244.00 ± 103.84	^184.62 ± 70.25	4.226	<0.001
		Experimental	^174.52 ± 63.16	^158.60 ± 51.98	1.684	0.099
	ALB (g/L)	Control	*41.20 (38.10, 42.70)	*39.90 (37.10, 42.60)	1.357	0.175
		Experimental	*42.75 (40.25, 44.85)	*41.40 (38.05, 43.60)	2.101	0.36
Tumor indexes (Unit, reference value)	SCC (ng/L, 0-3.00)	Control	*4.45 (2.17, 8.20)	*1.72 (0.80, 5.10)	3.900	<0.001
		Experimental	*3.29 (1.27, 6.46)	*1.20 (0.77, 2.08)	5.143	<0.001
	CEA (ng/ml, 0-5.00)	Control	*3.12 (2.10, 5.10)	*1.90 (1.3, 4.30)	2.857	0.004
		Experimental	*2.86 (1.43, 5.10)	*1.68 (1.10, 2.78)	5.208	<0.001
	CYRA21-1(ng/ml, 0-3.30)	Control	*3.02 (2.19, 4.07)	*2.07 (1.56, 2.88)	2.702	0.007
		Experimental	*3.01 (1.74, 3.93)	*2.16 (1.47, 3.15)	3.069	0.002
VEGF-A (pg/ml)		Control	+285.44 ± 53.25	+264.18 ± 49.24	4.183	<0.001
		Experimental	295.64 ± 73.44	273.13 ± 65.60	3.030	0.004

**Median and quaternary values (P_{25}, P_{75}). ^mean ± standard deviation.*

+Before and after treatment, t test was used to analyze VEGF-A levels in the two groups, and there was no statistical difference between the two groups (P > 0.05).

on the inhibition of VEGF-A with CCRT treatment. A decrease in VEGF-A levels has been significantly helpful in the prolongation of patient survival following treatment of various tumors (30, 31). However, a study of head and neck squamous cell carcinoma suggested that an increase in serum VEGF-A levels is a significant negative predictor of radiotherapy or chemoradiotherapy (P = 0.001) (32). Future research is needed to further explore the effect of Endostar on VEGF-A levels.

In the past, Endostar used intermittent intravenous infusion (IIV). In this study, we administered continuous intravenous (CIV) administration over a period of 120 hours with a portable infusion pump. In terms of treatment options, Endostar has a half-life of about 10 hours (33) and IIV causes drug concentrations to fluctuate greatly, but CIV can ensure a stable blood drug concentration in the body. In contrast, patients with LACSC received conventional fractionated radiotherapy once a day, Monday through Friday. The 120-hour CIV was administered from Monday to Friday to ensure that the Endostar treatment coincided with radiotherapy. It is important to note that, theoretically, stable drug concentrations have milder toxic side effects (34) and have been reported to support a possible survival benefit (35). LACSC patients with CCRT often present with gynecological symptoms and reduced abilities to carry out activities of daily living. The CIV is delivered in a portable manner, reducing patient time costs and improving compliance. In clinical practice, traditional IIV requires more infusion devices, while portable infusion pumps can reduce the cost of medical resources and reduce the workload of nursing staff. Therefore, CIV is a suitable way to use Endostar in combination with CCRT.

As CCRT has become the "gold standard" treatment for LACSC, there have been consistent efforts to improve CCRT to achieve better efficacy. Studies have reported that 5-year OS was higher in patients with a tri-weekly cisplatin regimen compared with a traditional weekly cisplatin regimen combined with CCRT (36). Carboplatin is a viable option for patients who cannot tolerate cisplatin in CCRT (37). A phase III clinical trial in Mexico showed that following 2 cycles of adjuvant chemotherapy after CCRT, the 3-year PFS increased from 65% to 74.4% for LACSC (38). When S-1 was added to the traditional CCRT regimen, the OS and PFS of patients with LACSC improved and there was no increase in the toxic side effects (39). When CCRT is combined with autologous cytokine-induced killer cell infusion, LACSC patients have better short-term efficacy and better quality of life (40). However, studies on CCRT combined with antiangiogenic therapy in patients with LACSC are rare, and this study is expected to provide new insight.

To the best of our best, the present study is the first trial exploring the efficacy and safety of Endostar in patients with LACSC. Limitations of this study include the small sample size and lack of long-term survival data, which may lower the power of the analysis. Currently, there is clinical evidence supporting the significant survival benefit of Endostar in the treatment of NSCLC. In addition, Endostar has been included in China's national medical insurance for the treatment of patients with advanced NSCLC. However, for other cancers, there is still a lack of broad, large clinical trials to support the benefits of Endostar, which is why Endostar is limited to the Chinese market. Therefore, more evidence is needed to determine the optimal dose, administration route, administration time window, and drug safety of Endostar. With more basic research we can better understand the potential value of Endostar in clinical application.

CONCLUSION

Endostar combined with CCRT in the treatment of LACSC can further improve the efficacy of CR rate and significantly reduce serum tumor indicators and VEGF-A levels, with mild and controllable AEs. For the treatment of LACSC, Endostar combined with CCRT could be extended to a broader clinical trial and is expected to be a new treatment regimen for LACSC.

DATA AVAILABILITY STATEMENT

The raw data supporting the conclusions of this article will be made available by the authors, without undue reservation.

ETHICS STATEMENT

The studies involving human participants were reviewed and approved by Ethics Committee of the First Affiliated Hospital of Anhui Medical University. The patients/participants provided their written informed consent to participate in this study.

AUTHOR CONTRIBUTIONS

YL and LC conceived and designed the study. HS analyzed the experimental data and drafted the manuscript. ZX, LX, and HZ collected the experimental data. WL and YD revised the manuscript for important intellectual content. All authors contributed to the article and approved the submitted version.

FUNDING

This work was supported by the China International Medical Foundation (CIMFz-2014-06-19413), China International Medical Foundation (CIMFz-2014-06-2102) and the Major Program of the Anhui Natural Science Foundation (KJ2016A754).

SUPPLEMENTARY MATERIAL

The Supplementary Material for this article can be found online at: https://www.frontiersin.org/articles/10.3389/fonc.2021.723193/full#supplementary-material

REFERENCES

1. Bray F, Ferlay J, Soerjomataram I, Siegel RL, Torre LA, Jemal A. Global Cancer Statistics 2018: GLOBOCAN Estimates of Incidence and Mortality Worldwide for 36 Cancers in 185 Countries. *CA Cancer J Clin* (2018) 68 (6):394–424. doi: 10.3322/caac.21492
2. Siegel RL, Miller KD, Fuchs HE, Jemal A. Cancer Statistics, 2021. *CA Cancer J Clin* (2021) 71(1):7–33. doi: 10.3322/caac.21654
3. Nicol AF, de Andrade CV, Russomano FB, Rodrigues LS, Oliveira NS, Provance DWJr., et al. HPV Vaccines: Their Pathology-Based Discovery, Benefits, and Adverse Effects. *Ann Diagn Pathol* (2015) 19(6):418–22. doi: 10.1016/j.anndiagpath.2015.07.008
4. Small WJr., Bacon MA, Bajaj A, Chuang LT, Fisher BJ, Harkenrider MM, et al. Cervical Cancer: A Global Health Crisis. *Cancer* (2017) 123(13):2404–12. doi: 10.1002/cncr.30667
5. Chen WQ, Li H, Sun KX, Zheng RS, Zhang SW, Zeng HM, et al. Report of Cancer Incidence and Mortality in China, 2014. *Zhonghua Zhong Liu Za Zhi.* (2018) 40(1):5–13. doi: 10.3760/cma.j.issn.0253-3766.2018.01.002
6. Morris M, Eifel PJ, Lu J, Grigsby PW, Levenback C, Stevens RE, et al. Pelvic Radiation With Concurrent Chemotherapy Compared With Pelvic and Para-Aortic Radiation for High-Risk Cervical Cancer. *N Engl J Med* (1999) 340 (15):1137–43. doi: 10.1056/nejm199904153401501
7. Whitney CW, Sause W, Bundy BN, Malfetano JH, Hannigan EV, Fowler WCJr., et al. Randomized Comparison of Fluorouracil Plus Cisplatin Versus Hydroxyurea as an Adjunct to Radiation Therapy in Stage IIB-IVA Carcinoma of the Cervix With Negative Para-Aortic Lymph Nodes: A Gynecologic Oncology Group and Southwest Oncology Group Study. *J Clin Oncol* (1999) 17(5):1339–48. doi: 10.1200/jco.1999.17.5.1339
8. Rose PG, Bundy BN, Watkins EB, Thigpen JT, Deppe G, Maiman MA, et al. Concurrent Cisplatin-Based Radiotherapy and Chemotherapy for Locally Advanced Cervical Cancer. *N Engl J Med* (1999) 340(15):1144–53. doi: 10.1056/nejm199904153401502
9. Chemoradiotherapy for Cervical Cancer Meta-analysis Collaboration (CCCMAC). Reducing Uncertainties About the Effects of Chemoradiotherapy for Cervical Cancer: Individual Patient Data Meta-Analysis. *Cochrane Database Syst Rev* (2010) 2010(1):Cd008285. doi: 10.1002/14651858.cd008285
10. Naga Ch P, Gurram L, Chopra S, Mahantshetty U. The Management of Locally Advanced Cervical Cancer. *Curr Opin Oncol* (2018) 30(5):323–9. doi: 10.1097/cco.0000000000000471
11. Folkman J. Tumor Angiogenesis: Therapeutic Implications. *N Engl J Med* (1971) 285(21):1182–6. doi: 10.1056/nejm197111182852108
12. Carmeliet P, Jain RK. Angiogenesis in Cancer and Other Diseases. *Nature* (2000) 407(6801):249–57. doi: 10.1038/35025220
13. Tewari KS, Sill MW, Long HJ3rd, Penson RT, Huang H, Ramondetta LM, et al. Improved Survival With Bevacizumab in Advanced Cervical Cancer. *N Engl J Med* (2014) 370(8):734–43. doi: 10.1056/NEJMoa1309748
14. Tewari KS, Sill MW, Penson RT, Huang H, Ramondetta LM, Landrum LM, et al. Bevacizumab for Advanced Cervical Cancer: Final Overall Survival and Adverse Event Analysis of a Randomised, Controlled, Open-Label, Phase 3 Trial (Gynecologic Oncology Group 240). *Lancet* (2017) 390(10103):1654–63. doi: 10.1016/s0140-6736(17)31607-0
15. Guan L. Endostar Rebuilding Vascular Homeostasis and Enhancing Chemotherapy Efficacy in Cervical Cancer Treatment. *Onco Targets Ther* (2020) 13:12811–27. doi: 10.2147/ott.S277644
16. Wu Y, Zheng Y, Shen Z, Ge W, Xie Y, Li C. Endostar Combined With Radiotherapy Increases Radiation Sensitivity by Decreasing the Expression of TGF-β1, HIF-1α and bFGF. *Exp Ther Med* (2014) 7(4):911–6. doi: 10.3892/etm.2014.1526
17. Wang J, Sun Y, Liu Y, Yu Q, Zhang Y, Li K, et al. [Results of Randomized, Multicenter, Double-Blind Phase III Trial of Rh-Endostatin (YH-16) in Treatment of Advanced Non-Small Cell Lung Cancer Patients]. *Zhongguo Fei Ai Za Zhi.* (2005) 8(4):283–90. doi: 10.3779/j.issn.1009-3419.2005.04.07
18. Jin T, Jiang F, Jin QF, Piao YF, Chen XZ. Endostar Combined With Gemcitabine and Cisplatin Chemotherapy for Patients With Metastatic Nasopharyngeal Carcinoma: An Update. *Transl Oncol* (2018) 11(2):286–91. doi: 10.1016/j.tranon.2018.01.002
19. Xing P, Zhang J, Yan Z, Zhao G, Li X, Wang G, et al. Recombined Humanized Endostatin (Endostar) Combined With Chemotherapy for Advanced Bone and Soft Tissue Sarcomas in Stage IV. *Oncotarget* (2017) 8(22):36716–27. doi: 10.18632/oncotarget.13545
20. Eisenhauer EA, Therasse P, Bogaerts J, Schwartz LH, Sargent D, Ford R, et al. New Response Evaluation Criteria in Solid Tumours: Revised RECIST Guideline (Version 1.1). *Eur J Cancer.* (2009) 45(2):228–47. doi: 10.1016/j.ejca.2008.10.026
21. Otrock ZK, Makarem JA, Shamseddine AI. Vascular Endothelial Growth Factor Family of Ligands and Receptors: Review. *Blood Cells Mol Dis* (2007) 38 (3):258–68. doi: 10.1016/j.bcmd.2006.12.003
22. Yu M, Han Y, Zhuo H, Zhang S. Endostar, a Modified Endostatin Induces Vascular Normalization to Improve Chemotherapy Efficacy Through Suppression of Src Signaling Pathway. *Cancer Biother Radiopharm.* (2018) 33(4):131–8. doi: 10.1089/cbr.2017.2399
23. Zhang SL, Han CB, Sun L, Huang LT, Ma JT. Efficacy and Safety of Recombinant Human Endostatin Combined With Radiotherapy or Chemoradiotherapy in Patients With Locally Advanced Non-Small Cell Lung Cancer: A Pooled Analysis. *Radiat Oncol* (2020) 15(1):205. doi: 10.1186/s13014-020-01646-9

24. Senior K. Infection Seems to Block Angiogenesis in Tumours. *Lancet* (2001) 357(9267):1507. doi: 10.1016/s0140-6736(00)04710-3
25. Davydova N, Harris NC, Roufail S, Paquet-Fifield S, Ishaq M, Streltsov VA, et al. Differential Receptor Binding and Regulatory Mechanisms for the Lymphangiogenic Growth Factors Vascular Endothelial Growth Factor (VEGF)-C and -D. *J Biol Chem* (2016) 291(53):27265–78. doi: 10.1074/jbc.M116.736801
26. Ling Y, Yang Y, Lu N, You QD, Wang S, Gao Y, et al. Endostar, a Novel Recombinant Human Endostatin, Exerts Antiangiogenic Effect *via* Blocking VEGF-Induced Tyrosine Phosphorylation of KDR/Flk-1 of Endothelial Cells. *Biochem Biophys Res Commun* (2007) 361(1):79–84. doi: 10.1016/j.bbrc.2007.06.155
27. Serkies K, Badzio A, Jassem J. Clinical Relevance of Hemoglobin Level in Cervical Cancer Patients Administered Definitive Radiotherapy. *Acta Oncol* (2006) 45(6):695–701. doi: 10.1080/02841860600833160
28. Gaarenstroom KN, Kenter GG, Bonfrer JM, Korse CM, Van de Vijver MJ, Fleuren GJ, et al. Can Initial Serum Cyfra 21-1, SCC Antigen, and TPA Levels in Squamous Cell Cervical Cancer Predict Lymph Node Metastases or Prognosis? *Gynecol Oncol* (2000) 77(1):164–70. doi: 10.1006/gyno.2000.5732
29. Malkin A, Kellen JA, Lickrish GM, Bush RS. Carcinoembryonic Antigen (CEA) and Other Tumor Markers in Ovarian and Cervical Cancer. *Cancer* (1978) 42(3 Suppl):1452–6. doi: 10.1002/1097-0142(197809)42:3+<1452::aid-cncr2820420813>3.0.co;2-9
30. Bernatz S, Monden D, Gessler F, Radic T, Hattingen E, Senft C, et al. Influence of VEGF-a, VEGFR-1-3, and Neuropilin 1-2 on Progression-Free: And Overall Survival in WHO Grade II and III Meningioma Patients. *J Mol Histol.* (2021) 52(2):233–43. doi: 10.1007/s10735-020-09940-2
31. Dinami R, Porru M, Amoreo CA, Sperduti I, Mottolese M, Buglioni S, et al. TRF2 and VEGF-a: An Unknown Relationship With Prognostic Impact on Survival of Colorectal Cancer Patients. *J Exp Clin Cancer Res* (2020) 39(1):111. doi: 10.1186/s13046-020-01612-z
32. Srivastava VK, Gara RK, Rastogi N, Mishra DP, Ahmed MK, Gupta S, et al. Serum Vascular Endothelial Growth Factor-a (VEGF-a) as a Biomarker in Squamous Cell Carcinoma of Head and Neck Patients Undergoing Chemoradiotherapy. *Asian Pac J Cancer Prev* (2014) 15(7):3261–5. doi: 10.7314/apjcp.2014.15.7.3261
33. Sim BK, Fogler WE, Zhou XH, Liang H, Madsen JW, Luu K, et al. Zinc Ligand-Disrupted Recombinant Human Endostatin: Potent Inhibition of Tumor Growth, Safety and Pharmacokinetic Profile. *Angiogenesis* (1999) 3 (1):41–51. doi: 10.1023/a:1009058931769
34. Hansma AH, Broxterman HJ, van der Horst I, Yuana Y, Boven E, Giaccone G, et al. Recombinant Human Endostatin Administered as a 28-Day Continuous Intravenous Infusion, Followed by Daily Subcutaneous Injections: A Phase I and Pharmacokinetic Study in Patients With Advanced Cancer. *Ann Oncol* (2005) 16(10):1695–701. doi: 10.1093/annonc/mdi318
35. Wang B, Xu L, Li Q, Man S, Jin C, Liu L, et al. Endostar Continuous Versus Intermittent Intravenous Infusion Combined With Chemotherapy for Advanced NSCLC: A Systematic Review and Meta-Analysis Including Non-Randomized Studies. *BMC Cancer.* (2020) 20(1):1021. doi: 10.1186/s12885-020-07527-4
36. Ryu SY, Lee WM, Kim K, Park SI, Kim BJ, Kim MH, et al. Randomized Clinical Trial of Weekly vs. Triweekly Cisplatin-Based Chemotherapy Concurrent With Radiotherapy in the Treatment of Locally Advanced Cervical Cancer. *Int J Radiat Oncol Biol Phys* (2011) 81(4):e577–81. doi: 10.1016/j.ijrobp.2011.05.002
37. Cetina L, Garcia-Arias A, Uribe Mde J, Candelaria M, Rivera L, Oñate-Ocaña L, et al. Concurrent Chemoradiation With Carboplatin for Elderly, Diabetic and Hypertensive Patients With Locally Advanced Cervical Cancer. *Eur J Gynaecol Oncol* (2008) 29(6):608–12.
38. Dueñas-González A, Zarbá JJ, Patel F, Alcedo JC, Beslija S, Casanova L, et al. Phase III, Open-Label, Randomized Study Comparing Concurrent Gemcitabine Plus Cisplatin and Radiation Followed by Adjuvant Gemcitabine and Cisplatin Versus Concurrent Cisplatin and Radiation in Patients With Stage IIB to IVA Carcinoma of the Cervix. *J Clin Oncol* (2011) 29(13):1678–85. doi: 10.1200/jco.2009.25.9663
39. Li Z, Mao W, Lin N, Han S. Concurrent Radiotherapy With s-1 Plus Cisplatin Versus Concurrent Radiotherapy With Cisplatin Alone for the Treatment of Locally Advanced Cervical Carcinoma: A Pilot Randomised Controlled Trial. *Clin Transl Oncol* (2016) 18(4):413–7. doi: 10.1007/s12094-015-1385-9
40. Li N, Tian YW, Xu Y, Meng DD, Gao L, Shen WJ, et al. Combined Treatment With Autologous CIK Cells, Radiotherapy and Chemotherapy in Advanced Cervical Cancer. *Pathol Oncol Res* (2019) 25(2):691–6. doi: 10.1007/s12253-018-0541-2

Conflict of Interest: The authors declare that the research was conducted in the absence of any commercial or financial relationships that could be construed as a potential conflict of interest.

frontiers in Oncology

ORIGINAL RESEARCH
published: 19 August 2021
doi: 10.3389/fonc.2021.698744

The Role of the Metabolic Parameters of ^{18}F-FDG PET/CT in Patients With Locally Advanced Cervical Cancer

Dunhuang Wang[1,2], Xiaoliang Liu[2], Weiping Wang[2], Li Huo[3], Qingqing Pan[3], Xue Ren[4], Fuquan Zhang[2†] and Ke Hu[2*†]*

[1] Department of Radiation Oncology, The First Affiliated Hospital of Xiamen University, Teaching Hospital of Fujian Medical University, Xiamen, China, [2] Department of Radiation Oncology, Peking Union Medical College Hospital, Chinese Academy of Medical Sciences & Peking Union Medical College, Beijing, China, [3] Department of Nuclear Medicine, Peking Union Medical College Hospital, Chinese Academy of Medical Sciences & Peking Union Medical College, Beijing, China, [4] Department of Radiology, Xiamen Humanity Hospital, Xiamen, China

OPEN ACCESS

Edited by:
John Varlotto, Marshall University, United States

Reviewed by:
Ozan Cem Guler, Başkent University, Turkey
Jung Sun Yoo, Hong Kong Polytechnic University, Hong Kong, SAR China
Jungsu S. Oh, University of Ulsan, South Korea

***Correspondence:**
Fuquan Zhang
zhangfq@pumch.cn
Ke Hu
huk@pumch.cn

†These authors have contributed equally to this work

Specialty section:
This article was submitted to Radiation Oncology, a section of the journal Frontiers in Oncology

Received: *22 April 2021*
Accepted: *30 July 2021*
Published: *19 August 2021*

Citation:
Wang D, Liu X, Wang W, Huo L, Pan Q, Ren X, Zhang F and Hu K (2021) The Role of the Metabolic Parameters of ^{18}F-FDG PET/CT in Patients With Locally Advanced Cervical Cancer. Front. Oncol. 11:698744. doi: 10.3389/fonc.2021.698744

Purpose: To evaluate the role of the pre-treatment cervical and lymph node (LN) metabolic parameters of ^{18}F-fluorodeoxyglucose positron emission tomography-computed tomography (^{18}F-FDG PET/CT) for locally advanced cervical cancer (LACC) patients receiving concurrent chemoradiotherapy or radiotherapy.

Methods: we reviewed 125 consecutive patients with LACC who underwent pre-treatment ^{18}F-FDG PET/CT examination and concurrent chemoradiotherapy or radiotherapy from February 2010 to December 2015 at our institute. The mean standardized uptake value (SUVmean), maximum standardized uptake value (SUVmax), metabolic tumor volume (MTV), and total lesion glycolysis (TLG) of cervical lesion and lymph node (LN) were recorded. Receiver operator characteristic curve, C-index, Kaplan-Meier method, and Cox proportional hazards models were performed.

Results: The median follow-up was 62 months (range, 4-114 months). For 125 included patients with cervical cancer, the 5-year overall survival (OS), disease-free survival (DFS), local control (LC) and distant metastasis-free survival (DMFS) rates were 83.6%, 75.1%, 92.3% and 79.9%, respectively. Cervical MTV (c-index 0.59-0.61) and cervical TLG (c-index 0.60-0.62) values calculated with a threshold of 40% SUVmax presented stronger prediction capability than cervical SUVmean (c-index 0.51-0.58) and cervical SUVmax (c-index 0.53-0.57) for OS, DFS, LC, and DMFS. In univariate analysis, cervical TLG ≥ 113.4 had worse DFS and DMFS. Cervical MTV ≥ 18.3 cm^3 had worse OS and DMFS. In multivariate analysis, cervical TLG ≥ 113.4 implied worse OS, DFS, and DMFS. In either univariate or multivariate analyses, cervical SUVmean and cervical SUVmax had no statistically significant correlation with OS, DFS, LC and DMFS. For 55 cervical cancer patients with positive LN, LN SUVmax presented strongest prediction capability for OS (c-index = 0.79), DFS (c-index = 0.72),

LC (c-index = 0.62), and DMFS (c-index = 0.79). In multivariate analysis, LN SUVmax remained significant biomarker linked to OS, DFS, and DMFS.

Conclusion: Pre-treatment cervical and LN metabolic parameters were associated with survival outcomes in patients with LACC. In our study, we found that pre-treatment cervical TLG and LN SUVmax may be important prognostic biomarkers for OS, DFS, and DMFS. However, further prospective studies with a large number of patients are required to evaluate the value of the metabolic parameters in survival outcomes prediction.

Keywords: cervical cancer, ^{18}F-FDG PET/CT, metabolic tumor volume, total lesion glycolysis, radiotherapy

INTRODUCTION

Cervical cancer is a global health problem and the leading cause of cancer death for women in developing countries (1). Cervical cancer ranks eighth in incidence and mortality in China (2). Almost half of the patients present with locally advanced disease at the time of diagnosis. Currently, the primary therapeutic method for patients with locally advanced cervical cancer (LACC) is concurrent chemoradiotherapy. In approximately 80% of patients with disease recurrence, disease failure of cervical cancer occurs within 2 years after initial treatment. Some prognostic factors have been associated with clinical outcomes, including age, stage, tumor pathology, primary tumor size, lymph node status, squamous cell carcinoma antigen, and human papillomavirus (3–6).

^{18}F-fluorodeoxyglucose positron emission tomography-computed tomography (^{18}F-FDG PET/CT) has become an essential imaging tool in oncology in addition to conventional radiologic methods such as computed tomography (CT) and magnetic resonance imaging (MRI) (7). It is widely used in the diagnosis, clinical staging, response evaluation, curative effect observation, failure mode and prognostic analysis of cervical cancer and other tumors (8–12). In recent years, the association between the metabolic parameters of pre- and post-treatment ^{18}F-FDG PET/CT and treatment failure or survival in cervical cancer has become a research hotspot. Metabolic parameters, such as the mean standardized uptake value (SUVmean), maximum standardized uptake value (SUVmax), metabolic tumor volume (MTV), and total lesion glycolysis (TLG), are the focus of attention (13). On the one hand, some studies have reported the correlations between metabolic parameters and the clinical outcomes of cervical cancer. Patients with cervical cancer with a high SUVmax primary lesion show a worse prognosis (14, 15). The baseline SUVmean can effectively predict the histopathological partial response of the primary tumor in LACC patients treated with chemoradiotherapy followed by surgery, suggesting the potential role of ^{18}F-FDG PET/CT in personalized treatment (16). Pre-treatment MTV and TLG are predictors of response to therapy and are correlated with overall survival in cervical cancer patients treated with chemoradiotherapy (17, 18). On the other hand, there are some dissenting views. The role of SUVmax and SUVmean as prognostic factors for cervical cancer is still controversial (19). Whether MTV and TLG are important prognostic indicators of cervical cancer remains to be further studied (20).

In this study, we reviewed cervical cancer patients with pre-treatment ^{18}F-FDG PET/CT and analyzed the associations between metabolic parameters and treatment failure or survival.

METHODS

Patients

We reviewed patients with LACC who received a pre-treatment ^{18}F-FDG PET/CT scan and were treated with concurrent chemoradiotherapy or radiotherapy between February 2010 and December 2015 at our institute. The inclusion criteria were as follows: (1) pathologically proven cervical cancer; (2) 2009 FIGO stage IB2, IIA2 and IIB-IVA; (3) underwent ^{18}F-FDG PET/CT scan before primary treatment; (4) no evidence of distant metastases; and (5) treated with concurrent chemoradiotherapy or radiotherapy. The exclusion criteria were as follows: (1) underwent conization of the cervix; (2) previous or concurrent diagnosis of secondary primary tumor; (3) Karnofsky performance score <70; and (4) diagnosis of diabetes mellitus.

Pre-treatment evaluations included history, physical, and gynecological examinations, complete blood count, liver function test, renal function studies, chest and abdomen CT or whole-body PET/CT, and pelvic MRI.

PET/CT Technique and Image Analysis

The imaging agent ^{18}F-FDG, which has both a radiochemical purity and chemical purity greater than 98% and negative 24 h bacterial culture and bacterial endotoxin test by the gel method, was synthesized by the PET center of Peking Union Medical College Hospital. All patients fasted for at least 4 hours and rested for 90 minutes before an intravenous administration of 3.7-7.4 (0.1-0.2 mCi) MBq/kg body weight ^{18}F-FDG. The blood glucose level was less than 8 mmol/l before the administration of the radiotracer. The PET images were acquired in 3-dimensional mode with a Siemens Biograph 64 PET/CT system from the skull base to the symphysis pubis 1 hour after injection.

The acquired data were reconstructed using the ordered-subset expectation maximization method (two iterations, eight subsets, Gaussian filter, image matrix size 168 × 168). The attenuation-corrected volumetric images were collected in axial, coronal, and sagittal views, and they were independently performed by 2 senior

PET physicians. The readers came to a consensus over controversial viewpoints. The SUVmax of the primary lesion of the cervix or positive lymph node (LN) was measured. A contouring around the primary cervical lesions or positive LN inside the boundaries was automatically determined, and the region of interest (ROI) with 40% SUVmax of the primary lesion of the cervix or positive LN within the contouring margin was delineated to define the cervical or LN MTV (20). The TLG of the primary lesion of the cervix or positive LN was calculated by multiplying the cervical or LN MTV by its SUVmean. The LN MTV and LN TLG analyzed in this study were calculated from the most FDG-avid lymph node (21).

Treatment

All patients were treated with external beam radiation therapy (EBRT) and high-dose-rate brachytherapy. EBRT was delivered with intensity-modulated radiation therapy (IMRT), volumetric-modulated arc therapy (VMAT), or helical tomotherapy (HT). A total of 50.4 Gy external radiation (1.8 Gy per fraction daily) was delivered to the elective regional lymphatics, and 59.36-61.6 Gy (2.12-2.2 Gy per fraction daily) was prescribed for the positive lymph nodes with simultaneous integrated boost (SIB) targets. For patients with para-aortic nodal involvement, the superior border extended to the level of renal vessels or to the upper margin of T12. High-dose-rate brachytherapy was delivered with an Ir-192 source, with 24-36 Gy (biologically effective dose 38.4-57.6 Gy) in four to six fractions to point A. The first-line recommendation of concurrent chemotherapy was weekly cisplatin (40 mg/m^2). A small number of patients received radical radiotherapy alone.

Follow-Up

Patients underwent follow-up examinations every 3 months in the first 2 years, every 6 months from 3 to 5 years, and once per year thereafter. Disease failure was confirmed by pathology or evidence of disease recurrence based on a series of imaging data. Overall survival (OS) was defined as the time from the start of treatment to death from any cause or the last follow-up. Disease-free survival (DFS) was defined as the time from the end of treatment to recurrence or the last follow-up. Local control (LC) was defined as the time from the end of treatment to local failure or the last follow-up. Distant metastasis-free survival (DMFS) was defined as the time from the end of treatment to distant metastasis or the last follow-up.

Statistical Analysis

R and SPSS software (version 26.0; SPSS Inc., Chicago, Illinois, USA) were used for statistical analyses. ROC curve analysis was performed to determine the cut-off values of SUVmax, SUVmean, MTV and TLG of the primary lesion of the cervix or positive lymph node that indicated the optimal trade-off by maximizing the sum of sensitivity and specificity for survival outcomes. The c-index values of SUVmean, SUVmax, MTV, and TLG of the primary lesion of the cervix or lymph node were calculated to present the prediction capability of the metabolic parameters for survival outcomes. The Kaplan–Meier method was used to estimate OS, DFS, LC, and DMFS. Univariate and multivariate analyses of the patient characteristics were performed using the log-rank test and Cox proportional hazards model. To avoid many of the previously significant relationships falling out of the 0.05 significance level, we decided to include variables with $p < 0.1$ values in the multivariate analysis, and $p < 0.05$ values were statistically significant.

RESULTS

A summary of the detailed characteristics of all patients is shown in **Table 1**. In accordance with the inclusion and exclusion criteria of the study, 125 of the 1560 patients were finally included in this study. A total of 112 patients (89.6%) presented with stage IIB or above cervical cancer. A total of 114 patients (91.2%) had squamous cell carcinoma, 9 patients (7.2%) had adenocarcinoma, 1 patient had clear cell carcinoma, and the remaining patient had Mullerian carcinosarcoma. Fifty-two patients (41.6%) had a tumor size greater than 4 cm by gynecological examination. Forty-three patients (34.4%) had positive pelvic metastatic lymph nodes (MLNs) and 2 patients (1.6%) had positive para-aortic MLNs confirmed by ^{18}F-FDG PET/CT; 10 patients (8%) with positive para-aortic MLNs had concomitant pelvic lymph nodes metastasis.

All 125 patients completed concurrent chemoradiotherapy or radiotherapy with a median time of 51 days (range, 42-98 days). Twelve patients (9.6%) received neoadjuvant chemotherapy followed by chemoradiotherapy or radiotherapy alone, 102 patients (81.6%) received concurrent chemoradiotherapy as the primary therapy, and the remaining 11 patients (8.8%) received radiotherapy alone. Ninety-seven patients (77.6%) completed more than or equal to four cycles of chemotherapy. A total of 111 patients (88.8%) underwent a total point A equivalent dose at 2 Gy (EQD_{2Gy}) greater than or equal to 85 Gy.

The median follow-up period for all patients was 62 months (range, 4-114 months). Of the 125 patients, 24% (n=30) experienced disease failure, including 6 patients with pelvic failure, 21 patients with distant metastases, and 3 patients with concurrent local and distant progression. The total local recurrence and distant failure rates were 7.2% and 19.2%, respectively. The cervix uterus was the most common site of pelvic recurrence, and the lung was the most common site of distant metastases. The 5-year overall survival, disease-free survival, local control and distant metastasis-free survival rates were 83.6%, 75.1%, 92.3% and 79.9%, respectively (**Figure 1**).

ROC curve analysis was carried out to determine the best cut-off values of SUVmean, SUVmax, MTV, and TLG of the primary lesion of the cervix or positive lymph node in predicting the prognosis of cervical cancer, considering the sensitivity and specificity for survival outcomes (**Figure 2**). The areas under the curves of cervical SUVmean, cervical SUVmax, cervical TLG, and cervical MTV were 0.54 (p=0.544; 95% CI 0.42–0.66), 0.53 (p=0.595; 95% CI 0.41–0.65), 0.57 (p=0.223; 95% CI 0.46–0.69), and 0.57 (p=0.267; 95% CI 0.45–0.68), respectively. The optimal cut-off points of cervical SUVmean, cervical SUVmax, cervical TLG and cervical MTV were 7.9, 12.8, 113.4 and 18.3 cm^3, respectively. The areas under the curves of LN SUVmean, LN SUVmax, LN TLG, and LN MTV were 0.82 (p=0.002; 95% CI

TABLE 1 | Characteristics for study patients.

Characteristic	Number of patients	Percent of patients
Median age, y	50 (range, 30-81)	
2009 FIGO stage		
IB	10	8%
IIA	3	2.4%
IIB	84	67.2%
IIIA	3	2.4%
IIIB	24	19.2%
IVA	1	0.8%
Histology		
Squamous cell carcinoma	114	91.2%
Adenocarcinoma	9	7.2%
Others	2	1.6%
Primary tumor size		
≤4 cm	73	58.4%
>4 cm	52	41.6%
Pelvic MLNs		
Yes	53	42.4%
No	72	57.6%
Para-aortic MLNs		
Yes	12	9.6%
No	113	90.4%
Treatment duration		
≤56 days	96	76.8%
>56 days	29	23.2%
Total point A EQD_{2Gy}		
<85 Gy	14	11.2%
≥85 Gy	111	88.8%
Concurrent chemoradiotherapy		
Yes	102	81.6%
No	23	18.4%
Cervical SUVmean		
<7.9	74	59.2%
≥7.9	51	40.8%
Cervical SUVmax		
<12.8	68	54.4%
≥12.8	57	45.6%
Cervical MTV		
<18.3 cm^3	59	47.2%
≥18.3 cm^3	66	52.8%
Cervical TLG		
<113.4	55	44%
≥113.4	70	56%
Lymph node SUVmean		
<2.2	29	52.7%
≥2.2	26	47.3%
Lymph node SUVmax		
<6.7	43	78.2%
≥6.7	12	21.8%
Lymph node MTV		
<9.8 cm^3	47	85.5%
≥9.8 cm^3	8	14.5%
Lymph node TLG		
<6.8	30	54.5%
≥6.8	25	45.5%

FIGO, International Federation of Gynecology and Obstetrics; MLN, metastatic lymph node; EQD_{2Gy}, equivalent dose at 2 Gy; SUV, standardized uptake value; MTV, metabolic tumor volume; TLG, total lesion glycolysis.

0.69–0.95), 0.84 (p=0.001; 95% CI 0.71–0.96), 0.77 (p=0.007; 95% CI 0.60–0.95), and 0.72 (p=0.032; 95% CI 0.52–0.92), respectively. The optimal cut-off points of LN SUVmean, LN SUVmax, LN TLG and LN MTV were 2.2, 6.7, 6.8 and 9.8 cm^3, respectively.

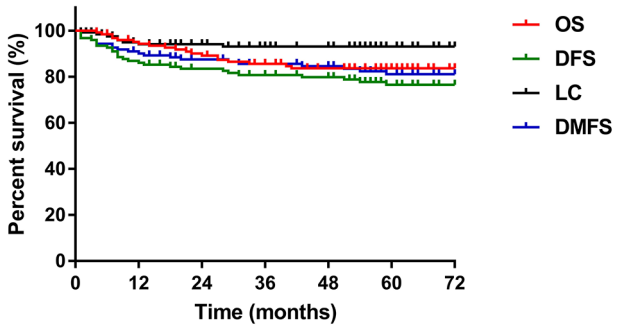

FIGURE 1 | The 5-year OS, DFS, LC, and DMFS curves of the study patients. OS, overall survival; DFS, disease-free survival; LC, local control; DMFS, distant metastasis-free survival.

The c-index values of SUVmean, SUVmax, MTV, and TLG of the primary lesion of the cervix or lymph node for OS, DFS, LC and DMFS were shown in **Table 2**. For 125 included patients with cervical cancer, cervical MTV (c-index 0.59-0.61) and cervical TLG (c-index 0.60-0.62) values calculated with a threshold of 40% SUVmax presented stronger prediction capability than cervical SUVmean (c-index 0.51-0.58) and cervical SUVmax (c-index 0.53-0.57) for OS, DFS, LC and DMFS. For 55 cervical cancer patients with positive LN, LN SUVmax presented strongest prediction capability for OS (c-index = 0.79), DFS (c-index = 0.72), LC (c-index = 0.62), and DMFS (c-index = 0.79).

The univariate analysis showed that para-aortic MLNs, total point A EQD_{2Gy}, and cervical TLG were significantly associated with DFS (**Table 3**). In multivariate analysis, para-aortic MLNs, total point A EQD_{2Gy} < 85 Gy, and cervical TLG ≥ 113.4 remained significant in predicting DFS (**Table 4**). Furthermore, in multivariate analysis, 2009 FIGO stage, para-aortic MLNs, total point A EQD_{2Gy}, and cervical TLG were significant prognostic factors for OS. Para-aortic MLNs was a poor prognostic factor for LC. Para-aortic MLNs, total point A EQD_{2Gy}, and cervical TLG had important impacts on DMFS in multivariate analysis. cervical MTV was an important prognostic factor for OS and DMFS in univariate analysis; however, no significant differences were identified for OS and DMFS in multivariate analysis. Moreover, in either univariate or multivariate analyses, cervical SUVmean and cervical SUVmax had no statistically significant correlation with OS, LC, DFS and DMFS.

The 5-year overall survival, disease-free survival, local control and distant metastasis-free survival rates for patients with cervical TLG levels <113.4 and ≥ 113.4 were 90.1% and 78% (p=0.055), 86.5% and 66.1% (p=0.015), 96.2% and 89.3% (p=0.136), and 90.9% and 71.2% (p=0.02), respectively (**Figure 3**). For the 70 patients with cervical TLG ≥ 113.4, the median follow-up period for all patients was 61 months (range, 4-110 months). The median DFS period was 56 months. Of these patients, 22 patients (31.4%) suffered from disease failure, including 4 patients with pelvic recurrence, 15 patients with distant metastases, 3 patients with concurrent local and distant

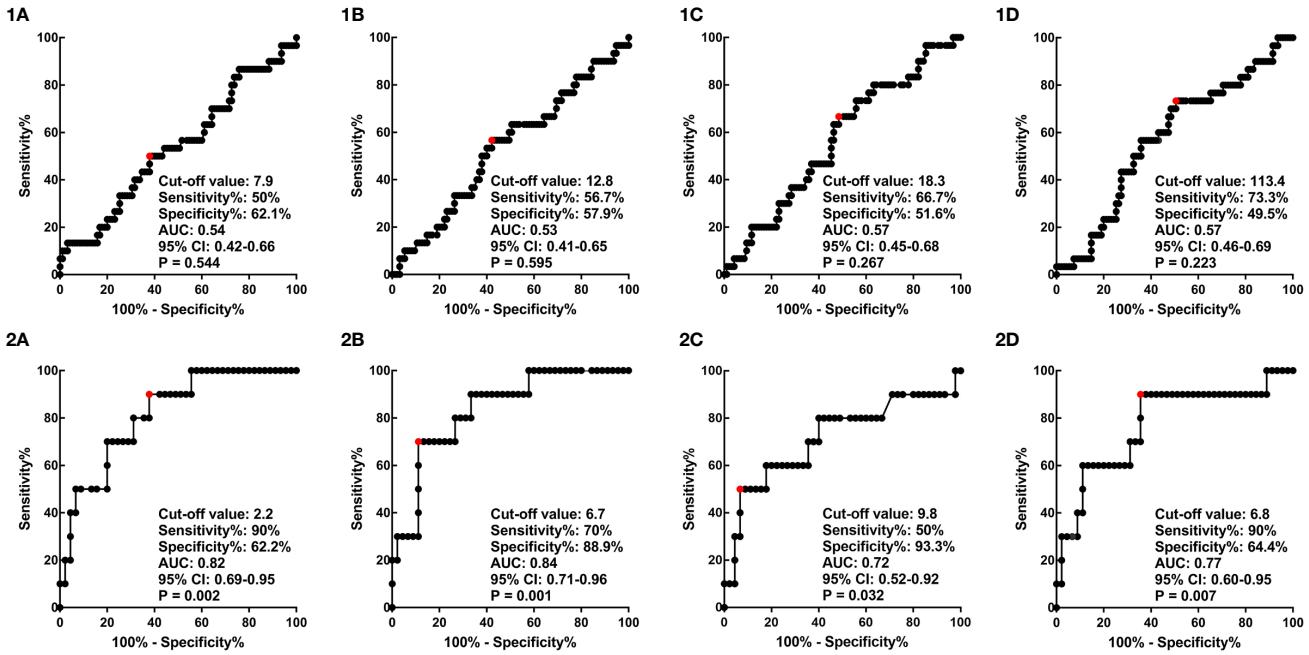

FIGURE 2 | ROC curves of cervical SUVmean **(1A)**, cervical SUVmax **(1B)**, cervical MTV **(1C)**, and cervical TLG **(1D)**, and ROC curves of LN SUVmean **(2A)**, LN SUVmax **(2B)**, LN MTV **(2C)**, and LN TLG **(2D)**. ROC, receiver operator characteristic; SUV, standardized uptake value; MTV, metabolic tumor volume; TLG, total lesion glycolysis; LN, lymph node.

progression. The total local recurrence and distant metastases rates were 10% and 25.7%, respectively. Of the 22 patients who suffered from disease failure, disease progression occurred within 2 years after primary treatment in 18 patients (81.8%) and within 5 years after primary treatment in all patients (100%). The 5-year OS, DFS, LC and DMFS rates for patients with cervical MTV levels <18.3 cm^3 and ≥ 18.3 cm^3 were 90.9% and 76.6% (p=0.03), 83.5% and 67.7% (p=0.051), 94.7% and 90.3% (p=0.32), and 88.4% and 71.8% (p=0.031), respectively.

Of the 125 included patients, 55 had pelvic or para-aortic nodal involvement. The 5-year OS, DFS, LC and DMFS rates for patients with positive LN were 80.4%, 72.2%, 86.1% and 81.4%, respectively. In univariate analysis, LN SUVmean, LN SUVmax, LN MTV, LN TLG, 2009 FIGO stage, para-aortic MLNs, treatment duration, and cycles of concurrent chemoradiotherapy were significantly associated with OS; LN SUVmax, LN MTV, LN TLG, 2009 FIGO stage, para-aortic MLNs, and treatment duration were significantly associated with DFS; LN SUVmean, LN SUVmax, LN MTV, LN TLG, 2009 FIGO stage, and para-aortic MLNs were significantly associated with DMFS; and only para-aortic MLNs was significantly associated with LC. In multivariate analysis, LN SUVmax remained significant biomarker linked to OS, DFS, and DMFS, and LN MTV was also connected with DMFS. The Kaplan-Meier curves of OS, DFS, LC, and DMFS for LN SUVmax were shown in **Figure 4**. However, SUVmean, SUVmax, MTV, and TLG of the primary lesion of the cervix had no correlation with survival outcomes in patients with positive LN.

TABLE 2 | The c-index values of SUVmean, SUVmax, MTV, and TLG of the primary lesion of the cervix or lymph node for OS, DFS, LC and DMFS.

	C-index			
	OS	**DFS**	**LC**	**DMFS**
Cervical				
SUVmax	0.53	0.56	0.57	0.53
SUVmean	0.51	0.56	0.58	0.53
MTV	0.61	0.59	0.59	0.60
TLG	0.61	0.61	0.62	0.62
Lymph node				
SUVmax	0.79	0.72	0.62	0.79
SUVmean	0.76	0.63	0.56	0.70
MTV	0.72	0.68	0.58	0.78
TLG	0.77	0.65	0.57	0.71

SUV, standardized uptake value; MTV, metabolic tumor volume; TLG, total lesion glycolysis; OS, overall survival; DFS, disease-free survival; LC, Local control; DMFS, distant metastasis-free survival.

DISCUSSION

At present, various metabolic parameters of PET, such as MTV and TLG, have particularly become a research hotspot for predicting the prognosis of cervical cancer. However, there are different opinions on the role of PET metabolic parameters in the prognosis of cervical cancer. Some studies have shown that metabolic parameters of PET, such as SUVmax, SUVmean, MTV and TLG, play an important role in predicting the prognosis of cervical cancer (**Table 5**). However, other studies have found no significant correlation between these parameters and survival. Therefore, in our study, we investigated the relationships between clinical characteristics

TABLE 3 | Results of the univariate analysis of clinical factors for disease-free survival.

Variable	Univariate analysis		
	HR	95%CI	P value
Age (continuous, year)	1.003	0.969-1.038	0.882
2009 FIGO stage			
I-II *vs.* III-IV	2.114	0.988-4.523	0.054
Histology			
Squamous *vs.* non-squamous	2.459	0.939-6.440	0.067
Primary tumor size			
≤4 cm *vs.* >4 cm	1.336	0.651-2.738	0.429
Pelvic MLNs			
Negative *vs.* Positive	1.368	0.667-2.805	0.393
Para-aortic MLNs			
Negative *vs.* Positive	6.166	2.711-14.024	< 0.001
Treatment duration			
≤56 days *vs.* >56 days	1.785	0.835-3.818	0.135
Total point A EQD_{2Gy}			
<85 Gy *vs.* ≥85 Gy	0.382	0.155-0.942	0.037
Cycles of concurrent chemoradiotherapy			
<4 *vs.* ≥4	0.839	0.360-1.956	0.684
Cervical SUVmean			
<7.9 *vs.* ≥7.9	1.555	0.759-3.187	0.227
Cervical SUVmax			
<12.8 *vs.* ≥12.8	1.788	0.867-3.688	0.116
Cervical MTV			
<18.3 cm^3 *vs.* ≥18.3 cm^3	2.095	0.980-4.480	0.056
Cervical TLG			
<113.4 *vs.* ≥113.4	2.629	1.169-5.914	0.019

HR, hazard ratio; CI, confidence interval; FIGO, International Federation of Gynecology and Obstetrics; MLN, metastatic lymph node; EQD_{2Gy}, equivalent dose at 2 Gy; SUV, standardized uptake value; MTV, metabolic tumor volume; TLG, total lesion glycolysis.

and PET metabolic parameters and the recurrence and long-term survival of cervical cancer. Our study shows that pre-treatment cervical TLG, LN SUVmax, Para-aortic MLNs, and Total point A EQD_{2Gy} are important independent prognostic factors for recurrence and survival.

SUV can reflect metabolic activity as a semiquantitative marker of tumor uptake and has been demonstrated to play an important role in predicting the prognosis of cervical cancer in previous studies. A meta-analysis demonstrated that a significantly worse prognosis was associated with a higher SUVmax of the primary lesion in cervical cancer. However, SUVmax was not a significant independent prognostic factor in most of the enrolled studies in that meta-analysis (14). There are various reasons for this contradictory result, especially publication bias, which cannot be ignored. In addition, there are several limitations, such as missing data, the small sample size of each enrolled study and inconsistent treatment methods in different medical centers, which may cause differences in results. Voglimacci et al. (15) also suggested that cervical SUVmax as a continuous variable was a critical predictive index for survival outcomes, but the difference was not statistically significant when using the cut-off value. Herrera et al. (19) reported that pre-treatment cervical SUVmean ≥ 5 was a significantly poor prognostic factor of OS (57% *vs.* 86%, p =0.03), DFS (36% *vs.* 88%, p = 0.004) and LC (65% *vs.* 88%, p = 0.04) in univariate analysis. However, statistically significant associations were not found between cervical SUVmean and survival outcomes in multivariate analysis. Meanwhile, the demonstration of an association between cervical SUVmax and prognosis would have been more challenging to interpret. In our study, cervical SUVmean and cervical SUVmax had no statistically significant correlation with OS, DFS, LC or DMFS. There are several articles with similar results to our study (13, 22). However, LN SUVmax was significant associated with survival outcomes. Similarly, Martinez et al. (21) indicated that LN SUVmax was significantly linked to para-aortic nodal involvement only in univariate analysis. SUV may be affected by many factors, including blood glucose level, body mass index, scan duration, and reconstruction algorithm (23–25). Therefore, the role of SUVmean and SUVmax in predicting the prognosis of cervical cancer is still controversial and remains to be further studied.

TABLE 4 | Results of the multivariate analysis of clinical factors for disease-free survival.

Variable	Multivariate analysis	
	HR (95% CI)	P value
Para-aortic MLNs		
Yes	Reference	
No	0.116 (0.048-0.278)	<0.001
Total point A EQD_{2Gy}		
≥85 Gy	Reference	
<85 Gy	3.296 (1.316-8.253)	0.011
Cervical TLG		
≥113.4	Reference	
<113.4	0.278 (0.121-0.640)	0.003

HR, hazard ratio; CI, confidence interval; MLN, metastatic lymph node; EQD_{2Gy}, equivalent dose at 2 Gy; TLG, total lesion glycolysis.

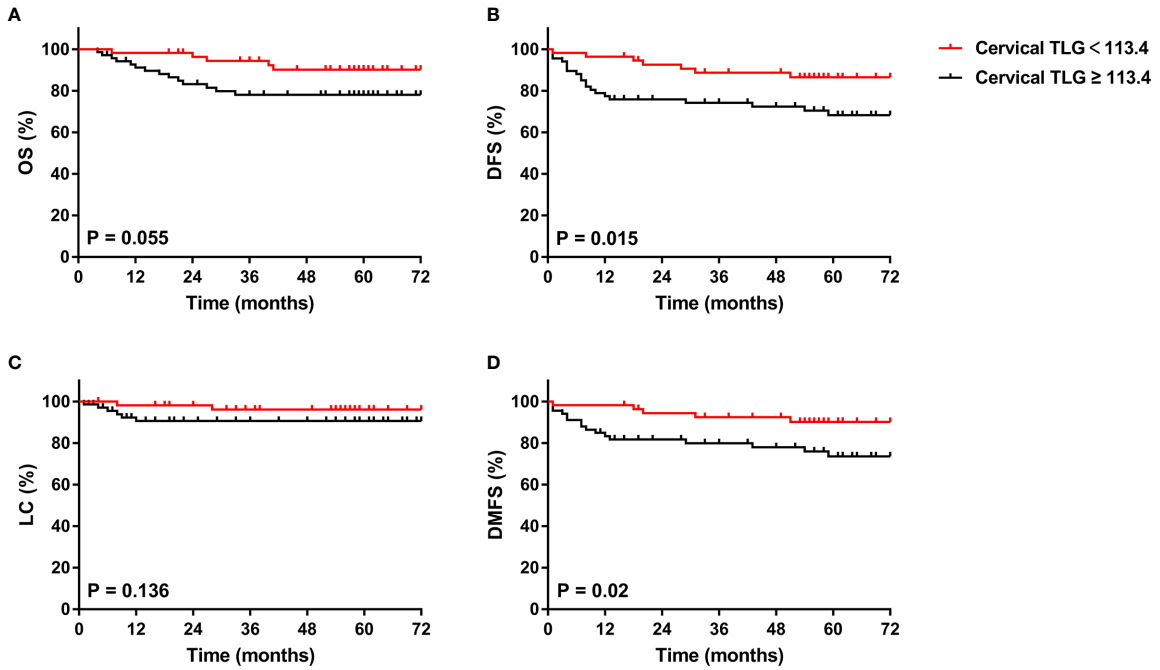

FIGURE 3 | Kaplan-Meier curves of OS **(A)**, DFS **(B)**, LC **(C)**, and DMFS **(D)** of all included patients with cervical cancer for cervical TLG. OS, overall survival; DFS, disease-free survival; LC, local control; DMFS, distant metastasis-free survival.

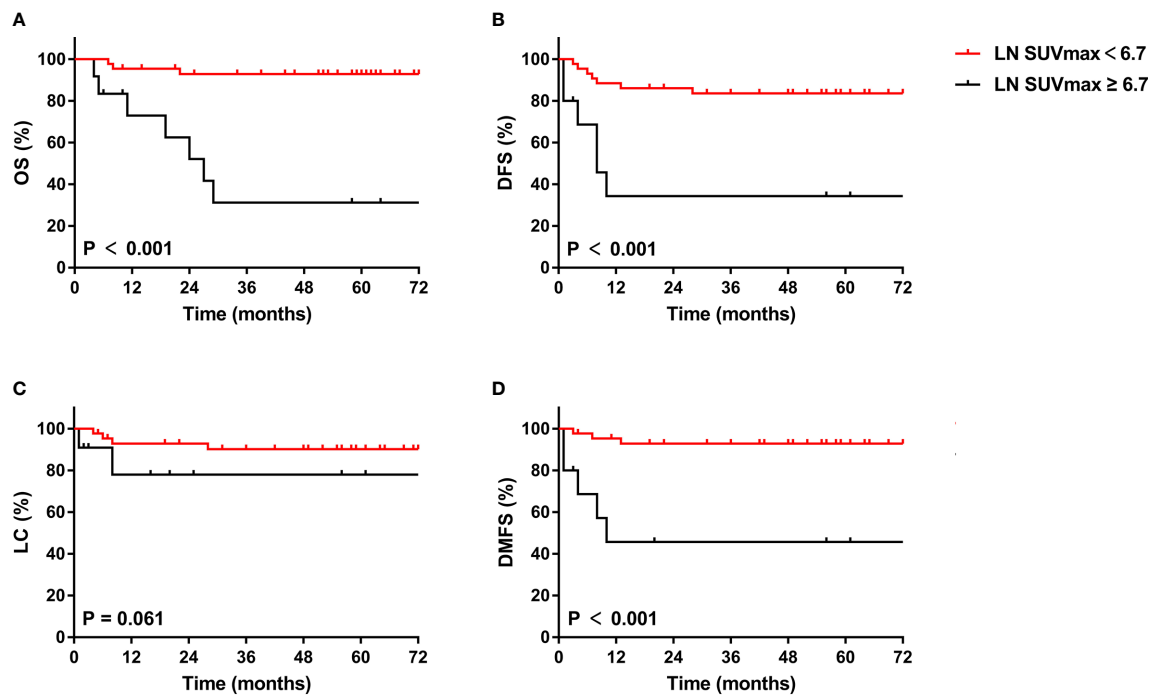

FIGURE 4 | Kaplan-Meier curves of OS **(A)**, DFS **(B)**, LC **(C)**, and DMFS **(D)** of cervical cancer patients with positive LN for LN SUVmax. OS, overall survival; DFS, disease-free survival; LC, local control; DMFS, distant metastasis-free survival.

TABLE 5 | Previous studies regarding pre-treatment metabolic parameters in patients with locally advanced cervical cancer.

Authors (year)	Design	N	FIGO stage	LN+ patients	Treatment	Statistical analysis	Pre-treatment Cervical metabolic parameters associated with survival outcomes	Pre-treatment LN metabolic parameters associated with survival outcomes
Voglimacci et al. (15)	R	93	IB2-IVA	33	CRT	Univariate analysis	SUVmax: OS and RFS	–
						Multivariate analysis	SUVmax: OS	–
Herrera et al. (19)	R	38	IB1-IVA	22	CRT	Univariate analysis	SUVmean: OS, DFS, and LRC TGV: OS, DFS, and LRC	–
						Multivariate analysis	TGV: OS and DFS	–
Leseur et al. (13)	P	53	IB2-IVA	Unknown	CRT/RT	Univariate analysis	MTV: OS and DFS TLG: OS and DFS	–
						Multivariate analysis	MTV: OS and DFS	–
Hong et al. (22)	R	56	IIB-IVA	51	CRT	Univariate analysis	MTV: RFS TLG: RFS	–
						Multivariate analysis	TLG: RFS	–
Martinez et al. (21)	R	125	IB2-IVA	47	CRT	Univariate analysis	MTV: para-aortic LN involvement TLG: para-aortic LN involvement	SUVmean: para-aortic LN involvement SUVmax: para-aortic LN involvement Pelvic LN/Cervical Tumor SUVmax ratio: para-aortic LN involvement MTV: para-aortic LN involvement TLG: para-aortic LN involvement
						Multivariate analysis	MTV: para-aortic LN involvement	–
Sun et al. (26)	R	91	IB1-IVB	26	Sur/Sur+CRT or ChT/CRT	Univariate analysis	SUVmax: OS MTV: OS TLG: OS	–
						Multivariate analysis	MTV: OS	–
Guler et al. (27)	R	129	IB2-IVA	76	CRT	Univariate analysis	SUVmean: OS and DFS SUVmax: OS and DFS MTV: OS and DFS TLG: OS and DFS	–
						Multivariate analysis	–	–
Yoo et al. (28)	R	73	I-IVB	28	Sur/sur+CRT/ CRT/RT/ChT	Univariate analysis	MTV: DFS TLG: DFS	–
						Multivariate analysis	TLG: DFS	–
Liang et al. (29)	R	67	IB-IVA	Unknown	Sur/Sur+CRT or RT/ CRT/ChT	Univariate analysis	Total SUVmax: OS and PFS Total MTV: OS and PFS	
						Multivariate analysis	Total TLG: OS and PFS Total TLG: OS and PFS	
Carpenter et al. (18)	P	30	IB1-IVA	24	CRT	Univariate analysis	Total MTV: OS, DFS, and DM Total TLG: OS and DM	
						Multivariate analysis	–	
Lima et al. (17)	R	82	IIA-IVA	44	CRT	Univariate analysis	Total MTV: response to therapy Total TLG: response to therapy	
						Multivariate analysis	Total MTV: response to therapy	
Our study	R	125	IB-IVA	55	CRT/RT/NAC + CRT or RT	Univariate analysis	TLG: DFS and DMFS	SUVmean: OS SUVmax: OS, DFS, and DMFS MTV: OS, DFS, and DMFS TLG: OS, DFS, and DMFS
						Multivariate analysis	TLG: OS, DFS, and DMFS	SUVmax: OS, DFS, and DMFS MTV: DMFS

N, number of patients; R, retrospective; P, prospective; FIGO, International Federation of Gynecology and Obstetrics; LN, lymph node; NAC, neoadjuvant chemotherapy; CRT, chemoradiotherapy; RT, radiotherapy; ChT, chemotherapy; Sur, surgery; SUV, standardized uptake value; MTV, metabolic tumor volume; TLG, total lesion glycolysis; TGV, tumor glycolytic volume; age, average; SD, standard deviation; OS, overall survival; RFS, relapse-free survival; DFS, disease-free survival; PFS, progression-free survival; LRC, Loco-regional control; DMFS, distant metastasis-free survival; DM, distant metastasis.

MTV represents the volume of metabolically active malignant lesions, which is similar but more accurate than the measurement of tumor size on physical examination and may be significantly correlated to the prognosis of the disease. Leseur et al. (13) demonstrated that cervical MTV calculated with a segmentation of 55% SUVmax from pre-treatment PET/CT was applicable for predicting patient survival outcomes after concurrent chemoradiotherapy for patients with locally advanced cervical cancer. Similarly, Sun et al. (26) also considered that cervical MTV accumulation with a threshold of 40% SUVmax was a critical prognostic factor for cervical cancer patients and should be used to guide oncologists in selecting individualized therapies. Martinez et al. (21) proposed that cervical MTV calculated with a threshold of 40% SUVmax was an independent prognostic biomarker on para-aortic nodal involvement prediction. Guler et al. (27) took the opposite view that the role of using cervical MTV, calculated with the primary cervical tumor equal to or greater than an SUV of 2.5, to predict the prognosis of patients with cervical cancer and to develop patient treatment strategies required further confirmation. In our study, cervical MTV, calculated with a threshold of 40% SUVmax, presented an obvious association with OS but failed to reach the 0.05 significance level for DFS in univariate analysis; however, there was no significant association between cervical MTV and OS in multivariate analysis. For cervical cancer patients with positive LN, LN MTV remained significant correlation with DMFS in multivariate. We considered that the reasons for these different results may be related to the inconsistency in the definition of MTV in different studies. Therefore, we believe that MTV alone is not rigorous enough to predict the prognosis of patients with cervical cancer in the absence of a consistent definition of MTV.

The combination of MTV and TLG is a more resultful prognostic factor that takes into consideration both tumor volume and metabolic activity as crucial parameters of tumor response to treatment. Yoo et al. (28) highlighted that cervical TLG (cut-off, 7600), a volume-based metabolic parameter for primary cervical tumors, was a significant predictor of recurrence in cervical cancer in both univariate analysis and multivariate analysis. Likewise, Liang et al. (29) reported that total TLG was obviously correlated with survival outcomes in patients with locally advanced cervical cancer. Similarly, Carpenter et al. (18) indicated that total TLG measured by ^{18}F-FDG PET/CT was correlated with OS in high-risk cervical cancer patients treated with chemoradiotherapy and brachytherapy. Lima et al. (17) also preliminary suggested that although its p value seems to be below the critical value, pre-treatment total TLG was a significant independent predictor of response to therapy. However, the sample sizes of these studies were less than 100 cases. In our group, we obtained similar results and had a larger sample size. Although TLG confronts the same challenges as MTV, we still believe that the combination of multiple parameters makes predictions more effective.

In our study, we found that distant metastasis in patients with LACC treated with chemoradiotherapy and brachytherapy was a major pattern of treatment failure. This finding was consistent with that of previous research. Importantly, we found that cervical TLG and LN SUVmax were important prognostic factors for OS, DFS, and DMFS. The role of additional chemotherapy included adjuvant chemotherapy or neoadjuvant chemotherapy is still controversial. Dueñas-González et al. (30) investigated 515 patients with locally controlled cervical cancer in a randomized study. The results showed that the 3-year PFS of concurrent chemoradiotherapy following two adjuvant cycles of cisplatin plus gemcitabine was significantly improved compared with standard therapy (74.4% *vs* 65.0%, p=0.029); the same result was found for OS (log-rank p= 0.0224; HR, 0.68; 95% CI, 0.49 to 0.95). However, the intervention group had more grade 3 and 4 toxicities than the control group (p<0.001). Adjuvant chemotherapy has not been widely accepted because further studies are needed to demonstrate the contributions of multiagent chemoradiotherapy and adjuvant chemotherapy to survival outcomes, and toxicity cannot be ignored. Da Costa et al. (31) conducted a randomized phase II trial to evaluate the efficacy and safety of neoadjuvant chemotherapy (NAC) followed by concurrent chemoradiotherapy (CRT) and reported that the addition of NAC with cisplatin and gemcitabine to CRT is not superior to standard CRT alone for LACC. Additionally, a phase III multicenter trial of weekly induction chemotherapy consisting of paclitaxel and carboplatin followed by standard CRT versus standard CRT alone in patients with LACC is undergoing (NCT01566240).

Local recurrence in cervical cancer patients treated with concurrent chemoradiotherapy or radiotherapy was another pattern of treatment failure. MRI-guided adaptive brachytherapy, which plays an important role, increased the radiation dose to the tumor and led to a significant improvement in the local control rate while minimizing the radiation dose delivered to surrounding normal tissues (32, 33). In our study, we also found that for the 22 patients with cervical TLG ≥ 113.4 who experienced treatment failure, disease recurrence occurred in all patients within 5 years after treatment. Thus, active follow-up for at least 5 years is essential. These findings may provide an early signal-individualized intensive therapeutic approach with either adjuvant chemotherapy or MRI-guided adaptive brachytherapy.

The present study demonstrates the value of the metabolic parameters of pre-treatment ^{18}F-FDG PET/CT as prognostic factors in patients with LACC. However, this study has several limitations. Most notably, this is a retrospective study with a small number of included patients and baseline data are easily to be incomplete. Moreover, this study includes a long-time span and changes in the treatment strategies may affect the results. In addition, positive LNs are identified on PET/CT and not by histopathologic verification. We cannot confirm that all FDG-avid LNs are histopathological lymphadenopathies. Finally, recently there are many promising methods such as radiomics, machine learning, and especially deep learning (34, 35). Combining these promising image analysis techniques may have more significant predictive values for the prognosis of cervical cancer. Further prospective randomized clinical trials with a large number of patients are required to evaluate the value of the metabolic parameters in survival outcomes prediction.

CONCLUSION

Pre-treatment cervical and lymph node metabolic parameters were associated with survival outcomes in patients with LACC. In our study, we found that pre-treatment cervical TLG and lymph node SUVmax may be important prognostic biomarkers for OS, DFS, and DMFS in patients with LACC. However, further prospective studies with a large number of patients are required to evaluate the value of the metabolic parameters in survival outcomes prediction.

DISCLOSURE

The abstract of this paper was presented at the 2020 ASTRO Conference name "The Role of Metabolic Parameters of Pre-treatment ^{18}F-FDG PET/CT in Patients with Locally Advanced Cervical Cancer" as a poster presentation with interim findings. The poster's abstract was published in "Poster Q&A Session" in International Journal of Radiation Oncology*Biology*Physics Journal name "The Role of Metabolic Parameters of Pre-treatment ^{18}F-FDG PET/CT in Patients with Locally Advanced Cervical Cancer": Hyperlink with DOI (https://doi.org/10.1016/j.ijrobp.2020.07.1572).

DATA AVAILABILITY STATEMENT

Data used in this study are not publicly available and can only be accessed, with appropriate approvals from data custodians and ethical clearance, from Peking Union Medical College Hospital. Requests to access the datasets should be directed to FZ, zhangfq@pumch.cn.

ETHICS STATEMENT

The studies involving human participants were reviewed and approved by Peking Union Medical College Hospital Ethics Committee [Protocol number S-K 1645]. The patients/participants provided their written informed consent to participate in this study.

AUTHOR CONTRIBUTIONS

FZ and KH contributed to the conception and the design of the study. DW wrote the first draft of the manuscript. WW and XL contributed to the review of literatures. LH and QP organized the database. XR performed the statistical analysis. All authors contributed to the article and approved the submitted version.

FUNDING

This study was funded by the National Key Research and Development Plan, the Ministry of Science and Technology of the People's Republic of China [grant number 2016YFC0105207] and the National Natural Science Foundation of China [grant number U19A2064] and the CAMS Innovation Fund for Medical Sciences (CIFMS) [grant number 2020-I2M-C&T-B-036].

ACKNOWLEDGMENTS

We would like to thank AJE (www.aje.com) for English language editing.

REFERENCES

1. Bray F, Ferlay J, Soerjomataram I, Siegel RL, Torre LA, Jemal A. Global Cancer Statistics 2018: GLOBOCAN Estimates of Incidence and Mortality Worldwide for 36 Cancers in 185 Countries. *CA Cancer J Clin* (2018) 68 (6):394–424. doi: 10.3322/caac.21492
2. Chen W, Zheng R, Baade PD, Zhang S, Zeng H, Bray F, et al. Cancer Statistics in China, 2015. *CA Cancer J Clin* (2016) 66(2):115–32. doi: 10.3322/caac.21338
3. Matsuo K, Machida H, Mandelbaum RS, Konishi I, Mikami M. Validation of the 2018 FIGO Cervical Cancer Staging System. *Gynecol Oncol* (2019) 152 (1):87–93. doi: 10.1016/j.ygyno.2018.10.026
4. Cohen PA, Jhingran A, Oaknin A, Denny L. Cervical Cancer. *Lancet (Lond Engl)* (2019) 393(10167):169–82. doi: 10.1016/S0140-6736(18)32470-X
5. Wang W, Liu X, Hou X, Lian X, Liu Z, Shen J, et al. Posttreatment Squamous Cell Carcinoma Antigen Predicts Treatment Failure in Patients With Cervical Squamous Cell Carcinoma Treated With Concurrent Chemoradiotherapy. *Gynecol Oncol* (2019) 155(2):224–8. doi: 10.1016/j.ygyno.2019.09.003
6. Nicolás I, Saco A, Barnadas E, Marimon L, Rakislova N, Fusté P, et al. Prognostic Implications of Genotyping and P16 Immunostaining in HPV-Positive Tumors of the Uterine Cervix. *Modern Pathol Off J United States Can Acad Pathol Inc* (2019) 33(1):128–37. doi: 10.1038/s41379-019-0360-3
7. Fletcher JW, Djulbegovic B, Soares HP, Siegel BA, Lowe VJ, Lyman GH, et al. Recommendations on the Use of 18F-FDG PET in Oncology. *J Nucl Med* (2008) 49(3):480–508. doi: 10.2967/jnumed.107.047787
8. Cantrell LA, Duska LR. PET Trumps Surgical Staging in Locally Advanced Cervical Cancer. *BJOG Int J Obstet Gynaecol* (2017) 124(7):1095. doi: 10.1111/1471-0528.14595
9. Yoon JW, Kim S, Kim SW, Kim YT, Kang WJ, Nam EJ. PET/CT Response Criteria (European Organization for Research and Treatment of Cancer) Predict Survival Better Than Response Evaluation Criteria in Solid Tumors in Locally Advanced Cervical Cancer Treated With Chemoradiation. *Clin Nucl Med* (2016) 41(9):677–82. doi: 10.1097/RLU.0000000000001269
10. Liu FY, Su TP, Wang CC, Chao A, Chou HH, Chang YC, et al. Roles of Posttherapy F-FDG PET/CT in Patients With Advanced Squamous Cell Carcinoma of the Uterine Cervix Receiving Concurrent Chemoradiotherapy. *Eur J Nucl Med Mol Imaging* (2018) 45(7):1197–204. doi: 10.1007/s00259-018-3957-8
11. Zaucha JM, Chauvie S, Zaucha R, Biggii A, Gallamini A. The Role of PET/CT in the Modern Treatment of Hodgkin Lymphoma. *Cancer Treat Rev* (2019) 77:44–56. doi: 10.1016/j.ctrv.2019.06.002
12. Cremonesi M, Gilardi L, Ferrari ME, Piperno G, Travaini LL, Timmerman R, et al. Role of Interim F-FDG-PET/CT for the Early Prediction of Clinical Outcomes of Non-Small Cell Lung Cancer (NSCLC) During Radiotherapy or Chemo-Radiotherapy. A Systematic Review. *Eur J Nucl Med Mol Imaging* (2017) 44(11):1915–27. doi: 10.1007/s00259-017-3762-9
13. Leseur J, Roman-Jimenez G, Devillers A, Ospina-Arango JD, Williaume D, Castelli J, et al. Pre- and Per-Treatment 18F-FDG PET/CT Parameters to Predict Recurrence and Survival in Cervical Cancer. *Radiotherapy Oncol J Eur Soc Ther Radiol Oncol* (2016) 120(3):512–8. doi: 10.1016/j.radonc.2016.08.008

14. Sarker A, Im HJ, Cheon GJ, Chung HH, Kang KW, Chung JK, et al. Prognostic Implications of the SUVmax of Primary Tumors and Metastatic Lymph Node Measured by 18F-FDG PET in Patients With Uterine Cervical Cancer: A Meta-Analysis. *Clin Nucl Med* (2016) 41(1):34–40. doi: 10.1097/RLU.0000000000001049
15. Voglimacci M, Gabiache E, Lusque A, Ferron G, Ducassou A, Querleu D, et al. Chemoradiotherapy for Locally Advanced Cervix Cancer Without Aortic Lymph Node Involvement: Can We Consider Metabolic Parameters of Pretherapeutic FDG-PET/CT for Treatment Tailoring? *Eur J Nucl Med Mol Imaging* (2019) 46(7):1551–9. doi: 10.1007/s00259-018-4219-5
16. Rufini V, Collarino A, Calcagni ML, Meduri GM, Fuoco V, Pasciuto T, et al. The Role of F-FDG-PET/CT in Predicting the Histopathological Response in Locally Advanced Cervical Carcinoma Treated by Chemo-Radiotherapy Followed by Radical Surgery: A Prospective Study. *Eur J Nucl Med Mol Imaging* (2019) 47(5):1228–38. doi: 10.1007/s00259-019-04436-y
17. Lima GM, Matti A, Vara G, Dondi G, Naselli N, De Crescenzo EM, et al. Prognostic Value of Posttreatment F-FDG PET/CT and Predictors of Metabolic Response to Therapy in Patients With Locally Advanced Cervical Cancer Treated With Concomitant Chemoradiation Therapy: An Analysis of Intensity- and Volume-Based PET Parameters. *Eur J Nucl Med Mol Imaging* (2018) 45(12):2139–46. doi: 10.1007/s00259-018-4077-1
18. Carpenter DJ, Jacobs CD, Wong TZ, Craciunescu O, Chino JP. Changes on Midchemoradiation Therapy Fluorodeoxyglucose Positron Emission Tomography for Cervical Cancer Are Associated With Prognosis. *Int J Radiat Oncol Biol Phys* (2019) 105(2):356–66. doi: 10.1016/j.ijrobp.2019.06.2506
19. Herrera FG, Breuneval T, Prior JO, Bourhis J, Ozsahin M. [F-18]FDG-PET/CT Metabolic Parameters as Useful Prognostic Factors in Cervical Cancer Patients Treated With Chemo-Radiotherapy. *Radiat Oncol* (2016) 11(43):1–11. doi: 10.1186/s13014-016-0614-x
20. Akkas BE, Demirel BB, Dizman A, Vural GU. Do Clinical Characteristics and Metabolic Markers Detected on Positron Emission Tomography/Computerized Tomography Associate With Persistent Disease in Patients With in-Operable Cervical Cancer? *Ann Nucl Med* (2013) 27(8):756–63. doi: 10.1007/s12149-013-0745-1
21. Martinez A, Voglimacci M, Lusque A, Ducassou A, Gladieff L, Dupuis N, et al. Tumour and Pelvic Lymph Node Metabolic Activity on FDG-PET/CT to Stratify Patients for Para-Aortic Surgical Staging in Locally Advanced Cervical Cancer. *Eur J Nucl Med Mol Imaging* (2020) 47(5):1252–60. doi: 10.1007/s00259-019-04659-z
22. Hong JH, Jung US, Min KJ, Lee JK, Kim S, Eo JS. Prognostic Value of Total Lesion Glycolysis Measured by 18F-FDG PET/CT in Patients With Locally Advanced Cervical Cancer. *Nucl Med Commun* (2016) 37(8):843–8. doi: 10.1097/MNM.0000000000000516
23. Wong KP, Sha W, Zhang X, Huang SC. Effects of Administration Route, Dietary Condition, and Blood Glucose Level on Kinetics and Uptake of 18F-FDG in Mice. *J Nucl Med* (2011) 52(5):800–7. doi: 10.2967/jnumed.110.085092
24. Lowe VJ, DeLong DM, Hoffman JM, Coleman RE. Optimum Scanning Protocol for FDG-PET Evaluation of Pulmonary Malignancy. *J Nucl Med* (1995) 36(5):883–7.
25. Jaskowiak CJ, Bianco JA, Perlman SB, Fine JP. Influence of Reconstruction Iterations on 18F-FDG PET/CT Standardized Uptake Values. *J Nucl Med* (2005) 46(3):424–8.
26. Sun Y, Lu P, Yu L. The Volume-Metabolic Combined Parameters From (18)F-FDG PET/CT May Help Predict the Outcomes of Cervical Carcinoma. *Acad Radiol* (2016) 23(5):605–10. doi: 10.1016/j.acra.2016.01.001
27. Guler OC, Torun N, Yildirim BA, Onal C. Pretreatment Metabolic Tumour Volume and Total Lesion Glycolysis Are Not Independent Prognosticators for Locally Advanced Cervical Cancer Patients Treated With Chemoradiotherapy. *Br J Radiol* (2018) 91(1084):20170552. doi: 10.1259/bjr.20170552
28. Yoo J, Choi JY, Moon SH, Bae DS, Park SB, Choe YS, et al. Prognostic Significance of Volume-Based Metabolic Parameters in Uterine Cervical Cancer Determined Using 18F-Fluorodeoxyglucose Positron Emission Tomography. *Int J Gynecol Cancer Off J Int Gynecol Cancer Soc* (2012) 22(7):1226–33. doi: 10.1097/IGC.0b013e318260a905
29. Liang Y, Li X, Wan H, Fang Y, Zheng R, Zhang W, et al. Prognostic Value of Volume-Based Metabolic Parameters Obtained by 18F-FDG-PET/CT in Patients With Locally Advanced Squamous Cell Cervical Carcinoma. *J Comput Assisted Tomogr* (2018) 42(3):429–34. doi: 10.1097/RCT.0000000000000708
30. Duenas-Gonzalez A, Zarba JJ, Patel F, Alcedo JC, Beslija S, Casanova L, et al. Open-Label, Randomized Study Comparing Concurrent Gemcitabine Plus Cisplatin and Radiation Followed by Adjuvant Gemcitabine and Cisplatin Versus Concurrent Cisplatin and Radiation in Patients With Stage IIB to IVA Carcinoma of the Cervix. *J Clin Oncol* (2011) 29(13):1678–85. doi: 10.1200/JCO.2009.25.9663
31. da Costa SCS, Bonadio RC, Gabrielli FCG, Aranha AS, Dias Genta MLN, Miranda VC, et al. Neoadjuvant Chemotherapy With Cisplatin and Gemcitabine Followed by Chemoradiation Versus Chemoradiation for Locally Advanced Cervical Cancer: A Randomized Phase II Trial. *J Clin Oncol* (2019) 37(33):3124–31. doi: 10.1200/JCO.19.00674
32. Mahantshetty U, Krishnatry R, Hande V, Jamema S, Ghadi Y, Engineer R, et al. Magnetic Resonance Image Guided Adaptive Brachytherapy in Locally Advanced Cervical Cancer: An Experience From a Tertiary Cancer Center in a Low and Middle Income Countries Setting. *Int J Radiat Oncol Biol Phys* (2017) 99(3):608–17. doi: 10.1016/j.ijrobp.2017.06.010
33. Serban M, Kirisits C, Potter R, de Leeuw A, Nkiwane K, Dumas I, et al. Isodose Surface Volumes in Cervix Cancer Brachytherapy: Change of Practice From Standard (Point A) to Individualized Image Guided Adaptive (EMBRACE I) Brachytherapy. *Radiother Oncol J Eur Soc Ther Radiol Oncol* (2018) 129(3):567–74. doi: 10.1016/j.radonc.2018.09.002
34. Lucia F, Visvikis D, Desseroit MC, Miranda O, Malhaire JP, Robin P, et al. Prediction of Outcome Using Pretreatment (18)F-FDG PET/CT and MRI Radiomics in Locally Advanced Cervical Cancer Treated With Chemoradiotherapy. *Eur J Nucl Med Mol Imaging* (2018) 45(5):768–86. doi: 10.1007/s00259-017-3898-7
35. Ferreira M, Lovinfosse P, Hermesse J, Decuypere M, Rousseau C, Lucia F, et al. [(18)F]FDG PET Radiomics to Predict Disease-Free Survival in Cervical Cancer: A Multi-Scanner/Center Study With External Validation. *Eur J Nucl Med Mol Imaging* (2021). doi: 10.1007/s00259-021-05303-5

Conflict of Interest: The authors declare that the research was conducted in the absence of any commercial or financial relationships that could be construed as a potential conflict of interest.

Publisher's Note: All claims expressed in this article are solely those of the authors and do not necessarily represent those of their affiliated organizations, or those of the publisher, the editors and the reviewers. Any product that may be evaluated in this article, or claim that may be made by its manufacturer, is not guaranteed or endorsed by the publisher.

frontiers | Frontiers in Oncology

TYPE Original Research
PUBLISHED 19 July 2022
DOI 10.3389/fonc.2022.943703

OPEN ACCESS

EDITED BY
John Varlotto,
Marshall University, United States

REVIEWED BY
Rakesh Kapoor,
Post Graduate Institute of Medical Education and Research (PGIMER), India
Fiori Alite,
Geisinger Commonwealth School of Medicine, United States

*CORRESPONDENCE
Tiejun Wang
drwangtiejun@yeah.net

SPECIALTY SECTION
This article was submitted to Radiation Oncology, a section of the journal Frontiers in Oncology

RECEIVED 14 May 2022
ACCEPTED 27 June 2022
PUBLISHED 19 July 2022

CITATION
Ren X, Fu Y, Liu Z, Lin X, Qiu L, Li Y, Li H, Bai Y and Wang T (2022) Image-guided interstitial brachytherapy for recurrent cervical cancer after radiotherapy: A single institution experience.
Front. Oncol. 12:943703.
doi: 10.3389/fonc.2022.943703

Image-guided interstitial brachytherapy for recurrent cervical cancer after radiotherapy: A single institution experience

Xiaojun Ren[1], Yingli Fu[2], Zhongshan Liu[1], Xia Lin[1], Ling Qiu[1], Yunfeng Li[1], Hanyang Li[1], Yuqi Bai[1] and Tiejun Wang[1*]

[1]Department of Radiation Oncology, The Second Hospital of Jilin University, Changchun, China, [2]Department of Clinical Epidemiology, The First Hospital of Jilin University, Changchun, China

Purpose: The aim of this study is to evaluate the efficacy and toxicity of image-guided high-dose rate (HDR) interstitial brachytherapy (ISBT) for the reirradiation of cervical cancer within a previously irradiated area.

Methods and materials: Twenty-three consecutive patients with cervical cancer were reirradiated with curative intent using brachytherapy (BT) with or without external beam irradiation. The median biologically equivalent dose in 2-Gy fractions (EQD2) for reirradiation was 64.0 Gy (range: 31.3–95.1 Gy), and the median cumulative EQD2 (for primary treatment and reirradiation) was 152.4 Gy (range: 97.8–200.9 Gy). The average clinical target volume was 82.9 cm^3 (range: 26.9–208.3 cm^3), and the median treatment-free interval (TFI) was 13 months (range: 3–93 months).

Results: The median follow-up time was 19 months (range: 2–59 months). The complete response rate after reirradiation was 56.5%. The 1-, 2- 3-, and 4-year post-relapse survival (PRS) rates were 65.2%, 43.5%, 33.8%, and 27.1%, respectively. The median reirradiation EQD2 D2cc of rectum and bladder was 39.5 Gy (range = 14.6–96.2 Gy) and 52.1 Gy (range = 29.1–114.2 Gy). The median cumulative EQD2 D2cc of rectum and bladder was 115.0 Gy (range = 84.4–189.3 Gy) and 130.5 Gy (range = 95.5–173.5 Gy). During follow-up, nine (39.1%) patients had experienced grade 3 or 4 late toxicities. Grade ≥3 rectal toxicity occurred in three patients (13.0%). Grade ≥3 urinary toxicity occurred in five patients (21.7%). One patient (4.3%) had both grade ≥3 urinary and rectal toxicity. Tumor volume, TFI, tumor invasion organ number, and local control were significant prognostic factors adversely affecting OS.

10.3389/fonc.2022.943703

Conclusions: For recurrent cervical cancer after radiotherapy, reirradiation of HDR-ISBT is feasible, even if the local tumor invasion is large, with a good chance of survival and acceptable side effects.

KEYWORDS

reirradiation (re-RT), recurrence, cervical cancer, brachytherapy, interstitial

Introduction

Cervical cancer is the fourth most common malignancy and the fourth leading cancer-related death in women worldwide (1). The recurrence rates of patients with IIA, IIB, IIIA, IIIB, IVA, and IVB stage cervical cancer were 21.2%, 27.8%, 40.9%, 44.7%, 64.3%, and 73.6%, respectively (2). A previous study reported that the recurrence rates of patients with stage IB, IIA, and IIB cervical cancer treated only by radiotherapy were 10%, 17%, and 23%, and the rates of patients treated by radiotherapy plus surgery respectively were 14%, 20%, and 29%, respectively (3). The 5-year survival rate for patients with cervical cancer who relapsed after radical surgery or radiotherapy was only 3.2%~13% (4, 5). The treatment of recurrent cervical cancer is challenging and mainly depends on the previous treatment and the site and extent of recurrence (2).

The retreatment of recurrent cervical cancer that develops in a previously irradiated field is a complex challenge for gynecologic oncologists (6). Surgery, which exhibits 5-year overall survival rates higher than 30%, could be a curative treatment option for patients who meet strict indications. However, surgery has been employed carefully because of a high rate of complications and positive surgical margins (7–10). In recent years, with the progress of radiotherapy technology and the development of computed tomography (CT)/magnetic resonance imaging (MRI)–guided brachytherapy (BT), the reirradiation of recurrent cervical cancer after radiotherapy has achieved a good curative effect, and the incidence of serious adverse reactions is low (11–15). Moreover, reirradiation can preserve the structure and function of the organ and thus improve the quality of life of the patients. Hence, reirradiation could be another potentially curative treatment option for recurrent cervical cancer after radiotherapy. However, there are few reports of reirradiation in patients with cervical cancer, and all of them are small sample studies. In addition, there are no recommendations in the literature for the reirradiation dose of interstitial brachytherapy (ISBT), either as a treatment alone or in combination with external beam radiation therapy (EBRT). This retrospective study aimed to evaluate the effectiveness and toxicity of high-dose rate (HDR)–ISBT as retreatment to develop clinical practice guidelines.

Materials and methods

Patients

A review of the database in the department of radiotherapy in the Second Hospital of Jilin University identified 23 patients who received HDR-BT reirradiation between November 2015 and August 2020 for a local recurrence (LR) occur within a previously treated volume, following radical or adjuvant RT for cervical cancer. Fifteen patients were not suitable for pelvic exenteration, and the others refused surgery for fear of surgical trauma. Twelve patients had LR identified by pathological examination, and the rest had LR confirmed by pelvic MRI and positron emission tomography (PET)/CT. Twelve patients were initially treated at other hospitals, and detailed doses of organs at risk (OARs) could not be obtained. When brachytherapy is used, radiation doses to the rectum and bladder should be limited to 65% and 75% of the tumor dose, respectively (16). The limit of the minimum dose delivered to 2 cm^3 (D2cc) rectum and sigmoid colon was 70–75 Gy, and that of the bladder was 90 Gy (17). For patients who were unable to obtain an accurate dose from the bladder and rectum during primary brachytherapy, we uniformly calculated the D2cc at 70% of the prescribed dose.

External beam radiation therapy

During reirradiation, the tumor location of some patients was too far from the vulva, leading to the use of external radiation therapy when the metal needles could not reach. Conformal EBRT was delivered to the tumors with a 0.7-cm margin using high-energy 6-MV photons with 1.8- to 2-Gy fractions to total doses of 30.0–50.4 Gy. The local tumor is the target of EBRT. The medical linear accelerator that we used is Varian Varianix-4702.The radiotherapy positioning system was Varian Eclipse 13.5. One hundred percent of the prescribed dose of EBRT was considered while calculating doses delivered to the tumor and the OARs.

High-dose rate interstitial brachytherapy

HDR-ISBT–based reirradiation was performed using three-dimensional (3D) planning in all patients. All the patients have pelvic MRI before brachytherapy. The Ir^{192} HDR brachytherapy machine, Oncentra brachytherapy planning system, and metal needle implantation are from Elekta, Sweden. The HDR ISBT was performed twice a week, 4–7 fractions in total, and 6–7 Gy for each fraction. Because of the large tumor volume and/or wide scope of invasion, ISBT was performed by freehand metal needle placement under CT guidance, resulting in excellent dose coverage. The patient underwent lumbar anesthesia in the operating room. After receiving anesthetic drugs, the patient was transferred to the large-caliber CT room dedicated to the Radiotherapy Department through a transfer bed. The anesthesiologist accompanied the patients all time to monitor vital signs. First, an intrauterine tandem was implanted in the uterine cavity. Then, some parallel and oblique metal needles (length of 18 cm, diameter of 1.3 mm, Elekta) were inserted into the tumor and lateral extensions at different degrees angled to the vagina at a width and depth of approximately 10 mm as initial implantation. The insertion position and number of these oblique needles were decided by T2-weighted MRI (Figure 1) and gynecological examination. Vaginal packing with gauze was used to push away the rectum and bladder. Finally, through multiple CT scans, we repeatedly adjusted the direction and depth of the needles until all the needles were evenly distributed within the tumor. In the treatment of all patients, including those with rectal and bladder involvement, the final position of the needle should be as far beyond the depth of invasion as possible, 0–1 cm, to obtain good target volume and dose distribution of the paddle in subsequent treatment plans (Figure 2).

Dose-volume-histograms analysis

3D plans were reported in high-risk clinical target volume (HR-CTV), defined as the cervix and the involved parametrium, vagina, vulva, urethra, pelvic wall, rectum, and bladder. The following dose–volume parameters were calculated for the HR-CTV and OARs (bladder and rectum): the percentage of the CTV receiving 100% of the prescribed dose (V100) and the dose that covered 90%, 98%, and 100% of the target volume (D90, D98, and D100, respectively). We calculated the D2cc of the rectum and bladder. The total doses (EBRT and HDR-BT) were recalculated as the biologically equivalent doses to 2-Gy fractions (EQD2) using the following equation: $EQD2 = nd\ (d + \alpha/\beta/2\ Gy + \alpha/\beta)$, where n = the number of fractions, d = dose (Gy) per fraction (assuming $\alpha/\beta = 10$ Gy for tumor control, and $\alpha/\beta = 3$ Gy for late normal tissue damage). For primary BT, the dose delivered by the two-dimensional (2D) treatment plan was calculated at point A and the rectum and bladder reference points, based on International Commission on Radiation Units and Measurements (ICRU)89 report (18).

Analysis of curative effect and toxicity after reirradiation

All time intervals were calculated from the final day of treatment. The tumor response was assessed 2 months after the reirradiation. The complete response (CR) was defined as the disappearance of the tumor, and the partial response (PR) was defined as a reduction of at least 30% in the sum of the maximum diameters of the tumor. Stable disease (SD) was defined as when none of the above conditions is applicable. Local control (LC) was defined as the length of time from the

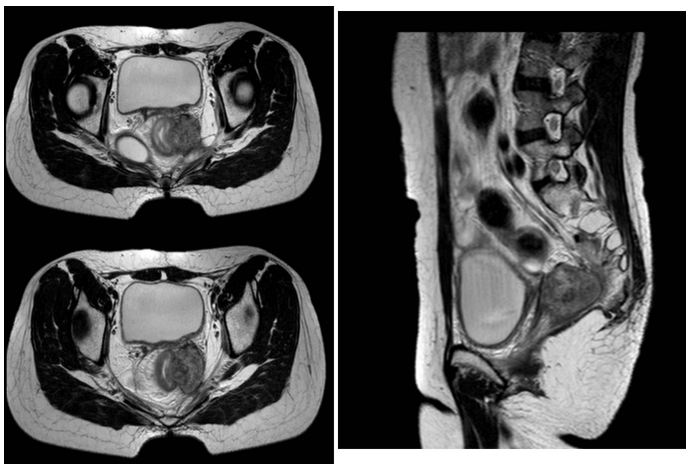

FIGURE 1
Pelvic MRI before reirradiation, recurrent tumors are shown in red circles.

FIGURE 2
Distribution of needles and dose curves.

end of treatment to LR. The post-relapse survival (PRS) was calculated from the date of relapse diagnosis to the date of death for disease or the date of the last follow-up.

The bladder and rectum complications were scored using the Radiation Therapy Oncology Group Acute and Late Radiation Morbidity Scoring Criteria (19).

Statistical analysis

PRS curves were derived from Kaplan–Meier estimates and compared using the log-rank test. The influence of potential prognostic factors on the risk of failure was assessed using a Cox model. *P*-values<0.05 were considered statistically significant.

Results

Patient characteristics

Table 1 listed the detailed characteristics of patients. The median age of the patients at diagnosis was 50.5 years (range = 24–68 years). According to the International Federation of Gynecology and Obstetrics (FIGO) Cervical Cancer Staging 2009 standard (20), the clinical stage at the initial diagnosis was stages I to II in 17 patients and stages III to IV in six patients. Twenty-one patients had SCC, and two patients displayed non-SCC histologic finding. Seventeen (73.9%) patients had been treated with definitive radiotherapy and others had been treated with postoperative radiotherapy in primary radiotherapy. The median EQD2 calculated for Primary EBRT + BT was 92.0 Gy (range = 31.3–109.7 Gy). The median treatment-free interval (TFI) (between the end of primary radiotherapy and reirradiation) was 13 months (range = 3–93 months). Eleven patients (47.8%) were diagnosed with recurrence within 12 months of the initial radiotherapy. All patients had a performance status of 0 to 1, and the median (mean) tumor diameter at the time of recurrence diagnosis was 51.0(56.6) mm. the median (mean) HR-CTV at the time of reirradiation was 70.8 (82.9) cm^3. Eleven patients had the number of tumor invasion organ including bladder, rectum, and pelvic wall greater than 1. The tumors of the other 12 patients did not invade the bladder, rectum, or pelvic wall.

Treatment outcome

There were 13 patients' tumors that reached CR after radiotherapy, nine had PR, and one had SD (Table 2). The CR rate after reirradiation was 56.5% (13 of 23). The median follow-up time was 19 months (range = 2–59months). Six patients are alive with no evidence of disease (NED), from 33 to 59 months post-treatment (median = 48 months). One patient is alive with disease (AWD), receiving chemotherapy. Sixteen patients died. No patients were lost to follow-up. Eight patients received HDR-ISBT combined with EBRT reirradiation. Fifteen patients received HDR-ISBT alone (Table 2).

The median EQD2 calculated for reirradiation was 64.0 Gy (range = 31.3–95.1 Gy), and the median cumulative EQD2 for primary treatment and reirradiation was 152.4 Gy (range = 97.8–200.9 Gy) (Table 2). The median D90, D98, and D100 were 37.8, 29.5, and 23.7 Gy in the re-radiotherapy planning, respectively. The median V100 was 93.4% (Table 2).

Tumor volume before reirradiation was found in six of the seven surviving patients was<80 cm^3. The tumor invasion in 12 patients did not include the rectum, bladder, and pelvic wall, and the average follow-up time was 31.9 months (9–59 months). Five of them were NED, one was AWD, five were dead of oncologic

TABLE 1 Baseline characteristics of involved patients (N = 23).

Characteristics	No. patients
Age (years)	
Median (range)	50.5 (24–68)
≤50	10 (43.5%)
>50	13 (56.5%)
FIGO stage*	
I–II	17 (73.9%)
III–IV	6 (26.1%)
Histologic finding	
SCC	21 (91.3%)
Non-SCC	2 (8.7%)
Prior radiotherapy	
Definitive	17 (73.9%)
Postoperative	6 (26.1%)
Primary EBRT + BT EQD2 (Gy)	
Median (range)	92.0 (31.3–109.7)
TFI(months)	
Median (range)	14 (3–93)
TFI ≤ 12	11 (47.8%)
TFI > 12	12 (52.2%)
Performance status	
0–1	23 (100%)
2–3	0 (0%)
Maximum tumor diameter (mm)	
Median (range)	51 (29–92)
≤50	11 (47.8%)
>50	12 (52.2%)
HR-CTV(cm^3)	
Median (range)	70.8 (20.3–208.3)
≤80	12 (52.2%)
>80	11 (47.8%)
Tumor invasion organ number (bladder, rectum, and pelvic wall)	
0	12 (52.2%)
≥1	11 (47.8%)

*Clinical stage at the time of the initial diagnosis.

disease (DOD), and one died due to cardiac sudden death. A total of 13 patients had CR in remission status after therapy, and the average follow-up time was 31.8 months. Among them, six were NED, one was AWD, three died due to LR or distant metastasis, two died due to complications of treatment, and one died due to cardiac sudden death. The treatment characteristics are detailed in (Supplemental Table 1).

The 1-, 2-, 3-, and 4-year PRS rates were 65.2% (95% CI = 42.3%–80.8%), 43.5% (95% CI = 23.3%–62.1%), 33.8% (95% CI = 15.6%–53.1%), and 27.1% (95% CI = 10.2%–47.3%), respectively. The survival curve of PRS after re-radiotherapy is shown in Figure 3.

Dosage delivered to OARs and toxicity

The median primary RT EQD2 D2cc of rectum and bladder was 73.5 Gy (range = 22.8–93.1 Gy) and 80.2 Gy (range = 22.8–106.0 Gy) (Table 3). The median reirradiation EQD2 D2cc of rectum and bladder was 39.5 Gy (range = 14.6–96.2 Gy) and 52.1 Gy (range = 29.1–114.2 Gy), respectively. The median cumulative EQD2 D2cc of rectum and bladder was 115.0 Gy (range = 84.4–189.3 Gy) and 130.5 Gy (range = 95.5–173.5 Gy), respectively. During follow-up, nine (39.1%) patients had experienced grade 3 or 4 late toxicities (Table 3). Grade ≥3 rectal toxicity occurred in three patients (13.0%). Grade ≥3 urinary toxicity occurred in five patients (21.7%). One patient (4.3%) had both grade ≥3 urinary and rectal toxicity. The dosimetric parameters of the OARs and radiation-related toxic effects are provided in Supplemental Table 2.

Predictors of survival after reirradiation

We performed Cox model analysis to identify independent predictors of treatment outcome in patients receiving re-radiotherapy (Table 4 and Figures 4A–D). Cox model analysis identified four independent prognostic factors that predicted good outcomes: Tumor volume (P = 0.008, Table 4 and Figure 4A), TFI (P = 0.024, Table 4 and Figure 4B), tumor invasion organ number (P = 0.009, Table 4 and Figure 4C), and LC (P = 0.001, Table 4 and Figure 4D).

The statistically significant factors, including tumor volume, TFI, tumor invasion organ number, and LC, were included in the multivariate Cox risk ratio model. The results showed that, after adjusting for TFI, tumor invasion organ number and LC were the independent factors for patient survival. The risk of death in patients with TFI≦12 months was 4.694 times higher than patients with >12 months (HR = 4.694, 95% CI = 1.445–15.247, Table 4 and Figure 4B). The risk of death in patients with tumor invasion organ number≥1 was 3.708 times higher than patients with = 0 (HR = 3.708, 95% CI = 1.048–13.116, Table 4 and Figure 4C). The risk of death in patients with no-CR was 3.617 times higher than patients with CR (HR = 3.617, 95% CI =1.155–11.330, Table 4 and Figure 4D).

Discussion

For patients with recurrent cervical cancer in the original irradiation field, the possible efficacy and potential toxicity should be considered during treatment. Previous studies have shown that the 5-year OS of patients with recurrent cervical cancer after radiotherapy is only 1% if they do not receive any treatments (21).

TABLE 2 Treatment outcomes of involved patients.

Clinical Outcomes		No. of Patients
Local control	CR	13 (56.5%)
	PR	9 (39.1%)
	SD	1 (4.3%)
Post-relapse survival (months)	Median (range)	19 (2–59)
Reirradiation modality	EBRT +ISBT	8 (34.8%)
	Only ISBT	15 (65.2%)
Reirradiation EBRT + BT EQD2 (Gy)	Median (range)	64.0 (31.3–95.1)
Reirradiation D90 (Gy)	Median (range)	37.8 (13.8–56.6)
Reirradiation D98 (Gy)	Median (range)	29.5 (10.9–47.1)
Reirradiation D100 (Gy)	Median (range)	23.7 (7.4–35.5)
Reirradiation V100 (%)	Median (range)	93.4 (78.4–98.4)
Primary RT + Reirradiation EQD2 (Gy)	Median (range)	152.4 (97.8–200.9)

ISBT can generate favorable LC in recurrent tumors that cannot be adequately covered by ICBT (22). Recent reports have shown that HDR-ISBT re-radiotherapy has good disease control and acceptable complications (11–15). Therefore, ISBT had been applied to patients with recurrent cervical cancer in our department. In our study, the 1-, 2-, 3-, and 4-year PRS rates were 65.2%, 43.5%, 33.8%, and 27.1%, respectively, and the median dose of EQD2 for reirradiation was 64 Gy. The CR rate after reirradiation was 56.5%. Nine (39.1%) patients had experienced grade 3 or 4 late toxicities. Grade ≥3 rectal toxicity occurred in three patients (13.0%). Grade ≥3 urinary toxicity occurred in five patients (21.7%). One patient (4.3%) had both grade ≥3 urinary and rectal toxicity. The doses used in our study were comparable to those in the current literature (11–14). Some of the toxicity symptoms are associated with a large recurrence of the rectum, bladder, urethra, etc. Because of its wide recurrence range and wide irradiation range, the damage of adjacent normal tissues is serious. In addition, some patients failed to achieve CR after treatment, and the corresponding toxic symptoms may be related to tumor control or HDR dose, which is difficult to identify. Therefore, we reported all the toxic symptoms of the patients and counted them as the toxic reactions caused by the treatment, which resulted in more toxic reactions in our study than in other reports. It is difficult to compare these results because the study cohorts were heterogeneous in terms of histopathology, tumor size, location of recurrence, treatment method, and RT schedules.

The main difficulty with re-radiotherapy is that the surrounding normal tissue is near the tumor but cannot receive high doses of radiation. A recent study showed that ISBT could be administered by injecting biodegradable hydrogels to increase the distance between the target and adjacent normal tissue, thereby reducing normal tissue exposure and therapeutic toxicity (23).

In our retrospective study, we found that, for patients with LR of gynecological tumors after radiotherapy, the use of HDR ISBT can cure the patient with acceptable side effects. In particular, patients with small local tumor volume and uninvaded pelvic wall, rectum, and bladder have a better chance of cure. If the local tumor reaches CR after treatment, then a good prognosis is suggested. However, there are no

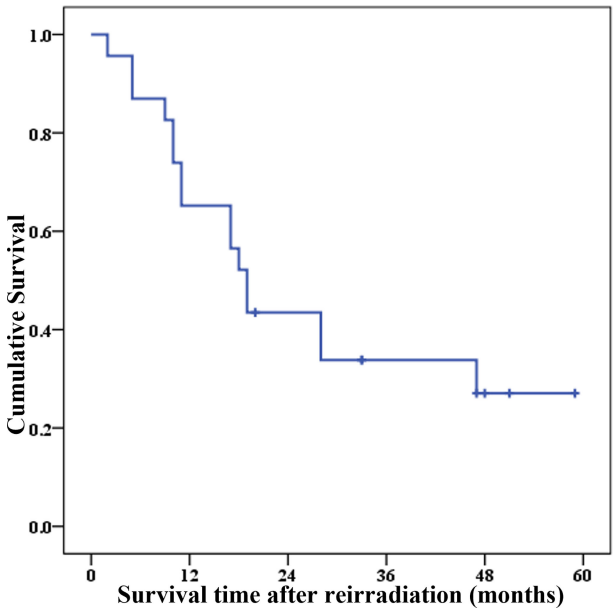

FIGURE 3
Survival curve of PRS after reirradiation in 23 patients with recurrent cervical cancer.

TABLE 3 Dosage delivered to OARs and toxicity.

Dosage and Toxicity		No. of Patients
Severe late toxicity	Patients with grade 3/4 toxicities	9 (39.1%)
Primary RT dose delivered to bladder EQD2 (Gy)	Median (range)	80.2 (22.8–106.0)
Reirradiation dose delivered to bladder EQD2 (Gy)	Median (range)	52.1 (29.1–114.2)
Cumulative dose delivered to the bladder after primary RT and reirradiation EQD2 (Gy)	Median (range)	130.5 (95.5–173.5)
Grade of late radiation damage to the bladder	<3	17 (73.9%)
	≥3	6(26.1%)
Primary RT dose delivered to rectum EQD2 (Gy)	Median (range)	73.5 (22.8–93.1)
Reirradiation dose delivered to rectum EQD2 (Gy)	Median (range)	39.5 (14.6–96.2)
Cumulative dose delivered to the rectum after primary RT and reirradiation EQD2 (Gy)	Median (range)	115.0 (84.4–189.3)
Grade of late radiation damage to the rectum	<3	19 (82.6%)
	≥3	4 (17.4%)

published guidelines for the dose and normal tissue limits of relapsing pelvic radiotherapy for cervical cancer. Current literature reports are all small sample studies.

Liu et al. (24) reported that freehand ISBT resulted in D90 HR-CTV of 87 Gy or greater in 85.7% of patients; however, D90 HR-CTV of ICBT was 87 Gy or greater only in 6.7% of the cases, which are bulky tumors and/or parametrial extension (tumor size>5 cm) after external beam radiotherapy. In our study, the average CTV was 88.5 cm^3 (range: 26.9–208.3 cm^3), and the median percentage volume of 100% prescription dose was 93.1%. This result suggests that freehand ISBT has better dose–volume histogram parameters for large volume tumors than conventional ICBT.

Permanent interstitial brachytherapy (PIB) is also a viable and potentially durable treatment modality that can be used to treat recurrent pelvic malignancies in the field of previous irradiation. Feddock et al. (25) reported on PIB for the treatment of recurrent pelvic malignancies with ^{131}Cs and ^{198}Au as an isotope of PIB. The 2-year success rate for reirradiation using PIB was 67.3%. Grade 3 to 4 toxicities were observed in eight patients (16.7%). However, the limitation in this series is the fact that majority of recurrences in this series were small volume, with an area of 6 cm^3. In our study, the average CTV was 88.5 cm^3.

To gain some insight from patients who benefited from re-radiotherapy, we performed a retrospective analysis of disease-free patients after treatment. Only one of the six NED patients involved the rectum and pelvic wall, and all of the remaining patients excluded the bladder, rectum, and pelvic wall. Additional external radiotherapy was used in only one patient with rectum and pelvic wall involvement, whereas brachytherapy was used in all of the patients. The TFI was 13.8 months (7–23 months), the mean tumor volume was 77.5cm^3 (39.7–136.9cm^3), the mean EQD2 of reirradiation was 69.8 Gy (51.3–95.1 Gy), the mean EQD2 calculated for primary RT and reirradiation was 157.3 Gy (143.3–184.4 Gy), and the mean follow-up time was 32 months (20–46 months). One patient underwent transverse colostomy prior to reirradiation for rectal invasion. Hence, the rectal dose of

TABLE 4 Univariate analysis of survival after reirradiation.

Characteristics		N (%)	Median OS	Log-Rank *P*
Tumor volume	≤80 cm^3	12 (50%)	47	0.008
	>80 cm^3	11 (90.9%)	11	
Treatment-free interval	≤12 m	11 (91.9%)	11	0.024
	>12 m	12 (50%)	47	
Tumor diameter	≤5cm	11 (54.5%)	47	0.197
	>5 cm	12 (83.3%)	17	
Tumor invasion organ number (bladder, rectum, and pelvic wall)	0	12 (50%)	47	0.009
	≥1	11 (90.9%)	17	
Reirradiation dose	≤64 Gy	12 (83.3%)	19	0.545
	>64GY	11 (54.5%)	17	
Local control	CR	13 (46.2%)	47	0.001
	No CR	10 (100%)	10	
FIGO stage	I–II	17 (70.6%)	18	0.678
	III–IV	6 (66.7%)	19	

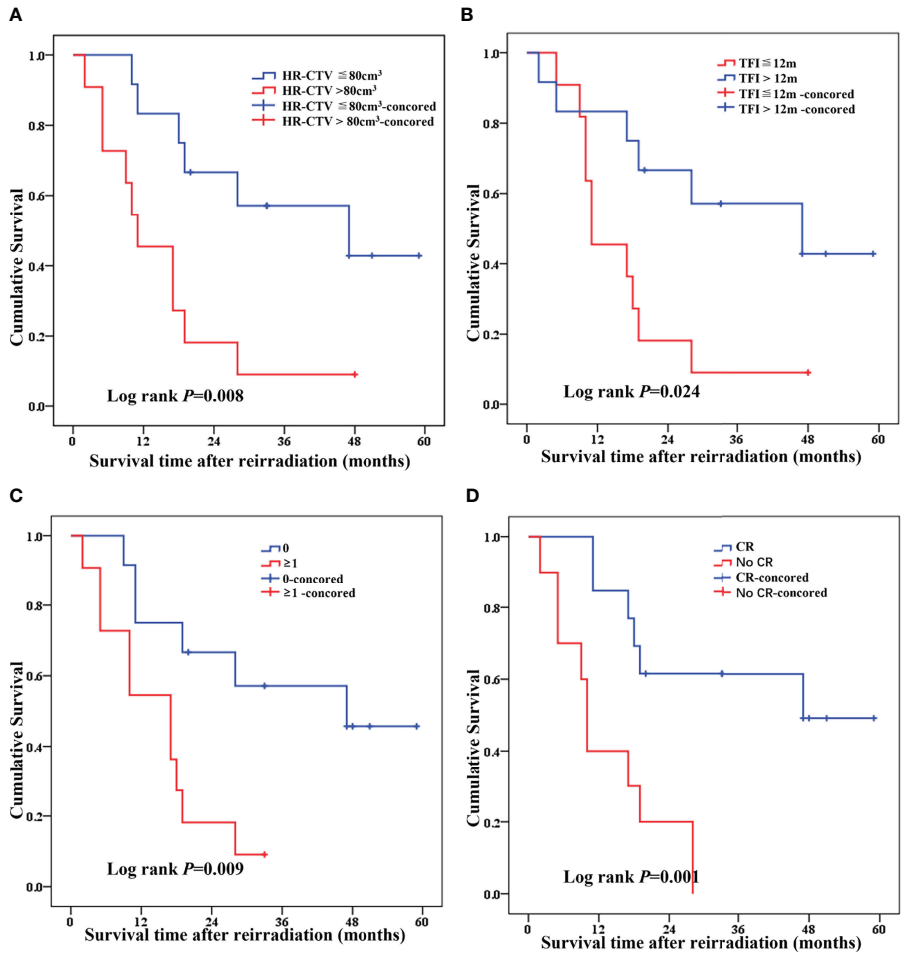

FIGURE 4
Cox model analysis of independent predictors of treatment outcome in recurrence patients receiving re-radiotherapy [**(A)** HR-CTV, **(B)** TFI, **(C)** tumor invasion organ number (bladder, rectum, and pelvic wall), and **(D)** local control].

this patient was not calculated. The average bladder and rectum doses of re-radiotherapy were 52.5 Gy (40.9–66.3 Gy) and 41.5 Gy (35.9–47.6 Gy), respectively. The median EQD2 calculated for primary RT and reirradiation of bladder and rectum were 136.0 Gy (90.5–148.8 Gy) and 120.0Gy (101.8–126.0 Gy), respectively. Two patients had a grade ≥3 urologic radiation response (two patients had a vaginal bladder fistula at 10 and 23 months, respectively), and one patient had a grade ≥3 gastrointestinal radiation response (1 patient had a colorectal fistula at 26 months after radiation) (Tables 1 and 2, supporting information). It has been reported that the cumulative dose of EQD2 in the bladder and rectum below 100 Gy is safe for HDR-BT reradiation (11). In our study, we found that, if the tumor could disappear, then the therapeutic toxicity caused by the cumulative dose of 136 and 120 Gy in the bladder and rectum was acceptable. If LC is poor, then serious complications may not occur before death.

Considering that HDR-ISBT reirradiation can lead to serious complications, selecting the individuals who would benefit from treatment is critical. Mabuchi et al. (14) suggested that tumor-free survival (>6 months), tumor diameter (<40 mm), and the initial FIGO staging (I–II) prognosis were good. The more the combined risk factors, the worse the prognosis and the lower the treatment benefit. In the study of Weitmann et al. (26), recurrence time > 2 years, initial tumor diameter ≤4cm, initial volume <15 cm^3, no pelvic lateral wall invasion, volume before BT< 7.5 cm^3, and the prescribed dose > 64 Gy were positive predictors. Mahantshetty et al. (13) suggested that patients who received >40-Gy EQD2 reirradiation dose and the interval between two radiotherapy sessions>25 months had a better prognosis. However, because of the sample size, these data were not statistically significant. Zolciak-Siwinska et al. (11) showed that the interval between initial RT and reirradiation ≤12 months and the tumor diameter > 3 cm had a poor prognosis.

Our results confirmed that tumor volume ≤ 80 cm^3 before reirradiation, TFI >12 months, local tumor reaching CR after reirradiation, and no tissue invasion of pelvic wall, rectum, and

bladder were the factors for a better prognosis. The dose level did not affect PRS. This observation may be due to the small size and heterogeneity of the study group or due to our higher prescribing dose. For patients with larger tumors and wider areas of invasion, we give higher doses, because we want to increase the local dose of the tumor to improve the LC rate, and the limitation of normal tissue is not too strict. Therefore, the prognosis of patients with the re-radiotherapy dose of > 64 Gy was worse. Further large-scale prospective clinical studies are needed to select suitable patients for HDR-ISBT reirradiation.

Conclusions

To sum up, our findings revealed that HDR-BT reirradiation is clinically feasible in patients with recurrent cervical cancer after radiotherapy, even if the local tumor invasion is large, there is a good chance of survival and an acceptable risk of complications. We suggest that the cumulative dose of EQD2 in the bladder and rectum can be relaxed to 136 and 120 Gy when ISBT re-radiotherapy is performed for recurrent cervical cancer with a chance of radical cure.

Data availability statement

The original contributions presented in the study are included in the article/supplementary material. Further inquiries can be directed to the corresponding author.

Ethics statement

The studies involving human participants were reviewed and approved by the ethics committee of the Second Hospital of Jilin University. The patients/participants provided their written informed consent to participate in this study. Written informed consent was obtained from the individual(s) for the publication of any potentially identifiable images or data included in this article.

Author contributions

XR conceived and designed the experiments, performed the experiments, analyzed the data, prepared figures and/or tables, authored or reviewed drafts of the paper, and approved the final draft. YF performed the experiments, analyzed the data, prepared figures and/or tables, authored or reviewed drafts of the paper, and approved the final draft. ZL analyzed the data, authored or reviewed drafts of the paper, and approved the final draft. XL conceived and designed the experiments, performed the experiments, and approved the final draft. LQ performed the experiments, prepared figures and/or tables, authored or reviewed drafts of the paper, and approved the final draft. YL performed the experiments, analyzed the data, authored or reviewed drafts of the paper, and approved the final draft. HL performed the experiments, authored or reviewed drafts of the paper, and approved the final draft. YB performed the experiments, authored or reviewed drafts of the paper, and approved the final draft. TW conceived and designed the experiments, performed the experiments, analyzed the data, authored or reviewed drafts of the paper, and approved the final draft. All authors contributed to the article and approved the submitted version.

Funding

This work was funded by the National Key Clinical Specialty Capacity Building Project (Application of Non-coplanar 3D Printing and Intertissue Interpolation Technology in Improving the Diagnosis and Treatment Ability of Recurrent and Refractory Cervical Cancer), Jilin Province Financial and Health Project (Research on the Differential Expression of Cyclic RNA in Cervical Cancer HeLa Cells and the Mechanism of Radiation Resistance under Radiation Induction), Jilin Provincial Department of Finance (Consortium of Medical Consortium for Diagnosis and Treatment of Difficult Women's Tumors and Precision Radiotherapy Training Base Construction Project), and Jilin Province Medical and Health Talent Special Project (2019SCZT010).

Conflict of interest

The authors declare that the research was conducted in the absence of any commercial or financial relationships that could be construed as a potential conflict of interest.

Publisher's note

Supplementary material

The Supplementary Material for this article can be found online at: https://www.frontiersin.org/articles/10.3389/fonc.2022.943703/full#supplementary-material

References

1. Sung H, Ferlay J, Siegel RL, Laversanne M, Soerjomataram I, Jemal A, et al. Global cancer statistics 2020: Globocan estimates of incidence and mortality worldwide for 36 cancers in 185 countries. *CA: Cancer J Clin* (2021) 71(3):209–49. doi: 10.3322/caac.21660

2. Quinn MA, Benedet JL, Odicino F, Maisonneuve P, Beller U, Creasman WT, et al. Carcinoma of the cervix uteri. figo 26th annual report on the results of treatment in gynecological cancer. *Int J Gynaecol Obstetrics* (2006) 95 Suppl 1:S43–103. doi: 10.1016/s0020-7292(06)60030-1

3. Perez CA, Grigsby PW, Camel HM, Galakatos AE, Mutch D, Lockett MA. Irradiation alone or combined with surgery in stage ib, iia, and iib carcinoma of uterine cervix: Update of a nonrandomized comparison. *Int J Radiat Oncol Biol Phys* (1995) 31(4):703–16. doi: 10.1016/0360-3016(94)00523-0

4. Hong JH, Tsai CS, Lai CH, Chang TC, Wang CC, Chou HH, et al. Recurrent squamous cell carcinoma of cervix after definitive radiotherapy. *Int J Radiat Oncol Biol Phys* (2004) 60(1):249–57. doi: 10.1016/j.ijrobp.2004.02.044

5. Eralp Y, Saip P, Sakar B, Kucucuk S, Aydiner A, Dincer M, et al. Prognostic factors and survival in patients with metastatic or recurrent carcinoma of the uterine cervix. *Int J Gynecol Cancer* (2003) 13(4):497–504. doi: 10.1046/j.1525-1438.2003.13325.x

6. Monk BJ, Tewari KS. Evidence-based therapy for recurrent cervical cancer. *J Clin Oncol* (2014) 32(25):2687–90. doi: 10.1200/jco.2014.56.8733

7. Mabuchi S, Matsumoto Y, Komura N, Sawada M, Tanaka M, Yokoi E, et al. The efficacy of surgical treatment of recurrent or persistent cervical cancer that develops in a previously irradiated field: A monoinstitutional experience. *Int J Clin Oncol* (2017) 22(5):927–36. doi: 10.1007/s10147-017-1134-x

8. Berek JS, Howe C, Lagasse LD, Hacker NF. Pelvic exenteration for recurrent gynecologic malignancy: Survival and morbidity analysis of the 45-year experience at ucla. *Gynecol Oncol* (2005) 99(1):153–9. doi: 10.1016/j.ygyno.2005.05.034

9. Chiva LM, Lapuente F, González-Cortijo L, González-Martín A, Rojo A, García JF, et al. Surgical treatment of recurrent cervical cancer: State of the art and new achievements. *Gynecol Oncol* (2008) 110(3 Suppl 2):S60–6. doi: 10.1016/j.ygyno.2008.05.024

10. Boers A, Arts HJ, Klip H, Nijhuis ER, Pras E, Hollema H, et al. Radical surgery in patients with residual disease after (Chemo)Radiation for cervical cancer. *Int J Gynecol Cancer* (2014) 24(7):1276–85. doi: 10.1097/igc.0000000000000171

11. Zolciak-Siwinska A, Bijok M, Jonska-Gmyrek J, Kawczynska M, Kepka L, Bujko K, et al. Hdr brachytherapy for the reirradiation of cervical and vaginal cancer: Analysis of efficacy and dosage delivered to organs at risk. *Gynecol Oncol* (2014) 132(1):93–7. doi: 10.1016/j.ygyno.2013.10.018

12. Martínez-Monge R, Cambeiro M, Rodríguez-Ruiz ME, Olarte A, Ramos LI, Villafranca E, et al. Phase ii trial of image-based high-Dose-Rate interstitial brachytherapy for previously irradiated gynecologic cancer. *Brachytherapy* (2014) 13(3):219–24. doi: 10.1016/j.brachy.2014.01.008

13. Mahantshetty U, Kalyani N, Engineer R, Chopra S, Jamema S, Ghadi Y, et al. Reirradiation using high-Dose-Rate brachytherapy in recurrent carcinoma of uterine cervix. *Brachytherapy* (2014) 13(6):548–53. doi: 10.1016/j.brachy.2014.06.005

14. Mabuchi S, Takahashi R, Isohashi F, Yokoi T, Okazawa M, Sasano T, et al. Reirradiation using high-Dose-Rate interstitial brachytherapy for locally recurrent cervical cancer: A single institutional experience. *Int J Gynecol Cancer* (2014) 24(1):141–8. doi: 10.1097/igc.0000000000000028

15. Badakh DK, Grover AH. Reirradiation with high-Dose-Rate remote afterloading brachytherapy implant in patients with locally recurrent or residual cervical carcinoma. *J Cancer Res Ther* (2009) 5(1):24–30. doi: 10.4103/0973-1482.48766

16. Demanes DJ, Rodriguez RR, Bendre DD, Ewing TL. High dose rate transperineal interstitial brachytherapy for cervical cancer: High pelvic control and low complication rates. *Int J Radiat Oncol Biol Phys* (1999) 45(1):105–12. doi: 10.1016/s0360-3016(99)00124-8

17. Georg P, Lang S, Dimopoulos JC, Dörr W, Sturdza AE, Berger D, et al. Dose-volume histogram parameters and late side effects in magnetic resonance image-guided adaptive cervical cancer brachytherapy. *Int J Radiat Oncol Biol Phys* (2011) 79(2):356–62. doi: 10.1016/j.ijrobp.2009.11.002

18. . doi: 10.1093/jicru/ndw042

19. Cox JD, Stetz J, Pajak TF. Toxicity criteria of the radiation therapy oncology group (Rtog) and the European organization for research and treatment of cancer (Eortc). *Int J Radiat Oncol Biol Phys* (1995) 31(5):1341–6. doi: 10.1016/0360-3016(95)00060-c

20. Pecorelli S, Zigliani L, Odicino F. Revised figo staging for carcinoma of the cervix. *Int J Gynaecol Obstetrics* (2009) 105(2):107–8. doi: 10.1016/j.ijgo.2009.02.009

21. Sommers GM, Grigsby PW, Perez CA, Camel HM, Kao MS, Galakatos AE, et al. Outcome of recurrent cervical carcinoma following definitive irradiation. *Gynecol Oncol* (1989) 35(2):150–5. doi: 10.1016/0090-8258(89)90033-4

22. Murakami N, Kobayashi K, Shima S, Tsuchida K, Kashihara T, Tselis N, et al. A hybrid technique of intracavitary and interstitial brachytherapy for locally advanced cervical cancer: Initial outcomes of a single-institute experience. *BMC Cancer* (2019) 19(1):221. doi: 10.1186/s12885-019-5430-x

23. Elledge CR, LaVigne AW, Bhatia RK, Viswanathan AN. Aiming for 100% local control in locally advanced cervical cancer: The role of complex brachytherapy applicators and intraprocedural imaging. *Semin Radiat Oncol* (2020) 30(4):300–10. doi: 10.1016/j.semradonc.2020.05.002

24. Liu ZS, Guo J, Zhao YZ, Lin X, Zhang BY, Zhang C, et al. Computed tomography-guided interstitial brachytherapy for locally advanced cervical cancer: Introduction of the technique and a comparison of dosimetry with conventional intracavitary brachytherapy. *Int J Gynecol Cancer* (2017) 27(4):768–75. doi: 10.1097/igc.0000000000000929

25. Feddock J, Cheek D, Steber C, Edwards J, Slone S, Luo W, et al. Reirradiation using permanent interstitial brachytherapy: A potentially durable technique for salvaging recurrent pelvic malignancies. *Int J Radiat Oncol Biol Phys* (2017) 99(5):1225–33. doi: 10.1016/j.ijrobp.2017.08.027

26. Weitmann HD, Knocke TH, Waldhäusl C, Pötter R. Ultrasound-guided interstitial brachytherapy in the treatment of advanced vaginal recurrences from cervical and endometrial carcinoma. *Strahlenther Und Onkol: Organ Der Deutschen Rontgengesellschaft* (2006) 182(2):86–95. doi: 10.1007/s00066-006-1420-4

frontiers | Frontiers in Oncology

TYPE Original Research
PUBLISHED 02 August 2022
DOI 10.3389/fonc.2022.945053

OPEN ACCESS

EDITED BY
Gene A. Cardarelli,
Brown University, United States

REVIEWED BY
Jan Egger,
University Hospital Essen, Germany
Francolini Giulio,
University of Florence, Italy

*CORRESPONDENCE
Wenjing Wu
wu_ermao@163.com
Xiaozhi Zhang
Zhang9149@sina.com
Yongkai Lu
luyongkai19931130@163.com

†These authors have contributed equally to this work and share first authorship

SPECIALTY SECTION
This article was submitted to Radiation Oncology, a section of the journal Frontiers in Oncology

RECEIVED 16 May 2022
ACCEPTED 04 July 2022
PUBLISHED 02 August 2022

CITATION
Li Y, Wu W, Sun Y, Yu D, Zhang Y, Wang L, Wang Y, Zhang X and Lu Y (2022) The clinical evaluation of atlas-based auto-segmentation for automatic contouring during cervical cancer radiotherapy.
Front. Oncol. 12:945053.
doi: 10.3389/fonc.2022.945053

The clinical evaluation of atlas-based auto-segmentation for automatic contouring during cervical cancer radiotherapy

Yi Li[1†], Wenjing Wu[2*], Yuchen Sun[1†], Dequan Yu[3†], Yuemei Zhang[1], Long Wang[1], Yao Wang[1], Xiaozhi Zhang[1*] and Yongkai Lu[1*]

[1]Department of Radiation Oncology, The First Affiliated Hospital of Xi'an Jiaotong University, Xi'an, China, [2]Department of Radiological Health, Xi'an Center for Disease Control and Prevention, Xi'an, China, [3]Department of Radiation Oncology, Tangdu Hospital, the Second Affiliated Hospital of Air Force Medical University, Xi'an, China

Purpose: Our purpose was to investigate the influence of atlas library size and CT cross-slice number on the accuracy and efficiency of the atlas-based auto-segmentation (ABAS) method for the automatic contouring of clinical treatment volume (CTV) and organs at risk (OARs) during cervical cancer radiotherapy.

Methods: Of 140 cervical cancer patients, contours from 20, 40, 60, 80, 100, and 120 patients were selected incrementally to create six atlas library groups in ABAS. Another 20 tested patients were automatically contoured with the ABAS method and manually contoured by the same professional oncologist. Contours included CTV, bladder, rectum, femoral head-L, femoral head-R, and spinal cord. The CT cross-slice numbers of the 20 tested patients included 61, 65, 72, 75, 81, and 84. The index of dice similarity coefficients (DSCs) and Hausdorff distance (HD) were used to assess the consistency between ABAS automatic contouring and manual contouring. The randomized block analysis of variance and paired t-test were used for statistical analysis.

Results: The mean DSC values of "CTV, bladder, femoral head, and spinal cord" were all larger than 0.8. The femoral head and spinal cord showed a high degree of agreement between ABAS automatic contouring and manual contouring, with a mean DC >0.80 and HD <1 cm in all atlas library groups. A *post-hoc* least significant difference comparison indicated that no significant difference had been found between different atlas library sizes with DSC and HD values. For ABAS efficiency, the atlas library size had no effect on the time of ABAS automatic contouring. The time of automatic contouring increased slightly with the increase in CT cross-slice numbers, which were 99.9, 106.8, 114.0, 120.6, 127.9, and 134.8 s with CT cross-slices of 61, 65, 72, 75, 81, and 84, respectively.

Conclusion: A total of 20 atlas library sizes and a minimum CT cross-slice number including CTV and OARs are enough for ensuring the accuracy and efficiency of ABAS automatic contouring during cervical cancer radiotherapy.

KEYWORDS
atlas, auto-segmentation, automatic contouring, cervical cancer, radiotherapy

Introduction

Radiotherapy, as an independent treatment strategy, plays an important role in cervical cancer treatment (1). Delineating the clinical target volume (CTV) and organs at risk (OARs) precisely is essential to ensuring the curative effect of radiotherapy. However, manual contouring is a time-consuming and complex process. Significant variance can be detected among contours that were delineated by different radiation oncologists or the same oncologist at different times (2–4). Compared with the manual segmentation process, atlas-based auto-segmentation (ABAS) could not only significantly save time but also reduce subjective bias among different radiation oncologists. In ABAS, segmented structures from the atlas library are propagated onto a subject image using the deformable image registration algorithm. Because multiple-ABAS uses a voting scheme for determining whether a voxel is inside or outside the structure, it is more susceptible to topological artifacts compared with single-ABAS (5).

The atlas library should be set before applying the ABAS method for delineating contours automatically. According to published results, multiple-ABAS could overcome the issues encountered with single-ABAS, such as large discrepancies in volume and location between the atlas library and subject data (6). However, the atlas library size varied a lot in different cases and no authorized guideline could be taken as the reference (7–10). Although there are several reports about atlas library size in pelvic radiotherapy (11–13), especially for endometrial and cervical cancer (14), limited atlas library groups and fewer test cases were available on the impact of atlas library size on the accuracy and efficiency of ABAS, which may lead to an inaccurate conclusion. Rare works have researched the effect of CT cross-slice numbers on the ABAS-performed efficiency. Therefore, the aim of our study is to investigate the influence of the atlas library size and CT cross-slice number on the accuracy and efficiency of ABAS automatic contouring and establish an optimal strategy for ABAS with atlas library size and CT cross-slice number during cervical radiotherapy.

Material and methods

Patients

This retrospective study included 140 patients with newly diagnosed, pathologically confirmed stage II–III cervical cancer (7th edition of the AJCC staging system). All patients were treated with volume-modulated arc therapy (VMAT) technology in the Radiation Oncology Department at the First Affiliated Hospital of Xi'an Jiaotong University from October 2020 to October 2021. The VMAT plan was delivered at the prescribed dose of 50 Gy (25 fractions) to the cervical tumor. Neoadjuvant, concurrent, or adjuvant chemotherapy was recommended for patients.

CT simulation

A total of 140 planning CT images from 140 patients were collected. All patients were immobilized using thermoplastic body mold in the supine position with hands raised and arms crossed with elbows on the top of the head during CT simulation. All patients were instructed that the rectum should be completely empty and the bladder should be filled with 300 ml of water 2 h before CT scanning. Each patient received a helical CT scanning under free breathing conditions on a 16-slice CT scanner (Big Bore, Philips Medical Systems, Cleveland, OH). The scanning parameters were as follows: pixel spacing 1.1543 mm × 1.1543 mm, matrix 512 × 512, pitch 0.85, 120 kV, 400 mAs, thickness 3 mm, and layer spacing 3 mm. The scanned images were sent to a MIM Maestro version 6.7 software (Cleveland, OH, USA) with ABAS function based on a computer (Intel(R), Xeon(R), E5-1603 CPU, 2.8 GHz, four processors, 32 G RAM).

Manual contouring

The professional oncologist manually contoured CTV and OARs on the CT-scanned images of all patients with reference to RTOG 0418 (15) and consensus guidelines (16, 17). CTV included the tumor volume and whole pelvic nodal volume. OARs included the bladder, femoral head-L, femoral head-R, rectum, and spinal cord. CTV and OARs were delineated manually by the same professional oncologist with the mediastinum window setting (L = 40 Hu, W = 350 Hu) to make the interobserver lowest as soon as possible, which were used as the atlas library data and tested the segmentation ground truth.

Atlas library creation and automatic contouring

Of 140 cervical cancer patients, 120 patients were randomly registered in six different atlas library groups with 20, 40, 60, 80,

100, and 120 patients incrementally for ABAS. The automatic segmentation process was performed in the 20 remaining tested patients with ABAS. The details are shown in Table 1. During library construction, a template subject was assigned, and the remaining subjects were registered to the template subject separately. To minimize the bias and maintain the consistency of the registration alignment, an additional intervention during registration was prohibited. The ABAS algorithm automatically matched the atlas subject according to the input tested set. The optimal number of the matched atlas template was set to three during ABAS automatic contouring. Based on the intensity and the freeform cubic spline interpolation, contours of CTV and OARs were deformed, registered, and transferred to the test set. The CT cross-slice number of the selected automatically contoured patients ranged from 61 to 84 (the average number was 72 slices per patient). Then, manual correction of ABAS automatic contours was performed in the 20 tested patients.

Quantitative evaluation of accuracy and efficiency of ABAS automatic contouring

Contours generated by ABAS automatic contours were compared with manually corrected ABAS automatic contours. The Dice similarity coefficient (DSC) and Hausdorff distance (HD) were used to evaluate the accuracy of automatic contouring (14). DSC was defined as $DSC = 2|A \cap B|/(A+B)$ with A equaling the volume of automatic contouring volume and B equaling the manual contouring volume. The results of DSC were between 0 and 1, where 0 represents no intersection and 1 reflects a perfect overlap of structures. In contrast, HD considered the degree of mismatch between two surfaces based on contour boundaries, eliminating the ambiguity of the volume-based DSC metric. Moreover, we timed the whole process to evaluate the efficiency of the ABAS method.

Statistical method

Random analysis of variance and paired-sample t-test were used to analyze the accuracy of automatic contouring results between the different atlas library sizes and CT cross-slice numbers. $P < 0.05$ was regarded as statistically significant. SPSS 22.0 was used for statistics analysis.

Results

DSC and HD values of contours of "CTV and OARs"

A total of 20 cervical cancer patients' CTV and OARs were delineated both by a radiation oncologist manually and ABAS automatically with an atlas library size of 20. The consistency between automatic and manual segmentation was assessed with DSC and HD values. According to the results, the mean DSC values of "CTV, bladder, femoral head, and spinal cord" were all larger than 0.8. However, the mean DSC value and HD value of the rectum were 0.695 and 2.508 cm, respectively. Therefore, the contours of the rectum needed to be corrected greatly before clinical application as shown in Figure 1 and Table 2.

The influence of atlas library size on the accuracy of ABAS automatic segmentation

ABAS was used to delineate the contours of "CTV and OARs" of cervical cancer patients under different atlas library groups (20, 40, 60, 80, 100, and 120, respectively). The DSC and HD values of CTV and OARs in the different atlas library groups are shown in Table 3 and Table 4. The results showed that different atlas library sizes had little impact on the accuracy of automatic contouring. Randomized block analysis of variance was adopted to further investigate the influence of atlas library size on the automatic contouring accuracy. *Post-hoc* least significant difference (LSD) comparisons indicated that no significant difference was found between different atlas library groups as shown in Table 5 and Table 6. Therefore, an atlas library size of 20 was enough to delineate CTV and OARs automatically with the ABAS method during cervical patients' radiotherapy.

TABLE 1 Characteristics of atlas library and tested patients.

	TestN = 20	Size of atlas library					
		N = 20	N = 40	N = 60	N = 80	N = 100	N = 120
Mean age (SD)	50.8 (11.3)	52.1 (12.5)	53.4 (12.2)	53.8 (11.7)	52.8 (12.3)	51.8 (11.9)	54.8 (12.6)
Mean height (SD), cm	157.0 (7.4)	158.0 (6.9)	159.7 (6.4)	157.4 (7.6)	158.4 (6.9)	157.4 (7.8)	159.4 (7.5)
Mean weight (SD), kg	62.7 (8.5)	62.5 (7.1)	61.3 (6.8)	61.7 (7.5)	62.9 (7.6)	61.6 (8.3)	62.7 (7.3)
Mean BMI (SD), kg/m^2	25.4 (4.5)	25.0 (4.3)	24.0 (3.9)	24.9 (4.1)	25.1 (3.8)	24.9 (4.2)	24.7 (4.4)

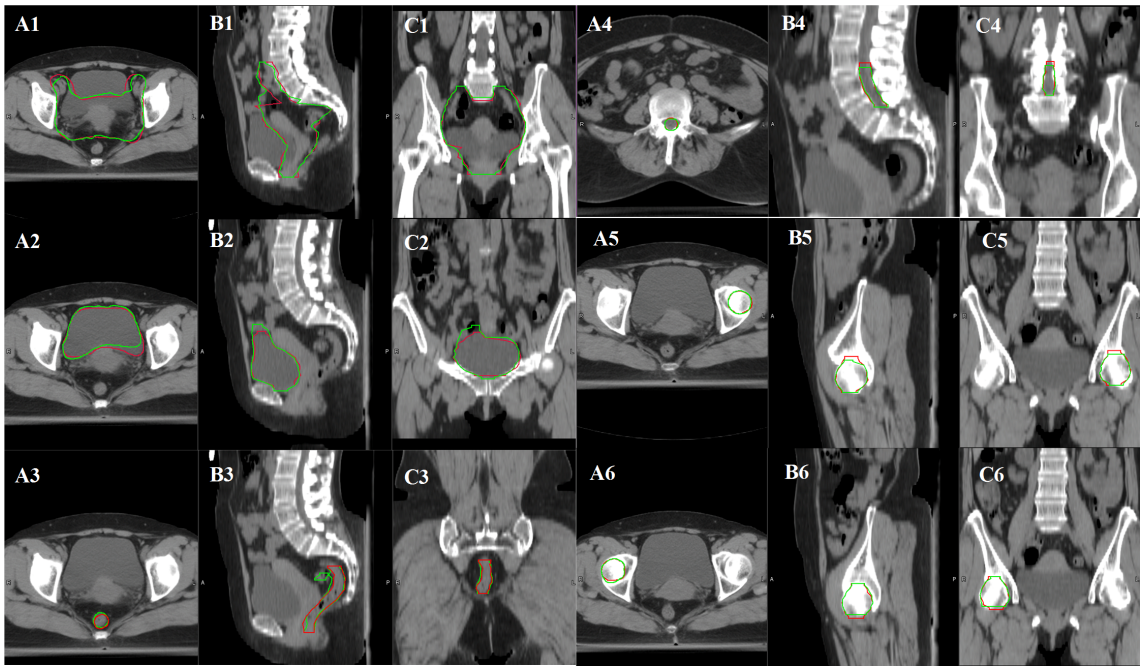

FIGURE 1
Variance between manual contours and ABAS automatic contours in CTV and OARs of cervical cancer patients with an atlas library size of 20 (**A1, B1, C1**: CTV contour comparison, **A2, B2, C2**: bladder contour comparison, **A3, B3, C3**: rectum contour comparison, **A4, B4, C4**: spinal cord comparison, **A5, B5, C5**: femoral head-L contour comparison, **A6, B6, C6**: femoral head-R contour comparison. Manual contours in red color, and automatic contours in green color).

Influence of atlas library size and CT cross-slice number on the efficiency of ABAS automatic contouring

One-way ANOVA was adopted to investigate the influence of atlas library size and CT cross-slice number on the efficiency of ABAS automatic contouring. The atlas library size had no effect on the time of ABAS automatic contouring, as shown in Table 7. The times of ABAS automatic contouring increased slightly with the increase in CT cross-slice numbers, which were 99.9, 106.8, 114.0, 120.6, 127.9, and 134.8 s with CT cross-slice numbers of 61, 65, 72, 75, 81, and 84, respectively, as shown in Table 8. As a result, a minimum CT cross-slice number was suggested for delineating the CTV and OARs automatically during cervical cancer radiotherapy.

Discussion

Our study investigated the influence of atlas library size and patients' CT cross-slice number on the accuracy and efficiency of ABAS and established an optimal atlas library and CT cross-slice for automatic contouring during cervical cancer radiotherapy, which was rarely discussed in previous studies. ABAS was introduced to delineate CTV and OARs automatically and reduce interobserver and intra-observer contouring variability.

TABLE 2 DSC and HD value of CTV and OARs with an atlas library size of 20.

Structure	DSC	HD (cm)
CTV	0.816 ± 0.046	2.195 ± 0.340
Bladder	0.866 ± 0.035	1.591 ± 0.340
Rectum	0.685 ± 0.048	2.508 ± 0.559
Femoral head-L	0.867 ± 0.039	0.843 ± 0.369
Femoral head-R	0.873 ± 0.047	0.789 ± 0.260
Spinal cord	0.858 ± 0.052	0.604 ± 0.205

TABLE 3 The DSC value of CTV and OARs in different atlas library groups (mean ± SD).

	20	40	60	80	100	120
CTV	0.816 ± 0.046	0.818 ± 0.046	0.819 ± 0.049	0.814 ± 0.036	0.819 ± 0.061	0.810 ± 0.046
Bladder	0.866 ± 0.035	0.857 ± 0.043	0.860 ± 0.034	0.854 ± 0.047	0.855 ± 0.043	0.861 ± 0.046
Rectum	0.685 ± 0.048	0.682 ± 0.041	0.693 ± 0.042	0.689 ± 0.048	0.682 ± 0.048	0.692 ± 0.053
Femoral head-L	0.867 ± 0.039	0.868 ± 0.047	0.865 ± 0.037	0.875 ± 0.046	0.864 ± 0.046	0.870 ± 0.038
Femoral head-R	0.873 ± 0.047	0.865 ± 0.041	0.870 ± 0.045	0.867 ± 0.042	0.869 ± 0.046	0.879 ± 0.037
Spinal cord	0.858 ± 0.052	0.857 ± 0.058	0.856 ± 0.053	0.851 ± 0.038	0.859 ± 0.037	0.858 ± 0.051

Previous studies (3, 18) demonstrated that contouring time could be reduced greatly using the ABAS method for head and neck cancer. Voet et al. (19) demonstrated that the delineation time was reduced from 180 to 66 min using the ABAS method despite necessary auto-contour editing. However, it should be noted that the manually corrected contouring times were difficult to assess accurately because manual correction times varied significantly with different oncologists or the same oncologist at different times. Therefore, we mainly focused on ABAS automatic contouring time without considering the manually corrected time. In clinical practice, it was a challenge to select the appropriate atlas library size. In our study, we found that a large atlas library size was not necessary for ABAS automatic contouring and an atlas library size of 20 could be enough to insure the accuracy of automatic contouring with the ABAS method. However, some authors validated ABAS based on a higher number of subjects for male pelvis CT images compared to what is concluded in the present article (20, 21). Some authors validated ABAS based on a lower number of subjects for prostate cancers if compared to what is concluded in the present article (7, 11). In addition, Ducote et al. concluded that the performance of ABAS was relatively insensitive to atlas size for various head and neck cancers (22). Kim et al. demonstrate that a different atlas library size had no impact on the accuracy of ABAS-OAR automatic contouring and the segmentation accuracy of ABAS-CTV improved with increasing library size with ABAS (14). In our opinion, the size of the atlas library is not an independent factor in determining the quality of auto-segmentation.

DSC was used to assess the overlap ratio between ABAS automatic contouring and manual contouring. In our study, we found that ABAS showed acceptable accuracy in delineating CTV and parts of OARs such as bladder, femoral head-L, femoral head-R, and spinal cord, with the mean DSC of 0.816, 0.866, 0.867, 0.873, and 0.858, which was larger than a good overlap standard of 0.7 according to a published paper (8). The femoral head and spinal cord showed a high degree of agreement between ABAS automatic contouring and manual contouring, with a mean DC >0.80 and HD <1 cm in all atlas library groups, which was similar to the result by Kim et al. (14). For ABAS efficiency, we found that the atlas library size had no effect on the time of ABAS automatic contouring and automatic contouring time increased with the increase in CT cross-slice number. Therefore, we suggested a minimum CT cross-slice number, which could include CTV and OARs, for ABAS automatic contouring during cervical patient radiotherapy.

Earlier work by Stuart Greenham et al. (12) evaluated the performance of ABAS automatic contouring, and the results showed that the bladder and CTV, which are the two largest structures in the pelvis, were delineated precisely in delineating the pelvic anatomy, which was similar with the results of our study. Among all the OARs, the bladder, femoral heads, and spinal cord achieved a higher DSC value and a lower HD value. This may be due to the relatively clear boundary and high contrast between these structures and the background. However, it should be noted that ABAS could not precisely delineate the rectum in this study. There are two reasons for this result. First, this could be caused by the unclear boundaries and the massive diversity in sizes, shapes, and locations for different patients. Even an experienced radiotherapy oncologist sometimes had to delineate the rectum boundary by experience instead of by images. To get accurate delineating results, manual corrections were suggested for rectum automatic contouring. In accordance with radiotherapy instructions, the rectum should be completely empty before CT scanning and the CT scanning time should be enough to acquire the images with contrast-enhanced

TABLE 4 The HD value of CTV and OARs in different atlas library groups (mean ± SD, cm).

	20	40	60	80	100	120
CTV	2.195 ± 0.340	2.335 ± 0.223	2.310 ± 0.265	2.345 ± 0.255	2.363 ± 0.275	2.074 ± 0.308
Bladder	1.591 ± 0.340	1.612 ± 0.257	1.566 ± 0.332	1.571 ± 0.293	1.614 ± 0.272	1.559 ± 0.298
Rectum	2.045 ± 0.562	2.097 ± 0.554	1.967 ± 0.381	1.956 ± 0.401	2.039 ± 0.429	1.925 ± 0.449
Femoral head-L	0.843 ± 0.369	0.727 ± 0.230	0.774 ± 0.204	0.690 ± 0.217	0.725 ± 0.297	0.730 ± 0.228
Femoral head-R	0.789 ± 0.260	0.730 ± 0.235	0.700 ± 0.140	0.635 ± 0.185	0.698 ± 0.195	0.673 ± 0.167
Spinal cord	0.604 ± 0.205	0.767 ± 0.336	0.640 ± 0.225	0.626 ± 0.267	0.677 ± 0.213	0.636 ± 0.161

10.3389/fonc.2022.945053

TABLE 5 Results of *post-hoc* least significant difference (LSD) with DSC value among different atlas library groups.

Atlasgroup	Atlasgroup	CTV	Bladder	Rectum	Femoral head-L	Femoral head-R	Spinal cord
20	40	0.753	0.694	0.291	0.592	0.610	0.240
	60	0.519	0.094	0.490	0.237	0.492	0.191
	80	0.954	0.372	0.268	0.883	0.877	0.062
	100	0.508	0.260	0.644	0.320	0.705	0.199
	120	0.745	0.886	0.104	0.592	0.722	0.163
40	20	0.753	0.694	0.291	0.592	0.610	0.240
	60	0.740	0.040	0.712	0.514	0.859	0.892
	80	0.797	0.200	0.958	0.697	0.722	0.477
	100	0.727	0.131	0.551	0.644	0.895	0.910
	120	0.991	0.591	0.558	1.000	0.877	0.820
60	20	0.519	0.094	0.490	0.237	0.492	0.191
	40	0.740	0.040	0.712	0.514	0.859	0.892
	80	0.556	0.425	0.673	0.299	0.594	0.565
	100	0.986	0.573	0.819	0.848	0.757	0.982
	120	0.749	0.124	0.342	0.514	0.740	0.928
80	40	0.954	0.372	0.268	0.883	0.877	0.062
	60	0.797	0.200	0.958	0.697	0.722	0.477
	80	0.556	0.425	0.673	0.299	0.594	0.565
	100	0.545	0.813	0.516	0.395	0.823	0.550
	120	0.788	0.453	0.594	0.697	0.841	0.628
100	20	0.508	0.260	0.644	0.320	0.705	0.199
	40	0.727	0.131	0.551	0.644	0.895	0.910
	60	0.986	0.573	0.819	0.848	0.757	0.982
	80	0.545	0.813	0.516	0.395	0.823	0.550
	120	0.736	0.325	0.240	0.644	0.981	0.910
120	20	0.745	0.886	0.104	0.592	0.722	0.163
	40	0.991	0.591	0.558	1.000	0.877	0.820
	60	0.749	0.124	0.342	0.514	0.740	0.928
	80	0.788	0.453	0.594	0.697	0.841	0.628
	100	0.736	0.325	0.240	0.644	0.981	0.910

ultrasound properly, which could improve the clarity of rectum boundaries and contouring accuracy. However, it was hard to control in clinical practice, which could result in poor automatic contouring and inaccurate manual contouring. Second, the atlas-based auto-segmentation method lacks necessary intervention methodologies and provides little final control by the medical doctor over the segmentation. Recently, auto-segmentation methodology with a user-defined template for the library construction could handle the variations in rectum anatomy. Luddemann et al. (23) have evaluated an interactive graph-based segmentation algorithm with a user-defined template by comparing the computer-assisted segmentation results with manual expert segmentation of the rectum/sigmoid colon and yielded a DSC of 83.58 ± 4.08% in gynecological brachytherapy. Therefore, auto-segmentation with a user-defined template can be used for rectosigmoid colon segmentation in gynecological external-beam radiation and gynecological brachytherapy.

Recently, the scope of auto-segmentation has been expanded to arterial intelligence (AI)-based contouring using deep learning algorithms (24–29). Earlier work by Liu (30) demonstrated that the mean DSC values of deep learning-based methods were 0.924 for the bladder, 0.906 for the femoral head-L, 0.900 for the femoral head-R, 0.791 for the rectum, and 0.827 for the spinal cord. The results of ABAS in this study had comparable performance with deep learning methods in the spinal cord but an inferior performance in the bladder, rectum, femoral head-L, and femoral head-R. The deep learning-based method outperformed the ABAS method in OAR automatic contouring. However, many radiotherapy departments have to use ABAS to automatically contour the target area and normal organs due to a lack of deep learning equipment or condition. This study provided a method for selecting appropriate atlas library sizes and CT cross-slices for the departments with ABAS.

There are several limitations in the current study. First, a cohort of patients was included in all the atlases used in six

TABLE 6 Results of *post-hoc* least significant difference (LSD) with HD value among different atlas library groups.

Atlasgroup	Atlasgroup	CTV	Bladder	Rectum	Femoral head-L	Femoralhead-R	Spinal cord
20	40	0.195	0.829	0.723	0.169	0.356	0.064
	60	0.287	0.789	0.602	0.413	0.164	0.637
	80	0.164	0.834	0.551	0.069	0.067	0.773
	100	0.120	0.813	0.970	0.162	0.153	0.340
	120	0.261	0.737	0.421	0.180	0.071	0.675
40	20	0.195	0.829	0.723	0.169	0.356	0.064
	60	0.816	0.629	0.382	0.574	0.638	0.098
	80	0.922	0.670	0.343	0.654	0.138	0.067
	100	0.791	0.983	0.696	0.981	0.610	0.240
	120	0.117	0.581	0.248	0.971	0.372	0.088
60	20	0.287	0.789	0.602	0.413	0.164	0.637
	40	0.816	0.629	0.382	0.574	0.638	0.098
	80	0.741	0.954	0.941	0.313	0.309	0.854
	100	0.618	0.614	0.628	0.558	0.969	0.628
	120	0.060	0.946	0.777	0.599	0.672	0.958
80	40	0.164	0.834	0.551	0.069	0.067	0.773
	60	0.922	0.670	0.343	0.654	0.138	0.067
	80	0.741	0.954	0.941	0.313	0.309	0.854
	100	0.867	0.655	0.576	0.671	0.328	0.504
	120	0.113	0.900	0.834	0.628	0.551	0.896
100	20	0.120	0.813	0.970	0.162	0.153	0.340
	40	0.791	0.983	0.696	0.981	0.610	0.240
	60	0.618	0.614	0.628	0.558	0.969	0.628
	80	0.867	0.655	0.576	0.671	0.328	0.504
	120	0.108	0.567	0.443	0.952	0.701	0.591
120	20	0.261	0.737	0.421	0.180	0.071	0.675
	40	0.117	0.581	0.248	0.971	0.372	0.088
	60	0.060	0.946	0.777	0.599	0.672	0.958
	80	0.113	0.900	0.834	0.628	0.551	0.896
	100	0.108	0.567	0.443	0.952	0.701	0.591

different atlas libraries. This pool could be overrepresented, and this issue could influence somehow the results of the work. Therefore, further investigations including a large number of independently tested patients are needed for evaluating the efficacy of the current ABAS library. Second, the research of this approach only evaluated the influence of CT cross-slice numbers on the time of ABAS automatic contouring. Future work will be required to evaluate the influence of CT cross-slice number on DSC and HD values of ABAS automatic contouring.

Conclusion

In our study, 20 atlases and a minimum CT cross-slice number could insure the accuracy and efficiency of ABAS automatic contouring during cervical cancer radiotherapy. Considering that ABAS could not delineate the rectum organ accurately, manual correction by a radiation oncologist is necessary. The data that we used in this study was from only one department, which means that the model may not apply to data with different situations. A larger

TABLE 7 The time of ABAS automatic segmentation among different atlas library sizes.

	Time (s)	Range	*P* value
20	114.3	108.7~119.9	
40	115.2	109.2~121.1	
60	114.1	100.2~128.1	0.974
80	115.8	103.9~127.8	
100	117.2	104.2~130.1	
120	119.2	105.8~136.7	

TABLE 8 Time for ABAS automatic contouring among different CT cross-slice numbers.

CT cross-slice number	61	65	72	75	81	84	P
Time (s)	99.9	106.8	114.0	120.6	127.9	134.8	0.032

dataset and more data sources could make the result more robust and have a better generalization capability.

Data availability statement

The original contributions presented in the study are included in the article/supplementary material. Further inquiries can be directed to the corresponding author/s.

Author contributions

WW and XZ planned and designed the research. YL, YS, and DY performed the experiment and wrote the manuscript. WW, YKL, and YZ revised the manuscript. YKL, LW, and YW analyzed the data. All authors contributed to the article and approved the submitted version.

Funding

This work was supported by the Key Research and Development Projects of Shaanxi Province, China (No. 2022SF-440).

Acknowledgments

All authors in this study and many colleagues helped to collect and analyze data. Their support and helps should be appreciated.

Conflict of interest

The authors declare that the research was conducted in the absence of any commercial or financial relationships that could be construed as a potential conflict of interest.

Publisher's note

References

1. Kokka F, Bryant A, Brockbank E, Powell M, Oram D. Hysterectomy with radiotherapy or chemotherapy or both for women with locally advanced cervical cancer. *Cochrane Database Syst Rev* (2015) 4:D10260. doi: 10.1002/14651858.CD010260.pub2

2. Young AV, Wortham A, Wernick I, Evans A, Ennis RD. Atlas-based segmentation improves consistency and decreases time required for contouring postoperative endometrial cancer nodal volumes. *Int J Radiat Oncol Biol Phys* (2011) 79:943–7. doi: 10.1016/j.ijrobp.2010.04.063

3. Teguh DN, Levendag PC, Voet PW, Al-Mamgani A, Han X, Wolf TK, et al. Clinical validation of atlas-based auto-segmentation of multiple target volumes and normal tissue (swallowing/mastication) structures in the head and neck. *Int J Radiat Oncol Biol Phys* (2011) 81:950–7. doi: 10.1016/j.ijrobp.2010.07.009

4. Langmack KA, Perry C, Sinstead C, Mills J, Saunders D. The utility of atlas-assisted segmentation in the male pelvis is dependent on the interobserver agreement of the structures segmented. *Br J Radiol* (2014) 87:20140299. doi: 10.1259/bjr.20140299

5. Sharp G, Fritscher KD, Pekar V, Peroni M, Shusharina N, Veeraraghavan H, et al. Vision 20/20: Perspectives on automated image segmentation for radiotherapy. *Med Phys* (2014) 41:50902. doi: 10.1118/1.4871620

6. Sykes J. Reflections on the current status of commercial automated segmentation systems in clinical practice. *J Med Radiat Sci* (2014) 61:131–4. doi: 10.1002/jmrs.65

7. Hwee J, Louie AV, Gaede S, Bauman G, D'Souza D, Sexton T, et al. Technology assessment of automated atlas based segmentation in prostate bed contouring. *Radiat Oncol* (2011) 6:110. doi: 10.1186/1748-717X-6-110

8. Anders LC, Stieler F, Siebenlist K, Schafer J, Lohr F, Wenz F. Performance of an atlas-based autosegmentation software for delineation of target volumes for radiotherapy of breast and anorectal cancer. *Radiother Oncol* (2012) 102:68–73. doi: 10.1016/j.radonc.2011.08.043

9. Warfield SK, Zou KH, Wells WM. Simultaneous truth and performance level estimation (STAPLE): An algorithm for the validation of image segmentation. *IEEE Trans Med Imaging* (2004) 23:903–21. doi: 10.1109/TMI.2004.828354

10. La Macchia M, Fellin F, Amichetti M, Cianchetti M, Gianolini S, Paola V, et al. Systematic evaluation of three different commercial software solutions for automatic segmentation for adaptive therapy in head-and-neck, prostate and pleural cancer. *Radiat Oncol* (2012) 7:160. doi: 10.1186/1748-717X-7-160

11. Wong WK, Leung LH, Kwong DL. Evaluation and optimization of the parameters used in multiple-atlas-based segmentation of prostate cancers in radiation therapy. *Br J Radiol* (2016) 89:20140732. doi: 10.1259/bjr.20140732

12. Greenham S, Dean J, Fu CK, Goman J, Mulligan J, Tune D, et al. Evaluation of atlas-based auto-segmentation software in prostate cancer patients. *J Med Radiat Sci* (2014) 61:151–8. doi: 10.1002/jmrs.64

13. Sjoberg C, Lundmark M, Granberg C, Johansson S, Ahnesjo A, Montelius A. Clinical evaluation of multi-atlas based segmentation of lymph node regions in head and neck and prostate cancer patients. *Radiat Oncol* (2013) 8:229. doi: 10.1186/1748-717X-8-229

14. Kim N, Chang JS, Kim YB, Kim JS. Atlas-based auto-segmentation for postoperative radiotherapy planning in endometrial and cervical cancers. *Radiat Oncol* (2020) 15:106. doi: 10.1186/s13014-020-01562-y

15. Jhingran A, Winter K, Portelance L, Miller B, Salehpour M, Gaur R, et al. A phase II study of intensity modulated radiation therapy to the pelvis for postoperative patients with endometrial carcinoma: Radiation therapy oncology group trial 0418. *Int J Radiat Oncol* (2012) 84:E23–8. doi: 10.1016/j.ijrobp.2012.02.044

16. Lim K, Small WJ, Portelance L, Creutzberg C, Jurgenliemk-Schulz IM, Mundt A, et al. Consensus guidelines for delineation of clinical target volume for intensity-modulated pelvic radiotherapy for the definitive treatment of cervix cancer. *Int J Radiat Oncol Biol Phys* (2011) 79:348–55. doi: 10.1016/j.ijrobp.2009.10.075

17. Small WJ, Bosch WR, Harkenrider MM, Strauss JB, Abu-Rustum N, Albuquerque KV, et al. NRG Oncology/RTOG consensus guidelines for delineation of clinical target volume for intensity modulated pelvic radiation therapy in postoperative treatment of endometrial and cervical cancer: An update. *Int J Radiat Oncol Biol Phys* (2021) 109:413–24. doi: 10.1016/j.ijrobp.2020.08.061

18. Lee H, Lee E, Kim N, Kim JH, Park K, Lee H, et al. Clinical evaluation of commercial atlas-based auto-segmentation in the head and neck region. *Front Oncol* (2019) 9:239. doi: 10.3389/fonc.2019.00239

19. Voet PW, Dirkx ML, Teguh DN, Hoogeman MS, Levendag PC, Heijmen BJ. Does atlas-based autosegmentation of neck levels require subsequent manual contour editing to avoid risk of severe target underdosage? a dosimetric analysis. *Radiother Oncol* (2011) 98:373–7. doi: 10.1016/j.radonc.2010.11.017

20. Casati M, Piffer S, Calusi S, Marrazzo L, Simontacchi G, Di Cataldo V, et al. Methodological approach to create an atlas using a commercial auto-contouring software. *J Appl Clin Med Phys* (2020) 21:219–30. doi: 10.1002/acm2.13093

21. Casati M, Piffer S, Calusi S, Marrazzo L, Simontacchi G, Di Cataldo V, et al. Clinical validation of an automatic atlas-based segmentation tool for male pelvis CT images. *J Appl Clin Med Phys* (2022) 23:e13507. doi: 10.1002/acm2.13507

22. Ducote JL, Sehgal V, Wong J, Al-Ghazi M. SU-E-J-102: The impact of the number of subjects for atlas-based automatic segmentation. *Med Phys* (2012) 39:3676. doi: 10.1118/1.4734938

23. Luddemann T, Egger J. Iterative-cuts: Longitudinal and scale-invariant segmentation *via* user-defined templates for rectosigmoid colon in gynecological brachytherapy. *J Med Imaging (Bellingham)* (2016) 3:24004. doi: 10.1117/1.JMI.3.2.024004

24. Lin L, Dou Q, Jin YM, Zhou GQ, Tang YQ, Chen WL, et al. Deep learning for automated contouring of primary tumor volumes by MRI for nasopharyngeal carcinoma. *Radiology* (2019) 291:677–86. doi: 10.1148/radiol.2019182012

25. Kim JR, Shim WH, Yoon HM, Hong SH, Lee JS, Cho YA, et al. Computerized bone age estimation using deep learning based program: Evaluation of the accuracy and efficiency. *AJR Am J Roentgenol* (2017) 209:1374–80. doi: 10.2214/AJR.17.18224

26. Nam JG, Park S, Hwang EJ, Lee JH, Jin KN, Lim KY, et al. Development and validation of deep learning-based automatic detection algorithm for malignant pulmonary nodules on chest radiographs. *Radiology* (2019) 290:218–28. doi: 10.1148/radiol.2018180237

27. Steiner DF, MacDonald R, Liu Y, Truszkowski P, Hipp JD, Gammage C, et al. Impact of deep learning assistance on the histopathologic review of lymph nodes for metastatic breast cancer. *Am J Surg Pathol* (2018) 42:1636–46. doi: 10.1097/PAS.0000000000001151

28. Ding Y, Chen Z, Wang Z, Wang X, Hu D, Ma P, et al. Three-dimensional deep neural network for automatic delineation of cervical cancer in planning computed tomography images. *J Appl Clin Med Phys* (2022) 23:e13566. doi: 10.1002/acm2.13566

29. Yoganathan SA, Paul SN, Paloor S, Torfeh T, Chandramouli SH, Hammoud R, et al. Automatic segmentation of magnetic resonance images for high-dose-rate cervical cancer brachytherapy using deep learning. *Med Phys* (2022) 49:1571–84. doi: 10.1002/mp.15506

30. Liu Z, Liu X, Xiao B, Wang S, Miao Z, Sun Y, et al. Segmentation of organs-at-risk in cervical cancer CT images with a convolutional neural network. *Phys Med* (2020) 69:184–91. doi: 10.1016/j.ejmp.2019.12.008

frontiers | Frontiers in Oncology

TYPE Original Research
PUBLISHED 30 August 2022
DOI 10.3389/fonc.2022.967436

OPEN ACCESS

EDITED BY
John Varlotto,
Marshall University, United States

REVIEWED BY
Saravanan Kandasamy,
Jawaharlal Institute of Postgraduate Medical Education and Research (JIPMER), India
Ramin Jaberi,
Tehran University of Medical Science, Iran

*CORRESPONDENCE
Jie Fu
fujie74@sjtu.edu.cn

†These authors have contributed equally to this work

SPECIALTY SECTION
This article was submitted to Radiation Oncology, a section of the journal Frontiers in Oncology

RECEIVED 12 June 2022
ACCEPTED 02 August 2022
PUBLISHED 30 August 2022

CITATION
Li Z, Chen K, Yang Z, Zhu Q, Yang X, Li Z and Fu J (2022) A personalized DVH prediction model for HDR brachytherapy in cervical cancer treatment.
Front. Oncol. 12:967436.
doi: 10.3389/fonc.2022.967436

A personalized DVH prediction model for HDR brachytherapy in cervical cancer treatment

Zhen Li[1†], Kehui Chen[2†], Zhenyu Yang[3], Qingyuan Zhu[1], Xiaojing Yang[1], Zhaobin Li[1] and Jie Fu[1*]

[1]Shanghai Jiao Tong University Affiliated Sixth People's Hospital, Shanghai, China, [2]Shuguang Hospital Affiliated to Shanghai University of Traditional Chinese Medicine, Shanghai, China, [3]Duke University, Durham, NC, United States

Purpose: Although the knowledge-based dose-volume histogram (DVH) prediction has been largely researched and applied in External Beam Radiation Therapy, it is still less investigated in the domain of brachytherapy. The purpose of this study is to develop a reliable DVH prediction method for high-dose-rate brachytherapy plans.

Method: A DVH prediction workflow combining kernel density estimation (KDE), k-nearest neighbor (kNN), and principal component analysis (PCA) was proposed. PCA and kNN were first employed together to select similar patients based on principal component directions. 79 cervical cancer patients with different applicators inserted was included in this study. The KDE model was built based on the relationship between distance-to-target (DTH) and the dose in selected cases, which can be subsequently used to estimate the dose probability distribution in the validation set. Model performance of bladder and rectum was quantified by $|\Delta D_{2cc}|$, $|\Delta D_{1cc}|$, $|\Delta D_{0.1cc}|$, $|\Delta D_{max}|$, and $|\Delta D_{mean}|$ in the form of mean and standard deviation. The model performance between KDE only and the combination of kNN, PCA, and KDE was compared.

Result: 20, 30 patients were selected for rectum and bladder based on KNN and PCA, respectively. The absolute residual between the actual plans and the predicted plans were 0.38 ± 0.29, 0.4 ± 0.32, 0.43 ± 0.36, 0.97 ± 0.66, and 0.13 ± 0.99 for $|\Delta D_{2cc}|$, $|\Delta D_{1cc}|$, $|\Delta D_{0.1cc}|$, $|\Delta D_{max}|$, and $|\Delta D_{mean}|$ in the bladder, respectively. For rectum, the corresponding results were 0.34 ± 0.27, 0.38 ± 0.33, 0.63 ± 0.57, 1.41 ± 0.99 and 0.23 ± 0.17, respectively. The combination of kNN, PCA, and KDE showed a significantly better prediction performance than KDE only, with an improvement of 30.3% for the bladder and 33.3% for the rectum.

Conclusion: In this study, a knowledge-based machine learning model was proposed and verified to accurately predict the DVH for new patients. This model is proved to be effective in our testing group in the workflow of HDR brachytherapy.

KEYWORDS

machine learning, brachytherapy, cervical cancer, dose prediction, radiation oncology

1 Introduction

Cervical cancer is the fourth most common cancer in women globally (1). The treatment of cervical cancer relies on a combination of external radiotherapy and HDR brachytherapy to increase the dose being delivered to the primary tumor (2, 3). Numerous studies have shown that high-dose-rate brachytherapy (HDR-BT) is strongly correlated with patients' survival rates and plays an essential curative role in cervical cancer (4, 5). It allows delivery of highly localized doses to the target and excellent sparing of surrounding organs at risk (OARs). High-quality planning is a critical component in gynecologic BT treatment. However, unlike in external-beam radiation therapy (EBRT), the planning workflow in BT necessitates the collaboration of multidisciplinary teamwork in the shortest possible time to minimize the patient's discomfort and movement. The pressures of a fast-paced and accurate planning will put the entire workflow under stress, raising the risk of planning errors. Additionally, the experience and preference of brachytherapy planners, as well as clinical expertise and intuition would result in large inter- and intra-plan quality variations, further introducing more uncertainties to the BT treatment.

In the last decade, Knowledge-based planning (KBP), a new set of data-driven methodologies has been developed to improve the quality and efficiency of EBRT planning based on the previous high-quality clinical plans (6–9). Many researchers have demonstrated KBP's strength and validity in guiding planners to achieve optimal dose-volume histograms (DVHs) for OARs in treatment planning (10–12). KBP methods in EBRT are usually classified into two major categories: (a) case and atlas-based methods; and (b) statistical modeling and machine learning methods. In general, case and atlas-based methods utilize geometric features to find the best-matched prior cases from a database to improve the current planning. The statistical modeling and machine learning approaches try to build dose prediction models based on regression models such as stepwise regression (13, 14), multivariate linear regression (15–17), support vector regression (18, 19), and logistic regression (20, 21). After years of development, KBP methods have been widely investigated and even clinically implemented in commercial treatment planning systems. RapidPlan™, a commercial software module integrated into Eclipse released by Varian (Varian Medical Systems, Palo Alto, CA, USA), is one such system that predicts the achievable doses and specifies the optimization objectives needed to achieve them based on the KBP method. The success of RapidPlan™ has demonstrated the KBP's practicability and effectiveness in EBRT (22, 23).

All these achievements verified the success KBP achieved in model accuracy, stability, and feasibility in clinical application in the area of EBRT. As mentioned above, the unique clinical workflow in BT makes it vulnerable to suboptimal plans. Quality control tools such as KBP are especially important, and promising in detecting suboptimal plans in BT. Moreover, current recommendations and guidelines have provided various dose constraints for BT planning. These population-based guides mainly concentrate on ensuring normal tissues do not exceed the dose limits, rather than guaranteeing individual patient receive the optimal dose distribution for their anatomy (24). Therefore, patient anatomy-based KBP, which could be used as patient-specific dose predictions to quantify currently unknown quality variations, would be particularly useful for brachytherapy.

However, despite great success achieved in EBRT, KBP is still far relatively unexplored in HDR brachytherapy due to some exceptional challenges in brachytherapy. The main reason is that the dose distribution in BT plans is highly constrained around the inserted applicator, resulting in insufficient freedom of dose modulation in planning. To the best of our knowledge, only two studies have investigated the possible application of KBP in brachytherapy, and both focused on tandem and ovoid applicator in an intracavitary setting. In Yusufaly et al.'s study (25), the authors used an established external-beam knowledge-based DVH estimation method to predict D_{2cc} in OARs. Zhou et al. (26) proposed a support vector machine model for dose prediction and effectively predicted D_{2cc}. Both studies demonstrated good results in predicting critical brachytherapy dose metrics using intracavitary brachytherapy applicators. Currently, only Tandem and Ovoid applicators were investigated in the knowledge-based planning strategies. However, various applicators with different geometry and source position would increase the dose distribution's versatility and complexity.

In this study, we proposed a KBP method to estimate the OAR dose distribution in HDR-BT treatment. To our knowledge, this work is the first application of knowledge-based dose estimation in HDR-BT with both intracavitary and interstitial cases included.

2 Method

2.1 Prediction pipeline

The study consists of two main tasks: (a) training dataset selection and (b) model training and validation. Figure 1 shows an overview of the entire workflow. Briefly, we first performed the principal component analysis (PCA) for all the training cases. Then, we retrieved the top k (bladder: k=30, rectum: k=20) plans from the training database based on PCA results using the k-nearest neighbor (kNN) algorithm. Cases in the new dataset have the most similar features to the cases in the validation dataset. These selected cases are then used to create a new training dataset to build training models. Subsequently, we used kernel density estimation (KDE) to develop a robust

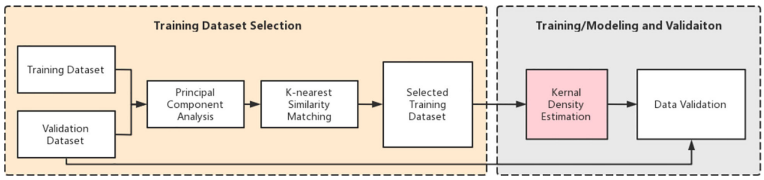

FIGURE 1
Pipeline of the DVH prediction.

prediction model based on the selected k plans. After training, a series of validation tests were conducted.

2.2 Patient database

79 HDR cervical patients previously treated in our center from 2019 to 2021 were included in this retrospective study. Each patient consists 2-4 fraction, with a total of 216 cases/fractions were involved. In this study, a 'case' indicates one single fraction containing a unique simulation CT and a treatment plan. All the cases were randomly divided into two datasets, with 170 cases in the training dataset and 46 cases in the validation dataset.

OARs and HRCTV were contoured based on CT images acquired at a GE 128 slice CT (Discovery, GE Healthcare, Inc.) using a tube setting of 120kV and 60mAs. All of the scans used identical parameters for image acquisition and reconstruction. The slice thickness and slice increment were 2.5*2.5mm. Each patient was treated with an applicator set among Tandem and Ovoid applicator (T+O), Ovoid applicator alone, Vaginal Multi-Channel applicator, 3D printed applicators, free needles, and a tandem applicator with up to 10 interstitial needles (T+N). The overview of the treatment characteristics is shown in Table 1.

According to the OARs dose constraint and the prescribed dose for the target (HR-CTV) recommended by the GEC-ESTRO, and the American Brachytherapy Society (ABS), all the treatment plans were created using the Oncentra treatment planning (Elekta, Stockholm, Sweden) system and based on TG 43 algorithm. The HRCTV was given an 80–90Gy EQD2 (biologically equivalent dose in 2-Gy fractions) prescription dose, assuming $\alpha/\beta = 10$. The bladder was given a maximum D_{2cc} of 90Gy EQD2, and the rectum was given a maximum D_{2cc} of 75 Gy EQD2, assuming $\alpha/\beta = 3$. The prescription dose in HDR brachytherapy ranges from 4-6 Gy/fraction (Table 1). In the treatment planning, we use a graphical optimization approach to repeatedly optimize the plan until the dose administered to 90% of the HRCTV reached the prescription dose. The dose distribution in each plan was scrutinized by physicians and physicists to ensure the dose distribution was clinically acceptable before treatment.

2.3 DVH prediction modeling

2.3.1 Feature reduction

Principal component analysis (PCA) has been applied to the brachytherapy plans to reduce the data dimensions and the model complexity (18, 27). PCA enables the transformation of a large set of variables into a smaller one containing most of the information. In this study, four features closely related to the dose distribution were processed using PCA to further reduce their dimensions: HRCTV volume, the distance between the centroids of the D_{2cc} and the HRCTV, prescription dose, and the average distance from D_{2cc} to the margin of the HRCTV. PCA simplifies the diversity of the dose distribution into a few principal component directions, and the individual variations can be represented by a small number of principal components. In our study, the first three principal components account for more than 90% of the variance (Figure 2) in both bladder and rectum, and thus were employed in the subsequent kNN similarity matching process for case selection.

TABLE 1 Treatment characteristics of included patients.

	Training Dataset	Test Dataset
Applicator Type		
Tandem + Needles	26	8
Vaginal	34	8
Tandem + Ovoid	45	15
Ovoid	28	5
Free Needles	26	6
3D_Printed	11	4
Total	170	46
Prescription Dose		
4	10	5
4.5	5	2
5	40	12
5.5	15	3
6	100	24
Total	170	46

Prescription dose and applicator types are grouped based on data from all included fractions(cases) per patient.

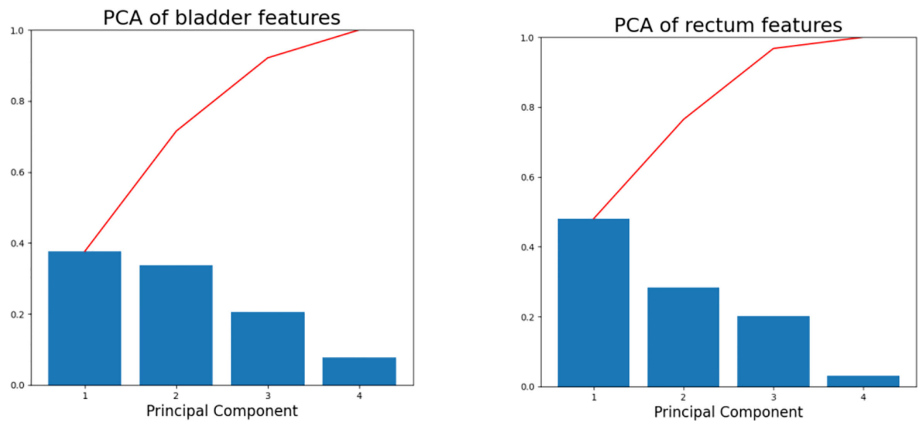

FIGURE 2
Scree plots of the bladder (left) and rectum (right) after PCA was applied to the training database. The percentage of variance represented by individual PC is plotted in descending order as blue bars, and the cumulative total is represented by red lines.

2.3.2 k-Nearest similarity matching

To take full advantage of the proposed feature, we incorporated k-Nearest Neighbors (kNN) similarity matching (28), a known robust non-parametric regression method to reduce model complexity. The purpose of kNN is to select a subset of training cases that matches closest to the validation case to create a new training dataset for subsequent model training. After recasting the training dataset along the principal component axes, the Euclidean distance between the single case in the validation set and each case in the training dataset was calculated separately in three principal component dimensions. kNN was thus used to retrieve k cases having the smallest Euclidean distance (bladder: k=30, rectum: k=20) in the training dataset.

2.3.3 Kernel density estimation

Considering that the determinant factor for dose levels near the HRCTV is the distance to the HRCTV, the histogram of distances from voxels in OARs to the HRCTV surface, which is the distance-to-target histogram (DTH), is a natural choice for predictive features. Thus, we implemented kernel density estimation (29, 30) for model training in this study. In KDE, for each voxel inside the OAR, we measure the closest distance from the voxel to the HRCTV boundary, and the distance was denoted by $x_i = x_1, x_2, \ldots x_i$ (Figure 3). The second step was to estimate the joint probability $P_{D,\,xi}$ (d, xi) of the dose d and the distance x, in which d was the corresponding dose in each voxel inside the OAR. Thirdly, we estimated the distance probability distribution P_{Xi} (xi), and calculated the conditional probability through: $P_{D|xi}$ (d|xi) = $P_{D,\,Xi}$ (d, xi)/P_{Xi}(xi)

In the prediction part, we estimated the new distance distribution probability $P^{\#}_{xi}$(xi) for each case from the validation set. Based on the calculated conditional probability in the training process, the prediction of the dose distribution for a new patient in the validation set can be calculated as: $P^{\#}_{D}(d) = \sum P_{D|Xi}(d|xi) \cdot P^{\#}_{xi}(xi)$. In the final step, DVH was defined as a function of the dose d and the probability that a random variable D was larger than or equal to d: $DVH(d) = 1 - P(D \le d) = 1 - \int_0^d P^{\#}_{D}(s)ds$.

2.4 Model validation

To quantitatively measure the prediction accuracy of the proposed model, we set the actual clinical plan DVHs as a baseline for comparison. Specific dose-volume indices including D_{2cc}, D_{1cc}, $D_{0.1cc}$, D_{max}, and D_{mean}, were extracted and analyzed, where D_{xcc} represented the minimum dose received by x cm^3 of an OAR. Absolute residuals of predicted value and the actual value ($|\Delta D_{2cc}|$, $|\Delta D_{1cc}|$, $|\Delta D_{0.1cc}|$, $|\Delta D_{max}|$, and $|\Delta D_{mean}|$) were calculated to assess the level of agreement between the predicted DVHs and the actual plan DVHs. Standard deviation (σ) over the residuals was considered a measure of model error. The mean squared error (MSE) was calculated for all planned and predicted D_{2cc} values.

2.5 Statistical analysis

Significant differences were determined using a two-sided paired t-test. Correlations between predicted parameters and actual parameters were tested by performing the Pearson correlation test. Kruskal-Wallis ANOVA was

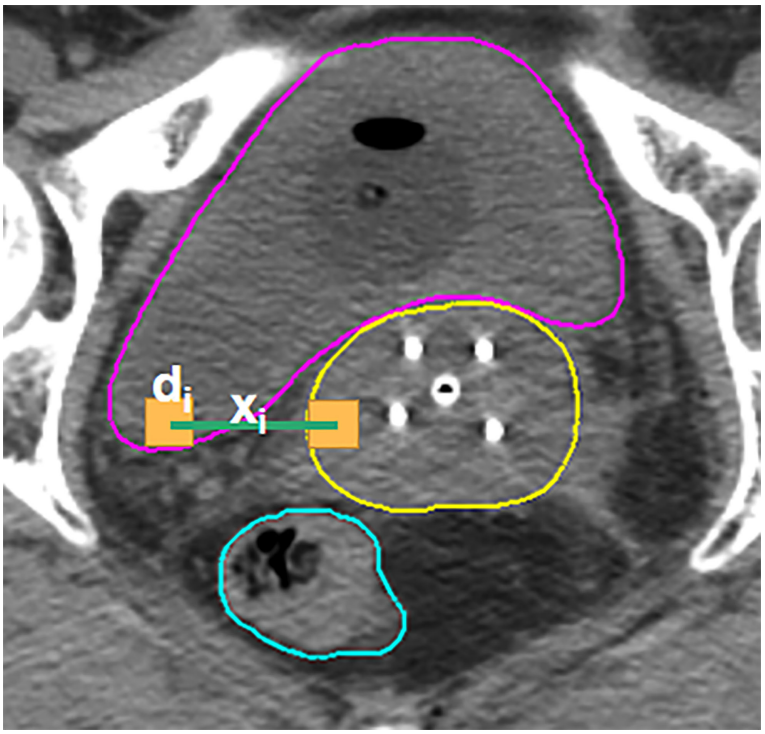

FIGURE 3
Illustration of the KDE method in the brachytherapy treatment planning. For each voxel in the OAR, xi is the distance between this voxel and its closest voxel on the HRCTV surface and di is the dose received in each voxel inside the OAR.

employed to identify differences among various applicators. All statistical data analyses were performed using Python.

3 Results

For each test case, we built a model trained with the selected k cases (bladder: k=30, rectum: k=20) from a total of 170 training cases. The model accuracy was evaluated using a separate validation dataset consisting of 46 cases. The kernel density model based on 170 cases is shown in Figure 4. There was no statistically significant difference between the predicted and actual D_{2cc} values for the bladder ($p = 0.74$), rectum ($p = 0.57$) in the validation group. As shown in Table 2, the MSE value of D_{2cc} for the bladder was 0.23, and for rectum was 0.18. In bladder, the absolute difference between predicted plans and actual plans in D_{2cc}, D_{1cc}, $D_{0.1cc}$, D_{max} and D_{mean}, were 0.38 ± 0.29, 0.4 ± 0.32, 0.43 ± 0.36, 0.97 ± 0.66 and 0.13 ± 0.09, respectively. For the corresponding rectum, the absolute difference values were 0.34 ± 0.27, 0.38 ± 0.33, 0.63 ± 0.57, 1.41 ± 0.99 and 0.23 ± 0.17, respectively. The model prediction error in D_{2cc} to the bladder, and rectum was within 0.3 Gy, as quantified by the standard deviation (Figure 5).

The model-predicted DVHs were compared to their corresponding DVHs in the actual plans to assess the model's prediction accuracy. The DVHs of one example in the validation set were plotted and compared, as shown in Figure 6.

4 Discussion

Knowledge-based planning in EBRT has demonstrated its effectiveness across multiple disease sites. However, it is still less investigated in high-dose-rate brachytherapy. This study developed a KBP method for DVH prediction in HDR-BT. Theoretically, such a KBP model can be trained using gold-standard datasets and serve as quality assurance tools in the clinic to identify suboptimal plans in treatment planning prospectively. Therefore, this KBP method has a great potential to assess the treatment plan quality and offer guidance for following plan optimization.

Different from previous studies, in which only T+O applicator was investigated (25, 26, 31), we involved different applicator sets including T+O, Vaginal Multi-Channel applicator, Ovoid applicator, free needles, 3D printed applicators, and T+N applicators. Overall, our results show slightly better accuracy in D_{2cc} than Yusufaly et al. (25): bladder σ was 0.36 Gy vs. 0.46 Gy,

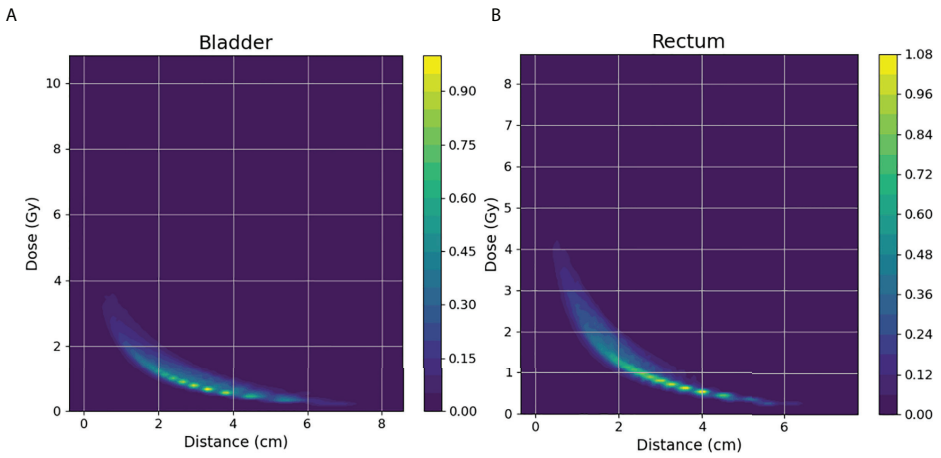

FIGURE 4
(A, B) depict the KDE model for bladder(left) and rectum(right) of 170 training cases.

rectum σ was 0.42 Gy vs. 0.47 Gy. (Since Yusufaly used relative error, here we also used the results of relative error for comparison.) To evaluate whether the applicator types would affect the predictive accuracy, we applied the Kruskal-Wallis analysis of variance (ANOVA) test in the validation dataset. The ANOVA revealed that D_{2cc} has no significant statistical difference among different applicators (p=0.109). A possible explanation for this might be that the combination of kNN and PCA selected similar training cases for each validation case, reducing the variation in dose distribution caused by different applicators.

TABLE 2 Model performances for bladder and rectum.

	MSE (D2cc)	|ΔD2cc|	|ΔD1cc|	|ΔD0.1cc|	|ΔDmax|	|ΔDmean|
Bladder	0.23	0.38 ± 0.29	0.4 ± 0.32	0.43 ± 0.36	0.97 ± 0.66	0.13 ± 0.09
Rectum	0.18	0.34 ± 0.27	0.38 ± 0.33	0.63 ± 0.57	1.41 ± 0.99	0.23 ± 0.17

The mean squared error and the absolute difference between predicted values and actual values were calculated.

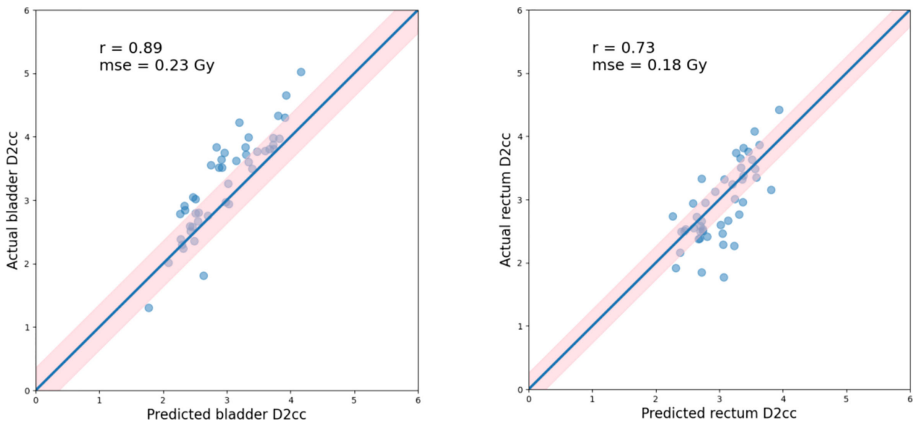

FIGURE 5
Actual vs. predicted D2cc for the bladder(left) and rectum(right), as well as the Pearson correlation coefficients (r), standard deviation (indicated by σ as well as light pink shaded area). Blue lines indicate the theoretically ideal predictions.

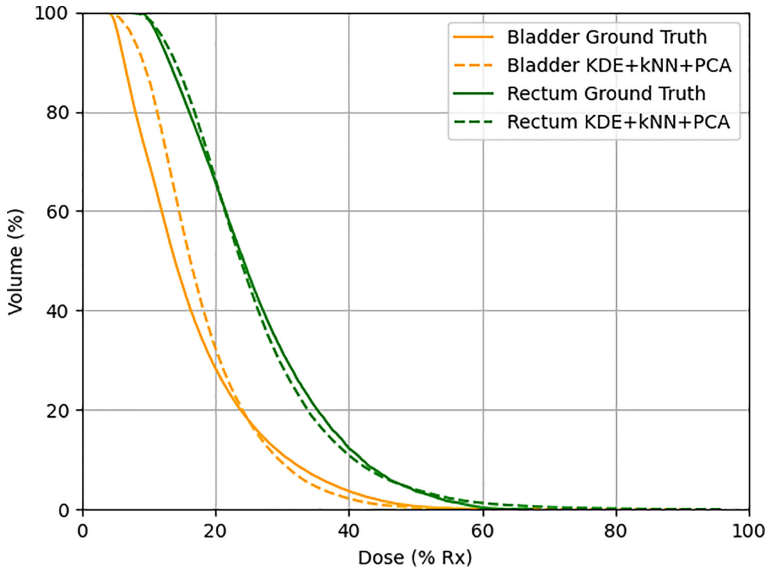

FIGURE 6
One example in the validation set demonstrating actual (solid line) and predicted (dotted line) DVHs. Orange lines represent the bladder, and green lines represent the rectum.

kNN was used to select k plans in the training dataset that mostly resemble the case in the validation dataset for model training. Once we determined the k value, we would neglect or hardly consider the information of other nearest neighbors. Thus, reducing the number of cases for training naturally comes at the expense of accuracy. The benefit of the case reduction is that smaller data set is easier to explore and analyze. It eliminates redundant and irrelevant variables and gives rise to an easier and faster training process in machine learning. A proper k value is crucial for model training and an inappropriate k value may yield unstable performance. To select the most appropriate k value, we run the kNN algorithm on 20 test cases with k values ranging from 10-40. The k value achieved the best model performance in D_{2cc} was used in model training (Table 3). Thus, we select k=30 for bladder and 20 for the rectum.

PCA was combined with kNN for better similarity matching in case selection. The main function of PCA was to reduce feature dimensionality in an interpretable way, while preserving as much information as possible at the same time. In our study, the first three principal components were used for kNN similarity matching. To verify the effectiveness of the PCA and kNN in model performance, we tested two different methods, KDE only, and KDE combined with kNN and PCA, separately. As shown in Table 4, results showed that the all-inclusive approach which combined KDE, kNN and PCA achieved the best D_{2cc} performance for both bladder and rectum. The all-inclusive method showed a significantly better prediction performance than KDE only, with an improvement of 30.3% for bladder and 33.3% for rectum. Figure 7 depicts one example predicted DVHs and actual DVHs (ground truth) for bladder and rectum. The DVHs predicted using all-inclusive method had the lowest difference from the actual DVHs.

TABLE 3 Mean square error of predicted D_{2cc} using different k values.

k	Bladder	Rectum
10	0.283	0.094
20	0.215	0.091
30	0.210	0.106
40	0.215	0.110

DVH prediction modeling is often a complex, not a simple problem. There are still several sources of error limiting the model"s ability to predict a satisfactory DVH. In this investigation, the main error came from the nonconformity of the HRCTV dose distribution, and 100% prescription dose line (contour of $V_{100\%}$). In KDE, since we do not have the contour of 100% prescription dose line for validation cases, we use HRCTV instead. We calculated the probability distribution based on the assumption that HRCTV achieved exactly 100% prescription dose. However, the dose distribution inside the HRCTV was determined by the source dwell position and dwell time, and the dose distribution in brachytherapy are highly constrained around applicators. The HRCTV and 100% prescription dose line can be slightly

TABLE 4 Comparison of model performances using different methods.

		MSE (D2cc)	|ΔD2cc|	|ΔD1cc|	|ΔD0.1cc|	|ΔDmax|	|ΔDmean|
Bladder	KDE	0.27	0.44 ± 0.28	0.47 ± 0.29	0.5 ± 0.42	2.1 ± 1.9	0.32 ± 0.2
	KDE+kNN+PCA	0.23	0.38 ± 0.29	0.4 ± 0.32	0.43 ± 0.36	0.97 ± 0.66	0.13 ± 0.09
Rectum	KDE	0.27	0.43 ± 0.31	0.45 ± 0.34	0.54 ± 0.49	0.93 ± 0.72	0.31 ± 0.23
	KDE+kNN+PCA	0.18	0.34 ± 0.27	0.38 ± 0.33	0.63 ± 0.57	1.41 ± 0.99	0.23 ± 0.17

The mean squared error and the absolute residual between predicted values and ground truth were calculated.

inconsistent if the case has inadequate or inappropriate applicator positions in some slices, especially in the slices at the beginning or the end of HRCTV. That is to say, the bias between the HRCTV contour and the 100% prescription dose line would cause error in the subsequent dose probability estimation. Thus, we applied a contour correction method to adjust the HRCTV contour.

$$\text{Mean} = \frac{1}{n}\sum \frac{1}{r_{i,j}^2}$$

where i = 1, 2, 3…n, n is the number of points in the HRCTV boundary, j = 1, 2, 3… m, m is the number of applicators, $r_{i,j}$ represents the distance between the point in the HRCTV boundary to the applicator.

Figure 8 shows the optimized HRCTV contour based on the correction method. The Dice Similarity Coefficient (DSC) value was used to evaluate the matching degree after correction. The DSC values between the optimized contour and 100% prescription dose line indicate a slightly better match degree than the original HRCTV contour, but ultimately these corrections made unstable and modest improvements ranging from -0.023-0.057 in D_{2cc} prediction accuracy. Thus, we did not integrate this correction into our machine learning algorithm. This limitation will become the direction of our future research.

To sum up, this work presents a KBP method to predict DVH for OARs in brachytherapy treatment. Patient anatomical features in previously treated cases were learned to predict DVHs for new patients. The predictions based on the individual patient geometry could motivate planners to go beyond the dosimetric constraints imposed by protocols to improve planning and provide better dose sparing for OARs. In our study, the entire process, including case selection, model construction, and DVH prediction, can be completed within one minute, which is acceptable in clinical application. Initial results have shown great potential in making this KBP model a quality control tool in treatment planning. Future studies will focus on the feasibility verification of using this model as a quality control tool in clinical practice. Another research direction is to re-plan those plans with D_{2cc} exceeding the prediction interval to improve plan quality and facilitate customized treatment planning for each patient.

5 Conclusion

In this paper, we proposed a machine learning method based on KDE, kNN, and PCA to predict the DVH in HDR-BT. The DVH for a new treatment plan was estimated using patient-specific anatomical information and an estimation model trained from prior plans. To our knowledge, this is the first KBP method that can predict the DVHs in patient who was treated with interstitial applicators, intracavitary applicators or both. The preliminary results have verified the

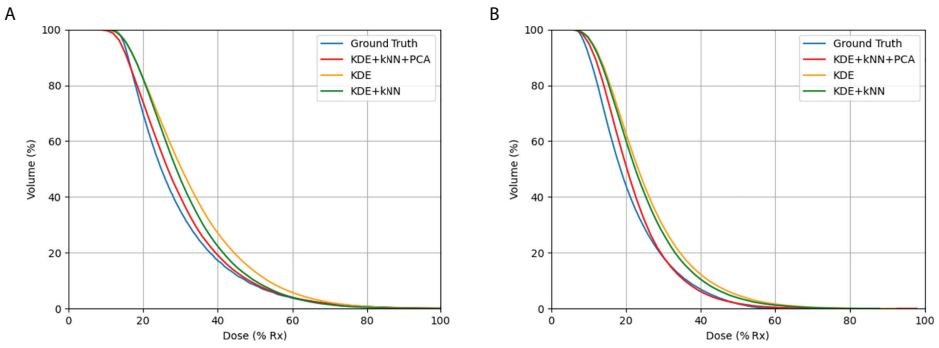

FIGURE 7
Comparison of DVHs in actual plan and the predicted DVHs using different methods: **(A)** bladder, **(B)** rectum. The method using KDE, kNN, and PCA produced the most accurate results when compared to actual DVHs.

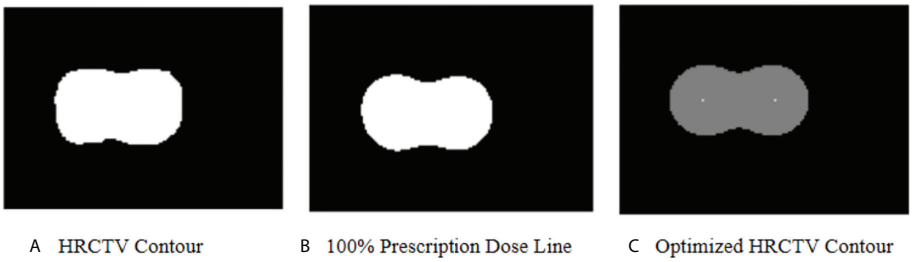

FIGURE 8
(A) shows the HRCTV contoured by a radiation oncologist in an actual plan. **(B)** shows the 100% prescription dose line in an actual plan. **(C)** shows the optimized HRCTV contour based on the correction method. In KDE method, we assume **(A)** matches with **(B)** perfectly. In this case, the optimized HRCTV has a better similarity with the 100% prescription dose line.

model's effectiveness in OAR dose estimation and its potential in providing guidance for brachytherapy planning in the future.

Data availability statement

The original contributions presented in the study are included in the article. Further inquiries can be directed to the corresponding author.

Ethics statement

The studies involving human participants were reviewed and approved by Shanghai Sixth People's Hospital. Written informed consent for participation was not required for this study in accordance with the national legislation and the institutional requirements.

Author contributions

ZL and KC : data acquisition, data processing, statistics, and writing; ZY, QZ, XY, ZL and JF: reviewing and editing. All authors contributed to the article and approved the submitted version.

Funding

This research was supported by the Science and Technology Project of Shanghai Municipal Science and Technology Commission (No.22Y31900500).

Conflict of interest

The authors declare that the research was conducted in the absence of any commercial or financial relationships that could be construed as a potential conflict of interest.

Publisher's note

All claims expressed in this article are solely those of the authors and do not necessarily represent those of their affiliated organizations, or those of the publisher, the editors and the reviewers. Any product that may be evaluated in this article, or claim that may be made by its manufacturer, is not guaranteed or endorsed by the publisher.

References

1. Buskwofie A, David-West G, Clare CA. A review of cervical cancer: Incidence and disparities. *J Natl Med Assoc* (2020) 112(2):229–32. doi: 10.1016/j.jnma.2020.03.002

2. Chargari C, Deutsch E, Blanchard P, Gouy S, Martelli H, Guerin F, et al. Brachytherapy: An overview for clinicians. *CA Cancer J Clin* (2019) 69(5):386–401. doi: 10.3322/caac.21578

3. Holschneider CH, Petereit DG, Chu C, Hsu IC, Ioffe JY, Klopp AH, et al. Brachytherapy: A critical component of primary radiation therapy for cervical cancer: From the society of gynecologic oncology (SGO) and the American brachytherapy society (ABS). *Brachytherapy* (2019) 18(2):123–32. doi: 10.1016/j.brachy.2018.11.009

4. Eifel PJ, Thoms WW Jr, Smith TL, Morris M, Oswald MJ. The relationship between brachytherapy dose and outcome in patients with bulky endocervical tumors treated with radiation alone. *Int J Radiat Oncol Biol Phys* (1994) 28(1):113–8. doi: 10.1016/0360-3016(94)90148-1

5. Tanderup K, Eifel PJ, Yashar CM, Pötter R, Grigsby PW. Curative radiation therapy for locally advanced cervical cancer: brachytherapy is NOT optional. *Int J Radiat Oncol Biol Phys* (2014) 88(3):537–9. doi: 10.1016/j.ijrobp.2013.11.011

6. Ge Y, Wu QJ. Knowledge-based planning for intensity-modulated radiation therapy: A review of data-driven approaches. *Med Phys* (2019) 46(6):2760–75. doi: 10.1002/mp.13526

7. Jiao SX, Wang ML, Chen LX, Liu XW. Evaluation of dose-volume histogram prediction for organ-at risk and planning target volume based on machine learning. *Sci Rep* (2021) 11(1):3117. doi: 10.1038/s41598-021-82749-5

8. Zhang J, Ge Y, Sheng Y, Yin FF, Wu QJ. Modeling of multiple planning target volumes for head and neck treatments in knowledge-based treatment planning. *Med Phys* (2019) 46(9):3812–22. doi: 10.1002/mp.13679

9. Nwankwo O, Mekdash H, Sihono DS, Wenz F, Glatting G. Knowledge-based radiation therapy (KBRT) treatment planning versus planning by experts: validation of a KBRT algorithm for prostate cancer treatment planning. *Radiat Oncol* (2015) 10:111. doi: 10.1186/s13014-015-0416-6

10. Zhang J, Wu QJ, Xie T, Sheng Y, Yin FF, Ge Y. An ensemble approach to knowledge-based intensity-modulated radiation therapy planning. *Front Oncol* (2018) 8:57. doi: 10.3389/fonc.2018.00057

11. Tol JP, Dahele M, Delaney AR, Slotman RJ, Verbakel WF. Can knowledge-based DVH predictions be used for automated, individualized quality assurance of radiotherapy treatment plans? *Radiat Oncol* (2015) 10:234. doi: 10.1186/s13014-015-0542-1

12. Janssen TM, Kusters M, Wang Y, Wortel G, Monshouwer R, Damen E, et al. Independent knowledge-based treatment planning QA to audit pinnacle autoplanning. *Radiother Oncol* (2019) 133:198–204. doi: 10.1016/j.radonc.2018.10.035

13. Wang J, Jin X, Zhao K, Peng J, Xie J, Chen J, et al. Patient feature based dosimetric pareto front prediction in esophageal cancer radiotherapy. *Med Phys* (2015) 42(2):1005–11. doi: 10.1118/1.4906252

14. Millunchick CH, Zhen H, Redler G, Liao Y, Turian JV. A model for predicting the dose to the parotid glands based on their relative overlapping with planning target volumes during helical radiotherapy. *J Appl Clin Med Phys* (2018) 19(2):48–53. doi: 10.1002/acm2.12203

15. Sheng Y, Ge Y, Yuan L, Li T, Yin FF, Wu QJ, et al. Outlier identification in radiation therapy knowledge-based planning: A study of pelvic cases. *Med Phys* (2017) 44(11):5617–26. doi: 10.1002/mp.12556

16. Faught AM, Olsen L, Schubert L, Rusthoven C, Castillo E, Castillo R, et al. Functional-guided radiotherapy using knowledge-based planning. *Radiother Oncol* (2018) 129(3):494–8. doi: 10.1016/j.radonc.2018.03.025

17. Younge KC, Marsh RB, Owen D, Geng H, Xiao Y, Spratt DE, et al. Improving quality and consistency in NRG oncology radiation therapy oncology group 0631 for spine radiosurgery via knowledge-based planning. *Int J Radiat Oncol Biol Phys* (2018) 100(4):1067–74. doi: 10.1016/j.ijrobp.2017.12.276

18. Zhu X, Ge Y, Li T, Thongphiew D, Yin FF, Wu QJ. A planning quality evaluation tool for prostate adaptive IMRT based on machine learning. *Med Phys* (2011) 38(2):719–26. doi: 10.1118/1.3539749

19. Zhang HH, Meyer RR, Shi L, D'Souza WD. The minimum knowledge base for predicting organ-at-risk dose-volume levels and plan-related complications in IMRT planning. *Phys Med Biol* (2010) 55(7):1935–47. doi: 10.1088/0031-9155/55/7/010

20. Boutilier JJ, Lee T, Craig T, Sharpe MB, Chan TC. Models for predicting objective function weights in prostate cancer IMRT. *Med Phys* (2015) 42(4):1586–95. doi: 10.1118/1.4914140

21. Lee T, Hammad M, Chan TC, Craig T, Sharpe MB. Predicting objective function weights from patient anatomy in prostate IMRT treatment planning. *Med Phys* (2013) 40(12):121706. doi: 10.1118/1.4828841

22. Yuan L, Ge Y, Lee WR, Yin FF, Kirkpatrick JP, Wu QJ. Quantitative analysis of the factors which affect the interpatient organ-at-risk dose sparing variation in IMRT plans. *Med Phys* (2012) 39(11):6868–78. doi: 10.1118/1.4757927

23. Li N, Carmona R, Sirak I, Kasaova L, Followill D, Michalski J, et al. Highly efficient training, refinement, and validation of a knowledge-based planning quality-control system for radiation therapy clinical trials. *Int J Radiat Oncol Biol Phys* (2017) 97(1):164–72. doi: 10.1016/j.ijrobp.2016.10.005

24. Yusufaly TI, Meyers SM, Mell LK, Moore KL. Knowledge-based planning for intact cervical cancer. *Semin Radiat Oncol* (2020) 30(4):328–39. doi: 10.1016/j.semradonc.2020.05.009

25. Yusufaly TI, Kallis K, Simon A, Mayadev J, Yashar CM, Einck JP, et al. A knowledge-based organ dose prediction tool for brachytherapy treatment planning of patients with cervical cancer. *Brachytherapy* (2020) 19(5):624–34. doi: 10.1016/j.brachy.2020.04.008

26. Zhou P, Li X, Zhou H, Fu X, Liu B, Zhang Y, et al. Support vector machine model predicts dose for organs at risk in high-dose rate brachytherapy of cervical cancer. *Front Oncol* (2021) 11:619384. doi: 10.3389/fonc.2021.619384

27. Söhn M, Alber M, Yan D. Principal component analysis-based pattern analysis of dose-volume histograms and influence on rectal toxicity. *Int J Radiat Oncol Biol Phys* (2007) 69(1):230–9. doi: 10.1016/j.ijrobp.2007.04.066

28. Salvador-Meneses J, Ruiz-Chavez Z, Garcia-Rodriguez J. Compressed kNN: K-nearest neighbors with data compression. *Entropy (Basel)* (2019) 21(3):234. doi: 10.3390/e21030234

29. Skarpman Munter J, Sjölund J. Dose-volume histogram prediction using density estimation. *Phys Med Biol* (2015) 60(17):6923–36. doi: 10.1088/0031-9155/60/17/6923

30. Fan J, Wang J, Zhang Z, Hu W. Iterative dataset optimization in automated planning: Implementation for breast and rectal cancer radiotherapy. *Med Phys* (2017) 44(6):2515–31. doi: 10.1002/mp.12232

31. Cortes KG, Kallis K, Simon A, Mayadev J, Meyers S, Moore KL. Knowledge-based three-dimensional dose prediction for tandem-and-ovoid brachytherapy. *Brachytherapy* (2022) 21(4):532–42. doi: 10.1016/j.brachy.2022.03.002

frontiers | Frontiers in Oncology

TYPE Original Research
PUBLISHED 27 October 2022
DOI 10.3389/fonc.2022.942016

OPEN ACCESS

EDITED BY
John Varlotto,
Marshall University, United States

REVIEWED BY
Yvonne Dzierma,
Saarland University Hospital, Germany
Hongfu Zhao,
China-Japan Union Hospital, Jilin University, China

*CORRESPONDENCE
Ailin Wu
wuailing@mail.ustc.edu.cn

†These authors have contributed equally to this work and share first authorship

SPECIALTY SECTION
This article was submitted to Radiation Oncology, a section of the journal Frontiers in Oncology

RECEIVED 12 May 2022
ACCEPTED 10 October 2022
PUBLISHED 27 October 2022

CITATION
Wu A, Cui H, Jiang X, Yan B, Wu A, Liu Y and Zhu L (2022) Development and validation of a scatter-corrected CBCT image-guided method for cervical cancer brachytherapy. *Front. Oncol.* 12:942016. doi: 10.3389/fonc.2022.942016

Development and validation of a scatter-corrected CBCT image-guided method for cervical cancer brachytherapy

Ailin Wu[1*†], Hehe Cui[2†], Xiao Jiang[2], Bing Yan[1], Aidong Wu[1], Yunqin Liu[1] and Lei Zhu[2]

[1]Department of Radiation Oncology, The First Affiliated Hospital of University of Science and Technology of China (USTC), Division of Life Sciences and Medicine, University of Science and Technology of China, Hefei, China, [2]Department of Engineering and Applied Physics, University of Science and Technology of China, Hefei, China

Background and purpose: Multiple patient transfers have a nonnegligible impact on the accuracy of dose delivery for cervical cancer brachytherapy. We consider using on-site cone-beam CT (CBCT) to resolve this problem. However, CBCT clinical applications are limited due to inadequate image quality. This paper implements a scatter correction method using planning CT (pCT) prior to obtaining high-quality CBCT images and evaluates the dose calculation accuracy of CBCT-guided brachytherapy for cervical cancer.

Materials and methods: The CBCT of a self-developed female pelvis phantom and five patients was first corrected using empirical uniform scatter correction in the projection domain and further corrected in the image domain. In both phantom and patient studies, the CBCT image quality before and after scatter correction was evaluated with registered pCT (rCT). Model-based dose calculation was performed using the commercial package Acuros®BV. The dose distributions of rCT-based plans and corrected CBCT-based plans in the phantom and patients were compared using 3D local gamma analysis. A statistical analysis of the differences in dosimetric parameters of five patients was also performed.

Results: In both phantom and patient studies, the HU error of selected ROIs was reduced to less than 15 HU. Using the dose distribution of the rCT-based plan as the baseline, the γ pass rate (2%, 2 mm) of the corrected CBCT-based plan in phantom and patients all exceeded 98% and 93%, respectively, with the threshold dose set to 3, 6, 9, and 12 Gy. The average percentage deviation (APD) of D_{90} of HRCTV and D_{2cc} of OARs was less than 1% between rCT-based and corrected CBCT-based plans.

Conclusion: Scatter correction using a pCT prior can effectively improve the CBCT image quality and CBCT-based cervical brachytherapy dose calculation accuracy, indicating promising prospects in both simplified brachytherapy processes and accurate brachytherapy dose delivery.

KEYWORDS

cervical cancer, CBCT, scatter correction, model-based dose calculation algorithm, brachytherapy

1 Introduction

Cervical cancer, the fourth most common cancer among women, is a worldwide disease with high incidence and mortality rates, especially in developing countries (1, 2). Benefiting from the steep dose curves and the short source-to-tumor distance, brachytherapy (BT) can deliver an ultrahigh dose to the target volume with maximal preservation of the organs at risk (OARs). Therefore, BT is considered essential to conventional radiotherapy for cervical cancer, and previous research reported that BT can significantly improve the local control rate of the tumor and the 5-year survival rate of patients in combination with external beam radiotherapy (EBRT) (3).

Despite the tremendous success, the inadequate rates of local control and recurrence still hamper the effectiveness of the treatment for advanced cervical cancer (4, 5). Further improvement in the patient survival rate requires more accurate dose delivery. Current BT dose delivery is usually compromised by two key factors. One is the error of the commonly used water-based dose calculation recommended by AAPM TG-43U1 (6). This dose estimation strategy omits the human tissue heterogeneity and the effect of the applicator with high-Z materials, and the difference in back scatter between the human body and water is not considered. As revealed in AAPM TG-186 (7), differences between water-based and media-based dose calculations may exceed a factor of 10 in specific situations. Therefore, the use of model-based dose calculation (MBDC) is advocated for clinical practice to promote dose calculation accuracy (8). Since MBDC makes use of tissue composition and mass density as estimated from CT images of BT patients, high-quality images are considered the essential assurance for accurate dose calculation.

The second adverse factor is patient organ variations and applicator displacement due to multiple transfers and long waits (9, 10). Since cumbersome x-ray/CT/MR machines have not been widely installed in the BT treatment room, patient transfers between the imaging room and the treatment room are inevitable, which usually not only increases patient suffering but also causes organ variations and applicator displacement. During scanning, planning, and treatment, this inconsistency in the patients' anatomy induces a large dose delivery error since the dose is sharply decreased (11). Due to its advantages, including low cost, volume imaging, and simple integration, cone-beam CT (CBCT) is promising for resolving all the above adverse factors. Provided a CBCT system is installed in the treatment room, the CBCT images obtained before treatment can provide consistent patient anatomy and applicator positions as those during BT dose delivery. More importantly, the calibrated physical quantities from CT numbers, such as electron density or Z-number (12, 13), can be used for MBDC. In this case, the applicator placement/adjustment and MBDC and BT dose delivery can be completed all in one room, indicating a much simplified treatment process, shortened treatment time, and improved patient comfort.

However, the severe photon scatter, a general CBCT issue (14, 15), unavoidably degrades the soft-tissue contrast and introduces large CT number bias, which consequently results in inaccurate organ delineation and dose calculation (16, 17). It is thus seen that effective and efficient scatter correction is critical for CBCT-based radiotherapy techniques. Various CBCT scatter corrections have been developed during the last two decades (18–22), which enhances its utility in dose calculation for adaptive EBRT planning (23). Recently, on-site CBCT has attracted increasing attention in adaptive BT (24). However, existing study results show that the current CBCT image quality is not adequate to meet the clinical requirements (24–26), and performance improvements of CBCT images are needed. Recall that cervical BT is always coupled with EBRT (3), and the prior information-based methods (27, 28) are especially suitable in BT since high-quality EBRT-CT routinely obtained for treatment planning can be used as a prior. However, the existing prior information-based methods are only carried out in the projection domain or in the image domain. The performance of those methods may be degraded when the CBCT is obtained under poor conditions.

In this work, we propose hybrid-domain CBCT scatter correction using EBRT-CT as a prior. A self-developed BT phantom is used in the first study, and the quantitative image analysis and accuracy evaluation of the dose calculation are carried out. The patient study presents the comparison of image quality and clinical dose assessment based on the rCT and scatter-corrected

CBCT images, which validates the clinical feasibility of scatter-corrected CBCT image-guided brachytherapy (IGBT).

2 Materials and methods

2.1 Hybrid-domain scatter correction

In the conventional IGBT process, the patient was first implanted with applicators in the gynecological room, then transferred to the x-ray/CT/MRI room to acquire images for treatment planning and dose calculation, and finally, the patient needs to be transferred to the BT room for treatment. However, this complex treatment process, coupled with the long wait times, inevitably caused applicator displacement and tissue variation. Because of a large dose gradient around the radiation source, even a small deviation can result in an unacceptable dose change to the tumor and OARs. As an ideal solution, CBCT IGBT was proposed, which realized applicator insertion, imaging, and treatment delivery in the same room. To ensure that CBCT images can not only meet the requirements of target delineation but also achieve accurate dose calculation, we put forward hybrid-domain CBCT scatter correction for BT. The workflow of this method is depicted in Figure 1. For simplicity, CT images acquired during the EBRT/BT are referred to as EBRT/BT-CT. To improve the HU accuracy of CBCT, we implemented a hybrid-domain scatter correction using EBRT-CT as a prior, which is illustrated in the dotted box of Figure 1, with each step summarized as follows:

Step 1: Obtain the linear attenuation coefficients (LAC) of four tissues (air, fat, muscle, and bone) from EBRT-CT, and their values are abbreviated as $\bar{\mu}_{air}, \bar{\mu}_{fat}, \bar{\mu}_{muscle}$, and $\bar{\mu}_{bone}$. Because of the high resolution and uniformity of EBRT-CT, the HU number of different tissues (air, adipose, muscle, and bone) can be easily distinguished in the CT histogram distribution. The mode of each tissue is obtained according to the histogram and used as the mean value of each tissue. Note that the directly obtained value is the CT number value with HU units and the LAC is then calculated based on Equation (1).

$$\mu_m = \frac{CT\ number}{1000} \times \mu_w + \mu_w \tag{1}$$

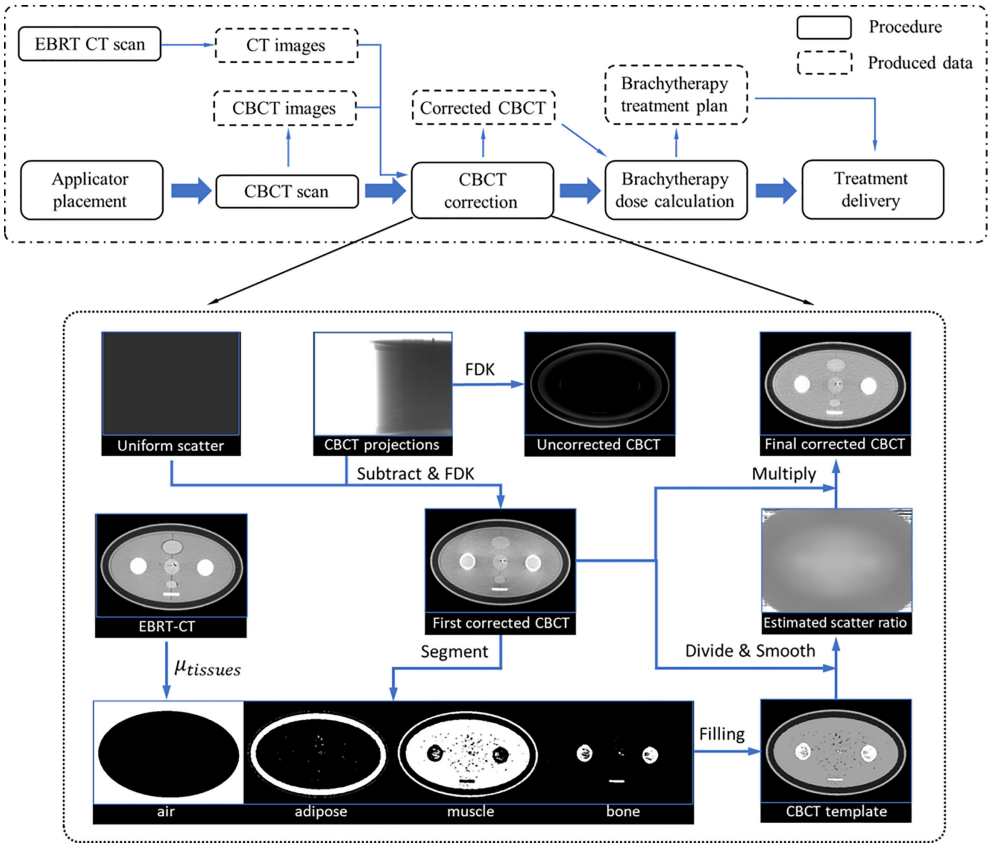

FIGURE 1
Dot-dash boxes: the flowchart of CBCT-based cervical brachytherapy. Dotted box: detailed workflow of the scatter correction.

μ_m and μ_w represent the LAC of the material and water, respectively.

Step 2: Generate the first-pass scatter-corrected projections (p_c) by subtracting an empirical uniform scatter ($\bar{s}$) from the raw CBCT projections (p_{raw}). Then, the CBCT image ($CBCT_c$) is reconstructed using p_c *via* the Feldkamp–Davis–Kress (FDK) algorithm.

Step 3: The $CBCT_c$ is segmented into four parts: air, fat, muscle, and bone, and the template image ($CBCT_t$) is generated by filling each part with the referenced LAC. Then, $CBCT_t$ is created using the LAC from EBRT-CT.

Step 4: The scatter ratio (r) is first calculated as $r = CBCT_t/CBCT_c$, and then a binary mask (f) is generated to sample the low-frequency signals on r:

$$f = \begin{cases} 0, & |r| > r_{\max} or |\nabla r| > G_{\max} \\ 1, & otherwise \end{cases} \quad (2)$$

r_{max} and G_{max} are the maximum intensity and the gradient of the scatter ratio, respectively. Their value is chosen such that 80% of all pixels is smaller than the chosen value.

Step 5: Sparse-sampled scatter ratio r is further smoothed and extended to the whole images *via* a local filtration technique (29):

$$r_f = \frac{(r \cdot f) ** w}{f ** w} \quad (3)$$

where ** represents the 2D convolution operation and w and r_f denote the Gaussian filter and the smoothed scatter ratio, respectively.

Step 6: Obtain the final corrected CBCT ($CBCT_{fc}$) by scaling the $CBCT_c$ by the smoothed ratio (r_f).

The CBCT images reconstructed from raw projections suffer severe nonuniformity, which hampers accurate tissue differentiation. To resolve this, an empirical uniform scatter correction is firstly performed in the projection domain to roughly alleviate the nonuniformity and facilitate segmentation. The uniform scatter correction method is inspired by the low-frequency feature of the scatter signal. In this method, a constant value is considered the scatter signal, and the corrected projection is generated by subtracting the value from the raw projection. In this work, the constant value is set such that 90% of the object projection signals are larger, and a soft-cut algorithm currently used in previous studies is adopted to ensure the corrected projection signal positivity (22). $CBCT_c$ is reconstructed using the corrected projections *via* FDK.

The CBCT segmentations are generated by transferring the EBRT-CT segmentation *via* the commercial software MIM (software version 7.1.2; MIM Software Inc., Cleveland, OH, USA). The segmentation of EBRT-CT is performed based on the threshold. The CT number of EBRT-CT in the range [−1,024 −500], [−125 −60], [15 85], and >190 HU is thought to be air, adipose, muscle, and bone tissues, respectively. Although the EBRT-CT is of high quality, the boundary between the two tissues is not easily distinguished automatically; the tissue whose CT number is not within the above interval was considered to be air. Then, the value of those values in the binary mask f is equal to 0, which means that the weight of those values in calculating the smoothed ratio r_f is 0.

Since the applicator used in this study is made of high-Z titanium, its HU value is much larger than that of human tissues. Considering that the applicator is not deformed during treatment, we performed a separate CT scan for the applicator and segmented it as the applicator ground truth. Then, the applicator in $CBCT_{fc}$ is segmented separately, and the applicator in the CT images is rigidly registered and transferred to the final corrected CBCT.

2.2 Data acquisition and processing

A self-developed female pelvis BT phantom is shown in Figure 2. The phantom dimension and organ position were determined based on Asian female patients with an elliptical cross-sectional area of 340 mm * 200 mm. The materials with similar CT numbers to the corresponding organs or tissues were selected to mimic the real female pelvis. As shown in Figure 2A, the molds of OARs, i.e., the bladder, intestine, and rectum, were made up of silica gel, peanut oil, polymethyl methacrylate (PMMA), polyoxymethylene (POM), and polytetrafluoroethylene (PTFE) were used to simulate adipose, muscle, cortical bone, and cancellous bone respectively. The uterus and vagina were connected with a 2-mm-diameter elastic channel in it to enable applicator movement. In the phantom study, a tandem applicator (AL07522000; Varian Medical Systems, Palo Alto, CA) was inserted. Figure 2B displays the real pelvis phantom with the inserted applicator. A phantom study was used to demonstrate the feasibility of the proposed method.

To further evaluate the proposed method in clinical applications, five patients with stage IIB–IIIB cervical cancer were selected for retrospective analysis. These patients received EBRT and image-guided radiotherapy (IGRT) boost in combination with 3D high-dose-rate (HDR) BT (30) in Anhui Provincial Cancer Hospital. Before each BT patient received EBRT, a BT-CBCT scan was performed after the BT-CT scan to confirm the position of applicators. During this procedure, an effective external immobilization and a 3D transfer bed were used. The patient transfer was performed by multiple staff members in a coordinated effort to minimize the applicator displacement. A titanium Fletcher-Suit Delclos (FSD)-Style Applicator Set (AL13030001; Varian Medical Systems, Palo Alto, CA) was used for implantation, along with gauze packing.

In both phantom and patient studies, the CT images (including EBRT-CT and BT rCT) were acquired by a 16-slice CT machine (Discovery CT590 RT, GE). The CT machine operated in standard pelvis mode and reconstructed images

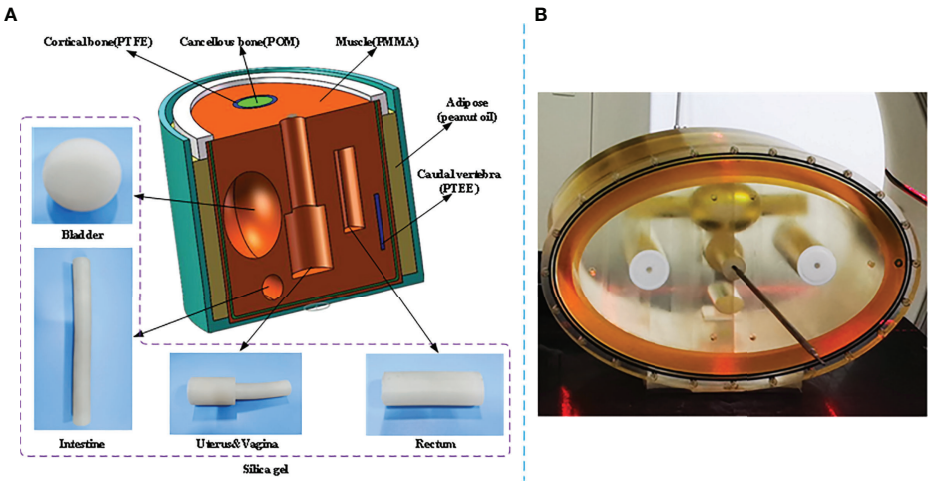

FIGURE 2
Illustration of the self-developed female pelvis BT phantom. **(A)** Structure diagram and materials of the phantom. **(B)** Pelvis phantom during a real CT scan.

with a size of 512 * 512 * 114 voxels, and the voxel size was 1.17 mm * 1.17 mm * 2.5 mm. The CBCT scan of the pelvis phantom was acquired in a tabletop CBCT system at the University of Science and Technology of China. The geometry of this system exactly matches that of a Varian On-Board Imager (OBI) CBCT system. To comprehensively evaluate the performance on scatter correction, the bowtie filter that can alleviate photon scatter was not installed in this system. The tube voltage, tube current, and pulse width were set to 125 kVp, 30 mA, and 10 ms, respectively. The patient CBCT scan was acquired on the commercial OBI system installed on Trilogy machine (Varian Medical Systems, Palo Alto, CA). The x-ray tube was operated at 125 kVp and 80 mA, with a bowtie filter mounted at the tube exit. Projection data were exported from the OBI CBCT system *via* the tabletop computer, and then the reconstructions were performed in MATLAB with and without scatter correction to obtain corrected CBCT and raw CBCT, respectively. The reconstructed volume had a size of 512 * 512 * 160 voxels, with a voxel size of 1 mm * 1 mm * 1 mm. Additionally, the rCT images and the corrected CBCT images were registered by using the MIM-Mastro DIR algorithm and the reg refine tool. For computation acceleration, FDK and the local filtration were implemented using CUDA C (NVIDIA, Santa Clara, CA).

2.3 Dose calculation

The rCT and $CBCT_{fc}$ of the phantom and patients were input into the commercial software BrachyVision (vision 15.5, Varian Medical Systems, Inc., Palo Alto, CA, USA). In the phantom dose calculation, the size of the dose-calculated volume was chosen as 386 * 245 * 200 voxels (1 mm * 1 mm * 1 mm for each voxel), which completely covered the entire area of the phantom. Ten dwell positions were manually defined, with a step size of 5 mm and a dwell time of 30 s at each position. The dose distributions (RD_CT) were obtained with MBDC *via* the Acuros®BV algorithm based on AAPM report TG-186. Since the phantom has no deformation, the rCT and $CBCT_{fc}$ were well matched. Using the same settings in the rCT dose calculation, the dose distribution RD_cor was obtained on $CBCT_{fc}$.

In the patient dose calculation, experienced oncologists first delineated the target volume and OARs on both rCT and $CBCT_{fc}$, then the physicist performed the applicator reconstruction on rCT images. To meet the dose recommendations by the gynecological (GYN) GEC-ESTRO working group (31, 32), the physical dose objectives of BT were 5.5 Gy/F for HR-CTV while the D_{2cc} of OARs was less than 5.3 Gy/F on the bladder and 4.15 Gy/F on the rectum, sigmoid, and intestine. Based on the rCT images, MBDC was completed by inverse planning *via* the Acuros BV optimization method and obtained the dose distribution RD_CT. Finally, the spatial coordinates of applicators, the dwell times, and the relative positions of radiation sources of the rCT plans were input into the $CBCT_{fc}$ plans. The obtained dose distribution in heterogeneous media was referred to as RD_cor. The dose matrix was set the same for both RD_CT and RD_cor while the size of the dose-calculated volume was chosen as 2.5 mm * 2.5 mm * 1 mm for each voxel.

2.4 Evaluation

2.4.1 CBCT image quality

Scatter always leads to severe cupping artifacts, indicating a much lower CT number, especially in the central area of CBCT images. The mean CT number value in selected ROIs is used to reflect the image accuracy on different tissues and the root-mean-square error (RMSE) is used to quantify the overall imaging accuracy, which is calculated as:

$$RMSE = \sqrt{\frac{1}{n}\sum_{i=1}^{n}(\overline{HU_{cbct}^{i}} - \overline{HU_{CT}^{i}})^2} \quad (4)$$

where $\overline{HU_{cbct}^{i}}$ and $\overline{HU_{CT}^{i}}$ are the mean CT number of the *i*th ROI in $CBCT_{fc}$ and rCT, respectively. In addition to CT number deviation, a low-frequency scatter signal also causes nonuniformity and contrast loss, which can be characterized by spatial nonuniformity (SNU) and the contrast-to-noise ratio (CNR):

$$SNU = \overline{HU}_{max} - \overline{HU}_{min} \quad (5)$$

$$CNR = \frac{|\overline{HU_r} - \overline{HU_b}|}{\sigma_r} \quad (6)$$

where $\overline{HU}_{max}$ and $\overline{HU}_{\min}$ are the maximal and minimum mean CT number of the same tissue among the selected ROIs, respectively. $\overline{HU_r}$ and $\overline{HU_b}$ are both the mean CT number in the selected ROI and background, and σ_r the standard deviation (STD) inside the ROI.

2.4.2 Dose distribution

In the phantom study, rCT and CBCTfc were strictly matched and shared an identical plan. Thus, phantom results were used to quantitatively evaluate the dose calculation accuracy. The 3D local γ -index (33) was first calculated under three different distance and dose difference criteria (δr, δD), i.e., (1%, 1 mm), (2%, 1 mm), and (2%, 2 mm). The dose distribution on the rCT was used as a reference, and the dose threshold was set to 3 Gy, 6 Gy, 9 Gy, and 12 Gy.

In patient studies, rCT was matched with the $CBCT_{fc}$ images by MIM software. Therefore, 3D gamma analysis with different criteria and dose thresholds was also performed to evaluate the local dose difference of patients between the RD_CT and RD_cor. In addition, the parameters commonly used in the clinical dosimetric evaluation were statistically analyzed, including D_{90} (minimal dose delivered to 90%) of HR-CTV and the minimum dose of the 2 cm^3 of the volume (D_{2cc}) received by the bladder, rectum, sigmoid, and intestine.

3 Results

3.1 Phantom study

3.1.1 CBCT image quality

Phantom images are displayed in Figures 3 and 4. Since a bowtie filter was not installed, raw CBCT images were severely contaminated by photon scatter such that no organ could be distinguished with the display window of [−200 300] HU, and the scatter-induced CT number error was spatially variant, as evidenced by the cupping 1D profiles in Figure 3 and the pixel-level CT number difference of CBCT and CT in Figure 4. Although the raw CBCT seems better at the display window of [−500 500] HU in Figure 4, the image quality is not substantially improved. After the proposed correction, organs such as the uterus, intestine, rectum, and bladder were observed with the display window of [−200 300] HU, and the nearly coincident profiles indicated that the proposed method achieved accuracy comparable to that of rCT on the soft tissues.

The quantitative analysis shown in Tables 1 and 2 further reveals the improvement in CT number accuracy. Excluding adipose tissue, each of the other nine ROIs suffered a CT number error of over 450 HU in the raw CBCT, which was reduced to less than 15 HU by the proposed correction. After scatter removal, the RMSE was reduced from 501 HU to less than 10 HU, the SNU was reduced to 16 HU from 107 HU and the CNR between the rectum and muscle was improved by a factor of 4.48. Although the improved CNR is still much lower than that of rCT, it is enough to differentiate the rectum from the background. Since the scatter removal amplifies the noise level (34), the standard deviation of CBCT corrected with the proposed method is larger than that in raw CBCT images.

3.1.2 Dose calculation precision

Figure 5 displays the γ-index map under three different criteria, with γ pass rates listed in Table 3. Using the criterion (1%, 1 mm), significant dose differences were observed in RD_cor at each dose level. Quite a few high-dose voxels (≥9 Gy) failed the γ-index test, as shown in Figures 5A, D. After relaxing the dose criterion to 2%, as observed in Figure 5B, most voxels at both ends of the applicator passed the γ-index test (Figure 4E). Quantitative analysis revealed that RD_cor achieved a γ pass rate of >97%, indicating significant improvement in the dose calculation accuracy after scatter correction. Furthermore, if the criteria were set to (2%, 2 mm), only scattered high-difference voxels were shown in the γ-index map.

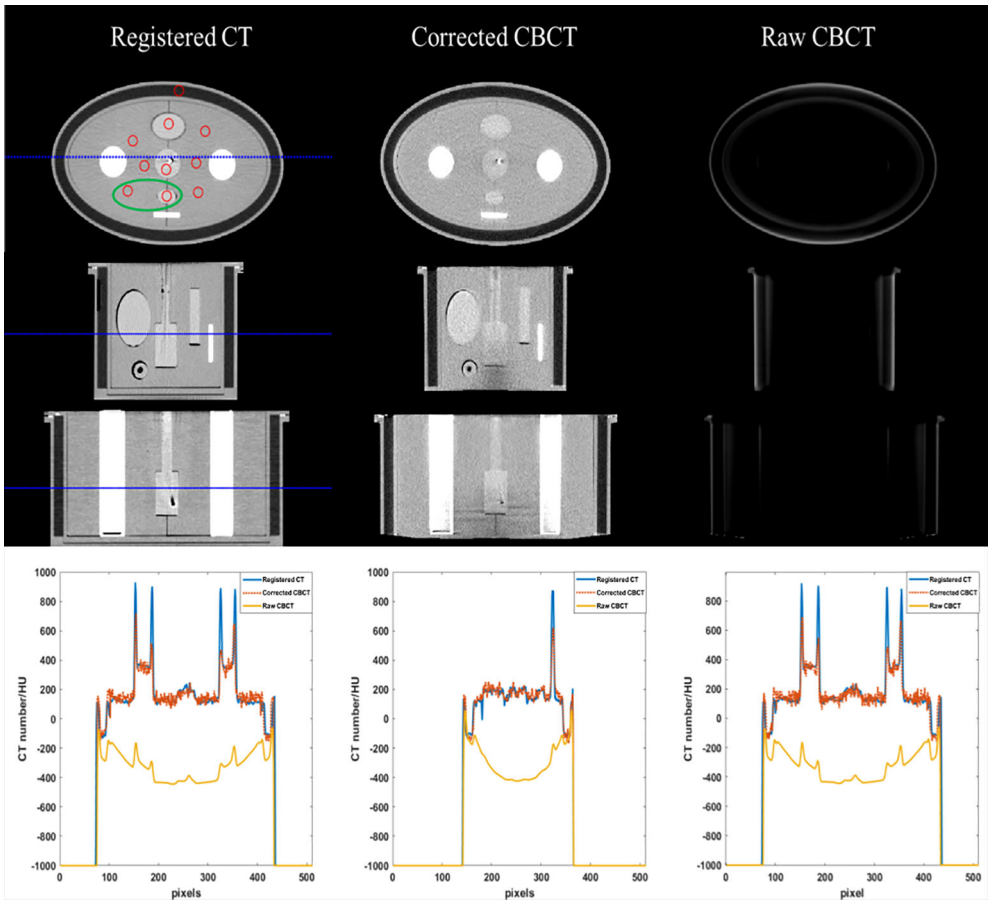

FIGURE 3
CT/CBCT images of the female pelvis phantom. The first three rows display the axial, sagittal, and coronal views from top to bottom; display window: [−200 300] HU. The mean CT number and SNU are calculated in the circle areas, and the CNR is calculated in the ellipse area. The 1D profiles indicated by the dotted lines are displayed in the last row.

3.2 Patient study

3.2.1 CBCT image quality

Figures 6 and 7 show the comparison views of a BT patient's images, with the CT number of this case in Table 4 and the quantitative analysis for five patients in Table 5. As shown in the absolute error images, the raw CBCT suffered a large CT number error around the patient margin, whereas the CT number of muscles around the cervix still had an error of more than 70 HU. Figures 6 and 7 show that the proposed correction not only compensated for the lower CT number of the marginal tissues but also improved the brightness of the central tissues to a level comparable to rCT.

In the patient study, the proposed method achieved similar CT number accuracy as the phantom study, and the error was limited to below 10 HU in each selected ROI. The RMSE of scatter-corrected CBCT was decreased to 5 ± 1 HU from 188 ± 25 HU in the raw CBCT, and SNU on adipose tissue and muscle was both reduced to ≤25 HU from ≥100 HU, indicating significantly improved image uniformity, and the CNR between adipose tissue and muscle was increased by a factor of 1.75.

3.2.2 Dose calculation precision

Using RD_CT as reference dose distributions, average γ pass rates with three different criteria for RD_cor of five patients are listed in Table 6. There are lower γ pass rates for high-dose thresholds under the same criterion. Except for the highest dose threshold of 12 Gy, the γ pass rate was >90% for all dose thresholds with the criterion (2%, 1 mm). This means that the further away from the radioactive source, the smaller the difference between RD_CT and RD_cor. Moreover, the RD_cor of patients could realize a γ pass rate of >93% with the criterion (2%, 2 mm) for different dose thresholds.

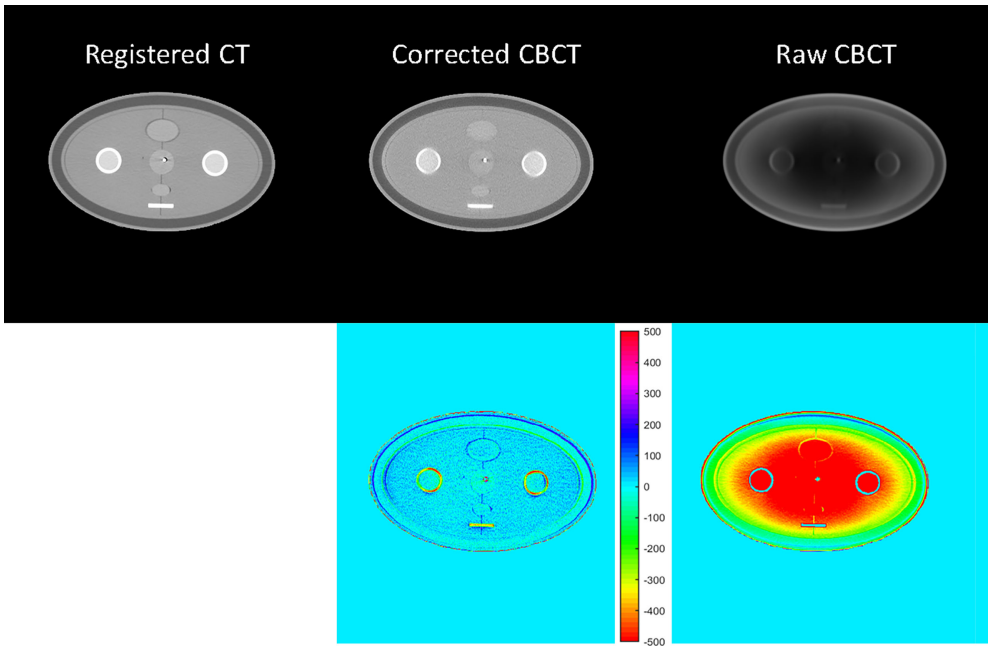

FIGURE 4
CT/CBCT images of the female pelvis phantom in the axial view and the CT number difference map of CBCT and CT; display window: [−500 500] HU.

TABLE 1 The CT number comparison of the 10 ROIs in Figure 3 (unit: HU).

	Registered CT			Corrected CBCT				Raw CBCT			
	CT #	STD	Range	CT #	STD	Range	HU error	CT #	STD	Range	HU error
Muscle	134	9	(112, 156)	140	26	(76, 201)	6	−384	11	(−404, −363)	−518
	127	10	(98, 151)	126	25	(69, 214)	−1	−441	3	(−447, −436)	−569
	134	10	(109, 162)	142	26	(77, 228)	8	−353	13	(−377, −329)	−487
	125	10	(166, 211)	138	25	(141, 283)	13	−334	13	(−359, −309)	−459
	121	12	(160, 238)	129	27	(123, 253)	9	−435	2	(−438, −431)	−556
	131	9	(165, 231)	139	25	(126, 273)	9	−375	10	(−395, −353)	−505
Adipose	−112	10	(106, 151)	−108	40	(75, 192)	4	−128	41	(−178, 25)	−16
Bladder	191	10	(89, 148)	205	27	(63, 220)	14	−340	15	(−367, −307)	−532
Uterus	196	15	(112, 154)	181	24	(72, 216)	−15	−416	4	(−431, −407)	−612
Rectum	199	10	(−133, −49)	199	28	(−177, 86)	0	−380	11	(−403, −355)	−579

STD, standard deviation.

TABLE 2 RMSE, SNU, and CNR in the images of the female phantom.

	Registered CT	Corrected CBCT	Raw CBCT
RMSE (HU)	N/A	9	510
SNU (HU)	13	16	107
CNR	6.96	2.24	0.50

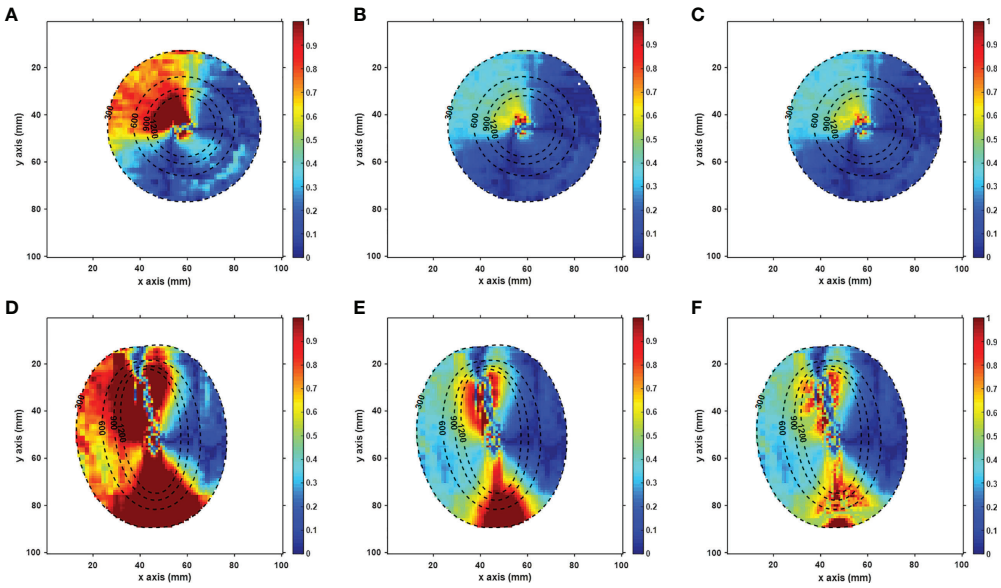

FIGURE 5
Axial **(A–C)** and sagittal **(D–F)** views of the gamma-index map of the RD_cor. In the gamma calculation, the distance and dose criteria were set to (1%, 1 mm) in a and d figures, (2%, 1 mm) in b and e figures, (2%,2 mm) in c and f figures, respectively, and the voxels with doses less than 3 Gy were not included. The dotted lines indicate the dose contour (unit: cGy).

Table 7 shows the dosimetric comparison of HRCTV and OARs based on different images. For both RD_CT and RD_cor, the D_{90} of HRCTV meets the dose requirements, while the D_{2cc} of OARs is below the threshold. Moreover, the average percentage deviation (APD) in these dosimetric parameters between RD_CT and RD_cor is<1%.

3.3 Computational efficiency

The CBCT reconstruction with scatter correction was implemented on a personal PC installed with NVIDIA RTX 2080ti GPU and Intel i9 9900k CPU, and the dose calculation was performed on the Intelligent cloud platform (Varian Medical Systems, Palo Alto, CA). The CBCT reconstruction took less than 30 s for 200 slice images using 656 projections with 1,024 * 768 pixels. Using the LBTE solver rather than Monte Carlo simulation, MBDC in the phantom study was completed within 2 min, while in the patient study, the time was increased to 8 min due to the process of volume optimization in inverse planning.

4 Discussion

IGBT has proved to be highly effective in cervical cancer treatment. Despite great success, the accuracy of dose delivery still suffers from anatomical variation and applicator displacement due to the transfer of the patient and the long treatment process. To complete image acquisition and treatment in a single room, CBCT guidance was introduced for cervical BT, which has the potential to avoid patient multiple transfers and CT scans, leading to a much simplified treatment process. In this work, we completed image acquisition and treatment in a single room, with the dose calculation finished in 10 min. Additionally, to facilitate accurate organ contouring and MBDC, a hybrid-domain scatter correction using EBRT-CT as a prior was implemented to improve the HU accuracy and soft-tissue contrast.

TABLE 3 γ pass rates for RD_cor for the phantom. The second column indicates the distance and dose difference criteria.

Threshold (Gy)		3	6	9	12
Pass rate of RD_cor (%)	1%, 1 mm	87.04	81.63	75.44	71.44
	2%, 1 mm	98.43	98.22	97.85	97.34
	2%, 2 mm	99.63	99.40	99.14	98.84

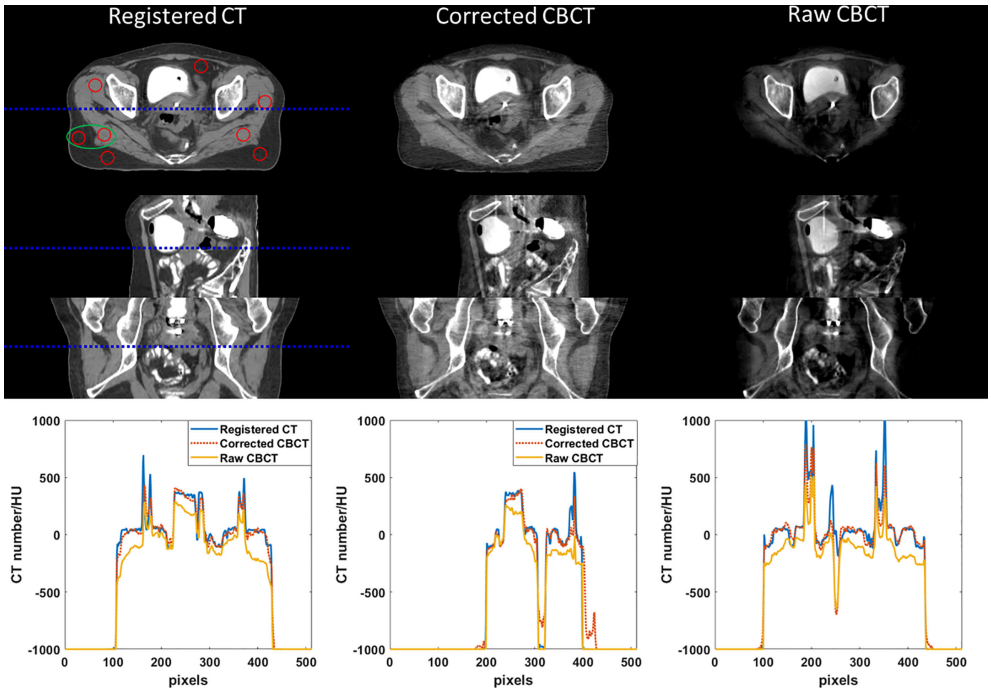

FIGURE 6
CT/CBCT images of one BT patient. The first three rows display the coronal, sagittal, and axial views from top to bottom; display window: [−200 300] HU. The 1D profiles indicated by the dotted lines are displayed in the last row. The mean CT number and SNU are calculated in the circle areas, and the CNR is calculated in the ellipse area.

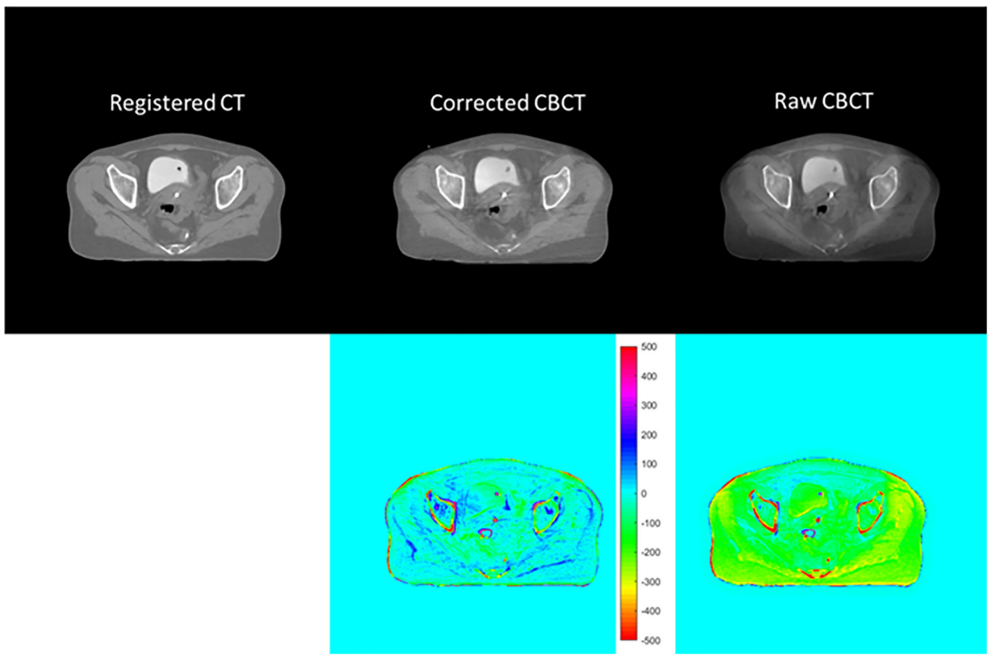

FIGURE 7
CT/CBCT images of the same patient in Figure 6 in the axial view and the CT number difference map of CBCT and CT; display window: [−500 500] HU.

TABLE 4 The CT number comparison of the eight ROIs in Figure 6 (unit: HU).

	Registered CT			Corrected CBCT				Raw CBCT			
	CT #	STD	Range	CT #	STD	Range	HU error	CT #	STD	Range	HU error
ROI-1	46	7	(15, 63)	51	14	(10, 82)	5	−102	17	(−149, −71)	−148
ROI-2	44	10	(3, 69)	48	17	(−14, 93)	4	−146	26	(−204, −83)	−190
ROI-3	46	8	(2, 68)	48	17	(−8, 90)	3	−196	9	(−230, −173)	−242
ROI-4	40	10	(−27, 61)	46	15	(0, 97)	6	−213	13	(−239, −182)	−253
ROI-5	−105	9	(−126, −77)	−104	19	(−152, −60)	1	−282	17	(−316, −245)	−178
ROI-6	−104	9	(−128, −79)	−101	13	(−138, −66)	3	−325	11	(−356, −286)	−221
ROI-7	−106	10	(−132, −75)	−99	15	(−138, −55)	7	−319	9	(−344, −291)	−213
ROI-8	−101	12	(−124, −43)	−104	11	(−133, −52)	−3	−138	10	(−164, −98)	−37

TABLE 5 Quantitative analysis of CT number error, CNR, SNU, and RMSE of five patients.

	CT number error/HU		SNU/HU		RMSE/HU	CNR
	Muscle	Adipose	Muscle	Adipose		
Registered CT	N/A	N/A	15 ± 5	12 ± 8	N/A	11.32 ± 2.80
Corrected CBCT	4 ± 2	4 ± 3	12 ± 4	12 ± 4	5 ± 1	6.65 ± 1.29
Raw CBCT	200 ± 63	154 ± 66	105 ± 56	154 ± 57	188 ± 25	3.80 ± 1.74

TABLE 6 Average γ pass rates for RD_cor of five patients. The second column indicates the distance and dose difference criteria ($\bar{x} \pm s$).

Threshold (Gy)		3	6	9	12
Pass rate of RD_cor (%)	1%, 1 mm	77.32 ± 14.26	74.81 ± 13.91	70.84 ± 12.32	65.92 ± 10.63
	2%, 1 mm	93.60 ± 8.70	93.21 ± 6.54	90.69 ± 5.34	87.19 ± 4.85
	2%, 2 mm	98.19 ± 2.00	96.96 ± 2.23	95.24 ± 2.20	93.07 ± 2.28

TABLE 7 Dosimetric comparison of HRCTV and OARs between RD_CT and RD_cor plans (unit: Gy; $\bar{x} \pm s$).

	HRCTV D_{90}	Bladder D_{2cc}	Rectum D_{2cc}	Intestine D_{2cc}	Sigmoid D_{2cc}
RD_CT	5.54 ± 0.19	4.58 ± 0.88	3.89 ± 0.32	3.35 ± 0.49	3.19 ± 0.88
RD_cor	5.54 ± 0.16	4.55 ± 0.93	3.88 ± 0.34	3.35 ± 0.49	3.18 ± 0.86
APD (%)	0.01 ± 0.57	−0.83 ± 1.87	−0.37 ± 1.40	−0.01 ± 0.21	−0.26 ± 0.65

APD, average percentage deviation.

Prior-information-based methods have advantages in accurate scatter estimation without extra patient dose (29) or hardware modification. These methods usually generate low-frequency scatter signals in the projection domain and require two successive CBCT reconstructions. The proposed scatter correction abandoned this commonly used strategy; instead, the constant scatter-corrected CBCT image was scaled by a low-frequency scatter ratio to remove scatter-induced artifacts in the image domain. Although this simplification inevitably sacrifices the HU accuracy, especially on the high-density bones, the proposed method is still suitable for CBCT-based BT. Due to the rapid dose fall-off, the BT dose was mainly concentrated within 5 cm around the radiation source, an area that is basically soft tissues. On the soft tissues, the proposed methods achieved high HU accuracy and could faithfully reflect the tissue heterogeneity; thus, the corrected CBCT images are accurate

enough for MBDC. Moreover, the proposed method could be accelerated using GPU, making the time to acquire BT images much lower than ~31 min (9) currently needed.

The feasibility of performing model-based dose calculations on corrected CBCT was verified in the phantom studies *via* γ analysis. Under each γ-index criterion, the γ pass rates decreased as the threshold dose increased. This phenomenon indicates that voxels with a large percentage dose error are mostly in the high-dose areas, which is consistent with the colored distributions in the γ-index map and may be caused by the slight applicator displacement between rCT and CBCT scans. When using the criterion of (2%, 1 mm) to (2%, 2 mm), the γ pass rates were all >97% in the $CBCT_{fc}$-based dose distribution, which revealed that the dose error of most voxels was limited to less than 2%. The patient study illustrated that the γ pass rates were all >93% with the criterion of 2% and 2 mm for both the high and lower dose thresholds. In $CBCT_{fc}$-based BT plans, the tumor target received almost the same dose as CT-based BT plans, while there was no additional dose to OARs. These results suggested that in the current clinical situation, the CBCT-guided BT could provide an optional solution for radiation therapists.

The proposed CBCT-guided BT can be further improved in some aspects. First, more patient cases could be studied to fully evaluate the stability of this method. The second is to investigate other scatter correction techniques, such as beam blocker-based (14) and primary modulation-based (22) methods, which may obtain accurate scatter estimation by combining hardware measurement and software processing. In addition, due to the lack of scatter-free and registered images, this study did not investigate the accuracy of dose calculation on the patient CBCT images. Future work will focus on creating scatter-free CBCT images *via* Monte Carlo simulation (20) and evaluating the patient dose accuracy. Currently, the CBCT scan and corresponding reconstruction take less than 90 s, and the dose calculation takes approximately 8 min; however, most of the time before treatment is spent on the manual organ delineation as indicated in Refs (9, 10).. To promote fast and accurate cervical BT, automated organ segmentation (35, 36) dedicated to cervical cancer should be developed and plugged into the workflow of BT.

5 Conclusion

In conclusion, scatter correction using planning CT (pCT) prior largely promoted the CBCT image quality, and a dosimetric study demonstrated the feasibility of using corrected CBCT for model-based BT dose calculation. This technique made full use of the pCT scan in EBRT and achieved an error of<15 HU without an extra CT scan or hardware modification. The accuracy of MBDC was also improved after scatter correction as indicated by the increased γ pass rate for prescription dose (>95%, criterion: 2%, 2 mm). Moreover, CBCT-based BT saved the patient transfer and setup to simplify BT treatment, while the real-time imaging avoided applicator displacement and organ deformation to facilitate more accurate dose delivery. Therefore, the proposed CBCT scatter correction and CBCT-based BT have promising prospects in cervical cancer radiotherapy.

Data availability statement

The original contributions presented in the study are included in the article/supplementary material. Further inquiries can be directed to the corresponding author.

Ethics statement

This is a retrospective study that analyzed data relating to previously treated patients retrospectively. None of the dose calculations involved in this study were performed on real humans.

Author contributions

ALW and LZ contributed to the study design and experiments. ALW, HC, and JX completed the data analysis and drafted the manuscript. YB helped with the phantom design and the use of software. ADW and YQL collected the data and evaluated the brachytherapy plans. All authors contributed to the article and approved the submitted version.

Funding

This research was supported by the National Natural Science Foundation of China (Grant Nos. 11805198 and 81671681), the Ministry of Science and Technology of China Key Research and Development Projects (Grant No. 2016YFC0101400), and the Fundamental Research Funds for the Central Universities (Grant No. WK2030040089).

Conflict of interest

The authors declare that the research was conducted in the absence of any commercial or financial relationships that could be construed as a potential conflict of interest.

Publisher's note

References

1. Kamangar F, Dores GM, Anderson WF. Patterns of cancer incidence, mortality, and prevalence across five continents: Defining priorities to reduce cancer disparities in different geographic regions of the world. *J Clin Oncol* (2006) 24(14):2137–50. doi: 10.1200/JCO.2005.05.2308

2. Bray F, Ferlay J, Soerjomataram I, Siegel RL, Torre LA, Jemal A. Global cancer statistics 2018: Globocan estimates of incidence and mortality worldwide for 36 cancers in 185 countries. *Ca-Cancer J Clin* (2020) 70(4):313–. doi: 10.3322/caac.21609

3. Mahmoud O, Kilic S, Khan AJ, Beriwal S, Small WJr. External beam techniques to boost cervical cancer when brachytherapy is not an option-theories and applications. *Ann Transl Med* (2017) 5(10):207. doi: 10.21037/atm.2017.03.102

4. Landoni F, Colombo A, Milani R, Placa F, Zanagnolo V, Mangioni C. Randomized study between radical surgery and radiotherapy for the treatment of stage ib-iia cervical cancer: 20-year update. *J Gynecol Oncol* (2017) 28(3):e34. doi: 10.3802/jgo.2017.28.e34

5. Liu YM, Ni LQ, Wang SS, Lv QL, Chen WJ, Ying SP. Outcome and prognostic factors in cervical cancer patients treated with surgery and concurrent chemoradiotherapy: A retrospective study. *World J Surg Oncol* (2018) 16(1):18. doi: 10.1186/s12957-017-1307-0

6. Rivard MJ, Butler WM, DeWerd LA, Huq MS, Ibbott GS, Li ZF, et al. Update of aapm task group no. 43 report: A revised aapm protocol for brachytherapy dose calculations. *Med Phys* (2004) 31(12):3532–3. doi: 10.1118/1.1812603

7. Beaulieu L, Tedgren AC, Carrier JF, Davis SD, Mourtada F, Rivard MJ, et al. Report of the task group 186 on model-based dose calculation methods in brachytherapy beyond the tg-43 formalism: Current status and recommendations for clinical implementation. *Med Phys* (2012) 39(10):6208–36. doi: 10.1118/1.4747264

8. Pappas EP, Zoros E, Moutsatsos A, Peppa V, Zourari K, Karaiskos P, et al. On the experimental validation of model-based dose calculation algorithms for (192)Ir hdr brachytherapy treatment planning. *Phys Med Biol* (2017) 62(10):4160–82. doi: 10.1088/1361-6560/aa6a01

9. Kim H, Houser CJ, Kalash R, Maceil CA, Palestra B, Malush D, et al. Workflow and efficiency in mri-based high-Dose-Rate brachytherapy for cervical cancer in a high-volume brachytherapy center. *Brachytherapy* (2018) 17(5):753–60. doi: 10.1016/j.brachy.2018.05.001

10. Mayadev J, Qi L, Lentz S, Benedict S, Courquin J, Dieterich S, et al. Implant time and process efficiency for ct-guided high-Dose-Rate brachytherapy for cervical cancer. *Brachytherapy* (2014) 13(3):233–9. doi: 10.1016/j.brachy.2014.01.004

11. Wu A, Tang D, Wu A, Liu Y, Qian L, Zhu L. Comparison of the dosimetric influence of applicator displacement on 2d and 3d brachytherapy for cervical cancer treatment. *Technol Cancer Res Treat* (2021) 20:15330338211041201. doi: 10.1177/15330338211041201

12. Hatton J, McCurdy B, Greer PB. Cone beam computerized tomography: The effect of calibration of the hounsfield unit number to electron density on dose calculation accuracy for adaptive radiation therapy. *Phys Med Biol* (2009) 54(15):N329–46. doi: 10.1088/0031-9155/54/15/N01

13. Constantinou C, Harrington JC, DeWerd LA. An electron density calibration phantom for ct-based treatment planning computers. *Med Phys* (1992) 19(2):325–7. doi: 10.1118/1.596862

14. Zhu L, Xie Y, Wang J, Xing L. Scatter correction for cone-beam ct in radiation therapy. *Med Phys* (2009) 36(6):2258–68. doi: 10.1118/1.3130047

15. Ning R, Tang X. Conover d. X-ray scatter correction algorithm for cone beam ct imaging. *Med Phys* (2004) 31(5):1195–202. doi: 10.1118/1.1711475

16. Guan HQ, Dong H. Dose calculation accuracy using cone-beam ct (Cbct) for pelvic adaptive radiotherapy. *Phys Med Biol* (2009) 54(20):6239–50. doi: 10.1088/0031-9155/54/20/013

17. Schroder L, Stankovic U, Remeijer P, Sonke JJ. Evaluating the impact of cone-beam computed tomography scatter mitigation strategies on radiotherapy dose calculation accuracy. *Phys Imag Radiat Onc* (2019) 10:35–40. doi: 10.1016/j.phro.2019.04.001

18. Maslowski A, Wang A, Sun MS, Wareing T, Davis I, Star-Lack J. Acuros cts: A fast, linear Boltzmann transport equation solver for computed tomography scatter - part I: Core algorithms and validation. *Med Phys* (2018) 45(5):1899–913. doi: 10.1002/mp.12850

19. Wang A, Maslowski A, Messmer P, Lehmann M, Strzelecki A, Yu E, et al. Acuros cts: A fast, linear Boltzmann transport equation solver for computed tomography scatter - part ii: System modeling, scatter correction, and optimization. *Med Phys* (2018) 45(5):1914–25. doi: 10.1002/mp.12849

20. Poludniowski G, Evans PM, Hansen VN, Webb S. An efficient Monte Carlo-based algorithm for scatter correction in kev cone-beam ct. *Phys Med Biol* (2009) 54(12):3847–64. doi: 10.1088/0031-9155/54/12/016

21. Nomura Y, Xu Q, Peng H, Takao S, Shimizu S, Xing L, et al. Modified fast adaptive scatter kernel superposition (Mfasks) correction and its dosimetric impact on cbct-based proton therapy dose calculation. *Med Phys* (2020) 47(1):190–200. doi: 10.1002/mp.13878

22. Zhu L, Bennett NR, Fahrig R. Scatter correction method for X-ray ct using primary modulation: Theory and preliminary results. *IEEE T Med Imaging* (2006) 25(12):1573–87. doi: 10.1109/Tmi.2006.884636

23. Dai ZH, Zhang YW, Zhu L, Tan JW, Yang G, Zhang BL, et al. Geometric and dosimetric evaluation of deep learning-based automatic delineation on cbct-synthesized ct and planning ct for breast cancer adaptive radiotherapy: A multi-institutional study. *Front Oncol* (2021) 11:725507. doi: 10.3389/fonc.2021.725507

24. Karius A, Strnad V, Lotter M, Kreppner S, Bert C. First clinical experience with a novel, mobile cone-beam ct system for treatment quality assurance in brachytherapy. *Strahlenther Onkol* (2022) 198:573–81. doi: 10.1007/s00066-022-01912-7

25. Karius A, Karolczak M, Strnad V, Bert C. Technical evaluation of the cone-beam computed tomography imaging performance of a novel, mobile, gantry-based X-ray system for brachytherapy. *J Appl Clin Med Phys* (2022) 23(2):e13501. doi: 10.1002/acm2.13501

26. Djukelic M, Waterhouse D, Toh R, Tan H, Rowshanfarzad P, Joseph D, et al. Evaluation of a mobile c-arm cone-beam ct in interstitial high-Dose-Rate prostate brachytherapy treatment planning. *J Med Radiat Sci* (2019) 66(2):112–21. doi: 10.1002/jmrs.331

27. Niu T, Al-Basheer A, Zhu L. Quantitative cone-beam ct imaging in radiation therapy using planning ct as a prior: First patient studies. *Med Phys* (2012) 39(6):4001–. doi: 10.1118/1.4736323

28. Niu TY, Sun MS, Star-Lack J, Gao HW, Fan QY, Zhu L. Shading correction for on-board cone-beam ct in radiation therapy using planning mdct images. *Med Phys* (2010) 37(10):5395–406. doi: 10.1118/1.3483260

29. Zhu L. Local filtration based scatter correction for cone-beam ct using primary modulation. *Med Phys* (2016) 43(11):6199–209. doi: 10.1118/1.4965042

30. Mahmoud O, Kilic S, Khan AJ, Beriwal S, Small W. External beam techniques to boost cervical cancer when brachytherapy is not an option–theories and applications. *Ann Trans Med* (2017) 5(10):207. doi: 10.21037/atm.2017.03.102

31. Potter R, Haie-Meder C, Van Limbergen E, Barillot I, De Brabandere M, Dimopoulos J, et al. Recommendations from gynaecological (Gyn) gec estro working group (Ii): Concepts and terms in 3d image-based treatment planning in cervix cancer brachytherapy-3d dose volume parameters and aspects of 3d image-based anatomy, radiation physics, radiobiology. *Radiother Oncol* (2006) 78(1):67–77. doi: 10.1016/j.radonc.2005.11.014

32. Haie-Meder C, Potter R, Van Limbergen E, Briot E, De Brabandere M, Dimopoulos J, et al. Recommendations from gynaecological (Gyn) gec-estro working group (I): Concepts and terms in 3d image based 3d treatment planning in cervix cancer brachytherapy with emphasis on mri assessment of gtv and ctv. *Radiother Oncol* (2005) 74(3):235–45. doi: 10.1016/j.radonc.2004.12.015

33. Hussein M, Clark CH, Nisbet A. Challenges in calculation of the gamma index in radiotherapy - towards good practice. *Phys Med* (2017) 36:1–11. doi: 10.1016/j.ejmp.2017.03.001

34. Zhu L, Wang J, Xing L. Noise suppression in scatter correction for cone-beam ct. *Med Phys* (2009) 36(3):741–52. doi: 10.1118/1.3063001

35. Mohammadi R, Shokatian I, Salehi M, Arabi H, Shiri I, Zaidi H. Deep learning-based auto-segmentation of organs at risk in high-dose rate brachytherapy of cervical cancer. *Radiother Oncol* (2021) 159:231–40. doi: 10.1016/j.radonc.2021.03.030

36. Zhang DG, Yang ZY, Jiang S, Zhou ZY, Meng MB, Wang W. Automatic segmentation and applicator reconstruction for ct-based brachytherapy of cervical cancer using 3d convolutional neural networks. *J Appl Clin Med Phys* (2020) 21(10):158–69. doi: 10.1002/acm2.13024

frontiers | Frontiers in Oncology

TYPE Clinical Trial
PUBLISHED 15 November 2022
DOI 10.3389/fonc.2022.1021453

OPEN ACCESS

EDITED BY
John Varlotto,
Marshall University, United States

REVIEWED BY
DeeDee Smart,
Radiation Oncology Branch, Center for Cancer Research, National Cancer Institute (NIH), Bethesda, United States
Seyed Alireza Javadinia,
Sabzevar University of Medical Sciences, Iran

*CORRESPONDENCE
Wan-Min Qiang
Qiangwanmin@sina.cn

SPECIALTY SECTION
This article was submitted to Radiation Oncology, a section of the journal Frontiers in Oncology

RECEIVED 17 August 2022
ACCEPTED 24 October 2022
PUBLISHED 15 November 2022

CITATION
Wang Y, Qiang W, Li J-Q, Shen A-M, Chen X-C, Li X-F, Zhang B-Z, Xie J, Yan R, Li X-H, Zhang Z-L, Wang C-L, and Li L-Y (2022) The effect of chronoradiotherapy on cervical cancer patients: A multicenter randomized controlled study.
Front. Oncol. 12:1021453.
doi: 10.3389/fonc.2022.1021453

The effect of chronoradiotherapy on cervical cancer patients: A multicenter randomized controlled study

Ying Wang[1], Wan-Min Qiang[1]*, Jia-Qian Li[1], Ao-Mei Shen[1], Xiao-Cen Chen[1], Xiao-Fang Li[1], Bao-Zhong Zhang[1], Juan Xie[2], Rong Yan[3], Xiang-Hua Li[4], Zhao-Li Zhang[5], Cui-Ling Wang[6] and Lai-You Li[7]

[1]Nursing Department, Tianjin Medical University Cancer Institute & Hospital, National Clinical Research Center for Cancer, Tianjin, China, [2]Radiotherapy Department, Shaanxi Provincial Cancer Hospital, Xian, China, [3]Nursing Department, Shandong Cancer Hospital, Qingdao, China, [4]Nursing Department, Cangzhou People's Hospital, Cangzhou, China, [5]Nursing Department, Chongqing Cancer Hospital, Chongqing, China, [6]Nursing Department, Shanxi Provincial Cancer Hospital, Taiyuan, China, [7]Nursing Department, The Fourth Hospital of Hebei Medical University, Shijiazhuang, China

Objectives: To investigate the short-term efficacy and radiotoxicity 3.543of chronoradiotherapy in patients with cervical cancer. We also examined the overall symptom score and quality of life (QOL) of patients who underwent morning radiotherapy and evening radiotherapy.

Methods: We conducted a multicenter randomized controlled trial to compare the effects of morning radiotherapy (9:00–11:00 AM) with evening radiotherapy (7:00–9:00 PM) in cervical cancer patients receiving radiotherapy. From November 2021 to June 2022, 114 cervical cancer patients admitted to eight cancer center hospitals in Tianjin, Chongqing, Hubei, Shanxi, Shandong, Shaanxi, Hebei, and Cangzhou were randomly divided into the morning radiotherapy group (MG; N = 61) and the evening radiotherapy group (EG; N = 53). The short-term efficacy of radiotherapy on cervical cancer patients at different time points and the occurrence of radiotoxicity were explored after patients had undergone radiotherapy.

Results: The total effective response (partial remission [PR] + complete remission [CR]) rate was similar across the two groups (93.5% vs. 96.3%, $p > 0.05$). However, the incidence of bone marrow suppression and intestinal reaction in the two groups were significantly different ($p < 0.05$). The patients in the MG had significantly higher Anderson symptom scores than patients in the EG (21.64 $\pm$ 7.916 vs. 18.53 $\pm$ 4.098, $p < 0.05$). In terms of physical activity, functional status, and overall QOL, the MG had significantly lower scores than the EG ($p < 0.05$). No other measures showed a significant difference between the groups.

Conclusion: The radiotherapy effect of the MG was consistent with that of the EG. The incidence of radiation enteritis and radiation diarrhea in the MG was significantly higher than that in the EG; however, bone marrow suppression and blood toxicity in the EG were more serious than in the MG. Because of the small sample size of the study, we only examined the short-term efficacy of radiotherapy. Therefore, further clinical trials are needed to verify the efficacy and side effects of chronoradiotherapy.

Clinical Trial Registration: http://www.chictr.org.cn/searchproj.aspx, Registration Number: ChiCTR2100047140.

KEYWORDS

radiotherapy, chronoradiotherapy, cervical cancer, radiation toxicity, radiotherapy effects

Introduction

A recent analysis revealed that cervical cancer remains a major threat to women. In 2020, there were an estimated 604,000 new cases of cervical cancer globally, which was the second most diagnosed cancer in women (1). Although cervical cancer is one of the leading causes of cancer-related death in women worldwide (2), nearly 90% of cervical cancer deaths occur in developing countries, with India and China accounting for 35% of the total cervical cancer burden (3).

Radiotherapy, alone or in combination with surgery or chemotherapy, is the main treatment for cervical cancer (4). Almost 80% of patients with cervical cancer undergo radiation therapy as part of their treatment (5). The aim of radiotherapy is to irradiate malignant tumors *via* ionizing radiation, and the cumulative effect of the irradiation dose destroys tumor cells (6). However, during the process of radiotherapy, although tumor cells are killed, the surrounding normal tissues are also damaged, which causes a series of toxic side effects.

Exposure to ionizing radiation during radiotherapy of the abdominopelvic region is associated with the development of treatment-limiting untoward symptoms. The consequences of damaging healthy cells can result in a series of adverse reactions ranging from acute radiation toxicity to organ damage and secondary cancers (7). Approximately 84% of patients undergo some form of acute radiation toxicity during radiation therapy for cervical cancer (7). The most common symptoms are hematological toxicity, gastrointestinal mucositis, diarrhea, nausea, and vomiting, which may lead to treatment interruptions, increased healthcare costs, and impaired quality of life (QOL) in patients undergoing irradiation. These adverse reactions are attributed to various factors, such as therapeutic, environmental, and genetic factors. In recent years, studies have explored how the time of day of radiotherapy administration affects radiation therapy outcomes to determine whether chrono-modulation may be beneficial (6–8).

The circadian rhythm is governed by an internal timing system that is regulated at the transcriptional level, creating networks of genes that oscillate on a 24-hour cycle (8). The cell cycle, proliferation, and cell death are closely intertwined with the circadian rhythm. Several recent studies have provided compelling evidence on the association between the circadian cycle and cancer; similar to healthy cells, tumor cells are rhythmic (9, 10), and their growth depends on circadian rhythms (11). It has been reported that each phase of the cell cycle corresponds to a different degree of radiosensitivity (12). Cells in or near mitosis (G2 and M phases) have the highest radiosensitivity, whereas cells in the S and G1 phases are less radiosensitive. Tumor cells also show time rhythms in metabolism and proliferation, which differ from those of healthy tissue cells. According to the different sensitivities of cells to radiation during different mitosis cycles, studies have investigated the time law of radiation sensitivity of tumor tissue and healthy tissue cells (12, 13). In line with circadian rhythm regularity, selecting a specific time to apply radiation therapy to tumors can significantly improve the efficacy of tumor radiation therapy (12, 13).

Chronoradiotherapy involves selecting the optimal radiotherapy time according to the body's rhythm changes. It is aimed at protecting normal tissues as much as possible while killing tumor cells to the greatest extent to attenuate toxicity and increase efficiency. Radiotherapy can achieve a good curative effect, but the dose is roughly the maximum that the body can tolerate, which significantly limits the treatment of tumors. Therefore, ways in which to further improve the curative effect and minimize

radiotoxicity is an important topic that requires urgent study. In this study, we investigated the radiation effects, radiotoxicity, and QOL in inoperable cervical cancer patients irradiated at different times of the day. Although chronoradiotherapy may be offered to cervical cancer patients as a new method, its efficacy and toxicity must be established. Current prospective randomized clinical data are lacking, and the use of chronoradiotherapy for the treatment of cervical carcinoma has not yet been established. Therefore, we conducted a multicenter prospective randomized study to assess the effectiveness of chronoradiotherapy in cervical cancer patients and to explore the relationship between the severity of acute gastrointestinal mucositis and the time of radiation in patients with carcinoma of the cervix.

Materials and methods

Study design

This was a multicenter randomized controlled trial (RCT) comparing morning radiotherapy (9:00–11:00 AM) with evening radiotherapy (7:00–9:00 PM) for cervical cancer patients undergoing radiotherapy. The study was registered with the Chinese Clinical Trial Registry (ref. Chi-CTR-2100047140) and was conducted from November 2021 to June 2022 at eight cancer center hospitals in the cities and provinces of Tianjin, Chongqing, Hubei, Shanxi, Shandong, Shaanxi, and Hebei. The Tianjin Medical University Cancer Institute and the Hospital Institutional Review Board approved the study protocol (approval number: bc2020185), and all caregivers provided informed consent. A total of 114 patients were registered during this period and were included in the study.

Study participants

Patients were eligible if they fulfilled the inclusion and exclusion criteria. The inclusion criteria were as follows: 1) aged between 18 and 65 years; 2) cervical cancer patients with Federation International of Gynecology and Obstetrics (FIGO) stage IIB-IVA tumors confirmed by pathological biopsy to be nonmetastatic cervical cell carcinoma (see Table 1 for details)

TABLE 1 2018 Federation International of Gynecology and Obstetrics (FIGO) Staging System for uterine cervical cancer.

Stage	Description
I	Carcinoma is strictly confined to the cervix (extension to the uterine corpus should be disregarded)
IA	Invasive carcinoma that can be diagnosed only with microscopy, with maximum depth of invasion < 5 mm
IA1	Stromal invasion < 3 mm in depth
IA2	Stromal invasion ≥ 3 mm and < 5 mm in depth
IB	Invasive carcinoma confined to the uterine cervix, with measured deepest invasion ≥ 5 mm
IB1*	Tumor measures < 2 cm in greatest dimension
IB2*	Tumor measures ≥ 2 cm and < 4 cm in greatest dimension
IB3*	Tumor measures ≥ 4 cm in greatest dimension
II	Carcinoma invades beyond the uterus but has not extended onto the lower third of the vagina or to the pelvic wall
IIA	Limited to the upper two-thirds of the vagina without parametrial involvement
IIA1	Tumor measures < 4 cm in greatest dimension
IIA2	Tumor measures ≥ 4 cm in greatest dimension
IIB	With parametrial involvement but not up to the pelvic wall
III	Carcinoma involves the lower third of the vagina and/or extends to the pelvic wall and/or causes hydronephrosis or nonfunctioning kidney and/or involves pelvic and/or para-aortic lymph nodes
IIIA	Involves the lower third of the vagina, with no extension to the pelvic wall
IIIB	Extension to the pelvic wall and/or hydronephrosis or nonfunctioning kidney from tumor
IIIC*	Involvement of pelvic and/or para-aortic lymph nodes, irrespective of tumor size and extent†
IIIC1*	Pelvic lymph node metastasis only
IIIC2*	Para-aortic lymph node metastasis
IV	Carcinoma has extended beyond the true pelvis or has involved (biopsy-proven) the mucosa of the bladder or rectum
IVA	Spread to adjacent pelvic organs
IVB	Spread to distant organs

Pathologic analysis, where available, can be used to supplement clinical findings for all stages. FIGO, International Federation of Gynecology and Obstetrics (adapted, under a CC BY license, from reference 1)
*New stages from the 2009 FIGO system.
†Stage IIIC should be annotated with r (radiology) or p (pathologic analysis) to indicate the method used to allocate this stage. Imaging modality or pathologic technique should also be documented.

(14); 3) a Karnofsky Performance Status (KPS) score of ≥ 70 points; 4) patients participated voluntarily and provided written informed consent.

The exclusion criteria were as follows: 1) clinically significant diseases (e.g., second primary tumor, severe infection, acute and chronic intestinal diseases or hemorrhoids, mental diseases, and systemic immune diseases) that might interfere with the primary endpoint assessment; 2) patients who had undergone major surgery within the 14 days before enrollment; 3) patients with serious liver, kidney, or another organ dysfunction.

Randomization, allocation concealment, and blinding

Randomization was performed before the beginning of the intervention using a random number table technique to ensure an equal number of participants in each group. The random allocation sequence was produced using the Statistical Analysis Software (SAS), version 9.4 (SAS Institute, Inc., Cary, NC, USA). Eight sets of random sequences with a sample size of 114 cases were generated by a computer, randomly grouped in a 1:1 ratio, and each center was divided into two sets of random sequences. After the participants provided informed consent and underwent baseline assessments, they were randomly assigned to receive either morning radiotherapy (i.e., the morning radiotherapy group [MG]) or evening radiotherapy (i.e., the evening radiotherapy group [EG]). Allocation concealment was assured by using sequentially numbered, opaque, sealed, and stapled envelopes that were distributed to the participants by the project manager. To avoid the disclosure of group assignment, aluminum foil was used to keep the envelope invisible, even under intense light. The group assignment (intervention or control group) was replaced by group A or B, so that the research assistant who collected and entered the study data into a database remained blinded to group allocation throughout the study.

Radiotherapy regimen

Both the MG and EG were treated with a uniform treatment combining external beam irradiation and high dose-rate (HDR) brachytherapy, without low dose-rate (LDR) brachytherapy. The external irradiation area has a large area to primarily address the problem of lymph node metastasis in the abdomen and pelvis. We used high-energy 6 MV and above X-rays for irradiation, and the irradiation dose was (50.4 Gy, 5–6 weeks, 28 fractions). HDR brachytherapy with iridium 192 HDR at a dose rate of 12–70/h, was initiated when the external radiation dose reached 30 Gy, and short-range radiation was added (30 Gy, five fractions). The samples in the MG received radiotherapy from 9:00 to 11:00 AM, whereas those in the EG received radiotherapy from 7:00 to 9:00 PM. In addition to radiotherapy, patients received a cisplatin chemotherapy regimen, (25 mg/m2 intravenously Guttae for 4–6 weeks). All the samples of this study in both groups received chemotherapy over the same time period, which was from 9:00 to 11:00 AM. We assessed the QOL of samples at baseline and the end of treatment. In addition, patients recorded any complaints of discomfort in a booklet we developed during this period to improve the compliance rate of patients.

Interventions

Before enrollment, patients in both groups received unified dietary guidance and radiotherapy-related health education. One day before radiotherapy, patients underwent blood tests, imaging examinations, such as chest X-ray, pelvic ultrasound, and electrocardiogram, and other baseline assessments. During radiation therapy, blood tests and radiotoxicity were assessed weekly by a trained observer blinded to group assignment. In addition, during radiotherapy, patients were instructed to use a uniform douche for vaginal douches twice per week. For radiotherapy-related symptoms, such as diarrhea and enteritis, we provided standardized treatments in strict accordance with the requirements of the protocol and maintained a complete record of the course of treatments. Finally, patients were evaluated for efficacy on the day following the final radiotherapy session (i.e., the day after the final brachytherapy).

Outcome measures

All outcomes were measured at baseline before the treatment and at the end of treatment. The curative effect of radiotherapy was evaluated according to the Response Evaluation Criteria in Solid Tumors (RECIST) 1.1 (see Table 2 for details) (15). Toxicity was assessed using the Radiation Therapy Oncology Group's common toxicity criteria (16). Myelosuppression was assessed using the myelosuppression grading of the World Health Organization. The Functional Assessment of Cancer Therapy-Cervix scale (17) was used to assess the QOL of patients during radiotherapy. Other radiation-related adverse reactions, such as pain, vomiting, sadness, and insomnia, were assessed using the M.D. Anderson Symptom Inventory (MDASI) (18). The case collection period was from August 2021 to December 2021. A trained observer assessed the results of patient assessments and completed unified case report forms, which included general information and relevant assessment results if patients visited the hospital for surveillance as an outpatient.

Sample size calculation

Before conducting the study, we calculated the approximate sample size considering the incidence of diarrhea in the two groups of chronoradiotherapy in relevant literature using the Power Analysis and Sample Size software version 15.0 (NCSS, Inc., USA). sample size calculation software: MG: 87.39%, EG: 68.18%, $\beta = 0.1$, test efficiency $1 - \beta = 80\%$, $\alpha = 0.05$, N1 = N2 = 47, a total of 94 cases. Accounting for a 10% dropout rate, we determined that a minimum sample size of 104 cases would be required with N1 = N2 = 52, respectively.

Statistical analysis

The data were analyzed using the Statistical Product and Service Solution version 21.0 (IBM Institute, Inc., Stanford, CA, USA). The count data are expressed as frequencies and percentages. Data that conformed to a normal distribution are described as means ± standard deviations, and those that were not normally distributed are described as medians and interquartile ranges. Baseline characteristics in the control and intervention groups were analyzed to assess whether there were between-group differences. To assess differences in mean scores between the intervention and control groups, we used a parametric test (t-test) for scores with a normal distribution and a non-parametric test (Mann–Whitney U test) for scores with non-normal distribution. Chi-square analysis was used to compare differences between the two groups after radiotherapy. Statistical significance was defined as a two-sided $p < 0.05$. Excel (Microsoft Office Home and Student 2019) was used for the analysis.

Results

Patients

Between November 2021 and June 2022, this study initially included 120 patients. However, three cases were excluded because they did not meet the inclusion criteria, and three cases dropped out of the study before the follow-up. Finally, 114 cases were included, which comprised 61 patients in the MG and 53 patients in the EG (Figure 1). All patients were pathologically diagnosed with cervical cancer with clinical stage IIB-IVA and had no indication for surgery. All the samples in this study had the same circadian rhythm sleeping at night and doing daily activities on daytime. Before the intervention, there were no statistical differences between the groups in terms of baseline characteristics, including general demographic, disease, or social data ($p < 0.05$). The baseline characteristics of MG and EG are shown in Table 3.

Efficacy of radiotherapy

The complete remission (CR) rate was 49.2%, and the partial remission (PR) rate was 44.3% in the MG. The CR rate was 64.2% and the PR rate was 32.1% in the EG. The total effective rates (PR + CR) of the MG and EG were 93.5% and 96.3%, respectively. The CR rate of the EG was slightly higher than that of the MG, although further analysis showed that there was no significant difference in the CR rate between the two groups ($p > 0.05$). The results are described in Table 4.

Radiotherapy toxicity, symptoms, and related QOL outcomes

In this study, the main toxic reactions were radioactive gastrointestinal reactions and myelosuppression, and the toxicity levels were 0, I, II, III, and IV. There were significant differences in the incidence of myelosuppression and intestinal reaction between the MG and EG ($p < 0.05$). The MDASI score of the MG was slightly higher than that of the EG (21.64 ± 7.916 vs. 18.53 ± 4.098, $p < 0.05$). In terms of QOL, physical activity, functional status, and overall QOL of the MG were significantly poorer than those of the EG ($p < 0.05$). No other measures showed a significant difference between the groups. The results are described in Tables 5–7.

TABLE 2 Response Evaluation Criteria in Solid Tumors (RECIST 1.1).

Grade	Efficacy evaluation criteria
CR	Disappearance of all pleural and non-pleural disease (including pleural thickening considered to represent tumor).
PR	Summed measurement decrease by at least 30% from the baseline scan summed measurement, which must be confirmed at a subsequent follow-up scan at least 4 weeks later (at which time the summed measurement must not exceed 70% of the baseline scan summed measurement).
SD	Summed measurement increase by at least 20% from the nadir of the summed measurements from all prior scans (up to and including the baseline scan), even if the summed measurement is < 70% of the baseline scan summed measurement; classification as PD also requires an absolute summed measurement increase of at least 5 mm over the nadir summed measurement. An unequivocal new non-pleural lesion or an unequivocal new focus of pleural thickening that exceeds the minimum measurable size (and represents either a pleural tumor mass physically distinct from that associated with existing measurement sites or a region of a previously existing pleural tumor mass that would now unequivocally qualify as a measurement site) would be considered progressive disease.
PD	A decrease in the summed measurement that does not qualify as PR, or an increase in the summed measurement that does not qualify as PD.

CR, complete remission; PR, partial remission; SD, stable disease; PD, progression of disease.

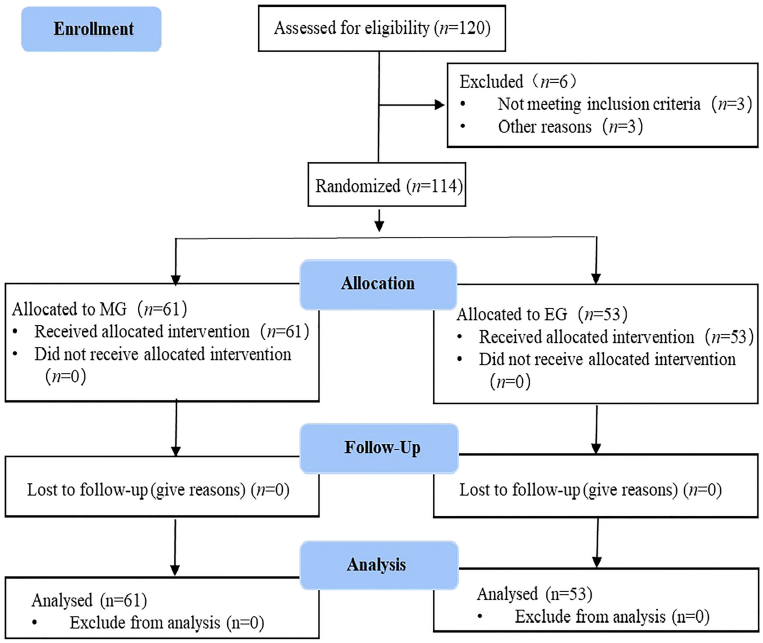

FIGURE 1
The CONSORT chart of the study.

Discussion

Radiotherapy toxicity

In nature, from simple single-celled organisms to complex mammals and humans, there are certain periodic life activities. Circadian rhythm is a special internal timing mechanism with a 24-hour cycle that is produced by the body, and it can self-regulate and change from day to night (19). The growth of normal human tissues and cells is precisely regulated by the circadian rhythm. Studies have shown that the cell cycle, proliferation, and cell death are closely related to the circadian clock; thus, the disruption of the circadian rhythm is likely involved in cancer development and progression (20). Radiotherapy remains the main treatment for cervical cancer at present (2). Basic research results have confirmed that the sensitivity of different cells to radiation varies significantly depending on its cycle, and each stage of the cell cycle corresponds to different degrees of radiation sensitivity (21, 22). The sensitivity of cells to radiation varies with the cell cycle; therefore, selecting an appropriate radiotherapy time is crucial. Radiotherapy aimed at the sensitive period of tumor cells while avoiding the sensitive period of healthy tissues can achieve the maximum killing effect on cancer cells and minimize damage to healthy cells (22).

In this study, we implemented chronoradiotherapy under the condition of ethical review. For observations of acute radiation adverse reactions, we found that the incidence of radiation enteritis in the morning was higher than that in the evening (above grade II: 32.8% vs. 11.3%, $p < 0.05$). Diarrhea in the MG was more serious than that in the EG, and the diarrhea of grade II and above was significantly more serious in the MG than in the EG (above grade II: 21.3% vs. 13.2%, $p < 0.05$). Additionally, the degree of myelosuppression was more severe in the EG than in the MG (above grade II: 22.9% vs. 41.5%, $p < 0.05$). Chang et al. (23) randomly divided 67 patients into MG (9:00–11:00 AM) and EG (9:00–11:00 PM) groups, and results showed that the incidence of grade III–IV diarrhea in the MG and EG was 12.5% and 6.1%, respectively. In the EG, the incidence of serious hematological toxicity was significantly higher than that in the MG, which is consistent with our results. A systematic Cochrane review in 2018 included two RCTs with a total sample size of 294 patients treated with radiotherapy for cervical cancer (24). Results showed that the incidence of grade I–II diarrhea in cancer patients was lower in the EG than in MG.

Diarrhea caused by radiotherapy in the pelvic region is mainly caused by intestinal crypt cell apoptosis (25). In a study of the intestinal crypt in mice, an obvious circadian rhythm was observed in the number of apoptotic cells in the intestinal crypt during the administration of radiotherapy at different times, which indicated that radiotherapy-induced apoptosis occurs in a time-dependent manner (26, 27). Studies on the effects of radiation therapy on mice have shown that the

10.3389/fonc.2022.1021453

TABLE 3 Baseline characteristics of patients.

Characteristic	Morning Group (n = 61)	Evening Group (n = 53)	t/x^2	P
Age (years)	56.85 ± 9.80	55.72 ± 9.55	0.625[a]	0.533
Weight (kg)	62.47 ± 12.00	62.77 ± 8.65	0.154[a]	0.427
Height (cm)	156.11 ± 19.03	160.26 ± 5.30	1.535[a]	0.193
Body surface area (m^2)	1.61 ± 0.14	1.64 ± 0.11	1.19[a]	0.072
Blood pressure (mmHg)	94.23 ± 12.19	92.74 ± 12.26	0.651[a]	0.519
Body temperature (°C)	36.30 ± 0.20	36.29 ± 0.22	0.194[a]	0.303
Pulse (time)	79.72 ± 10.08	79.55 ± 8.82	0.097[a]	0.062
Breath	18.87 ± 1.638	18.58 ± 1.865	0.866[a]	0.329
Job category				
Retired	9 (14.8)	5 (9.4)	3.543[b]	0.471
Staff	9 (14.8)	6 (11.3)		
Peasant	19 (31.1)	23 (43.4)		
Freelancer	3 (4.9)	5 (9.4)		
Unemployed	21 (34.4)	14 (26.4)		
Educational level				
Primary and below	24 (39.3)	17 (32.1)	4.019[b]	0.547
Junior high school	26 (42.6)	20 (37.7)		
High school	5 (8.2)	11 (20.8)		
Technical secondary school	2 (3.3)	1 (1.9)		
College				
Junior college	3 (4.9)	3 (5.7)		
Bachelor's degree or above	1 (1.6)	1 (1.8)		
Marital status				
Unmarried	1 (1.6)	0 (0)	2.020[b]	0.364
Married	60 (98.4)	52 (98.1)		
Remarried	0 (0)	1 (1.9)		
Divorced	0 (0)	0 (0)		
Other	0 (0)	0 (0)		
Per capita monthly household income (yuan)				
< 3000				
3000–5000	14 (23.0)	8 (15.1)	2.289[b]	0.515
5001–10000	30 (49.2)	28 (52.8)		
> 10000	14 (23.0)	16 (30.2)		
	3 (4.9)	1 (1.9)		
Medical payment method				
Worker health	12 (19.7)	7 (13.2)	2.433[b]	0.488
Residents of social security	35 (57.4)	35 (66.0)		
At own expense	0 (0)	10 (1.9)		
new rural cooperative medical system	14 (23.0)	10 (18.9)		
Fertility history				
Yes	60 (98.4)	52 (98.1)	0.010[b]	0.92
No	1 (1.6)	1 (1.9)		
FIGO staging				
IIB	31 (50.8)	30 (56.6)	6.488[b]	0.166
IIIA	5 (8.2)	4 (7.5)		
IIIB	8 (13.1)	2 (3.8)		
IIIC	14 (23.0)	17 (32.1)		
IVA	3 (4.9)	0 (0)		

(Continued)

TABLE 3 Continued

Characteristic	Morning Group (n = 61)	Evening Group (n = 53)	t/x^2	P
Pathological classification				
Squamous carcinoma	56 (91.8)	47 (88.7)	0.317[b]	0.537
Adenocarcinoma	5 (8.2)	6 (11.3)		
Past medical history				
No	45 (73.8)	36 (67.9)	2.074[b]	0.557
Hypertension	11 (18.0)	8 (15.1)		
Diabetes	1 (1.6)	2 (3.8)		
Heart disease	4 (6.6)	7 (13.2)		
KPS				
70	3 (4.9)	3 (5.7)	0.836[b]	0.405
80	16 (26.2)	15 (28.3)		
90	22 (36.1)	23 (43.4)		
100	20 (32.8)	12 (22.6)		

[a]t-test; [b]X^2 test.
FIGO, Federation International of Gynecology and Obstetrics; KPS, Karnofsky Performance Status.

TABLE 4 Radiotherapy efficacy and efficacy rate.

Group	CR (%)	PR (%)	SD (%)	PD (%)	x^2	p
MG	30 (49.2)	27 (44.3)	3 (4.9)	1 (1.6)	3.177	0.365
EG	34 (64.2)	17 (32.1)	2 (3.7)	0 (0)		

CR, complete remission; PR, partial remission; SD, stable disease; PD, progression of disease.

TABLE 5 Radiotherapy toxicity.

Group	Number	Grade 0	Grade 1	Grade 2	Grade 3	Grade 4	x^2	p
Radiation enteritis (%)								
MG	61	17 (27.9)	24 (39.3)	17 (27.9)	3 (4.9)	0 (0)	11.026	0.012
EG	53	29 (54.7)	18 (34.0)	5 (9.4)	1 (1.9)	0 (0)		
Diarrhea (%)								
MG	61	21 (34.4)	27 (44.3)	8 (13.1)	4 (6.6)	1 (1.6)	10.141	0.038
EG	53	33 (62.3)	13 (24.5)	6 (11.3)	1 (1.9)	0 (0)		
Radiocystitis (%)								
MG	61	45 (73.8)	9 (14.8)	5 (8.2)	2 (3.3)	0 (0)	1.350	0.717
EG	53	39 (73.6)	5 (9.4)	7 (13.2)	2 (3.8)	0 (0)		
Nausea/vomiting (%)								
MG	61	20 (32.8)	20 (32.8)	14 (23.0)	6 (9.8)	1 (1.6)	5.199	0.267
EG	53	26 (49.6)	15 (28.3)	10 (18.9)	1 (1.9)	1 (1.9)		
Radiodermatitis (%)								
MG	61	45 (73.8)	8 (13.1)	7 (11.5)	1 (1.6)	0 (0)	3.643	0.303
EG	53	41 (77.4)	10 (18.9)	2 (3.8)	0 (0)	0 (0)		
Myelosuppression (%)								
MG	61	24 (39.3)	23 (27.7)	13 (21.3)	1 (1.6)	0 (0)	10.462	0.033
EG	53	14 (26.4)	17 (32.1)	12 (22.6)	9 (17.0)	1 (1.9)		

MG, morning radiotherapy group; EG, evening radiotherapy group.

TABLE 6 M.D. Anderson Symptom Inventory scores.

Group	Number	Average score (mean ± standard deviation)	*t*	*p*
MG	61	21.64 ± 7.916	2.576	0.002
EG	53	18.53 ± 4.098		

MG, morning radiotherapy group; EG, evening radiotherapy group.

TABLE 7 Quality of life (QOL) scores.

Dimension	MG (mean ± standard deviation)	EG (mean ± standard deviation)	*t*	*p*
Physical activity	13.11 ± 4.53	14.53 ± 2.55	7.189	0.047
Family status	15.13 ± 5.83	16.34 ± 4.23	1.249	0.214
Emotional status	7.18 ± 3.55	7.49 ± 3.47	0.470	0.639
Functional status	14.03 ± 2.65	15.15 ± 3.10	2.075	0.040
Additional	13.80 ± 5.49	14.64 ± 5.73	0.797	0.427
Total QOL score	63.26 ± 8.68	68.15 ± 10.04	2.789	0.006

MG, morning radiotherapy group; EG, evening radiotherapy group; QOL, quality of life.

induction of apoptosis peaks between 9:00 AM and 11:00 AM and troughs between 7:00 PM and 9:00 PM. Therefore, the occurrence of toxic reactions, such as diarrhea and mucositis, is more serious in the morning than in the evening (13). Myelosuppression and hematological toxicity are more serious in the evening after radiotherapy, which may be because proliferation and apoptosis of bone marrow cells exhibit circadian rhythm changes; indeed, apoptosis in the evening group was significantly higher than that in the morning group (28, 29).

Radiotherapy effect

Before radiotherapy, there were no significant differences in general demographic, disease, or social data between the two groups of patients. In this study, RECIST 1.1 was used to evaluate the efficacy of radiotherapy in patients with cervical cancer. After radiotherapy, the total effective rates (CR + PR) of the MG and EG were similar (93.5% vs. 96.3%, $p > 0.05$). Moreover, no significant differences in treatment response or disease progression were found between the MG and EG.

The results of this study are consistent with the report of Chang et al. (23) on the treatment of patients with cervical cancer by chronoradiotherapy. Chang et al. (23) randomized 67 cervical cancer patients to evaluate the efficacy of radiotherapy delivered using RECIST 1.1 in the morning and evening. Results showed that the effects were similar in the MG and the EG, and the total effective rates (CR + PR) were 100%, which was consistent with the results of our study. However, Guo et al. (30) evaluated the short-term efficacy of chronoradiotherapy using RECIST 1.1 in 25 cervical cancer patients and found that the effective rates of the MG and EG were 61.5% and 80.0%, respectively, which were significantly different. This finding is inconsistent with the results of our study. Possible reasons for this discrepancy are our sample size was too small, affecting the statistical analyses; or the efficacy of chronoradiotherapy was evaluated after the treatment, and the tumors of some patients regressed, which may have affected the evaluation results. Therefore, we plan to follow up patients over a longer period to evaluate long-term efficacy.

General condition of symptoms and QOL

The results of this study showed that the MDASI score in the MG was significantly higher than that in the EG (21.64 ± 7.916 vs. 18.53 ± 4.098, $p < 0.05$). Cervical cancer patients experience different degrees of symptoms during radiotherapy, including fatigue, nausea, vomiting, diarrhea, and pain (31). This may be because, during radiotherapy for cervical cancer, the deep penetration of radiation and the numerous organs in the pelvic cavity with similar anatomical positions results in normal tissues and organs being affected by radiation, inducing a series of corresponding symptoms and reactions (32). The MDASI scores were slightly higher in the MG than in the EG, which may be attributed to the higher incidence of radiation enteritis and diarrhea in the MG. Most patients experience nausea, vomiting, loss of appetite, pain, fatigue, and other symptoms (2, 33), which seriously affect the daily lives and QOL of patients, which may explain the higher total MDASI score in the MG than in the EG.

In terms of QOL, the total QOL score in the MG (63.26 ± 8.68) was lower than that in the EG (68.15 ± 10.04). In addition, the scores of physical activity and functional activity in the MG were also slightly lower than those in the EG. A previous study (34, 35) on the application of chronoradiation in patients with head and neck cancer found that the QOL score of the EG was higher than that of the MG during the first and second weeks after the start of

radiotherapy, although the difference was not significant. The discrepancy between the results of the two studies may be due to the different biological rhythms and time points of radiosensitivity between the two cancer types. Patients with cervical cancer have a higher incidence of gastrointestinal reactions in the morning, whereas head and neck cancer patients have a higher incidence of oral mucosa in the evening. Alternatively, the time points for the QOL life assessments may have been inconsistent between the two studies.

Limitations

In this study, the sample size was small, and the observation time for efficacy was short. We only examined the short-term efficacy of radiotherapy. Thus, further longitudinal investigations of the long-term efficacy and toxicity of radiotherapy are needed.

Conclusion

This multicenter randomized controlled trial focused on the short-term efficacy and side effects of chronoradiotherapy in patients with cervical cancer. We verified that the efficacy of radiotherapy was similar irrespective of whether it was administered in the morning or the evening. However, toxicity and side effects differed depending on the time of radiotherapy administration. That is, more severe hematologic toxicity and greater bone marrow suppression were observed in the EG, whereas more severe gastrointestinal toxicity was observed in the MG. Post-radiation assessment revealed that the overall severity of symptoms in the MG was greater than that in the EG; moreover, the QOL of the MG was lower than that of the EG.

Data availability statement

The original contributions presented in the study are included in the article/supplementary material. Further inquiries can be directed to the corresponding author.

Ethics statement

The studies involving human participants were reviewed and approved by Medical Ethics Committee of Tianjin Medical University Cancer Institute & Hospital, China. The patients/participants provided their written informed consent to participate in this study. Written informed consent was obtained from the individual(s) for the publication of any potentially identifiable images or data included in this article.

Author contributions

Study design: WY, QWM. Clinical subject recruitment: ZBZ. Clinical data collection: CXC, LXF, XJ, YR, LXH, ZZL, WCL and LYL. Primary outcome assessor: LJQ and SAM. Data interpretation: All authors. All authors contributed to the article and approved the submitted version.

Funding

This study was supported by the Basic Scientific Research Fund of Tianjin Medical University (general project 2020KJ144).

Conflict of interest

The authors declare that the research was conducted in the absence of any commercial or financial relationships that could be construed as a potential conflict of interest.

Publisher's note

References

1. Sung H, Ferlay J, Siegel RL, Laversanne M, Soerjomataram I, Jemal A. Global cancer statistics 2020: GLOBOCAN estimates of incidence and mortality worldwide for 36 cancers in 185 countries. *CA Cancer J Clin* (2021) 71(3):209–49. doi: 10.3322/caac.21660

2. Cohen PA, Jhingran A, Oaknin A, Denny L. Cervical cancer. *Lancet* (2019) 393(10167):169–82. doi: 10.1016/S0140-6736(18)32470-X

3. Arbyn M, Weiderpass E, Bruni L, de Sanjosé S, Saraiya M, Ferlay J, et al. Estimates of incidence and mortality of cervical cancer in 2018: A worldwide analysis. *Lancet Glob Health* (2020) 8(2):e191–203. doi: 10.1016/S2214-109X(19)30482-6

4. Marth C, Landoni F, Mahner S, McCormack M, Gonzalez MA, Colombo N, et al. Cervical cancer: ESMO clinical practice guidelines for diagnosis, treatment and follow-up. *Ann Oncol* (2017) 28(4):72–83. doi: 10.1093/annonc/mdx220

5. Li Z, Zhang Y, Sui S, Hua Y, Zhao A, Tian X, et al. Targeting HMGB3/hTERT axis for radio resistance in cervical cancer. *J Exp Clin Cancer Res* (2020) 39(1):1–17. doi: 10.1186/s13046-020-01737-1

6. Shen H, Cook K, Gee HE, Hau E. Hypoxia, metabolism, and the circadian clock: New links to overcome radiation resistance in high-grade gliomas. *J Exp Clin Cancer Res* (2020) 39(1):129. doi: 10.1186/s13046-020-01639-2

7. Rivina L, Davoren M, Schiestl RH. Radiation-induced myeloid leukemia in murine models. *Hum Genomics* (2014) 8(1):13. doi: 10.1186/1479-7364-8-13

8. Radojevic MZ, Tomasevic A, Karapandzic VP, Milosavljevic N, Jankovic S, Folic M. Acute chemoradiotherapy toxicity in cervical cancer patients. *Open Med* (2020) 15(1):822–32. doi: 10.1515/med-2020-0222

9. Sato F, Bhawal UK, Yoshimura T, Muragaki Y. DEC1 and DEC2 crosstalk between circadian rhythm and tumor progression. *J Cancer* (2016) 7(2):153–9. doi: 10.7150/jca.13748

10. Nelson N, Lombardo J, Matlack L, Smith A, Hines K, Shi WY, et al. Chronoradiobiology of breast cancer: The time is now to link circadian rhythm and radiation biology. *Int J Mol Sci* (2022) 23(3):1331. doi: 10.3390/ijms23031331

11. Liu X, Yu R, Zhu L, Hou X, Zou K. Bidirectional regulation of circadian disturbance and inflammation in inflammatory bowel disease. *Inflammation Bowel Dis* (2017) 23(10):1741–51. doi: 10.1097/MIB.0000000000001265

12. Pawlik TM, Keyomarsi K. Role of cell cycle in mediating sensitivity to radiotherapy. *Int J Radiat Oncol Biol Phys* (2004) 59(4):928–42. doi: 10.1016/j.ijrobp.2004.03.005

13. Bermúdez GL, Blanco SA, Ramírez ZJ, Lovo E. The time for chronotherapy in radiation oncology. *Front Oncol* (2021) 11:687672. doi: 10.3389/fonc.2021.687672

14. Lee SI, Atri M. 2018 FIGO staging system for uterine cervical cancer: Enter cross-sectional imaging. *Radiol* (2019) 292(1):15–24. doi: 10.1148/radiol.2019190088

15. Armato SG, Anna KN. Revised modified response evaluation criteria in solid tumors for assessment of response in malignant pleural mesothelioma (Version 1.1). *J Thorac Oncol* (2018) 13(7):1012–21. doi: 10.1016/j.jtho.2018.04.034

16. Cox JD, Stetz J, Pajak TF. Toxicity criteria of the radiation therapy oncology group (RTOG) and the European organization for research and treatment of cancer (EORTC). *Int J Radiat Oncol Biol Phys* (1995) 31(5):1341–6. doi: 10.1016/0360-3016(95)00060-C

17. Cella DF, Tulsky DS, Gray G, Sarafian B, Linn E, Bonomi A, et al. The functional assessment of cancer therapy scale: Development and validation of the general measure. *J Clin Oncol* (1993) 11(3):570–9. doi: 10.1200/JCO.1993.11.3.570

18. Cleeland CS, Mendoza TR, Wang XS, Chou C, Harle MT, Morrissey M, et al. Assessing symptom distress in cancer patients: The M.D. Anderson symptom inventory. *Cancer* (2000) 89(7):1634–46. doi: 10.1002/1097-0142(20001001)89:7<1634:aid-cncr29>3.0.co;2-v

19. Sancar A, Van Gelder RN. Clocks, cancer, and chronochemotherapy. *Science* (2021) 371:6524.eabb0738. doi: 10.1126/science.abb0738

20. Shilts J, Chen G, Hughey JJ. Evidence for widespread dysregulation of circadian clock progression in human cancer. *PeerJ* (2018) 31:6:e4327. doi: 10.7717/peerj.4327

21. Zhang Y, Chen X, Ren P, Su Z, Cao H, Zhou J, et al. Synergistic effect of combination topotecan and chronomodulated radiation therapy on xenografted human nasopharyngeal carcinoma. *Int J Radiat Oncol Biol Phys* (2013) 87(2):356–62. doi: 10.1016/j.ijrobp.2013.05.047

22. Chan S, Rowbottom L, McDonald R, Bjarnason GA, Tsao M, Danjoux C, et al. Does the time of radiotherapy affect treatment outcomes? a review of the literature. *Clin Oncol* (2017) 29(4):231–8. doi: 10.1016/j.clon.2016.12.005

23. Chang L, Li L, Li W, Jiang M, Jv Y, Wang L, et al. Research on radiotherapy at different times of the day for inoperable cervical cancer. *Int J Clin Pharmacol Ther* (2016) 54(11):856–64. doi: 10.5414/CP202654

24. Lawrie TA, Green JT, Beresford M, Wedlake L, Burden S, Davidson SE, et al. Interventions to reduce acute and late adverse gastrointestinal effects of pelvic radiotherapy for primary pelvic cancers. *Cochrane Database Syst Rev* (2018) 1(1):CD012529. doi: 10.1002/14651858.CD012529.pub2

25. Wang L, Wang X, Zhang G, Ma Y, Zhang Q, Zheng L, et al. The impact of pelvic radiotherapy on the gut microbiome and its role in radiation-induced diarrhoea: A systematic review. *Radiat Oncol* (2021) 16(1):187. doi: 10.1186/s13014-021-01899-y

26. Harper E, Talbot CJ. Is it time to change radiotherapy: The dawning of chronoradiotherapy? *Clin Oncol* (2019) 31(5):326–35. doi: 10.1016/j.clon.2019.02.010

27. Qiu G, Yu Y, Wang Y, Wang X. The significance of probiotics in preventing radiotherapy-induced diarrhea in patients with cervical cancer: A systematic review and meta-analysis. *Int J Surg* (2019) 65:61–9. doi: 10.1016/j.ijsu.2019.03.015

28. Benderitter M, Reyes EH, Gigov Y, Souleau B, Huet C, Trompier F, et al. Hematopoietic recovery using multi-cytokine therapy in 8 patients presenting radiation-induced myelosuppression after radiological accidents. *Radiat Res* (2021) 196(6):668–79. doi: 10.1667/RADE-21-00169.1

29. Corbeau A, Kuipers SC, Boer SM, Horeweg N, Hoogeman MS, Godart J, et al. Correlations between bone marrow radiation dose and hematologic toxicity in locally advanced cervical cancer patients receiving chemoradiation with cisplatin: A systematic review. *Radiother Oncol* (2021) 164:128–37. doi: 10.1016/j.radonc.2021.09.009

30. Guo P, Wang H, Jiang R, Wang Z. The clinical effect study on malignant tumors with chronoradiotherapy. *Biol Rhythm Res* (2015) 46(2):249–55. doi: 10.1080/09291016.2014.985001

31. Chargari C, Peignaux K, Escande A, Renard S, Lafond C, Petit A, et al. Radiotherapy of cervical cancer. *Cancer Radiother* (2022) 26(1-2):298–308. doi: 10.1016/j.canrad.2021.11.009

32. Vande Wetering FT, Verleye L, Andreyev HJN, Maher J, Vlayen J, Pieters BR, et al. Non-surgical interventions for late rectal problems (Proctopathy) of radiotherapy in people who have received radiotherapy to the pelvis. *Cochrane Database Syst Rev* (2016) 4(4):CD003455. doi: 10.1002/14651858.CD003455.pub2

33. Moezian GSA, Javadinia SA, Sales SS, Fanipakdel A, Elyasi S, Karimi G. Oral silymarin formulation efficacy in management of AC-T protocol induced hepatotoxicity in breast cancer patients: A randomized, triple blind, placebo-controlled clinical trial. *J Oncol Pharm Pract* (2022) 28(4):827–35. doi: 10.1177/10781552211006182

34. Bjarnason GA, Mackenzie RG, Nabid A, Hodson ID, Sayed SE, Grimard L, et al. Comparison of toxicity associated with early morning versus late afternoon radiotherapy in patients with head-and-neck cancer: A prospective randomized trial of the national cancer institute of Canada clinical trials group (HN3). *Int J Radiat Oncol Biol Phys* (2009) 73(1):166–72. doi: 10.1016/j.ijrobp.2008.07.009

35. Salek R, Dehghani M, Mohajeri SA, Talaei A, Fanipakdel A, Javadinia SA. Amelioration of anxiety, depression, and chemotherapy related toxicity after crocin administration during chemotherapy of breast cancer: A double blind, randomized clinical trial. *Phytother Res* (2021) 35(9):5143–53. doi: 10.1002/ptr.7180

frontiers | Frontiers in Oncology

TYPE Original Research
PUBLISHED 16 November 2022
DOI 10.3389/fonc.2022.1041839

OPEN ACCESS

EDITED BY
Gene A. Cardarelli,
Brown University, United States

REVIEWED BY
Chenyang Shen,
University of Texas Southwestern Medical Center, United States
Maria F. Chan,
Memorial Sloan Kettering Cancer Center, United States

*CORRESPONDENCE
Sara Trivellato
s.trivellato@asst-monza.it;
saratrive89@libero.it

SPECIALTY SECTION
This article was submitted to Radiation Oncology, a section of the journal Frontiers in Oncology

RECEIVED 11 September 2022
ACCEPTED 25 October 2022
PUBLISHED 16 November 2022

CITATION
Trivellato S, Caricato P, Pellegrini R, Montanari G, Daniotti MC, Bordigoni B, Faccenda V, Panizza D, Meregalli S, Bonetto E, Arcangeli S and De Ponti E (2022) Comprehensive dosimetric and clinical evaluation of lexicographic optimization-based planning for cervical cancer.
Front. Oncol. 12:1041839.
doi: 10.3389/fonc.2022.1041839

Comprehensive dosimetric and clinical evaluation of lexicographic optimization-based planning for cervical cancer

Sara Trivellato[1]*, Paolo Caricato[1,2], Roberto Pellegrini[3], Gianluca Montanari[1], Martina Camilla Daniotti[1,2], Bianca Bordigoni[1,4], Valeria Faccenda[1,2], Denis Panizza[1,5], Sofia Meregalli[5,6], Elisa Bonetto[6], Stefano Arcangeli[5,6] and Elena De Ponti[1,5]

[1]Medical Physics Department, Azienda Socio Sanitaria Territoriale (ASST) Monza, Monza, Italy, [2]Department of Physics, University of Milan, Milan, Italy, [3]Global Clinical Science, Elekta AB, Stockholm, Sweden, [4]Department of Physics, University of Milan Bicocca, Milan, Italy, [5]School of Medicine and Surgery, University of Milan Bicocca, Milan, Italy, [6]Department of Radiation Oncology, Azienda Socio Sanitaria Territoriale (ASST) Monza, Monza, Italy

Aim: In this study, a not yet commercially available fully-automated lexicographic optimization (LO) planning algorithm, called mCycle (Elekta AB, Stockholm, Sweden), was validated for cervical cancer.

Material and methods: Twenty-four mono-institutional consecutive treatment plans (50 Gy/25 fx) delivered between November 2019 and April 2022 were retrospectively selected. The automatic re-planning was performed by mCycle, implemented in the Monaco TPS research version (v5.59.13), in which the LO and Multicriterial Optimization (MCO) are coupled with Monte Carlo calculation. mCycle optimization follows an *a priori* assigned priority list, the so-called Wish List (WL), representing a dialogue between the radiation oncologist and the planner, setting hard constraints and following objectives. The WL was tuned on a patient subset according to the institution's clinical protocol to obtain an optimal plan in a single optimization. This robust WL was then used to automatically re-plan the remaining patients. Manual plans (MP) and mCycle plans (mCP) were compared in terms of dose distributions, complexity (modulation complexity score, MCS), and delivery accuracy (perpendicular diode matrices, gamma analysis-passing ratio, PR). Their clinical acceptability was assessed through the blind choice of two radiation oncologists. Finally, a global quality score index (SI) was defined to gather into a single number the plan evaluation process.

Results: The WL tuning requested four patients. The 20 automated re-planning tasks took three working days. The median optimization and calculation time can be estimated at 4 h and just over 1 h per MP and mCP, respectively. The dose comparison showed a comparable organ-at-risk spare. The planning

target volume coverage increased ($V_{95\%}$: MP 98.0% [95.6–99.3]; mCP 99.2% [89.7–99.9], p >0.05). A significant increase has been registered in MCS (MP 0.29 [0.24–0.34]; mCP 0.26 [0.23–0.30], p <0.05) without affecting delivery accuracy (PR (3%/3mm): MP 97.0% [92.7–99.2]; mCP 97.1% [95.0–98.6], p >0.05). In the blind choice, all mCP results were clinically acceptable and chosen over MP in more than 75% of cases. The median SI score was 0.69 [0.41–0.84] and 0.73 [0.51–0.82] for MP and mCP, respectively (p >0.05).

Conclusions: mCycle plans were comparable to clinical manual plans, more complex but accurately deliverable and registering a similar SI. Automated plans outperformed manual plans in blinded clinical choice.

KEYWORDS

lexicographic optimization, automated planning, cervical cancer, VMAT (volumetric modulated arc therapy), plan quality, plan comparison

1 Introduction

Recent studies focused on the implementation and commissioning of automatic tools in the typical radiotherapy workflow steps (1–3). The main characteristic of these tools is their mimicking of human planners' interactions with the treatment planning system (TPS). Three paradigms have been exploited in commercially available auto-planning solutions: knowledge-based planning (KBP), protocol-based algorithms, and multicriterial optimization (MCO). The KBP (e.g., RapidPlan in Eclipse TPS, Varian Medical Systems, Palo Alto, California) is based on a library of clinically accepted, high-quality plans. KBP suggests how good a plan could be by comparing the new patient's anatomy with the plan library, as a planner would learn from experienced colleagues' suggestions (4). Protocol-based algorithms (e.g., Autoplanning in Pinnacle^3 TPS, Philips Medical Systems, Fitchburg, Wisconsin) automatically repeat a known sequence of inverse planning actions, simulating the planner's presence at the TPS (5). On the other hand, the MCO sequentially tries to get an organ at risk (OAR) spared as well as possible without compromising the target coverage by substituting the planner in the typical trial-and-error procedure. In particular, the MCO looks for optimal solutions belonging to the so-called Pareto's surface, meaning that a plan cannot be further improved on any objective without degrading the results on at least one of the others. This surface navigation is done by the TPS in the *a priori* MCO, proposing only one planning solution respecting the listed requests (e.g., Monaco TPS, Elekta AB, Stockholm, Sweden). In the a-posteriori approach, the user can navigate between the generated multiple plans to choose the plan that best meets the clinical requests (e.g., Eclipse TPS, Varian, and Raystation TPS, RaySearch Laboratories AB, Stockholm, Sweden).

Together with the MCO, lexicographic optimization (LO) can be listed as a hierarchical optimization approach. LO is based on the imitation of the plan discussion process between radiation oncologists and planners, characterized by given clinical dose constraints, distribution evaluation, and compromise between conflicting planning goals (6). To do so, the given planning criteria are subdivided into constraints, which cannot be violated, and prioritized objectives with an assigned relevance order. Compared to MCO, in the LO sequential iterations, the obtained objective results are turned into constraints so that the following iterations cannot invalidate what has already been reached. The set of constraints, objectives, and priorities is called a Wish List (WL). The LO was first introduced and implemented at the Erasmus MC Cancer Institute of Rotterdam in the iCycle software (7). It is now implemented in the research version of Monaco TPS v5.59 combined with the *a priori* MCO as a research-available tool for photon beams and called mCycle (Elekta AB, Stockholm, Sweden). Although iCycle and mCycle are conceptually similar, their implementation is strongly different. The Rotterdam workflow is composed of two steps in the iCycle optimizer and in Monaco TPS, respectively. It starts with a fluence map

Abbreviations: LO, lexicographic optimization; MCO, multicriterial optimization; WL, wish list; MP, manual plans; mCP, mCycle plans; SI, scoring index; OAR, organ-at-risk; PTV, planning target volume; TPS, treatment planning system; KBP, knowledge-based planning; VMAT, volumetric-modulated arc therapy; CTV, clinical target volume; CP, control points; FMO, Fluence matrix optimization; SSO, segment shape optimization; SWO, segment weight optimization; CC, clinical constraint; PC, planning constraint; FP, first pass; SP, second pass; PGDSSO, pseudo-gradient descent segment shape optimizer; MUs, monitor units; MCS, modulation complexity score; ROs, radiation oncologists.

optimization (FMO) in the iCycle multicriterial optimizer. The obtained distribution is the input to define a patient-specific Monaco template, which is subsequently used for final plan generation with the Monaco TPS. On the other hand, mCycle is completely embedded in the Monaco environment and no passages are needed. mCycle automated planning starts with a wish-list driven multicriterial FMO but the FMO dose distribution is directly input for a multi-criterial optimization of MLC segments answering again to the WL. The WL is defined by translating the physician's main and secondary planning requests into a sequence of clinical (CC) and planning constraints (PC) and the following objectives. Usually, CC are the inviolable clinical requests (e.g., spinal cord maximum dose), and they are assigned a higher weight than PC. Objectives get weighted proportionally to their priority in the WL. Each constraint and objective must be translated into one or more cost functions associated with the contoured structures.

A completely new code has been written to embed this approach in the Monaco environment with a different mathematical solver, a different patient model, the typical Monaco cost functions, and a Monte Carlo Algorithm (XVMC) (8). The published experiences are mainly focused on iCycle application in several anatomic sites, while applications of the novel mCycle are reported only for head and neck, prostate and rectal cancer volumetric-modulated arc therapy (VMAT) treatment planning (8, 9), and prostate treatment on an MR-Linac (10). This is the first feasibility study of mCycle implementation for cervical cancer treatment. This pelvic anatomic site was chosen to study the possibility of reducing planner workload. Cervical cancer treatments are characterized by large and irregular-shaped targets that pose challenges to the generation of high-quality plans (11). They cover more than 10% of VMAT plans at our institution, contributing to the annual workload almost as much as prostate cancer treatments. This feasibility study thoroughly investigates mCycle performances to produce a plan quality at least comparable to accepted clinical manual plans obtained with clinical Monaco *a priori* MCO. The analysis included a comparison of plan dose distributions, complexity, delivery accuracy, and clinical acceptability. A plan quality score was introduced to globally assess manual and automatic plans, as suggested by previous studies claiming how powerful these indexes are to discern plan quality (12).

2 Materials and methods

2.1 Patient population

This retrospective planning study included a mono-institutional consecutive cohort of 24 cervical cancer patients previously treated with the VMAT technique between November 2019 and April 2022. All patients were treated at an Elekta VersaHD linear accelerator equipped with the Agility Multileaf Collimator (MLC, 160 leaves, 5 mm thickness, up to 6.5 cm/s, MU calibration 1 MU = 1 cGy). The main inclusion criterion was a prescription dose of 50 Gy in 25 fractions. To cover all the possible scenarios, the selected population included 9 patients who had undergone surgery and 15 patients who had not. This challenged the mCycle algorithm to manage different target volumes. The presence of a mono- or bilateral femoral prosthesis was considered an exclusion criterion. All patients underwent a CT simulation with a 3 mm slice thickness in the supine position, with rectum- and bladder-specific preparation instructions before the simulation and each treatment fraction. The originally segmented structure sets included clinical target volumes, CTVs (cervix, uterus if present, proximal vagina, and pelvic nodes), and OARs (rectum, bladder, small bowel, and femoral heads). These structure sets were used in the automatic re-optimization and the following data analysis. According to the institutional protocol, the planning target volume (PTV) was defined as the isotropic 7-mm expansion of the CTV. All patient-related information was deeply anonymized before conducting the research. The institutional review board denied the need for written informed consent from the participants as there was no impact on treatment and the applied patient data in this retrospective dosimetric planning study.

2.2 Manual treatment planning

All manual plans were generated with the clinical *a priori* MCO of the Monaco TPS (version 5.51.10). A 6-MV coplanar dual 330°-arc was optimized with up to 150 control points (CP), a minimum segment width of 1.0 cm, and highly smoothed fluence. A 3-mm dose grid and a 1%-statistical uncertainty per Monte Carlo calculation have been used. The manual optimization used the so-called MCO-constrained modality: the the PTV-related requests will be satisfied after the fulfillment of OAR cost functions because PTV and OAR cost functions were handled as first-order objectives and first-order constraints, respectively. The main limitation of this approach is the strong dependence on how the cost functions are manually defined, i.e., the defined parameters are manually modified, iteration by iteration, to modulate the PTV-OAR compromise in search of the best clinical plan. In MP, both Fluence Matrix Optimization (FMO, phase 1) and Segment Shape and Segment Weight Optimization (SSO and SWO, phase 2) phases have been performed with MCO. A final re-normalization of the dose distribution to reach the minimum PTV coverage or to fulfill the small bowel constraint was allowed. The minimum target coverage of $V_{95\%}$ >95% was requested with a $D_{1\%}$ <107%. Institutional OAR tolerance doses were rectum $D_{50\%}$ <44.7 Gy, bladder $D_{50\%}$ <57.3 Gy, small bowel V_{45Gy} <195 cm^3, femoral heads $D_{5\%}$ <44.7 Gy (13–16). If it was not possible to respect the

protocol constraints, minor or major deviations were discussed and accepted by the approving clinician.

2.3 mCycle auto-planning

As previously described, in mCycle, constraints and prioritized objectives are managed by the planner through the mCycle WL, which represents a dialogue between the radiation oncologist and the planner. The WL has to be tuned accordingly to the institution's clinical protocol to obtain an optimal clinical plan in a single optimization process. As described by Hussein et al. (3), the tuning process is a multi-step iterative method on a subset of patients in which the current WL is evaluated in terms of the optimized plans. From a practical standpoint, the creation of a WL starts from a robust template of the manual planning process, following these simple guidelines:

a. Identifying what the prescriptions are, whose violation would prevent the acceptance of the plans and indicate them as WL CC;
b. Identifying those prescriptions that are normally inserted to determine dose gradients and indicating them as WL PC;
c. If the priority is a minimal target coverage (for example, 95% of the prescription dose to 95% of the volume), assign this prescription as the first priority-objective
d. Assign all subsequent priorities to the OARs according to the clinical relevance discussed with the radiation oncologist;
e. If there is still room for optimization, assign lower-order priorities to ask again for certain OAR sparing or target coverage.

The user then iteratively acts on the type of cost function, their priority order, and their related goals. This iterative process continues on until the results satisfy the defined clinical protocol for a subset of patients without incurring the cost of not accurately delivering plans.

The WL is used in a two-pass automated lexicographic MCO during mCycle fluence optimization. During the first pass (FP), the fluence is optimized to sequentially get, for each defined cost function, a value lower than the requested goal. The obtained value is then used to constrain its cost function in the following second pass (SP). In the SP, all the objectives that were below their goal in the FP are further optimized till they reach their lowest possible value or till a specified "sufficient value" is reached. On the other hand, the objectives that were higher than their goal after the FP are constrained to the value reached during the FP. This sequential definition of new constrained values allows for the avoidance of repetitive manual interventions on the cost function parameters and for achieving the clinically desired plan in only one optimization.

The obtained optimized fluence map distribution is input for the following multi-criterial optimization of MLC segments using the new Pseudo-Gradient Descent Segment Shape Optimizer (PGDSSO), which, again, deals with the WL. Starting from the collection of beamlets and for each segment, it computes the benefit of including or excluding the i-th beamlet with an optimization method similar to gradient descent.

The WL definition requires initial tweaking using a subset of CTs and structure sets to get robust WL-producing automatic plans at least comparable to the retrospectively selected manual plans. To avoid any bias, the patients used to tune the WL have been excluded from the following analysis. The tuned WL has been exploited to automatically re-plan the final selection of treatment plans. The same arc configuration has been used with a 6-MV coplanar dual 330°-arc with up to 150 CP, 1-cm minimum segment width, highly smoothed fluence, 3-mm dose grid, and 3%-statistical uncertainty per CP in the Monte Carlo calculation. No further WL changes were allowed in this test phase. The only accepted manual intervention on the mCycle plans (mCP) was limited to minimal fine-tuning to obtain the minimum clinical acceptability, namely a second optimization reducing the minimum segment width to 0.75 cm or, as in MP, a final re-normalization of the dose distribution to reach the minimum PTV coverage or to fulfill the small bowel constraint. As indicated before, this normalization step is often done in the clinical manual routine to obtain minor adjustments in dose distributions, being careful to not invalidate plan deliverability (i.e., losing segments with a low number of monitor units (MU)).

2.4 Plan comparison

2.4.1 Dosimetric comparison

To guarantee an unbiased comparison, all plans were recalculated using a statistical uncertainty of 0.5%. The MP and mCP PTV coverages have been compared in terms of the PTV $V_{100\%}$, $V_{95\%}$, and $D_{1\%}$. The dose distributions have been compared in terms of the conformality index ($CI_{95\%}$ and $CI_{50\%}$), defined by the ratio between the total volume covered by the specified dose (95% and 50% of the prescription dose) and the volume of the PTV. The analyzed OAR metrics were the mean doses (D_{mean}), the rectum and bladder $D_{50\%}$, the bowel V_{45Gy}, and the femoral heads $D_{5\%}$.

2.4.2 Plan complexity and delivery accuracy

The two planning modes have also been analyzed in terms of the total number of monitor units (MU) and segments. Furthermore, the plan complexity has been quantified through the modulation complexity score (MCS), as defined by McNiven (17).

The plan delivery has been evaluated in terms of the agreement between the calculated and measured dose

distributions, tested by performing a gamma analysis (ɣ). All plans have been recalculated on the CT scan of the Delta^{4+} phantom (ScandiDos, Uppsala, Sweden) using a 2-mm grid and a 0.5% statistical uncertainty. All plans, including MP, were delivered on the phantom on the same day to avoid daily delivery variations. The local ɣ has been performed with Scandidos software (version 1.00.0180). As established in the institutional QA protocol for conventional treatment plans, the gamma passing rate has been evaluated with a 3%/3 mm criteria (PR_33) neglecting any pixel registering a dose lower than 8% of the maximum dose (threshold). For sake of completeness, the 2%/2 mm criteria (PR_22), maximum gamma value ($ɣ_{max}$), mean gamma value ($ɣ_{mean}$), and confidence interval ($ɣ_{CI}$ = $ɣ_{mean}$ + 1.5 standard deviation) have been evaluated (18).

2.4.3 Physicians' blind choice

To clinically evaluate the mCycle results, two senior radiation oncologists (ROs) performed an independent, blind choice between MP and mCP, based on dose distribution, dose-volume histograms, and clinical objectives. All patients were anonymized and no information about the planning technique was given. Cohen's kappa coefficient (k) has been used to measure inter-rater reliability.

2.4.4 Plan quality score

The basic concept of a plan quality score was first introduced by Nelms (19), and it was here adapted to gather into a single number the plan evaluation process of our clinical team. The scoring index (SI) was defined as the quadratic mean of four sub-metrics representing target coverage, OAR-sparing, plan delivery accuracy, and plan complexity, each one of them ranging from 0 to 1 (Figure 1). The target coverage and OAR sparing sub-metrics are composed of the evaluated dose metrics as indicated in Figure 1. For each sub-metric, the score is proportional to the constraint fulfillment. For example, the PTV $D_{1\%}$ has a null score if it is higher than 107% as requested by the clinical protocol. The score increases as the PTV $D_{1\%}$ decreases.

2.5 Statistical analysis

Firstly, the normality test of Shapiro–Wilk has been performed on each sample of comparison metrics to establish whether to conduct the parametric t-test or the nonparametric Wilcoxon rank-sum test. The Bonferroni correction for multiple tests has been applied and the selected significance level has been set at 5% (p = 0.05). The variances of the two groups have also been compared with Bartlett's test and Levene's test (5) for normal and non-normal distributions, respectively. All statistical tests have been performed using Rstudio (2021.09.0).

3 Results

3.1 WL tweaking and automatic planning

The WL definition requested a tweak on four patients in five working days, acting on cost functions, their priority order, and their related goals. If a double PTV was present (PTV uterus and PTV pelvis), the PTV requests were simply doubled and kept both as first-priority objectives.

The final WL is presented in Table 1. The fulfillment of the bowel bag (CC), which violation implies plan rejection most of the time, is followed by dose gradient requests (PC). Finally, the objectives sequence asks for PTV coverage (first priority) and the iterative research of OAR doses as low as possible (following lower priorities).

The following automatic re-planning for the remaining 20 test patients took three working days. Excluding the contouring and the plan finalizing process, the median optimization and Monte Carlo calculation time can be estimated at 4 h and just over 1 h per MP and mCP, respectively. The manual fine-tuning was limited to six out of 20 plans (30%). A small re-normalization has been applied to get the minimum acceptable coverage or to satisfy the bowel constraint. In two cases, the re-normalization did not allow us to fulfill the clinical protocol bowel request and a re-optimization with a 0.75-cm minimum segment width was needed.

3.2 Plan comparison

3.2.1 Dosimetric comparison

The selected patients registered a median PTV of 1,073.7 cm^3 [608.4–1,453.9]. The MP and mCP dose results and their box-and-whisker plots are reported in Table 2 and Figure 2. Statistically significant differences resulted in median values of target metrics, even if the significance remained only in $D_{1\%}$ once the multiple-tests correction is applied. Furthermore, the variance test showed a statistically significant difference for the PTV $CI_{95\%}$ with an associated mCP distribution larger than the MP one.

On the other hand, results in OAR sparing showed comparable performances in all considered metrics. A slight decrease in OAR metrics can be observed in mCP, but it did not register statistical significance. It is worth noticing the mCP high repeatability of the bowel V_{45Gy} with an extremely narrow boxplot just below the constraint.

The dose distributions for a representative patient are graphically reported in Figure 3. This shows a slight increase in the PTV coverage and a significant improvement in rectum and bladder sparing. The bowel $V_{45\ Gy}$ respected the clinical constraints in both plans, but it is worth noticing the greater extent of the low doses in mCP than in MP.

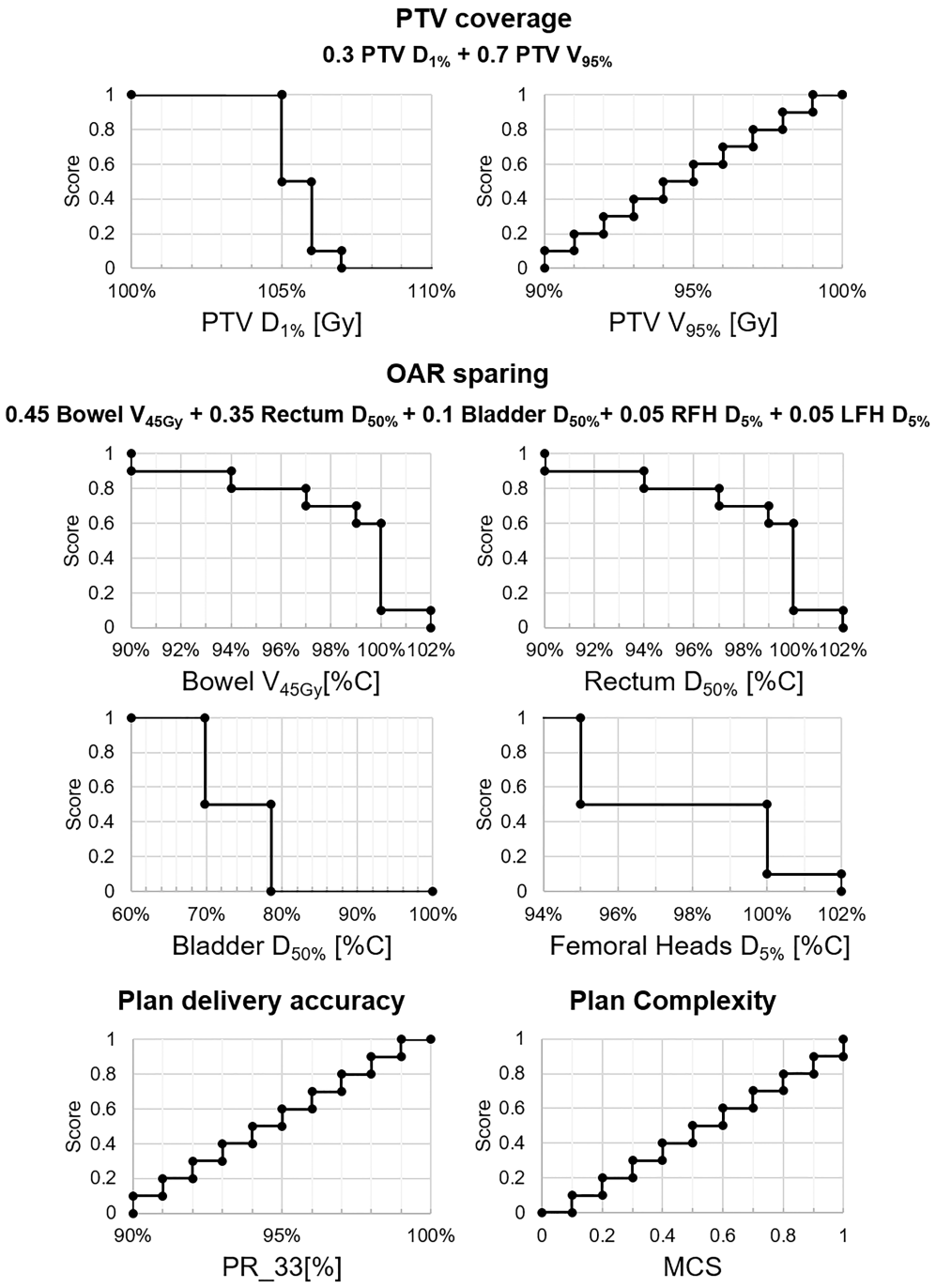

FIGURE 1
Scoring index components and definition. The weighting of target coverage and OAR sparing index components are reported in the formulae. Abbreviations: PTV, planning target volume; OAR, organ-at-risk; $D_{\#}$, dose received by the # % of contoured volume; $V_{\#}$, volume receiving more than # Gy; RFH, right femoral head; LFH, left femoral head; PR_33, 3%/3 mm gamma passing ratio; MCS, modulation complexity score.

3.2.2 Complexity and delivery accuracy comparison

Plan complexity and delivery results and their box-and-whiskers plots are reported in Table 3 and Figure 4, respectively. The mCP registered a MU slight increase and a statistically significant MCS decrease ($p < 0.001$). On the other hand, a decrease in the number of segments has been registered thanks to the novel PGDSSO. A significant narrowing of data variance is

registered for the MCS and number of segments. The increased complexity had no effect on plan delivery accuracy, as shown by the gamma passing ratios reported in Table 3 with their p-values.

3.2.3 Blind choice results

Out of 20 patients, all manual and automated plans were considered clinically acceptable. Only two MPs presented a major deviation from the protocol criteria due to unfavorable anatomy.

Other minor deviations in OAR constraints were clinically accepted (2 MP and 3 mCP). The ROs chose the mCP over the MP in 75.0% and 80.0% of cases, with a moderate agreement (k = 0.51). The preferred MP plans registered a slightly better OAR spare with lower PTV coverage.

3.2.4 Plan scoring

The target coverage, OAR sparing, plan delivery accuracy, and plan complexity median scores for MP and mCP were 0.90, 0.79, 0.75, 0.20, and 1.00, 0.81, 0.80, and 0.20, respectively. The median SI was 0.69 [0.41–0.84] and 0.73 [0.51–0.82] for MP and mCP, respectively. On a single patient-basis, the mCP median score variation with respect to MP was 5.8% [−17.0% to +72.0%]. No statistically significant difference was registered between the single metrics and the SI distributions. All data are listed in Table 4.

4 Discussion

To the knowledge of the authors, this work is the first feasibility study of mCycle implementation in the VMAT

TABLE 1 mCycle wish-list for auto-planning of cervical cancer (50 Gy in 25 fractions).

Clinical Constraints

	Structure	*Cost Function (parameter)*	*Shrink margin (cm)*	*Limit*
	PTV	Quadratic Overdose (52 Gy)	/	<0.02 Gy
	Bowel bag	Overdose DVH (45 Gy)	/	<195.0 cm^3
	External	Maximum Dose	/	53.4 Gy

Planning Constraints

	Structure	*Cost Function (parameter values)*	*Shrink margin (cm)*	*Limit*
	External	Quadratic Overdose (50 Gy)	0.0	<0.1 Gy
	External	Quadratic Overdose (45 Gy)	0.3	<0.2 Gy
	External	Quadratic Overdose (40 Gy)	0.6	<0.2 Gy
	External	Quadratic Overdose (35 Gy)	0.9	<0.2 Gy
	External	Quadratic Overdose (25 Gy)	2.5	<0.3 Gy

Objectives

Priority	*Structure*	*Cost Function (parameter values)*	*Shrink margin (cm)*	*Goal value (sufficient)*
1	PTV	Target EUD (0.5)		50.0 Gy
1	PTV	Target Penalty (99%)		50.0 Gy
2	Rectum	Parallel (40 Gy, k = 3)	0.3	<30.0%
2	Bladder	Parallel (40 Gy, k = 3)	0.3	<33.5%
3	Rectum	Serial (k = 15)		<46.0 Gy
3	Bowel bag	Parallel (40 Gy, k = 3)	0.3	<20.0%
3	Bowel bag	Serial (k = 15)		<43.0 Gy
3	Bladder	Serial (k = 15)		<47.0 Gy
4	Bowel bag	Overdose DVH (45 Gy)		<14.0% (7.0%)
4	Right femoral head	Serial (k = 15)		<38.0 Gy
4	Left femoral head	Serial (k = 15)		<38.0 Gy
5	External	Conformality		<0.75
6	Right femoral head	Serial (k = 1)		<30.0 Gy
6	Left femoral head	Serial (k = 1)		<30.0 Gy
7	Rectum	Serial (k = 1)		<30.0 Gy
8	Bladder	Serial (k = 1)		<35.0 Gy

Priority: order list according to which the objectives (cost functions) are optimized. Shrink margin: creates a buffer zone between the PTV and overlapping structures to avoid conflict between the applied cost functions of each of the structures. PTV, planning target volume; DVH, dose volume histogram; EUD, equivalent uniform dose.

10.3389/fonc.2022.1041839

TABLE 2 Comparison of original manual plans and mCycle plans in terms of PTV and OAR dose metrics.

DOSE METRICS	MP	mCP	Wilcoxon or t test	Levene's or Bartlett's test
PTV				
$V_{100\%}$ (%) (2)	63.3 [54.2–80.3]	72.4 [43.3–87.7]	**0.040**/1.000	0.597
$V_{95\%}$ (%) (2)	98.0 [95.6–99.3]	99.2 [89.7–99.9]	**0.004**/0.108	0.391
$D_{1\%}$ (%) (2)	103.6 [103.0–105.5]	104.3 [103.4–105.2]	**0.001**/**0.027**	0.066
$CI_{95\%}$ (1)	1.2 [1.1–1.3]	1.2 [1.0–1.4]	0.218/1.000	**0.018**
$CI_{50\%}$ (1)	4.2 [3.6–5.0]	4.2 [3.5–5.3]	0.379/1.000	0.376
Bowel				
$V_{45\ Gy}$ (cm^3) (2)	179.2 [56.5–414.0]	188.3 [92.6–209.0]	0.344/1.000	0.080
D_{mean} (Gy) (1)	25.0 [19.3–31.7]	26.7 [20.8–30.8]	0.142/1.000	0.518
Rectum				
$D_{50\%}$ (Gy) (1)	41.7 [30.2–47.0]	40.3 [31.4–45.8]	0.713/1.000	0.430
D_{mean} (Gy) (1)	39.1 [29.7–44.0]	37.7 [30.4–42.1]	0.404/1.000	0.273
Bladder				
$D_{50\%}$ (Gy) (2)	42.0 [28.8–47.4]	41.6 [26.7–48.1]	0.583/1.000	0.631
D_{mean} (Gy) (1)	39.7 [30.9–45.4]	38.4 [30.3–43.1]	0.293/1.000	0.661
Left femoral head				
$D_{5\%}$ (Gy) (1)	40.9 [33.9–49.0]	41.3 [30.5–48.9]	0.872/1.000	0.239
D_{mean} (Gy) (1)	30.1 [25.8–37.2]	29.0 [20.9–38.4]	0.186/1.000	0.060
Right femoral head				
$D_{5\%}$ (Gy) (1)	42.3 [34.0–49.8]	41.3 [32.8–47.9]	0.734/1.000	0.973
D_{mean} (Gy) (1)	30.5 [23.2–37.8]	28.4 [19.8–34.3]	0.126/1.000	0.416

MP, manual plans; mCP, mCycle plans; PTV, planning target volume; $V_{\#}$, volume receiving more than # Gy; $D_{\#}$, dose received by the # % of contoured volume; $CI_{\#\%}$, conformality index of the #% of the prescription dose; D_{mean}, mean dose; (1), Gaussian distribution; (2), not normal distribution. In Wilcoxon and t test column, non-corrected and Bonferroni-corrected p-values are reported (p-value/corrected p value). Bold: Statistical significance ($p < 0.05$). Median values and ranges are reported.

planning of cervical cancer treatment. This novel tool differs from iCycle by exploiting Monaco cost functions, a new mathematical solver, and a new patient model, providing a single solution in which LO and MCO are coupled with Monte Carlo calculation. This qualitative and quantitative comparison with the clinically accepted plans generated by experienced medical physicists included a quantitative scoring of global plan quality. Results proved the mCycle capability to generate plans at least comparable to manual plans with a strongly limited manual plan fine-tuning. The number of patients needed to tune the WL is not defined in the literature, but the presented results are in line with Bijman et al.'s (8) experience on other anatomic sites. Furthermore, the automatic re-planning took only three working days to obtain 20 clinically acceptable and deliverable mCP, showing how mCycle would strongly reduce planners' workload in the clinical routine of cervical treatment planning. In terms of dosimetric comparison, mCP was comparable to MP obtaining a target coverage increase. The registered increase of the PTV $D_{1\%}$ showed statistical significance, although not clinically relevant and respecting the institutional protocol. These results were obtained with a very narrow distribution of bowel-sparing results, proving the strength and repeatability of LO when a clinical constraint is given. It is worth noticing that the blind choice revealed that slightly lower OAR doses or a smaller low dose extent in MP, as shown in Figure 3, was preferred to the extremely high target coverage of the opposing mCP. The analysis of plan complexity and delivery accuracy proved that mCycle generates more complex plans even if the implementation of a new segment shape optimization led to a lower number of segments. The newer PGDSSO is faster and more efficient in merging similar segments than the previous algorithm (used in the MP), thus resulting in a lower global number of segments while keeping the modulation degree as high as needed by the plan. Nevertheless, the gamma analysis results showed that the accuracy of plan delivery was preserved and guaranteed. These results are limited to the available sample size, which was strongly dependent on the inclusion criteria. Further investigations will be needed to confirm these results on a larger dataset (20).

The mCycle capability to mimic manual planning has thus been verified in an anatomic site only investigated in a few other auto-planning experiences reported in the literature. Hussein et al. (21) and Tinoco et al. (22) have reported the KBP capability to produce IMRT and VMAT treatment plans with comparable OAR sparing and better conformity than the original clinically accepted plans. Sharfo et al. investigated IMRT versus VMAT

strategies for cervical cancer with their in-house Erasmus-iCycle optimizer (23) and demonstrated that the plan quality of automatically generated plans was superior to manually-generated plans (24).

Comparing this mCycle implementation with the published results on KBP (11, 21, 22, 25, 26) the main difference can be identified in the KBP need for a model optimization based on a high-quality plan library (21). As claimed by Cilla (5), KBP

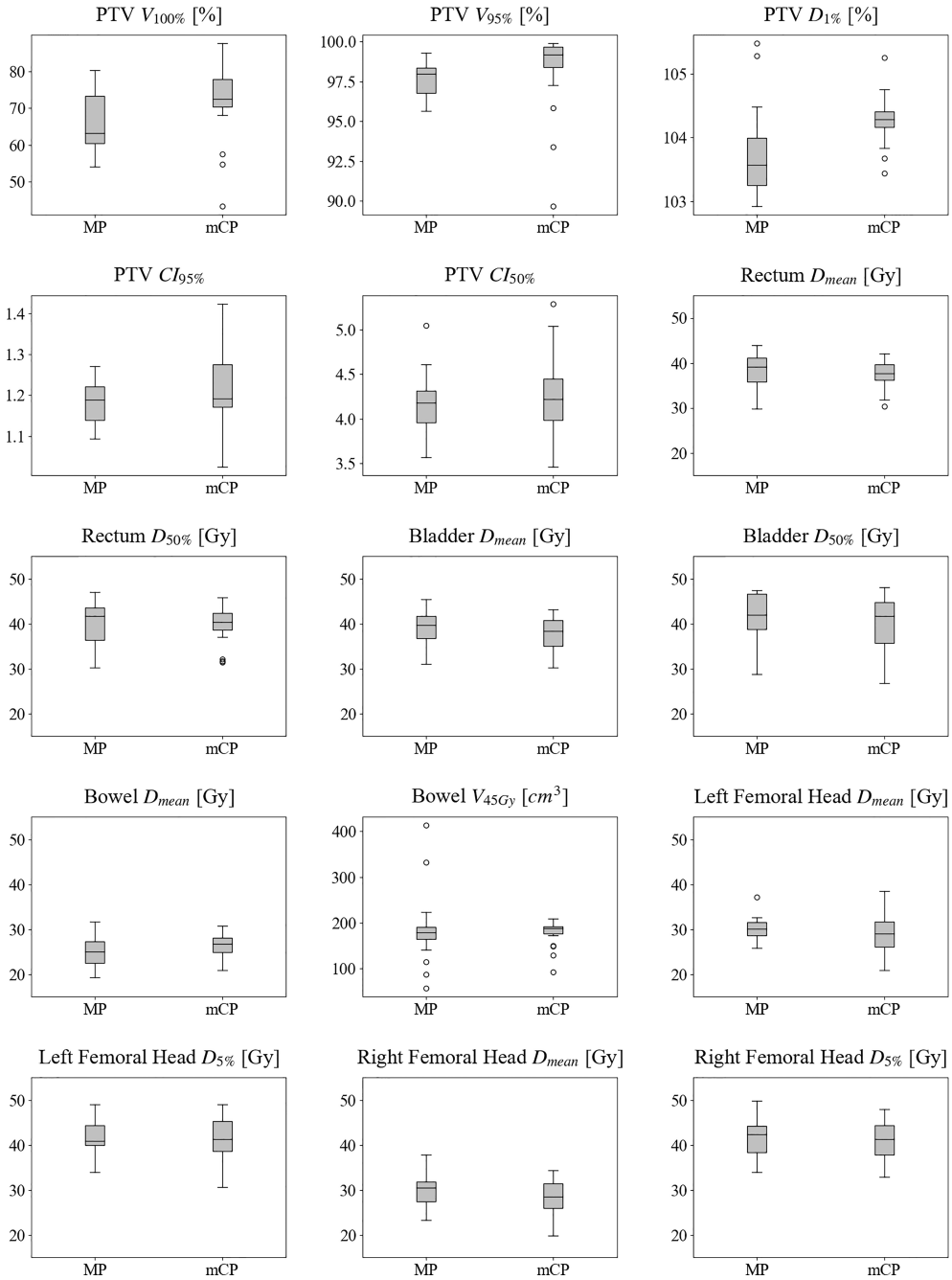

FIGURE 2
Box-and-whisker plots of computed dosimetric metrics for manual plans and mCycle plans. The box is delimited by the first (25%) and the third (75%) quartiles, and the bold line represents the median value. The whiskers point to the minimum and maximum data without counting boxplot outliers that in case there exist are represented with circles. An outlier is defined as a value exceeding the 1.5 interquartile range [1.5 (third−first quartile)]. MP, manual plans; mCP, mCycle plans; PTV, planning target volume; $V_{\#}$, volume receiving more than # Gy; $D_{\#}$, dose received by the # % of contoured volume; $CI_{\#}$, conformality index of the # dose; D_{mean}, mean dose.

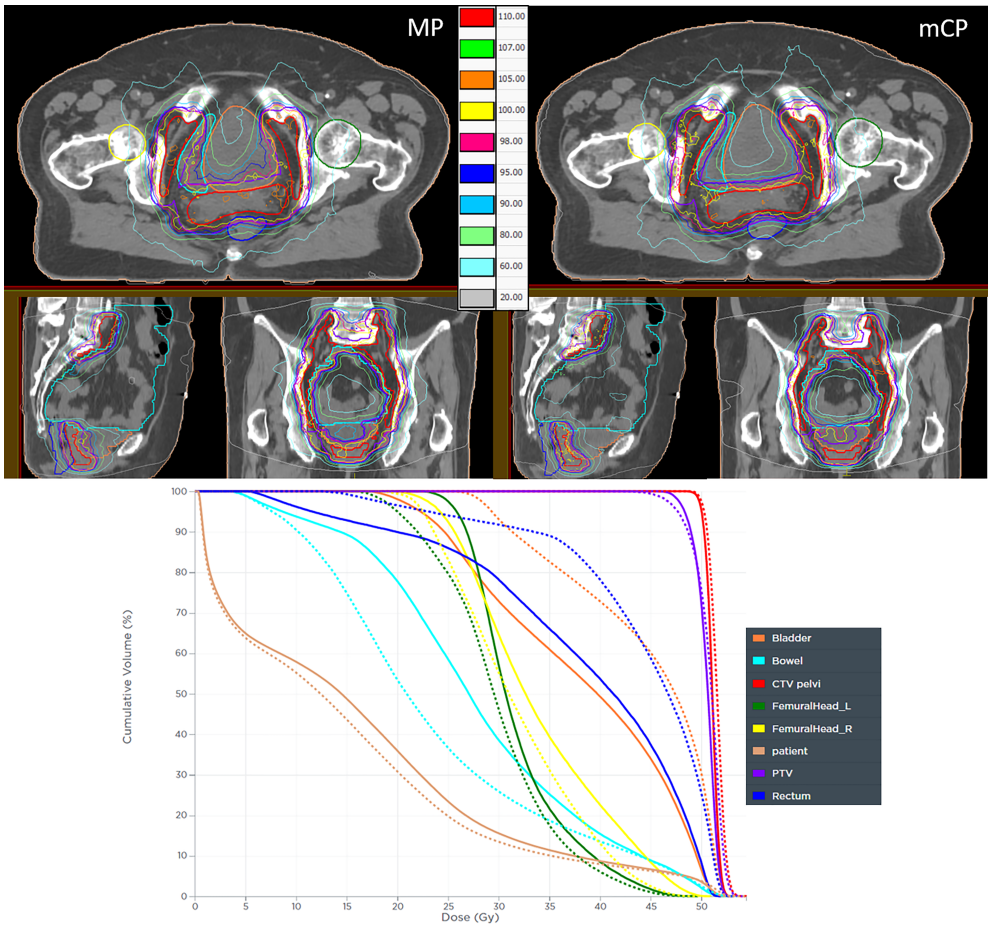

FIGURE 3
Dose distribution comparison of a manual plan (MP) and a mCycle plan (mCP). The isodose color legend is reported while the contoured structures are CTV (red), PTV (purple), rectum (blue), bladder (orange), bowel (cyan), right femoral head (yellow), left femoral head (green), and patient (pink). The DVH curves are reported as solid lines for mCP and dotted lines for MP.

TABLE 3 Comparison of original manual plans and mCycle plans in terms of plan complexity and plan delivery. Median values and ranges are reported.

PLAN COMPLEXITY	MP	mCP	Wilcoxon or t test	Levene's or Bartlett's test
MCS[(1)]	0.29 [0.24–0.34]	0.26 [0.23–0.30]	**<0.001/0.002**	**0.047**
MU [(2)]	751.2 [644.1–875.2]	783.5 [721.2–985.1]	0.086/1.000	0.188
Segments [(2)]	211 [134–257]	148 [133–196]	**0.001/0.027**	**<0.001**
PLAN DELIVERY ACCURACY	**MP**	**mCP**	**Wilcoxon or t test**	**Levene's or Bartlett's test**
PR (3%/3 mm) (%) [(1)]	97.0 [92.7–99.2]	97.1 [95.0–98.6]	0.441/1.000	**0.018**
PR (2%/2 mm) (%) [(1)]	89.2 [79.2–96.7]	90.3 [84.3–96.1]	0.331/1.000	**0.031**
γ_{mean} [(2)]	0.33 [0.24–0.45]	0.32 [0.22–0.39]	0.498/1.000	0.055
γ_{max} [(2)]	2.01 [1.67–3.44]	2.62 [1.58–3.92]	0.079/1.000	0.190
γ_{CI} [(1)]	0.75 [0.57–0.98]	0.75 [0.55–0.97]	0.911/1.000	0.274

MP, manual plans; mCP, mCycle plans; MCS, modulation complexity score; MU, monitor units; PR, gamma passing ratio; γ_{mean}, mean gamma index value; γ_{max}, maximum gamma index value; γ_{CI}, gamma confidence interval; [(1)], Gaussian distribution; [(2)], not normal distribution. In Wilcoxon and t test column, non-corrected and Bonferroni-corrected p-values are reported (p-value/corrected p-value). Bold: Statistical significance ($p < 0.05$).

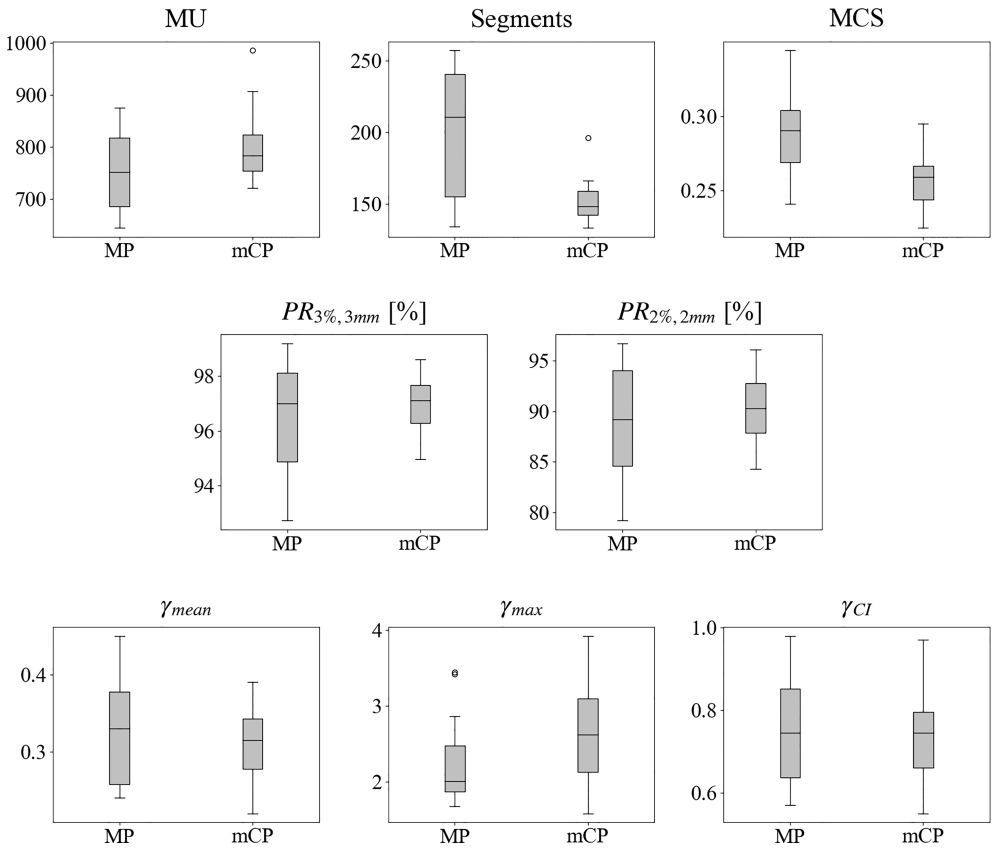

FIGURE 4
Box-and-whisker plots of computed complexity and delivery metrics for manual plans (MP) and mCycle plans (mCP). The box is delimited by the first (25%) and the third (75%) quartiles, and the bold line represents the median value. The whiskers point to the minimum and maximum data without counting boxplot outliers that in case there exist are represented with circles. An outlier is defined as a value exceeding the 1.5 interquartile range (1.5 (third−first quartile)). Abbreviations: MP, manual plans; mCP, mCycle plans; MU, monitor units; MCS, modulation complexity score; PR_33, 3%/3 mm gamma passing ratio; PR_22, 2%/2 mm gamma passing ratio; γ_{mean}, mean gamma index value; γ_{max}, maximum gamma index value; γ_{CI}, gamma confidence interval.

mainly depends on the model strength, i.e., on the original plan quality and the correct identification of plan outliers. On the other hand, mCycle asks for a WL optimization, which appears very simple and intuitive, resembling a template optimization that can be easily learned by any Monaco user. Furthermore, if a new clinical protocol is introduced, KBP needs a new database of high-quality manually generated plans. On the contrary, mCycle and the Autoplanning of Pinnacle allow implementing automatic plan generation only adapting the WL or the Pinnacle technique, respectively, using the very first patients' CT scans and structures.

In this context of protocol updates, a single dose prescription WL can be considered to be a limitation. In fact, lymph node boosts are often included in external beam radiotherapy. Despite

TABLE 4 Comparison of plan scoring index and its sub-metrics for plans and mCycle plans. Median values and ranges are reported.

SUBMETRIC*	MP	mCP	Wilcoxon	Levene's test
Target coverage	0.90 [0.57–1.00]	1.00 [0.30–1.00]	0.013/0.195	0.722
OAR sparing	0.79 [0.32–1.00]	0.81 [0.05–1.00]	0.507/1.000	0.135
Plan delivery accuracy	0.75 [0.30–1.00]	0.80 [0.60–0.90]	0.466/1.000	**0.002**
Plan complexity	0.20 [0.20–0.30]	0.20 [0.20–0.20]	**0.004**/0.060	**0.003**
SCORE INDEX	0.69 [0.41–0.84]	0.73 [0.51–0.82]	0.159/1.000	0.302

*All metrics showed a not normal distribution. Abbreviations: MP, manual plans; mCP, mCycle plans. Non-corrected and Bonferroni-corrected p-values are reported (p-value/corrected p-value). Bold: Statistical significance ($p < 0.05$).

the capabilities of mCycle to deal with multiple dose prescriptions, in the current study, we only dealt with a single dose prescription. As it has already been demonstrated by other authors in head and neck cases (9) or prostate with simultaneous boost (10), multiple prescriptions are easily handled by mCycle WL exploiting the LO capability to spare OAR as much as possible without affecting a higher dose target coverage: the PTV coverage request should be doubled and differentiated for the PTV boost, and the goal values of OAR cost functions coherently adapted. This would lead to fine-tune the presented WL on a different subset.

Furthermore, three considerations on the WL optimization can be done. As already mentioned, even if mCP were all defined as clinically acceptable, their extremely wide target coverage was sometimes ranked lower than a slightly better OAR sparing in MP. Secondly, the planner's manual intervention has been reduced to a very small number of clicks, but 10% of mCP asked for a second optimization. Finally, the compared manual plans were obtained in the clinical routine by expert planners with limited available time, while Sharfo et al. proved an LO plan quality superior to manual plans even when generated by an expert planner without time pressure (24).

These considerations led to a further investigation into the possible WL tuning to explore the possibility of further sparing the surrounding OARs without any manual intervention and challenging a planning expert with no planning time limits. To do so, the LO gives the possibility to introduce multiple requests and priority levels, while the presented WL is now very straightforward. Further studies are ongoing to investigate the possibility to tune a second more complex WL highly demanding on OAR sparing, increasing the plan complexity, and, of course, the risk to affect plan deliverability. Having two WLs, it would be possible to choose the preferred compromise between dose distribution and plan complexity for each patient.

The RATING guidelines for treatment planning studies were used by three authors (PC, MCD, and BB) to independently score this study (27). The RATING scores were 93%, 89%, and 94%.

5 Conclusions

This is the first retrospective feasibility study on mCycle planning for cervical cancer treatment. The presented results showed that mCycle is an effective tool to generate automatic, high-quality VMAT treatment plans according to the cervical treatment institutional protocol. In fact, this comprehensive dosimetric and clinical evaluation showed that mCycle plans were comparable to clinical manual plans at the dosimetric comparison, more complex but equally deliverable. In addition, they registered a slightly higher global quality score. Furthermore, the needed planning time has been reduced by nearly a quarter. Finally, automated plans outperformed manual plans in blinded clinical scoring. As soon as it becomes commercially available, its implementation into the clinical routine will lead to reduced planning workload and dosimetric and clinical advantages. Future studies will broaden its use to other anatomic sites.

Data availability statement

The raw data supporting the conclusions of this article will be made available by the authors, without undue reservation.

Author contributions

ST was the lead author, who participated in study design, data collection, data and statistical analysis, manuscript drafting, table/figure creation, and manuscript revision. PC contributed to study design, participated in data collection and analysis, manuscript drafting, table/figure creation, study rating, and manuscript revision. RP participated in data collection, data analysis, and manuscript revision. GM participated in data collection and analysis, and manuscript revision. MD participated in table/figure creation, study rating, and manuscript revision. BB participated in study rating and manuscript revision. VF and DP aided in data analysis and manuscript revision. SM and EB participated in the plan blind choice and manuscript revision. SA is a senior author who aided in data analysis and manuscript revision. EP is a senior author who aided in the study design, contributed to statistical analysis, and revised the manuscript. All authors contributed to the article and approved the submitted version.

Conflict of interest

RP serves as Director of Clinical Science at Elekta AB.

The remaining authors declare that the research was conducted in the absence of any commercial or financial relationships that could be construed as a potential conflict of interest.

Publisher's note

References

1. Vandewinckele L, Claessens M, Dinkla A, Brouwer C, Crijns W, Verellen D, et al. Overview of artificial intelligence-based applications in radiotherapy: Recommendations for implementation and quality assurance. *Radiother Oncol* (2020) 153:55–66. doi: 10.1016/j.radonc.2020.09.008

2. Hansen CR, Hussein M, Bernchou U, Zukauskaite R, Thwaites D. Plan quality in radiotherapy treatment planning - review of the factors and challenges. *J Med Imaging Radiat Oncol* (2022) 66(2):267–78. doi: 10.1111/1754-9485.13374

3. Hussein M, Heijmen BJM, Verellen D, Nisbet A. Automation in intensity modulated radiotherapy treatment planning - a review of recent innovation. *Br J Radiol* (2018) 91:20180270. doi: 10.1259/bjr.20180270

4. Momin S, Fu Y, Lei Y, Roper J, Bradley JD, Curran WJ, et al. Knowledge-based radiation treatment planning: A datadriven method survey. *J Appl Clin Med Phys* (2021) 22(8):16–44. doi: 10.1002/acm2.13337

5. Cilla S, Ianiro A, Romano C, Deodato F, Macchia G, Buwenge M, et al. Template-based automation of treatment planning in advanced radiotherapy: A comprehensive dosimetric and clinical evaluation. *Sci Rep* (2020) 10. doi: 10.1038/s41598-019-56966-y

6. Jee KW, McShan DL, Fraass BA. Lexicographic ordering: Intuitive multicriteria optimization for IMRT. *Phys Med Biol* (2007) 52(7):1845–61. doi: 10.1088/0031-9155/52/7/006

7. Breedveld S, Storchi PRM, Voet PWJ, Heijmen BJM. iCycle: Integrated, multicriterial beam angle, and profile optimization for generation of coplanar and noncoplanar IMRT plans. *Med Phys* (2012) 39(2):915–63. doi: 10.1118/1.3676689

8. Bijman R, Sharfo AW, Rossi L, Breedveld S, Heijmen B. Pre-clinical validation of a novel system for fully-automated treatment planning. *Radiother Oncol* (2021) 158:253–61. doi: 10.1016/j.radonc.2021.03.003

9. Biston MC, Costea M, Gassa F, Serre AA, Voet P, Larson R, et al. Evaluation of fully automated a priori MCO treatment planning in VMAT for head-and-neck cancer. *Phys Med* (2021) 87:31–8. doi: 10.1016/j.ejmp.2021.05.037

10. Naccarato S, Rigo M, Pellegrini R, Voet P, Akhiat H, Gurrera D, et al. Automated planning for prostate stereotactic body radiation therapy on the 1.5 T MR-linac. *Adv Radiat Oncol* (2022) 7(3):100865. doi: 10.1016/j.adro.2021.100865

11. Yusufaly TI, Meyers SM, Mell LK, Moore KL. Knowledge-based planning for intact cervical cancer. *Semin Radiat Oncol* (2020) 30(4):328–39. doi: 10.1016/j.semradonc.2020.05.009

12. Leung LH, Kan MW, Cheng AC, Wong WK, Yau CC. A new dose-volume-based plan quality index for IMRT plan comparison. *Radiother Oncol* (2007) 85 (3):407–17. doi: 10.1016/j.radonc.2007.10.018

13. Marks LB, Yorke ED, Jackson A, Ten Haken RK, Constine LS, Eisbruch A, et al. Use of normal tissue complication probability models in the clinic. *Int J Radiat Oncol Biol Phys* (2010) 76(3 Suppl):S10–9. doi: 10.1016/j.ijrobp.2009.07.1754

14. Buckey CR, Swanson GP, Stathakis S, Papanikolaou N. Optimizing prostate intensity-modulated radiation therapy (IMRT): Do stricter constraints produce better dosimetric results? *Eur J Clin Med Oncol* (2010) 2(2):139–44.

15. Roeske JC, Bonta D, Mell LK, Lujan AE, Mundt AJ. A dosimetric analysis of acute gastrointestinal toxicity in women receiving intensity-modulated whole-pelvic radiation therapy. *Radiother Oncol* (2003) 69(2):201–7. doi: 10.1016/j.radonc.2003.05.001

16. Lawton CA, Michalski J, El-Naqa I, Buyyounouski MK, Lee WR, Menard C, et al. RTOG GU radiation oncology specialists reach consensus on pelvic lymph node volumes for high-risk prostate cancer. *Int J Radiat Oncol Biol Phys* (2009) 74 (2):383–7. doi: 10.1016/j.ijrobp.2008.08.002

17. McNiven AL, Sharpe MB, Purdie TG. A new metric for assessing IMRT modulation complexity and plan deliverability. *Med Phys* (2010) 37(2):505–15. doi: 10.1118/1.3276775

18. Venselaar J, Welleweerd H, Mijnheer B. Tolerances for the accuracy of photon beam dose calculations of treatment planning systems. *Radiother Oncol* (2001) 60(2):191–201. doi: 10.1016/s0167-8140(01)00377-2

19. Nelms BE, Robinson G, Markham J, Velasco K, Boyd S, Narayan S, et al. Variation in external beam treatment plan quality: An inter-institutional study of planners and planning systems. *Pract Radiat Oncol* (2012) 2(4):296–305. doi: 10.1016/j.prro.2011.11.012

20. Fogliata A, Belosi F, Clicio A, Navarria P, Nicolini G, Scorsetti M, et al. On the pre-clinical validation of a commercial model-based optimisation engine: Application to volumetric arc therapy for patients with lung or prostate cancer. *Rad Oncol* (2014) 113:385–91. doi: 10.1016/j.radonc.2014.11.009

21. Hussein M, South CP, Barry MA, Adams EJ, Jordan TJ, Stewart AJ, et al. Clinical validation and benchmarking of knowledge-based IMRT and VMAT treatment planning in pelvic anatomy. *Radiother Oncol* (2016) 120(3):473–9. doi: 10.1016/j.radonc.2016.06.022

22. Tinoco M, Waga E, Tran K, Vo H, Baker J, Hunter R, et al. RapidPlan development of VMAT plans for cervical cancer patients in low- and middle-income countries. *Med Dosim* (2020) 45(2):172–8. doi: 10.1016/j.meddos.2019.10.002

23. Sharfo A, Voet P, Breedveld S, Mens J, Hoogeman M, Hejimen B. Comparison of VMAT and IMRT strategies for cervical cancer patients using automated planning. *Radiother Oncol* (2015) 114:395–401. doi: 10.1016/j.radonc.2015.02.006

24. Sharfo AWM, Breedveld S, Voet PWJ, Heijkoop ST, Mens JWM, Hoogeman MS, et al. Validation of fully-automated VMAT plan generation for library-based plan-of-the-day cervical cancer radiotherapy. *PloS One* (2016) 11(12). doi: 10.1371/journal.pone.0169202

25. Ma C, Huang F. Assessment of a knowledge-based RapidPlan model for patients with postoperative cervical cancer. *Prec Radiat Oncol* (2017) 1(3):102–7. doi: 10.1002/pro6.23

26. Li N, Carmona R, Sirak I, Kasanova L, Followill D, Michalski J, et al. Highly efficient training, refinement, and validation of a knowledge-based plan quality control system for radiotherapy clinical trials. *Int J Radiat Oncol Biol Phys* (2017) 97(1):164–72. doi: 10.1016/j.ijrobp.2016.10.005

27. Hansen CR, Crijns W, Hussein M, Rossi L, Gallego P, Verbakel W, et al. Radiotherapy treatment plannINg study guidelines (RATING): A framework for setting up and reporting on scientific treatment planning studies. *Radiother Oncol* (2020) 153:67–78. doi: 10.1016/j.radonc.2020.09.033

Frontiers in Oncology

Advances knowledge of carcinogenesis and tumor progression for better treatment and management

The third most-cited oncology journal, which highlights research in carcinogenesis and tumor progression, bridging the gap between basic research and applications to imrpove diagnosis, therapeutics and management strategies.

Discover the latest Research Topics

See more →

Frontiers

Avenue du Tribunal-Fédéral 34
1005 Lausanne, Switzerland
frontiersin.org

Contact us

+41 (0)21 510 17 00
frontiersin.org/about/contact